TAMPEREEN TEKNILLINEN YLIOPISTO
TAMPERE UNIVERSITY OF TECHNOLOGY

Mikko Salminen

Shear Resistance of Thin Metal Plate at Non-Uniform Elevated Temperatures

Julkaisu 1012 • Publication 1012

Tampere 2012

Tampereen teknillinen yliopisto. Julkaisu 1012
Tampere University of Technology. Publication 1012

Mikko Salminen

Shear Resistance of Thin Metal Plate at Non-Uniform Elevated Temperatures

Thesis for the degree of Doctor of Science in Technology to be presented with due permission for public examination and criticism in Rakennustalo Building, Auditorium RN201, at Tampere University of Technology, on the 13th of January 2012, at 12 noon.

Tampereen teknillinen yliopisto - Tampere University of Technology
Tampere 2012

ISBN 978-952-15-2697-8
ISSN 1459-2045

ABSTRACT

The shear resistance of thin metal plate consists of three components: shear buckling, the tension field effect and contribution of the flanges. This study considers the first two. The shear resistance of metal plate at elevated temperatures is known when temperature across the plate is constant. However, in many practical applications, such as webs of all-metal sandwich panels and slim floor beams in fire, the temperature distribution across the plate is non-uniform.

This study presents the results of a FEM analysis of thin carbon steel, aluminium and stainless steel plates at different non-uniform elevated temperatures. The temperature distributions were motivated by fire tests in literature (on slim floor beam and sandwich panel) and FEM calculations based on the general heat transfer theory. Material and geometric non-linearity were applied in the model. The material models were obtained from the most novel EN standards. The imperfections for the analysis are introduced by superimposing the eigenmodes of the plates.

The benchmarking cases used to validate the FEM models are resistances of the plates at uniform elevated temperatures. These results are compared to the test results available in literature.

Two methods for predicting the shear buckling, post-buckling and ultimate shear resistances of thin metal plates at non-uniform elevated temperatures are proposed. Design methods are given for carbon steel, aluminium and stainless steel and comparison against the FEM and EN results is made. The proposed methods are calibrated so that they give safe results compared to the considered FEM results.

TIIVISTELMÄ

Ohuen metallilevyn leikkauskestävyys koostuu kolmesta osasta: leikkauslommahdus, vetokenttä ja ympäröivien rakenteiden osuus. Tässä tutkimuksessa käsitellään kahta ensimmäistä. Mikäli uuman lämpötila on tasainen, kirjallisuudesta löytyy kokeiden tuloksia ja teorioita leikkauskestävyyden laskemiseen. Epätasaisen lämpötilan vaikutusta ei sen sijaan ole tutkittu aiemmin. Kuumia epätasaisia lämpötiloja leikkausrasitetuissa levyissä voi esiintyä esimerkiksi metallikennojen ja hattupalkkien uumissa tulipalotilanteessa.

Tässä tutkimuksessa esitetään numeerisen laskennan tulokset ohuille hiiliteräksestä, alumiinista ja ruostumattomasta teräksestä valmistetuille levyille erilaisissa epätasaisissa lämpötilajakautumissa. Lämpötilajakaumat on valittu kirjallisuudesta löytyvien polttokokeiden (matalalattiapalkille ja metallikennolle) ja suoritettujen numeeristen laskelmien perusteella mahdollisimman realistisiksi. Laskentamallissa otetaan huomioon sekä geometrinen että materiaalimallien epälineaarisuudet. Korkeiden lämpötilojen materiaalimallit ovat uusimpien EN standardien mukaiset. Levyjen alkuhäiriöt on muodostettu yhdistelemällä alimpia ominaismuotoja.

Numeerisen laskentamallin käyttökelpoisuus todetaan laskemalla leikkauskestävyyksiä kuumissa, tasaisissa lämpötiloissa. Saatuja tuloksia verrataan kirjallisuudesta löytyviin koetuloksiin.

Tutkimuksessa esitellään kaksi menetelmää ohuen metallilevyn leikkauskestävyyden laskemiseksi kuumassa epätasaisessa lämpötilassa. Menetelmät esitetään hiiliteräksestä, alumiinista ja ruostumattomasta teräksestä tehdyille levyille ja menetelmien antamia tuloksia verrataan numeerisella laskennalla ja EN standardeilla saatuihin arvoihin. Laskentamenetelmät ovat kalibroitu siten, että ne antavat varmalla puolella olevia tuloksia numeeriseen laskentaan verrattuna.

PREFACE

This study was carried out in the Research Centre of Metal Structures at Tampere University of Technology between June 2009 and November 2011. The study was financially supported by the Research Centre of Metal Structures and Rautaruukki Oyj. The financiers are gratefully acknowledged. Emil Aaltonen Foundation is thanked for funding the participation for a short-course in Berlin.

First and foremost, I would like to thank my supervisor Professor Markku Heinisuo for his competent guidance and support. I also wish to express my thanks to all the staff members of the Research Centre of Metal Structures. It has been a pleasure to work in such an active, inspiring and supporting atmosphere.

The reviewers of the thesis, Professor František Wald from Czech Technical University in Prague and Professor Pentti Mäkeläinen from Aalto-yliopisto are kindly acknowledged for their comments and valuable suggestions to improve the manuscript. I am grateful for Professor František Wald and Professor Mikko Malaska from University of Oulu for agreeing to act as opponents during the defense of the thesis.

CSC – IT Center for Science Ltd is thanked for providing the software used in this study. Especially the assistance of Mr. Reijo Lindgren in constructing the numerical models is gratefully acknowledged. The English language has been revised by Mr. Jorma Tiainen to whom I express my thanks for his contribution to my work.

I wish to thank my mother Marja, father Rauno and little sister Anumaria for their strong support throughout my life.

Finally, I would like to thank my dear wife Eeva and son Eemil for their love, understanding and faith in me.

Tampere, December 2011

Mikko Salminen

CONTENTS

NOTATIONS

Roman characters

a	distance between stiffeners of the web plate
a_g	length of the gusset plate
b_f	width of flange
c	width or depth of a cross-section
d	factor related to method of reference temperature
E	elastic modulus
f_a	ultimate strength for aluminium
f_o	strength for overall yielding for aluminium
f_{of}	strength for overall yielding for aluminium flanges
f_u	ultimate strength
f_y	yield strength
f_{yf}	yield strength of flange material
h	height of the plate
h_g	height of the gusset plate
h_w	height of the web
k, k_θ	reduction factor
k_E, $k_{E,\theta}$	reduction factor of elastic modulus
$k_{p0.2,\theta,web}$	reduction factor for design yield strength at average temperature of plate
k_τ	shear buckling coefficient
$k_{y,\theta,web}$	reduction factor for yield strength at average temperature of plate
L	length
M, M_b	bending moment
M_{Ed}	design bending moment
R	resistance
t	thickness
t_f	thickness of flange
t_{lf}	thickness of lower flange
u_x, u_y, u_z	displacements
V	shear force
$V_{b,Rd}$, V_{Rd}	shear force resistance at ambient temperature
$V_{bf,Rd}$, $V_{f,Rd}$	contribution of flanges to shear resistance
$V_{bw,Rd}$, $V_{w,Rd}$	contribution of web to shear resistance
V_{cr}	shear buckling load
$V_{fi,t,Rd}$	shear resistance at elevated temperatures
V_{pb}	post-buckling resistance

V_{ult}	ultimate shear resistance
x, y, z	co-ordinates

Greek characters

α	thermal expansion coefficient
χ_w	shear buckling factor for carbon and stainless steel
ε	coefficient dependent on f_y
γ_{M0}	partial factor for resistance of cross-sections
γ_{M1}	partial factor related to instability of member
$\gamma_{M,fi}$	partial factor for relevant material property, for fire situation
η	factor for shear area
λ, λ_w	slenderness parameter
ν	Poisson's ratio
θ	temperature
θ_a	material temperature
θ_{cold}	coldest plate temperature
θ_{hot}	hottest plate temperature
θ_{mid}	temperature in the middle of the height of plate
θ_{web}	average plate temperature
ρ_v	shear buckling factor for aluminium
σ	normal stress
σ_1, σ_2	principal stresses
τ	shear stress
τ_{cr}	critical shear stress
$\tau_{cr,g}$	critical shear stress for the gusset plate
τ_u, $\tau_{u,D}$, $\tau_{u,D,d}$	ultimate shear stress
τ_y	shear yield stress

1 INTRODUCTION

1.1 Background and history

Fire resistance of structures has drawn much more attention since the collapse of the World Trade Center towers [Duthinh et al, 2008], [Quintiere et al, 2002], [Dai et al, 2010]. The safety of the people and property inside buildings in a fire situation is a major concern. People inside or in the neighbourhood should be able to escape safely before a structure or a part thereof fails at elevated temperatures. The structures of ships, trains and other vehicles need to be designed fire resistant, too. Elevated temperatures occur also in hot gas ducts and similar industrial structures.

Many structures of buildings, vehicles and industrial products are composed of thin plates. Webs of slim floor beams in buildings and the all-metal sandwich panels mainly used in ships in fire are examples of possible applications of this study, also illustrated in Figure 1.1.

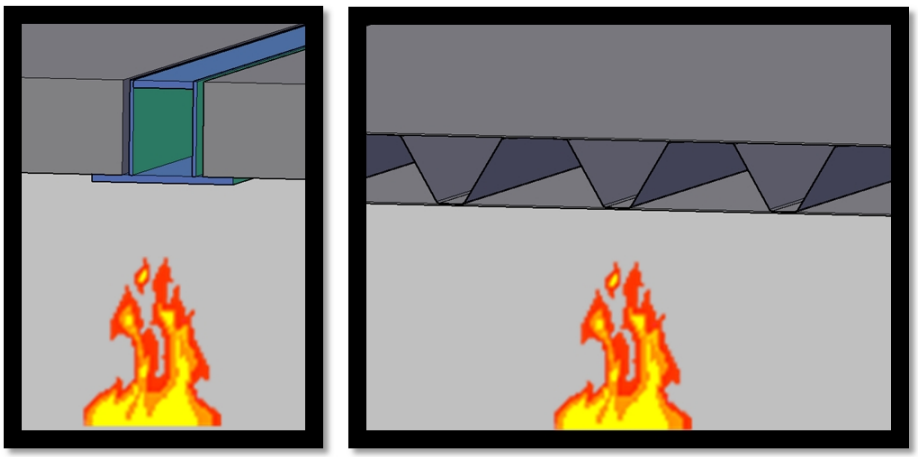

Figure 1.1. Metal plates (webs) under shear loading at non-uniform elevated temperatures.

The main focus of this study is on plates made of metal (carbon steel, aluminium and stainless steel). The shear resistance of thin metal plate at non-uniform elevated temperatures is an important, unsolved factor as regards the many applications mentioned above.

A thin metal plate is capable of carrying considerable additional shear load in excess of its elastic shear buckling load. After buckling occurs, a new load carrying mechanism

develops, whereby any additional shear loading is supported by an inclined tensile stress field. Material yielding and geometrical buckling are two independent phenomena, but they may well interact with each other and produce complex behaviours [Gheitasi, Alinia, 2010]. As the applied loading increases, the tensile membrane stress grows until the yield stress of the material is reached. When the web has yielded, final collapse will occur when plastic hinges form in the supporting structures [Real et al, 2007].

Wilson was the first to discover post-buckling behaviour as early as 1886 [Wilson, 1886]. The first calculation model was developed by Rode in 1916, when he adopted a tension field width of 50 times the thickness of the plate [Rode, 1916] (left-hand side of Fig. 1.2). His theory was never used in design, because it had not been verified by tests. In the 1930's Wagner presented a pure tension field theory for aircraft structures [Wagner, 1931] (right-hand side of Fig. 1.2). That theory is suitable only for extremely thin aircraft structures attached to very rigid boundary elements. Even though the existence of post-buckling shear capacity was discovered, it was not considered directly in the design of plate girders in civil engineering. Post-buckling strength was accounted for only indirectly in design by lowering safety factors [Alinia et al, 2009(c)]. Elastic buckling remained the basis for plate girder design until the 1960's.

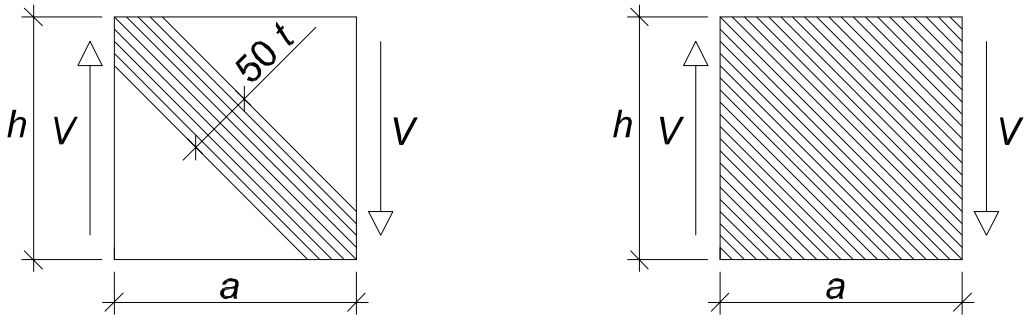

Figure 1.2. Tension field theories by Rode [Rode, 1916] (left) and Wagner [Wagner, 1931] (right).

In 1959, Basler and Thurlimann performed an extensive study on the post-buckling behavior of plate girder web panels under shear loading [Basler, Thurlimann, 1959]. The American Institute of Steel Construction (AISC) was the first to include post-buckling shear strength in its specifications [AISC, 1963] as a result of the above study and another two by Basler [Basler, 1961(a)], [Basler, 1961(b)]. According to Basler's theory, the tension field is anchored only to the vertical stiffeners because of the lack of rigidity of the flanges (left-hand side of Fig. 1.3).

Basler and Thurlimann's theory was followed by modified failure theories intended to achieve better correlation between theory and tests. Rockey and his co-workers proposed a theory, which assumed that flanges could develop plastic hinges after tension field action [Rockey et al, 1978] (right-hand side of Fig. 1.3). This theory was

eventually included in the British Standard [BS 5950, 1990]. According to Lee et al, the majority of all steel bridges in the world have been designed and built based on theories by Basler and Rockey or their derivatives [Lee et al, 2008].

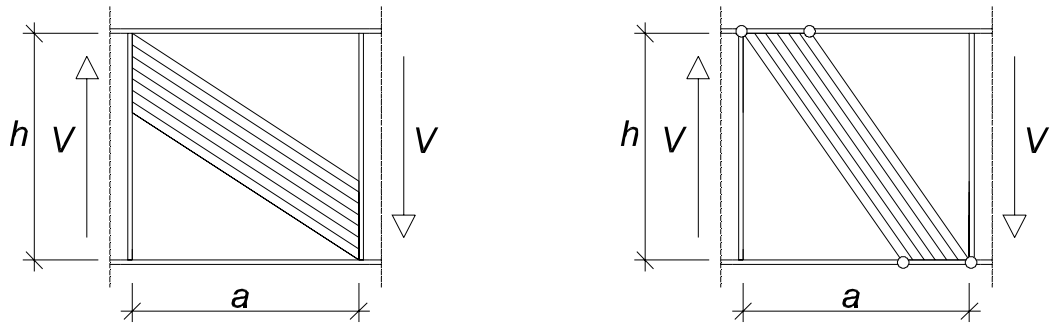

Figure 1.3. Tension field theories by Basler [Basler, 1961] (left) and Rockey et al. [Rockey et al, 1978] (right).

In Eurocodes [EN 1993-1-5, 2005], the shear resistance of slender plates is based on the rotated stress field theory as proposed by Höglund [Höglund, 1972] (left-hand side of Fig. 1.4). The tension field theory by Dubas and Gehri also agrees well with the test results [Dubas, Gehri, 1986] (right-hand side of Fig. 1.4). These theories are described in more detail later in this thesis.

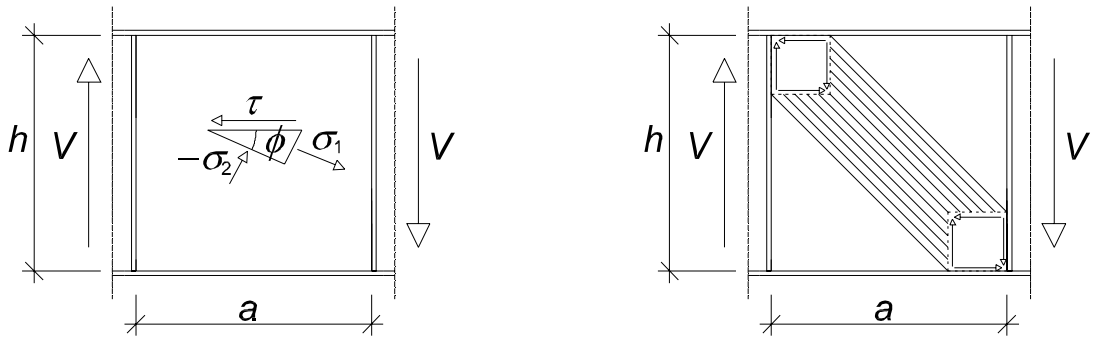

Figure 1.4. Tension field theories by Höglund [Höglund, 1972] (left) and Dubas & Gehri [Dubas, Gehri, 1986] (right).

In addition to the tension field theories illustrated in Figures 1.2–1.4, a large number of different theories concerning ultimate shear resistance of web panels have been presented. For example, the tension field theories of Fujii [Fujii, 1968], [Fujii, 1971] Komatsu [Komatsu, 1971] and Chern and Ostapenko [Chern, Ostapenko, 1969] assume that the tension field develops all over the plate, but the intensity of the tension varies in the perpendicular direction. According to Yoo and Lee, this might be the largest number of failure theories devoted to a single topic in structural mechanics. The ultimate strength state is so complex that any attempt to address it using classical closed form

solutions appears to be a futile exercise [Yoo, Lee, 2006]. Behind the classical theories mentioned above, is the fundamental assumption that compressive stresses do not increase after shear buckling has occurred. That assumption yields to theory that the tension field must be anchored by flanges and stiffeners. However, recent numerical analyses [Yoo, Lee, 2006], [Alinia et al, 2011] have revealed that tension field action is possible also for unanchored plates. The analysis by Yoo and Lee showed that all forces developed during post-buckling are self-equilibriated within the plate and that diagonal compression increases near the edges of the plate after shear buckling, which is contrary to the fundamental assumption of classical failure theories [Yoo, Lee, 2006]. Thus, it can be concluded that there is no single theory that explains the behaviour of thin plate under shear loading even at ambient temperature. Obviously, the phenomenon becomes even more complex at elevated temperatures, especially when temperature distribution across the plate is non-uniform.

In addition to the research performed by Yoo and Lee [Yoo, Lee, 2006], numerous other numerical analyses concerning the post-buckling behaviour of steel plates at ambient temperature have been conducted. Alinia et al. [Alinia et al, 2009(b)] described the different stages of the post-buckling behaviour of thin shear panels using the finite element method (FEM). Their research showed that after buckling, differences between in-plane stresses on the two sides of plates started to develop and widen with the applied loading. It was also shown that material yielding starts earlier on one face, but at the ultimate load stage both faces have full yield bands. Moreover, Alinia et al concluded that support conditions do not have a significant effect on the through-thickness bending stresses and tension fields of plates [Alinia et al, 2009(b)]. In another research by Alinia et al. [Alinia et al, 2009(c)], they analysed numerically a number of full-scale plate girders with a thin web and determined their shear failure characteristics. Moreover, they compared the results from FEM to different theories. They concluded that Eurocodes [EN 1993-1-1, 2005], [EN 1993-1-5, 2005] gave the most conservative results while e.g. Rockey's [Rockey et al, 1978] and Basler's [Basler, 1961] tension field models always overestimated the girders' ultimate shear resistance. Moreover, Höglund's [Höglund, 1972] theory for thicker flanges was always on the safe side and reasonably close to FEM results [Alinia et al, 2009(c)].

During the past decade, experimental and analytical research on the shear resistance of web plates at elevated temperatures has been conducted. Test results and FEM calculations on 18 steel-plate girders loaded primarily in shear at elevated temperatures are presented in the reference [Vimonsatit, Tan, Qian, 2007]. Vimonsatit et al concluded that the shear strength of a plate girder section reduces significantly with increasing temperature and that the more slender sections have lower shear capacity at a certain temperature [Vimonsatit, Tan, Qian, 2007]. These test series will be considered in more detail later in this thesis. Moreover, the most slender web will be used as the benchmark case for the numerical analyses of this study.

An article by Tan and Qian deals with experimental and numerical investigation of a thermally restrained plate girder loaded in shear at elevated temperatures [Tan, Qian, 2007]. Tan and Qian observed that ultimate shear resistance decreased significantly under a thermal restraint effect involving an axial force [Tan, Qian, 2007].

A theoretical model for predicting the failure load of a plate girder subjected to a specified uniform elevated temperature is presented in [Vimonsatit, Tan, Ting, 2007]. That model is based on Rockey's investigations [Rockey et al, 1978] on shear resistance at ambient temperature, which has been extended to uniform elevated temperatures by reducing material properties. The predicted shear strengths from that research agreed well with the predictions from numerical analysis [Vimonsatit, Tan, Ting, 2007].

In another article Qian and Tan analysed the plate girder out-of-plane and in-plane deformations at elevated temperatures in order to obtain pre- and post-buckling stiffnesses [Qian, Tan, 2009]. Qian and Tan proposed analytical equations for out-of-plane and in-plane deflections which were verified by experimental measurements and FEM analysis [Qian, Tan, 2009].

All experimental and analytical investigations on shear resistance at elevated temperatures consider the case where temperature distribution across the plate is uniform. However, in many applications (e.g. hat beam webs and all-metal sandwich panel webs in fire, hot gas ducts) the temperature distribution is non-uniform. Temperatures at opposite edges of a plate may vary significantly when the plate is part of a larger structure. This has been shown for example in fire tests for hat beams [Teräsnormikortti 21/2009, 2009] and all-metal sandwich panels [Heinisuo, Ylihärsilä, 2006] as well as in numerical analyses of all-metal sandwich panels [Salminen, 2010], [Ala-Outinen et al, 2006]. For example, in the fire tests on hat beams, the difference between the hottest and the coldest temperature of the web was in some cases approximately 300 ^{o}C and exceeded 800 ^{o}C in the numerical analysis of an insulated all-metal sandwich panel [Ala-Outinen et al, 2006]. Thus, the material properties may vary significantly across the height of the plate.

In some studies on the resistance of metal structures at elevated temperatures, non-uniform temperature distributions have also been considered. The article by Feng et al presents the results of a numerical investigation of cold-formed thin-walled steel channels at non-uniform elevated temperatures [Feng et al, 2003]. The non-uniform temperature distributions across the cross-section were derived from thermal analysis of thin-walled panels, which are commonly used in wall construction as load-bearing studs with interior insulation and planar gypsum board sheeting on both sides. Feng et al reported that the non-uniform temperature distributions in the cross-section of the column may be simplified by assuming uniform temperatures in the flanges and a linear

temperature distribution in the web in order to develop a hand-calculation method to evaluate the column strength [Feng et al, 2003].

The article by Yin and Wang presents the results of numerical analyses conducted for lateral torsional buckling of steel I-beams at non-uniform elevated temperatures in the cross-section [Yin, Wang, 2003]. According to their article, the lateral torsional buckling behaviour of the beam is controlled by the average elastic modulus of the cross-section at low load ratios, and the temperature of the less heated flange dominates beam behaviour at high load ratios. According to Yin and Wang, British standards [BS 5950, 1990] and Eurocodes [EN 1993-1-2, 2005] predict much lower beam failure temperatures (often much more than 100 ^{o}C) than numerical analyses in the case of non-uniform temperature distribution [Yin, Wang, 2003].

The articles by Tan and Yuan consider buckling of steel columns under longitudinal non-uniform temperature distribution [Tan, Yuan, 2008], [Tan, Yuan, 2009]. The motivation for these studies came from zone modeling of a compartment fire where the gas layers were artificially divided into two zones: the hotter upper zone and the cooler lower zone. Across the cross-section temperature was assumed to be uniform. The results of these analytical studies show that the buckling load or failure duration is significantly underestimated when using uniform temperature distribution conservatively based on the top column (hottest) temperature [Tan ,Yuan, 2008].

Kaitila carried out an FEM analysis on cold-formed thin-walled channel sections subjected to compressive axial force under a temperature gradient in the cross-section [Kaitila, 2002]. He found that the stiffness of the member is affected by the temperature gradient difference between the flanges. He concluded that the design method based on average temperature gave results that were on the safe side compared to FEM analysis in the cases of flexural and torsional-flexural buckling. The maximum temperature in Kaitila's analysis was 750 ^{o}C and the maximum temperature difference in the cross-section 300 ^{o}C.

Although shear capacity has been widely investigated for carbon steel plates, only limited studies have been carried out for stainless steel plates. Stainless steel design rules have been based on those developed for carbon steel even though these materials exhibit completely different mechanical behaviour [Estrada et al, 2007]. Recent studies concerning stainless steel shear buckling at ambient temperature have been carried out for example by Real, Estrada and Olsson [Real et al, 2007], [Real, 2001], [Estrada, 2005], [Olsson, 2001]. The calculation models for aluminium structures at elevated temperatures are also partially based on research of steel structures due to the lack of researches on aluminium structures at elevated temperatures [Maljaars, 2008].

1.2 Scope of the work

The shear resistance of a thin plate consists of three phases both at ambient and elevated temperatures as the load increases [Vimonsatit, Tan, Ting, 2007]: the buckling phase, the post-buckling phase and yielding of supporting structures (Fig. 1.5). The first two are considered in this study. The buckling phase alone was studied numerically in an earlier research [Salminen, 2010] which showed that when the reduction factor based on the average temperature of the plate at non-uniform temperatures is used, the results are almost always clearly on the unsafe side compared to FEM analysis.

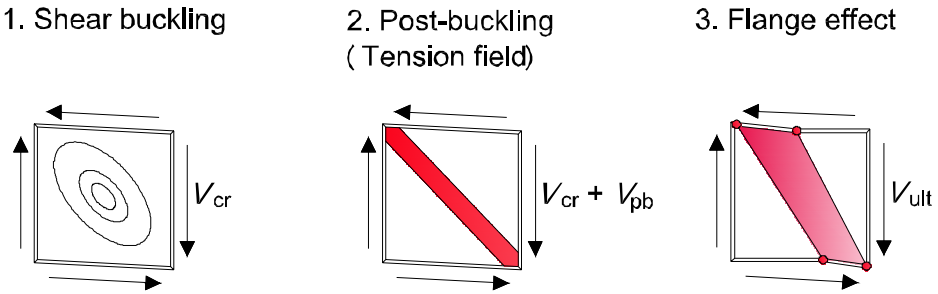

Figure 1.5. Three stages of plate before collapse as the load increases.

This study examines rectangular, isolated metal plates of different properties under shear loading. It covers the range of Eurocodes for carbon steel, stainless steel and aluminium plates [EN 1993-1-1, 2005], [EN 1993-1-2, 2005], [EN 1993-1-4, 2006], [EN 1999-1-1, 2007], [EN 1999-1-2, 2007]. All considered plates were selected so thin that elastic shear buckling precedes yielding at ambient temperature meaning that the post-buckling phase occurs. The effects of the boundary conditions (simply supported/clamped), slenderness, aspect ratio and yield strength of the plate to shear resistance are studied at different kinds (linear and non-linear) of temperature distributions.

In reality, there are no isolated plates under pure shear loading in structures, and it is recognised that a simply supported or clamped plate in shear cannot exactly represent the behaviour of a plate girder web. According to Alinia et al [Alinia et al, 2009(c)], the following differences occur in the behaviour of a plate in pure shear and a plate girder web:

- In a web plate, bending moment due to lateral loading is always present,
- The actual behaviour of a flange-web joint is something between simply supported and clamped,
- The flanges of a beam are allowed to move towards or away from each other which makes their weak axis second moment an important factor. In a plate

model, it is assumed that the plate edges' in-plane movement is either free or restrained, and

- The effects from end-posts and sub-plates due to intermediate stiffeners are ignored in the plate model.

The effects of stiffeners or surrounding members (flanges) are not considered in this study. All cases involve only the shear in the plane of the plate. Nor are interactions with other stress components considered even though there are cases where significant compressive and tensile forces can occur in heated beams due to thermal expansion and catenary action, respectively [Liu et al, 2002], [Allam et al, 2002], [Wald et al, 2009], [Ma, Mäkeläinen, 2006], [Yin, Wang, 2005(a)] and [Yin, Wang, 2005(b)]. Moreover, it has been shown that many kinds of behaviour occur due to the interaction of members. Often the behaviour of real structures is better than predicted from standards for isolated members. However, the current design codes for fire resistance of structures are based on isolated members and, for example, in the Cardington fire test Eurocodes [EN 1991-1-2, 2002], [EN 1993-1-2, 2005] gave good and conservative predictions of structural behaviour [Wald et al, 2006]. Thus, it can be concluded that resistance to pure shear is an important factor when considering the resistance of metal structures at ambient as well as elevated temperatures. The surrounding structures are left for future studies. However, the relation between the isolated plates analysed in this study and real structures needs to be shown by comparison to applicable test results available in literature.

Figure 1.6 presents the cases of this study in principle. For carbon steel, yield strengths from 235 to 460 N/mm^2 are considered. In the case of aluminium and stainless steel, the range of alloys and grades is rather wide. In this study, aluminium alloy 5083-H111 and 5083-O and stainless steel grade 1.4301 are considered. According to Maljaars and Estrada et al, they are commonly used in structural applications [Maljaars, 2008], [Estrada et al, 2007]. The material models for carbon and stainless steel at elevated temperatures are taken from EN 1993-1-2 [EN 1993-1-2, 2005] and for aluminium based on the test results presented in dissertation of Maljaars [Maljaars, 2008]. It should be noted that this study uses basic values of Eurocodes for the material properties even though it is possible to use also nationally determined parameters.

The height of the plate is in every case 305 mm (same as in the benchmark case). Other dimensions of the plate (distance between stiffeners a and thickness t) vary in the analysis. It should be noted that the displacements in the plane of the plate are constrained only at one point whereby no horizontal forces can develop at the vertical edges of the plate like many tension field theories, such as the rotated stress field theory [Höglund, 1972], predict. The boundary conditions shown in Figure 1.6 are applied because it makes possible to observe the plate under pure shear loading. Shear loading is applied as a uniform stress along the edges of the plate. In reality, the distribution is

not uniform and depends on the cross-section. However, in the case of a thin web, shear load can be assumed to be distributed uniformly across the beam web without leading to a significant error. The use of uniform shear stresses is justified in more detail in Chapter 2.

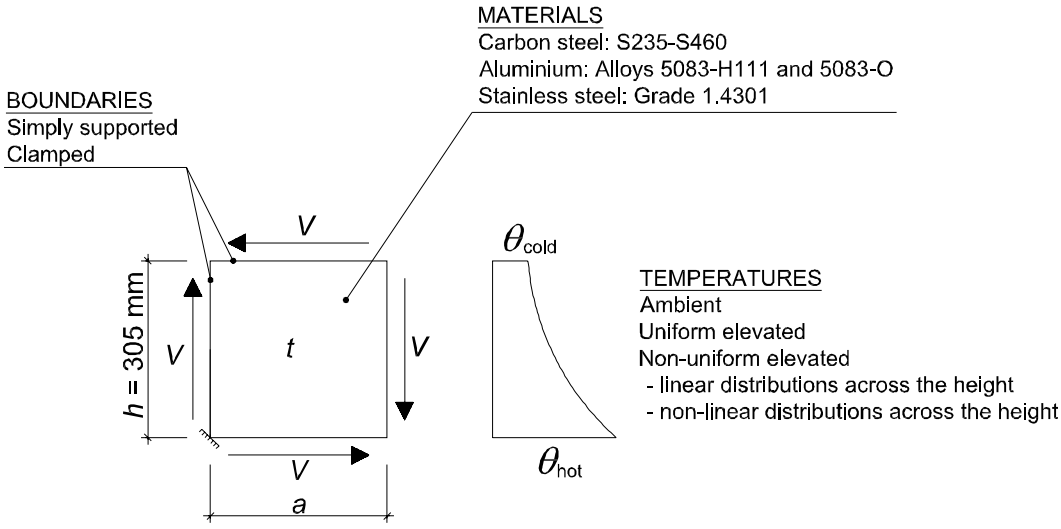

Figure 1.6. Studied cases.

1.3 Method of study

This study concentrates merely on numerical analysis – no mechanical loading tests are conducted. The shear resistances of metal plates of different properties are calculated at numerous non-uniform elevated temperatures using commercial ABAQUS FEM software [ABAQUS, 2010], which has been widely used in other recent analyses of shear buckling and resistance of thin plates at ambient temperature, such as [Alinia et al, 2009(c)], [Habasbi, Alinia, 2009], [Estrada et al, 2008], [Real et al, 2006]. The verification of FEM models is done by comparing their results to the test results at ambient and uniform elevated temperatures presented in reference [Vimonsatit, Tan, Qian, 2007]. Moreover, a comparison to resistances according to Eurocodes [EN 1993-1-1, 2005], [EN 1993-1-2, 2005], [EN 1993-1-4, 2006], [EN 1999-1-1, 2007], [EN 1999-1-2, 2007] at ambient and elevated temperatures is also done. Then, FEM models are applied at non-uniform elevated temperatures. The non-uniform temperature distributions are motivated by fire tests on hat beams [Teräsnormikortti 21/2009, 2009], an all-metal sandwich panel [Heinisuo, Ylihärsilä, 2006] and FEM analysis of an all-metal sandwich panel [Salminen, 2010], [Ala-Outinen et al, 2006]. In the FEM analysis, the temperatures of the plate are set first and then mechanical loading is applied until maximum resistance is reached (steady-state method), which makes the observation of the different stages presented in Figure 1.5 possible. Unfortunately, no test results on shear resistance at non-uniform temperatures are available.

1.4 Goal and outline of the study

The main interest of this study is to determine how the ultimate shear resistance of an isolated, thin plate decreases at non-uniform elevated temperatures compared to ambient temperature resistance. It is believed that Eurocodes [EN 1993-1-1, 2005], [EN 1993-1-4, 2006], [EN 1999-1-1, 2007] predict the shear resistance of metal plates at ambient temperature reliably. Thus, the goal of this study is to develop an analytical design method to reduce the ambient temperature shear resistance of a thin metal plate in cases where temperature varies across the height (constant temperature in the longitudinal direction) of the plate. The design method is based on the equations and reduction factors given in Eurocodes [EN 1993-1-2, 2005] and [EN 1999-1-2, 2007].

This thesis divides into six chapters. In all chapters, the main focus is on carbon steel which is considered first. Then, the differences compared to aluminium and stainless steel are pointed out, where necessary. The first chapter presents the background and motivation for the study as well as its methods and goal. The theoretical background for calculating shear resistance at ambient and elevated temperatures is presented in Chapters 2 and 3, respectively. Different theories and test results are also compared.

The fourth chapter presents the procedure and results of the numerical calculations used to verify the proposed design methods. Firstly, the FEM model is validated by comparing the results at ambient and uniform elevated temperature to the results of the reference [Vimonsatit, Tan, Qian, 2007]. Then, numerous analyses of different cases at non-uniform elevated temperatures are conducted. The fifth chapter presents the proposed design methods for the cases where temperature varies across the height of the plate. Use of the methods is also demonstrated by worked examples. Moreover, a comparison of the results from FEM, the Eurocodes and the proposed methods is made. Finally, Chapter 6 summarises the results of the study and makes suggestions for further research.

2 SHEAR RESISTANCE OF THIN METAL PLATE AT AMBIENT TEMPERATURE

The behaviour of a thin plate can be divided into three stages: shear buckling V_{cr}, post-buckling (tension field) resistance V_{pb} and the effect of the flanges. The first two (Fig. 2.1) are considered in this study. The contribution of the flanges according to Eurocodes [EN 1993-1-5, 2005], [EN 1999-1-1, 2007], [EN 1993-1-4, 2006] is only dealt with briefly.

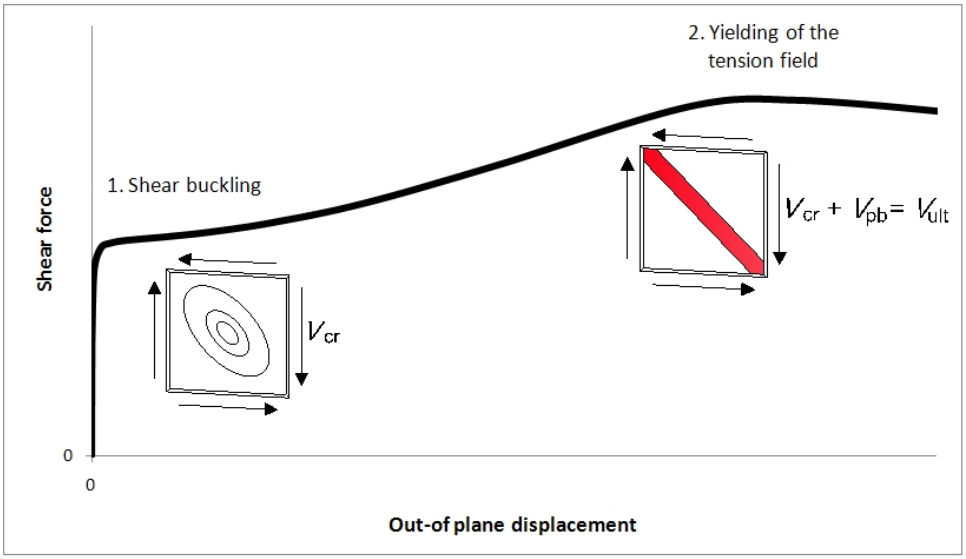

Figure 2.1. Two phases of thin plate loaded with pure shear as the load increases.

It was assumed in all cases of this study, that the shear load is distributed uniformly along the edges of the plate. In reality, the vertical distribution depends on the dimensions of the cross-section and is non-uniform. According to Jourawski's formula, the distribution of shear stresses in the web of the symmetric I-profile shown in Figure 2.2 can be derived from Equation (2.1) [Outinen, Salmi, 2004].

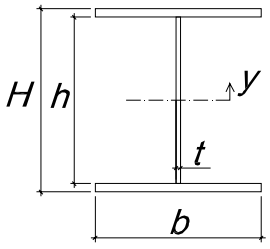

Figure 2.2. Dimensions of the I-profile.

$$\tau(y) = \frac{Vb}{8I_z t}\left[\left(H^2 - h^2\right) + \frac{t}{b}\left(h^2 - 4y^2\right)\right] \tag{2.1}$$

where

$$I_z = \frac{1}{12}bH^3 - \frac{1}{12}(b-t)h^3 \tag{2.2}$$

Vertical distributions of shear stresses are calculated for five example cases. Table 2.1 presents the dimensions and slenderness ratios λ_w (Eq. (2.25)) of the tested beams (TG1−TG5) considered in reference [Vimonsatit, Tan, Qian, 2007]. Beam TG5 is used as a benchmark case in this study.

Table 2.1. Dimensions of the tested beams of reference [Vimonsatit, Tan, Qian, 2007].

Beam	H [mm]	b [mm]	h [mm]	t [mm]	λ_w
TG1	152.6	152.4	139	6.1	0.25
TG2	206	203.9	181	8	0.24
TG3	317	80	305	2	1.51
TG4	317	80	305	2.7	1.01
TG5	317	80	305	1.5	2.17

Figure 2.3 presents the calculated distributions (Eqs. (2.1) and (2.2)) of shear stresses for the beam webs shown in Table 2.1.

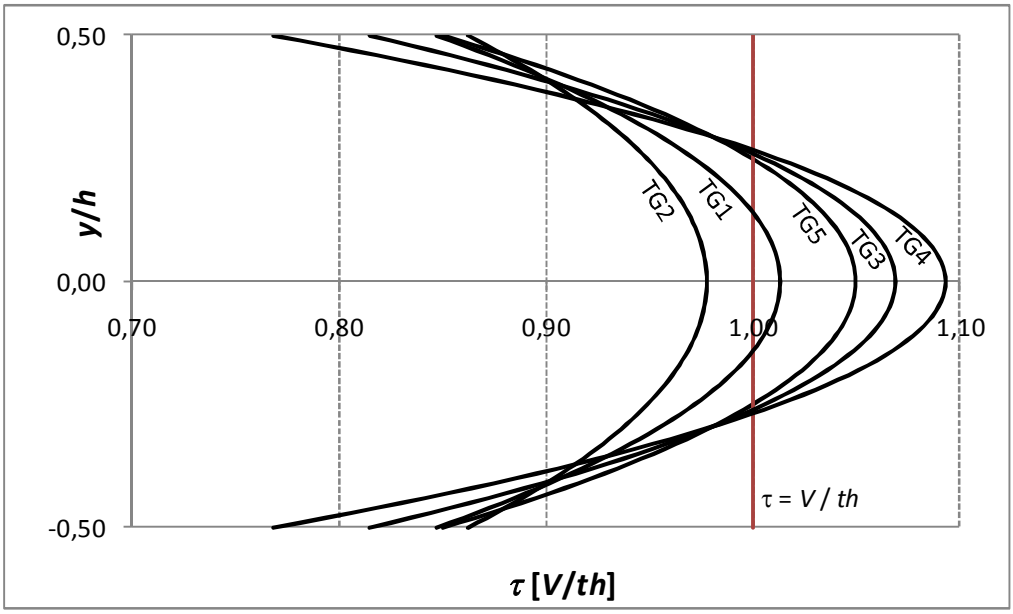

Figure 2.3. Distributions of shear stresses for beam webs TG1−TG5.

Figure 2.3 shows that the distribution of shear stress is not uniform in the considered cases. Table 2.2 lists the minimum, average and maximum values of shear stresses (τ_{min}, τ_{avg} and τ_{max}, respectively) for the considered beam webs.

Table 2.2. Minimum, average and maximum values of shear stresses for the considered beams [V/th].

	TG1	TG2	TG3	TG4	TG5
τ_{min}	0.85	0.86	0.81	0.77	0.85
τ_{avg}	0.96	0.94	0.98	0.98	0.98
τ_{max}	1.01	0.98	1.07	1.09	1.05

Figure 2.3 and Table 2.2 reveal that in all considered cases minimum shear stress was 23 % lower and maximum shear stress 9 % than uniform distribution. The following analytical formulas were derived from Equation (2.1) for τ_{min} and τ_{max}:

$$\tau_{\min} = \tau(0.5h) = \frac{Vb}{8I_z t}\left(H^2 - h^2\right) \tag{2.3}$$

$$\tau_{\max} = \tau(0) = \frac{Vb}{8I_z t}\left[H^2 - h^2\left(1 - \frac{t}{b}\right)\right] \tag{2.4}$$

According to Equations (2.3) and (2.4), if t decreases, the difference between τ_{min} and τ_{max} also decreases. Thus, it can be concluded that in the case of structures with a thin web compared to overall width, the assumption of uniformly distributed shear stress is justified.

2.1 Shear buckling

The shear load that causes a plate to buckle is given by:

$$V_{cr} = ht\tau_{cr} \tag{2.5}$$

where
- h is the height of the plate,
- t is the thickness of the plate,
- τ_{cr} is the critical shear stress.

The critical shear stress τ_{cr} can be calculated from the classical stability theory for plates by Timoshenko [Timoshenko, 1936]:

$$\tau_{cr} = k_\tau \frac{\pi^2 E}{12(1-\nu^2)}\left(\frac{t}{h}\right)^2 \tag{2.6}$$

where
- E is the elastic modulus of the plate material,
- ν is the Poisson's ratio of the plate material, and
- k_τ, the shear buckling coefficient, is obtained for simply supported plates from:

$$k_t = 5.34 + 4\left(\frac{h}{a}\right)^2 \text{ for } a \geq h \tag{2.7}$$

$$k_t = 5.34\left(\frac{h}{a}\right)^2 + 4 \text{ for } a \leq h \tag{2.8}$$

where
- a is the distance between the stiffeners of the plate.

Historically, shear buckling in steel plates has been determined by assuming that web panels are simply supported at the joint between the supporting structures and the web. This assumption has turned out to be conservative since the geometrical properties of the structure modify the boundary conditions and influence the behavior in shear. It has been known for long that the boundary conditions of a web plate are somewhere between simply supported and clamped, but it has not been taken into account, mainly due to the lack of means to evaluate it in a rational manner [Estrada et al, 2008]. In this study, boundary conditions are assumed to be either simply supported or clamped. The shear buckling coefficient for clamped plates can be derived from Equations (2.9) and (2.10) [Timoshenko, 1936]:

$$k_t = 8.98 + 5.6\left(\frac{h}{a}\right)^2 \text{ for a} \geq \text{h} \tag{2.9}$$

$$k_t = 5.6\left(\frac{h}{a}\right)^2 + 8.98 \text{ for a} \leq \text{h} \tag{2.10}$$

The shear buckling coefficient for simply supported and clamped plates as a function of ratio a/h is shown in Figure 2.4 (left). Moreover, the right-hand side of Figure 2.4 illustrates how much higher the shear buckling coefficients of clamped plates $k_{\tau,cl}$ are compared to the corresponding coefficients of simply supported plates $k_{\tau,ss}$.

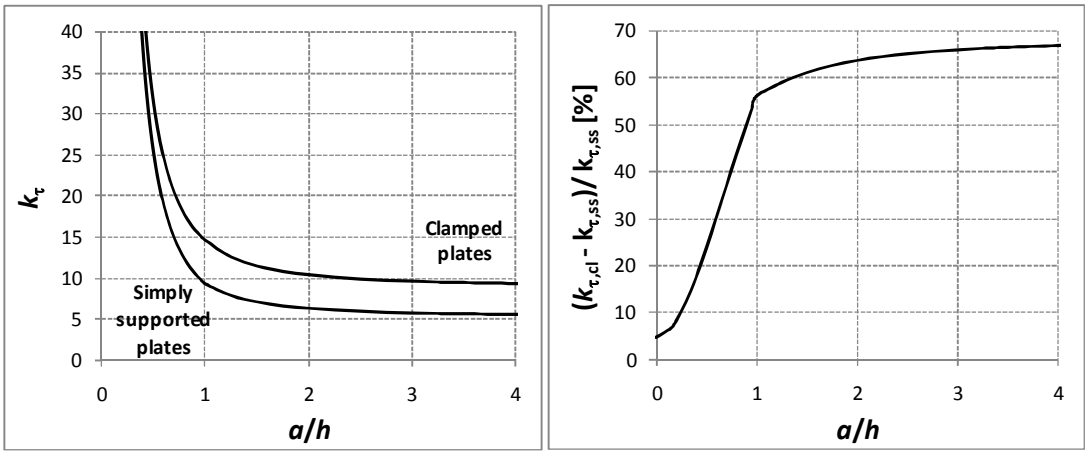

Figure 2.4. Shear buckling coefficients for simply supported and clamped plates (left) and their percentage difference (right).

Figure 2.4 shows that the difference between the shear buckling coefficients for clamped and simply supported plates is significant. When the ratio a/h exceeds 0.9, the shear buckling coefficient for a clamped plate is at least 50 % higher than that for a simply supported plate.

It should be noted that Equation (2.6) is only valid for elastic behaviour. When the proportionality limit is exceeded, most current standards introduce the effect of material non-linearity into the formulation of critical shear buckling stress by including a plasticity reduction factor η [Estrada et al, 2008].

The material coefficients E and ν for carbon steel, aluminium and stainless steel at ambient temperature according to Eurocodes [EN 1993-1-1, 2005], [EN 1999-1-1, 2007] and [EN 1993-1-4, 2006] are shown in Table 2.3. EN 1993-1-4 gives three values for elastic modulus of stainless steel depending on its grade. This study uses stainless steel grade 1.4301 whereby E = 200 000 N/mm^2.

Table 2.3. Material coefficients E and ν at ambient temperature according to Eurocodes.

Material	E [N/mm^2]	ν
Carbon steel	210 000	0.3
Stainless steel	200 000 195 000 220 000	0.3
Aluminium	70 000	0.3

2.2 Tension field resistance

When a thin plate reaches critical shear strength V_{cr}, any increase in shear load is carried by tensile membrane stresses in the tension field. Figure 2.5 illustrates stress development in a plate loaded with pure shear before (top) and after (bottom) buckling. Before critical shear strength is reached, each element maintains the pure shear stress state with equal magnitudes of diagonal tensile and compressive stresses. When critical shear stress is reached, compressive stress can no longer increase (a fundamental assumption in many tension field theories) and equilibrium is violated by stresses on the vertical and horizontal planes as shown in Figure 2.5. This necessitates the development of normal stresses σ_{11} and σ_{22} [Yoo, Lee, 2006].

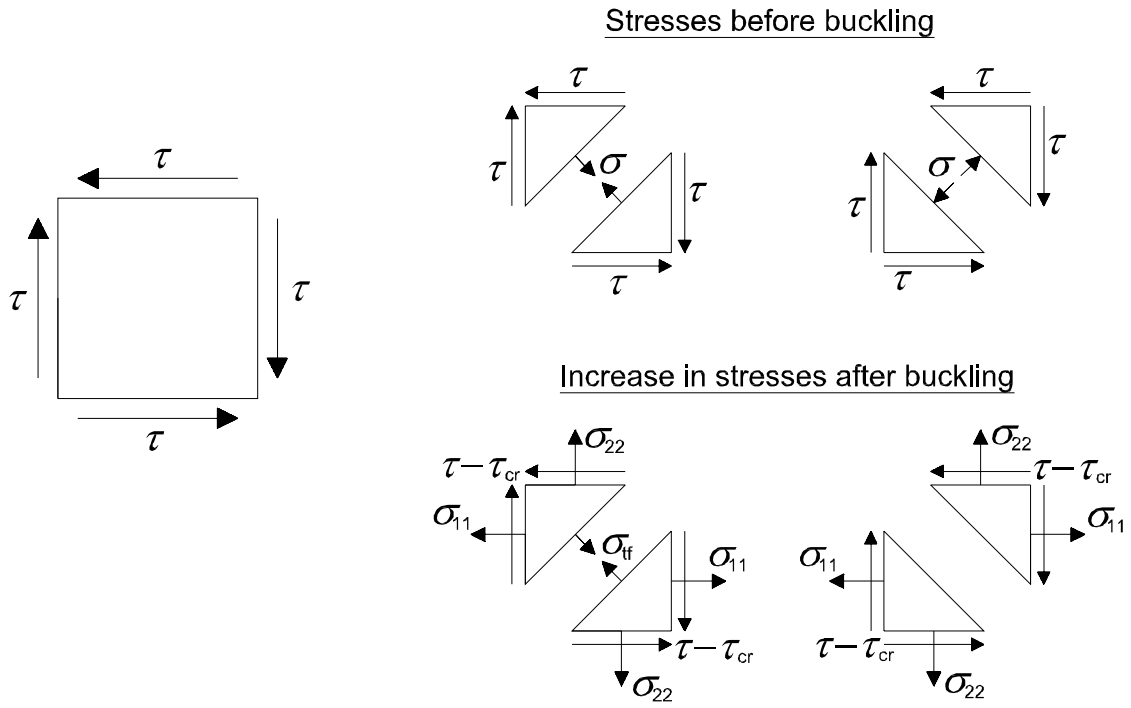

Figure 2.5. Stress developments before and after buckling.

If the fundamental assumption is valid across the plate, then vertical normal stresses σ_{22} must be resisted by the flanges and horizontal normal stresses σ_{11} by adjacent panels [Yoo, Lee, 2006]. According to reference [Dubas, Gehri, 1986], tension field action is possible only if the panel is surrounded by stiffening members. Moreover, according to the tension field theory proposed by Höglund [Höglund, 1972], the resulting tensile forces must be anchored to the end-posts (see Chapter 2.2.2).

This study considers only isolated plates where vertical and horizontal normal stresses σ_{11} and σ_{22} cannot be anchored to flanges or stiffeners. If the fundamental assumption is correct, no tension field (post-buckling behaviour) can occur there. However, according to FEM analyses and the test series conducted by Yoo and Lee, no anchoring system,

such as flanges, is needed for the development of post-buckling strength [Yoo, Lee, 2006]. Yoo and Lee noticed that vertical and horizontal axial stresses reduce to zero at the edges of vertical and horizontal strips. That observation clearly explains why a thin plate without anchors (flanges or stiffeners) is also able to develop its post-buckling strength [Yoo, Lee, 2006].

Numerous tension field theories are found in literature as shown in Chapter 1. Any attempt to describe this phenomenon based on classical closed form solutions appears a futile exercise [Yoo, Lee, 2006]. However, the following two tension field theories are in close agreement with the test results: the tension field theory by Dubas and Gehri [Dubas, Gehri, 1986] and the rotated stress field theory by Höglund [Höglund, 1972].

2.2.1 Tension field theory by Dubas and Gehri

The tension field theory by Dubas and Gehri [Dubas, Gehri, 1986] is illustrated in Figure 2.6.

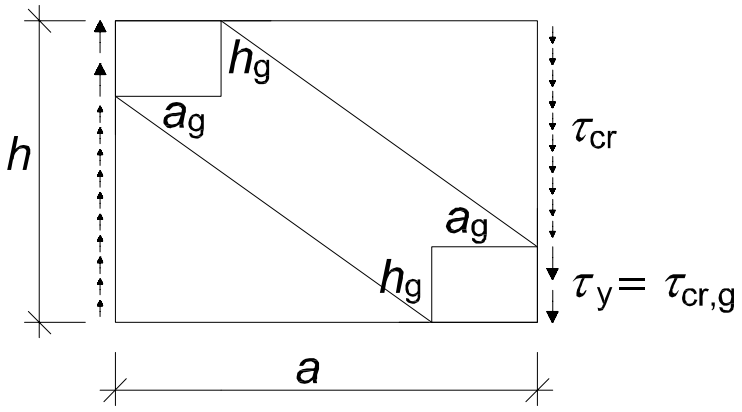

Figure 2.6. Tension field theory by Dubas and Gehri.

This theory supposes that a tension field develops between two gusset plates. The gussets are assumed to act as a simply supported plate under pure shear and to have the same shear buckling coefficient k_τ and aspect ratio as the whole plate meaning that $\frac{a_g}{h_g} = \frac{a}{h}$, notations as in Figure 2.6. The dimension h_g results from the assumption that the critical buckling strength for the gusset plate $\tau_{cr,g}$ equals the shear yield stress of the whole plate τ_y defined in Equation (2.11).

$$\tau_y = \frac{f_y}{\sqrt{3}} \tag{2.11}$$

The critical shear stresses for the gusset plate and the whole plate are thus:

$$\tau_{cr,g} = k_t \frac{\pi^2 E}{12(1-\nu^2)}\left(\frac{t}{h_g}\right)^2 = \tau_y \tag{2.12}$$

$$\tau_{cr} = k_\tau \frac{\pi^2 E}{12(1-\nu^2)}\left(\frac{t}{h}\right)^2 \tag{2.13}$$

By combining Equations (2.12) and (2.13), the size of the gusset plate can be obtained from:

$$k_\tau \frac{\pi^2 E}{12(1-\nu^2)} = \tau_y\left(\frac{h_g}{t}\right)^2 = \tau_{cr}\left(\frac{h}{t}\right)^2 \Rightarrow \tag{2.14}$$

$$h_g = h\sqrt{\frac{\tau_{cr}}{\tau_y}} \tag{2.15}$$

$$a_g = a\sqrt{\frac{\tau_{cr}}{\tau_y}} \tag{2.16}$$

The ultimate shear load $V_{u,D}$ (where D represents Dubas) of the plate is (see Fig. 2.6):

$$V_{u,D} = ht\tau_{cr} + h_g t(\tau_y - \tau_{cr}) = ht\tau_{cr} + h\sqrt{\frac{\tau_{ct}}{\tau_y}}t(\tau_y - \tau_{cr}) \tag{2.17}$$

$$= ht\left[\tau_{cr} + \sqrt{\frac{\tau_{cr}}{\tau_y}}(\tau_y - \tau_{cr})\right]$$

The ultimate stress is:

$$\tau_{u,D} = \frac{V_{u,D}}{ht} = \sqrt{\tau_{cr}\tau_y}\left[1 + \left(\sqrt{\frac{\tau_{cr}}{\tau_y}} - \frac{\tau_{cr}}{\tau_y}\right)\right] \le \tau_y \tag{2.18}$$

The first term corresponds to the ultimate strength from the von Karman assumption and the second one is an enhancement factor with a maximum value of 1.25. In order to achieve a better correlation between test results and theory, Dubas proposed the following design formula where the enhancement factor is ignored and a factor of 0.9 is applied:

$$\tau_{u,D,d} = 0.9\sqrt{\tau_{cr}\tau_y} \le \tau_y \tag{2.19}$$

Equation (2.19) correlates closely with test results and is suitable for design [Dubas, Gehri, 1986].

2.2.2 Rotated stress field theory by Höglund

The rotated stress field theory presented by Höglund [Höglund, 1972] was originally developed for girders with web stiffeners only at the supports − a structure for which other tension field methods give very conservative results [Höglund, 1997]. The method is capable of predicting the resistance of short as well as long panels [Johansson et al, 2001]. First, the method is presented as in the references [Höglund, 1997], [Johansson et al, 2001] and [Maquoi, Skaloud, 2000] (Fig. 2.7 and Eqs. (2.20)−(2.26)) followed by illustrations in Figures 2.8, 2.9 and Equations (2.27)−(2.36).

Figure 2.7 presents the state of stress in a slender girder web after shear buckling and the idea of the rotated stress field theory.

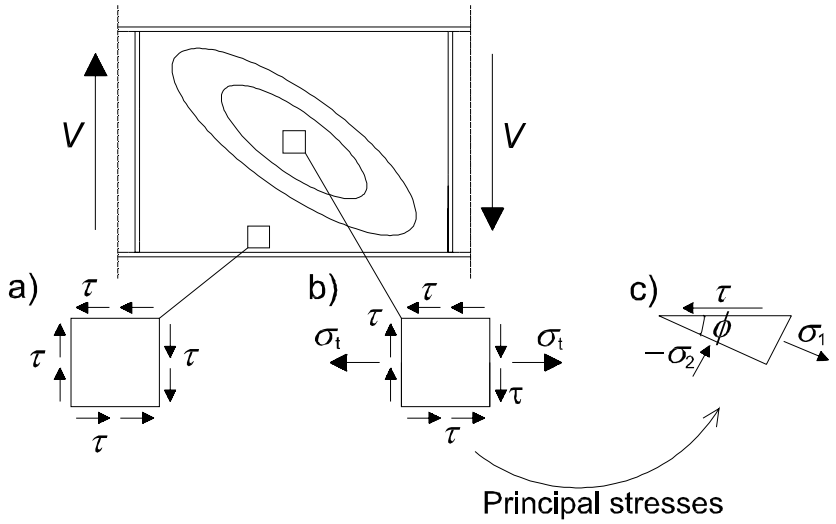

Figure 2.7. Rotated stress field theory by Höglund.

A more or less pure shear state of stress exists close to the flanges (Fig. 2.7 (a)), but in the middle area of the plate there are also membrane stresses σ_t (Fig. 2.7 (b)). Membrane stresses in the transverse direction are zero, because only the web prevents the flanges from moving towards each other. The principal stresses (σ_1 and σ_2) of stress state b are also drawn in Figure 2.7. The conditions for the equilibrium of the principal stresses are (Fig. 2.7 (c)):

$$\sigma_1 = \tau / \tan \varphi \tag{2.20}$$

$$\sigma_2 = -\tau \tan \varphi \tag{2.21}$$

Based on test results, a fundamental assumption is made that the compressive stress remains close to critical shear stress meaning that (see also Eq. (2.6)):

$$\sigma_2 = -\tau_{cr} = -k_\tau \frac{\pi^2 E t^2}{12(1-\nu^2)h^2} \tag{2.22}$$

Ultimate strength of the web plate is assumed to be reached when it yields according to the von Mises yield criterion, defined in this case as:

$$f_y = \sigma_{mises} = \sqrt{\sigma_1^2 + \sigma_2^2 - \sigma_1 \sigma_2} \tag{2.23}$$

Shear resistance τ_u can then be solved from Equations (2.20)–(2.23):

$$\frac{\tau_u}{\tau_y} = \frac{\sqrt[4]{3}}{\lambda_w} \sqrt{\sqrt{1 - \frac{1}{4\lambda_w^4}} - \frac{1}{2\sqrt{3}\lambda_w^2}} \tag{2.24}$$

where

$$\lambda_w = \sqrt{\frac{\tau_y}{\tau_{cr}}} = \sqrt{\frac{f_y}{\sqrt{3}\tau_{cr}}} \tag{2.25}$$

It should be noted that in the references [Johansson et al, 2001] and [Maquoi, Skaloud, 2000] Equation (2.24) is miswritten ($\sqrt[3]{4}$ should be $\sqrt[4]{3}$).

The resultant of the tensile stresses σ_t, shown in Figure 2.7, the force N_t, can be derived from Equation (2.26) assuming the state of stress used in Equations (2.20) and (2.21) is uniform across the depth of the plate.

$$N_t = ht\tau_y \left[\frac{1}{\lambda_w^2} - \left(\lambda_w \frac{\tau_u}{\tau_y} \right)^2 \right] \tag{2.26}$$

The actual force N_t is smaller because the state of stress close to the flanges is close to pure shear. However, the resulting tension in the web plate has to be anchored at the end-posts. The test results for girders with rigid end-posts agree well with the theory, while the resistances of girders with non-rigid end-posts are clearly smaller [Johansson et al, 2001]. The requirements for the stiffness and strength of rigid end-posts are given in EN 1993-1-5 [EN 1993-1-5, 2005].

The EN 1993-1-5 [EN 1993-1-5, 2005] resistances (Table 2.4 and Fig. 2.12) are somewhat reduced compared to the rotated stress field theory to allow for scatter in test

results as a result of initial imperfections and plastic buckling [Höglund, 1997]. Moreover, in EN 1993-1-5, the design resistance of steel plate is given using simpler expressions than in Equation (2.24) by curve fitting.

An alternative way of illustrating the rotated stress field theory is presented in the following. Figure 2.8 and Equations (2.27)−(2.36) present an optimization problem, where shear stress τ is maximized by changing τ and σ_t so that constraints (Eqs. (2.28) and (2.29)) are satisfied.

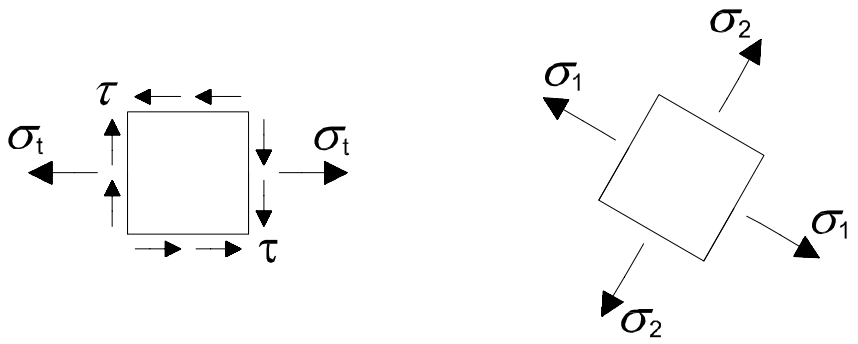

Figure 2.8. Shear and membrane stresses (left) and principal stresses (right).

$$\text{maximize } \tau(\tau, \sigma_t) \tag{2.27}$$

subject to

$$\sqrt{\sigma_1^2 + \sigma_2^2 - \sigma_1\sigma_2} \le f_y \tag{2.28}$$

$$\sigma_2 \ge -\tau_{cr}(\lambda_w) \tag{2.29}$$

It should be noted that positive σ_2 is tension and positive τ_{cr} is compression (Eq. (2.6)) which explains the sign in Equation (2.29). The relation between the principal plane stresses σ_1 and σ_2 and plane stresses τ and σ_t is shown by Equations (2.30) and (2.31) [Outinen, Salmi, 2004].

$$\sigma_1 = \frac{1}{2}\sigma_t + \frac{1}{2}\sqrt{\sigma_t^2 + 4\tau^2} \tag{2.30}$$

$$\sigma_2 = \frac{1}{2}\sigma_t - \frac{1}{2}\sqrt{\sigma_t^2 + 4\tau^2} \tag{2.31}$$

When replacing the principal stresses σ_1 and σ_2 in Equation (2.28) by the values of Equations (2.30) and (2.31), the first constraint (Eq. (2.28), von Mises yield criterion) can be written as:

$$\tau \le \sqrt{\frac{f_y^2 - \sigma_t^2}{3}} \tag{2.32}$$

The second constraint (Eq. (2.29), fundamental assumption) can be formulated as shown in Equation (2.33) by using Equations (2.6) and (2.31).

$$\frac{1}{2}\sigma_t - \frac{1}{2}\sqrt{\sigma_t^2 + 4\tau^2} \geq -\tau_{cr} \tag{2.33}$$

Equation (2.33) can be formulated as:

$$\tau \leq \sqrt{\sigma_t \tau_{cr} + \tau_{cr}^2} \tag{2.34}$$

Critical shear stress τ_{cr} can be written as shown in Equation (2.35) (see Eq. (2.25)).

$$\tau_{cr} = \frac{f_y}{\sqrt{3}\lambda_w^2} \tag{2.35}$$

Equation (2.34) can then be written in the following form:

$$\tau \leq \sqrt{\frac{f_y^2}{3\lambda_w^4} - \frac{f_y \sigma_t}{\sqrt{3}\lambda_w^2}} \tag{2.36}$$

Figure 2.9 presents both constraints (Eqs. (2.28) and (2.29)) drawn for slenderness ratios λ_w = 1.1, 1.2, 1.3, 1.5, 2, 2.5 and 3. It should be noted that the first constraint (Eq. (2.28), von Mises yield criterion) does not depend on the slenderness of the plate. Relative stresses (σ_t/f_y and τ/τ_y) are used in order to plot a graph which applies to all yield stresses f_y.

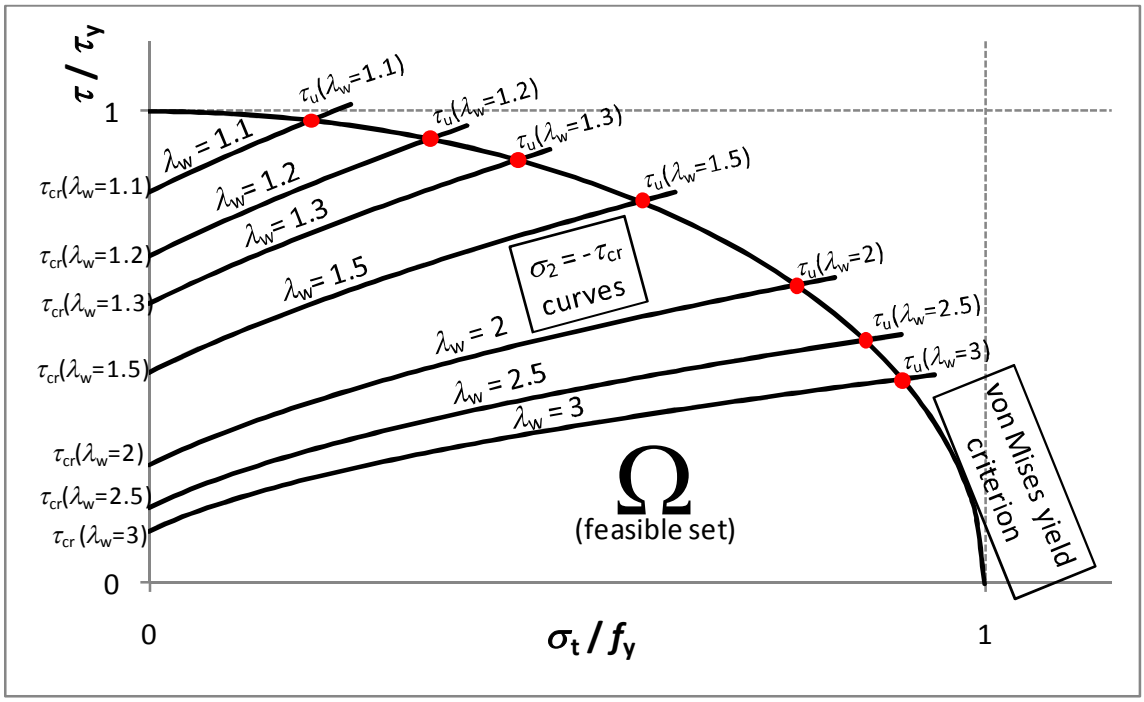

Figure 2.9. Rotated stress field as an optimization problem.

Figure 2.9 shows that the maximum values of shear stress, τ_u at different slenderness can be found from the intersections of the constraints (Eqs. (2.28) and (2.29), red points in Fig. 2.9) in the considered cases. Furthermore, the illustration also shows that according to the rotated stress field theory [Höglund, 1972], the development of post-buckling strength is possible only when a tensile stress component σ_t is introduced. In the case of slender webs, tensile stresses are significant at the maximum values of shear strength τ_u. Figure 2.9 reveals that, for example, a plate with a slenderness ratio $\lambda_w = 3$ reaches its maximum shear strength when tensile stress σ_t is approximately 90 % of yield strength f_y.

It must be reminded that the optimization approach presented above is equivalent to Equations (2.20)−(2.26) and Figure 2.7. In that approach, the value of τ_u is calculated explicitly. The purpose of the optimization approach was to provide an alternative way to illustrate the basic ideas of the rotated stress field theory.

2.3 Shear resistance of web according to the Eurocodes

Here follows a presentation of how the shear resistances of thin metal plates at ambient temperature are calculated according to EN 1993-1-5 [EN 1993-1-5, 2005], EN 1999-1-1 [EN 1999-1-1, 2007] and EN 1993-1-4 [EN 1993-1-4, 2006] for carbon steel, aluminium and stainless steel plates, respectively. Chapters 2.3.1 and 2.3.2 only deal with the shear resistance of plates made of carbon steel. The differences in the cases of aluminium and stainless steel are considered in Chapters 2.3.3 and 2.3.4, respectively. Standard EN 1993-1-1 [EN 1993-1-1, 2005] states that the shear buckling resistance of

webs without intermediate stiffeners should be calculated according to EN 1993-1-5 [EN 1993-1-5, 2005], if

$$\frac{h}{t} > 72\frac{\varepsilon}{\eta} \tag{2.37}$$

where

- $\varepsilon = \sqrt{\frac{235}{f_y}}$, (2.38)
- η = 1.2 when $\theta \leq 400\ ^{o}$C and steel grade is not higher than S460. In all other cases η = 1.0 according to the Finnish National Annex to EN 1993-1-5 [Kansallinen liite standardiin 1993-1-5, 2008].

The maximum shear strength in EN 1993-1-5 [EN 1993-1-5, 2005] is put to $1.2f_y/\sqrt{3} \sim 0.7f_y$ for steel grades S460 and lower because of strain hardening and the contribution from the flanges. With higher grades the strain hardening is less pronounced and no test results are available. Therefore, a more conservative shear strength of $f_y/\sqrt{3} \sim 0.6f_y$ is applied [Johansson et al, 2001]. It should be noted that in EN 1993-1-5 [EN 1993-1-5, 2005] the height of the web h is defined as the clear web depth between flanges.

EN 1993-1-5 [EN 1993-1-5, 2005] gives the slenderness parameter λ_w:

$$\lambda_w = 0.76\sqrt{\frac{f_y}{\tau_{cr}}} \tag{2.39}$$

Since $\sqrt{1/\sqrt{3}} \approx 0.76$, Equation (2.39) has basically the same formula as Equation (2.25).

Theoretically, shear buckling may occur when $\tau_{cr} < \tau_y$ meaning that $\lambda_w > 1$. The corresponding slenderness limit according to EN 1993-1-1 [EN 1993-1-1, 2005] is considered next. Equation (2.39) can be written in the form (see Eq. (2.6)):

$$\lambda_w = 0.76\sqrt{\frac{12 f_y (1-\nu^2) h^2}{k_\tau \pi^2 E t^2}} \tag{2.40}$$

When the EN 1993-1-1 [EN 1993-1-1, 2005] condition for shear buckling (Eqs. (2.37) and (2.38)) is inputted in Equation (2.40), the condition according to EN 1993-1-1 becomes:

$$\lambda_w > 0.76\sqrt{\frac{12 f_y (1-\nu^2)\cdot 72^2 \varepsilon^2}{k_\tau \pi^2 E \eta^2}} = 0.76\sqrt{\frac{14618880\cdot(1-\nu^2)}{k_\tau \pi^2 E \eta^2}} \tag{2.41}$$

When the properties defined for carbon steel in EN 1993-1-1 [EN 1993-1-1, 2005] (E = 210 000 N/mm^2, ν = 0.3) are used, the following curves for cases η = 1.0 and η = 1.2 can be drawn (Fig. 2.10). Plates that are more slender than the drawn curves should be designed for shear buckling.

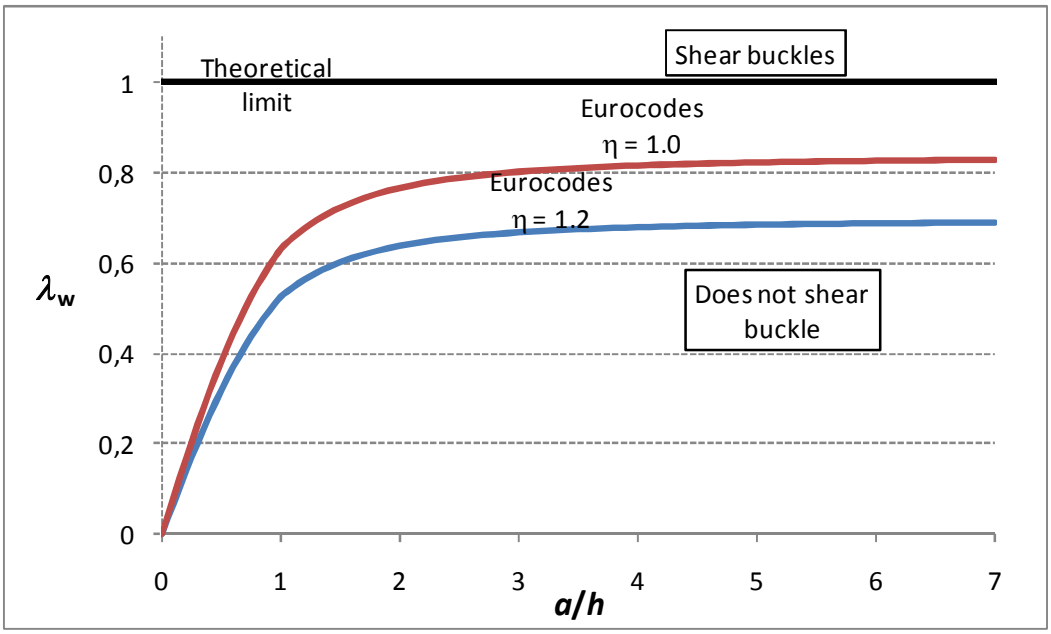

Figure 2.10. Plate slendernesses at which shear buckling should be considered.

In relation to the ratio h/t, theoretical Equation (2.6) can be written in the following form, meaning that the plate buckles if:

$$\frac{h}{t} > \sqrt{\frac{\sqrt{3} k_\tau \pi^2 E}{12(1-\nu^2) f_y}} \tag{2.42}$$

Figure 2.11 presents the maximum h/t value for the plate at which it does not buckle theoretically (Eq (2.42)) and according to EN 1993-1-1 [EN 1993-1-1, 2005] (Eq. (2.37)). Steel grades S235, S355 and S460 are considered here.

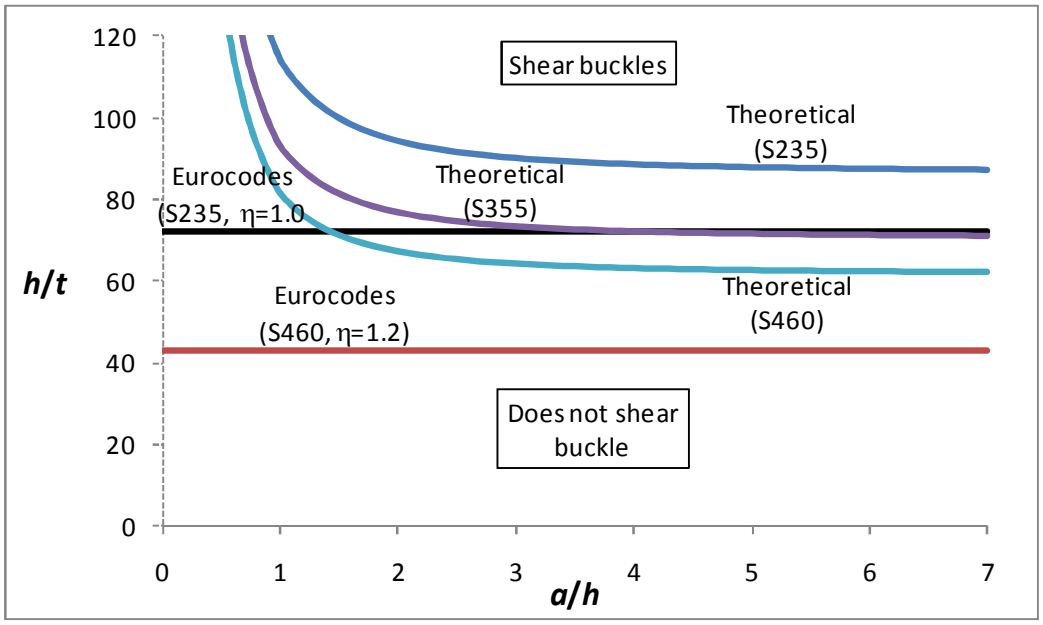

Figure 2.11. Plate h/t ratios at which shear buckling should be considered.

According to EN 1993-1-1 [EN 1993-1-1, 2005], shear buckling should be considered in each case if $\lambda_w > 0.83$ for $\eta = 1.0$ and if $\lambda_w > 0.69$ for $\eta = 1.2$. It is obvious from Figure 2.11 that the distance between the stiffeners has no effect in the EN 1993-1-1 [EN 1993-1-1, 2005] condition. Figure 2.11 shows that the maximum h/t ratio for the shear buckling condition decreases when yield strength or factor η increases. Moreover, it can be seen that according to EN 1993-1-1 [EN 1993-1-1, 2005], shear buckling should be considered in the case of clearly thicker plates than when using theoretical Equation (2.6). It has been long accepted that the existence of initial imperfections in thin-walled structures can reduce their buckling resistance [Alinia et al, 2009(a)].

In this study, all considered plates are assumed to be so thin that they buckle before yielding. Therefore, the design resistance of the plate for shear is calculated according to EN 1993-1-5 [EN 1993-1-5, 2005] as follows:

$$V_{b,Rd} = V_{bw,Rd} + V_{bf,Rd} \leq \frac{\eta f_y h t}{\sqrt{3}\gamma_{M1}} \tag{2.43}$$

where
- $V_{bw,Rd}$ is the contribution of the web (see Chapter 2.3.1),
- $V_{bf,Rd}$ is the contribution from the flanges (see Chapter 2.3.2),
- $\gamma_{M1} = 1.00$ [EN 1993-1-1, 2005].

2.3.1 Contribution of the web

The contribution from the web is obtained from the following [EN 1993-1-5]:

$$V_{bw,Rd} = \frac{\chi_w f_y h t}{\sqrt{3}\gamma_{M1}} \tag{2.44}$$

where
- χ_w is the factor for the contribution of the web shown in Table 2.4 and Figure 2.12,
- γ_{M1} = 1.00 [EN 1993-1-1, 2005].

Table 2.4. Contribution from the web (χ_w) for shear resistance according to EN 1993-1-5 [EN 1993-1-5, 2005].

	Rigid end post	Non-rigid end post
$\lambda_w < 0.83/\eta$	η	η
$0.83/\eta \le \lambda_w < 1.08$	$0.83/\lambda_w$	$0.83/\lambda_w$
$\lambda_w \ge 1.08$	$1.37/(0.7+\lambda_w)$	$0.83/\lambda_w$

Figure 2.12 presents the formulas of Table 2.4 graphically for all cases (η = 1.0 and 1.2, rigid and non-rigid end post). Moreover, theoretical shear buckling resistance (Eq. (2.6)) is plotted in order to illustrate that EN 1993-1-5 [EN 1993-1-5, 2005] takes the post-buckling strength into account in the design of slender webs.

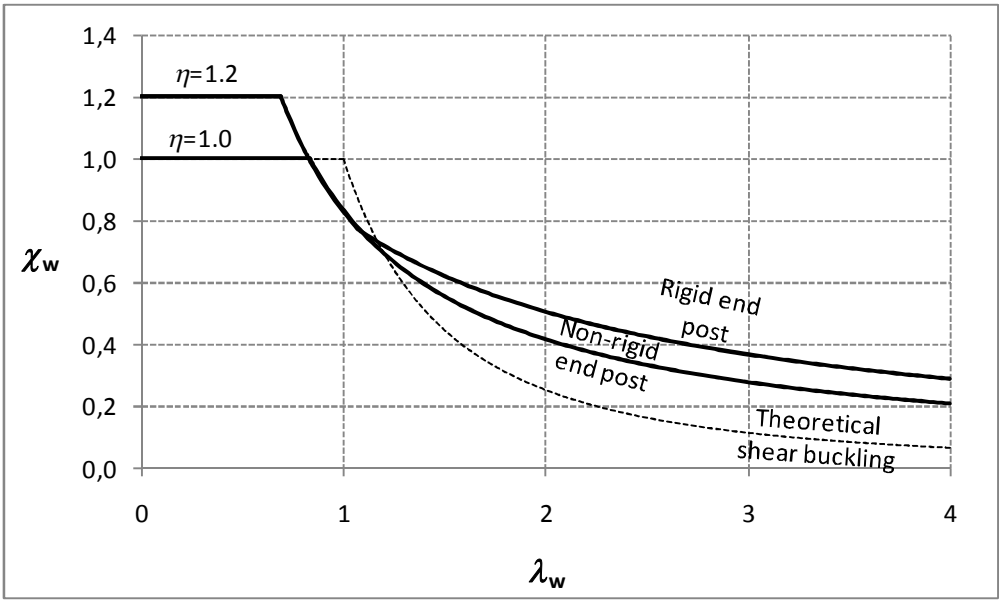

Figure 2.12. Contribution from the web according to EN 1993-1-5 [EN 1993-1-5, 2005].

Critical shear stress τ_{cr}, which is needed in the calculation of slenderness parameter λ_w (Eq. (2.39)), is obtained according to the informative Annex A of EN 1993-1-5 [EN 1993-1-5, 2005]. The plates of this study have no transverse stiffeners, which means that the EN 1993-1-5 equations for the shear buckling coefficient and critical shear stress are the same as with the classical theory illustrated by Equations (2.6)−(2.8).

It should be noted that calculation of post-buckling resistance according to EN 1993-1-5 [EN 1993-1-5, 2005] is permitted for all a/h ratios and end panels. For example, in the American Standard [AISC, 2005(b)], tension field action is not permitted for end panels with transverse stiffeners and for members when a/h exceeds 3.

2.3.2 Contribution from the flanges

According to EN 1993-1-5 [EN 1993-1-5, 2005], the contribution from flanges to shear resistance is obtained from:

$$V_{bf,Rd} = \frac{b_f t_f^2 f_{yf}}{c\gamma_{M1}} \left(1 - \left(\frac{M_{Ed}}{M_{f,Rd}} \right)^2 \right) \tag{2.45}$$

where
- b_f is the width of the flange,
- t_f is the thickness of the flange,
- f_{yf} is the yield strength of the flanges,
- M_{Ed} is the design bending moment,
- $M_{f,Rd} = M_{f,k}$ (when $\gamma_{M0} = 1.00$), the moment resistance of the cross section consisting of the effective area of the flanges only,
- $\gamma_{M1} = 1.00$ [EN 1993-1-1, 2005], and
- $c = a\left(0.25 + \frac{1.6 b_f t_f^2 f_{yf}}{t h^2 f_{yw}} \right)$. (2.46)

The width b_f and thickness t_f of the flange are taken for the flange which provides the least axial resistance so that the maximum value for b_f is $15\varepsilon t_f$ on both sides of the web. The value of $M_{f,Rd}$ should be reduced by multiplying it by the factor shown in Equation (2.47) when an axial force N_{Ed} is present.

$$\left(1 - \frac{N_{Ed}}{(A_{f1} + A_{f2}) f_{yf}} \right) \tag{2.47}$$

where
- A_{f1} is the area of the top flange and
- A_{f2} is the area of the bottom flange.

2.3.3 Aluminium

According to EN 1999-1-1 [EN 1999-1-1, 2007], the design resistance of aluminium plate girders with transverse and longitudinal stiffeners for shear buckling is the sum of the contributions from the web and flanges. For aluminium web plates with transverse stiffeners only at supports, web contribution alone is considered. The contribution from the web is determined as follows:

$$V_{w,Rd} = \rho_v th \frac{f_o}{\sqrt{3}\gamma_{M1}} \tag{2.48}$$

where
- ρ_v is the factor for shear buckling (see Table 2.5 and Fig. 2.13),
- f_o is the characteristic value of 0.2 % proof strength,
- γ_{M1} = 1.10 [EN 1999-1-1, 2007].

The factor for shear buckling is obtained from Table 2.5 or Figure 2.13 [EN 1999-1-1, 2007].

Table 2.5. Factor ρ_v for shear buckling according to EN 1999-1-1 [EN 1999-1-1, 2007].

	Rigid end post	Non-rigid end post
$\lambda_w < 0.83/\eta$	η	η
$0.83/\eta \le \lambda_w < 0.937$	$0.83/\lambda_w$	$0.83/\lambda_w$
$\lambda_w \ge 0.937$	$2.3/(1.66+\lambda_w)$	$0.83/\lambda_w$

The factor η is obtained from the following in the case of aluminium web plate [EN 1999-1-1, 2007]:

$$\eta = 0.7 + 0.35\frac{f_a}{f_o} \le 1.2 \tag{2.49}$$

where
- f_o is the strength for overall yielding and
- f_a is the ultimate strength of the web material.

Figure 2.13 presents the formulas of Table 2.5 graphically for cases η = 1 and 1.2 as well as for rigid and non-rigid end posts.

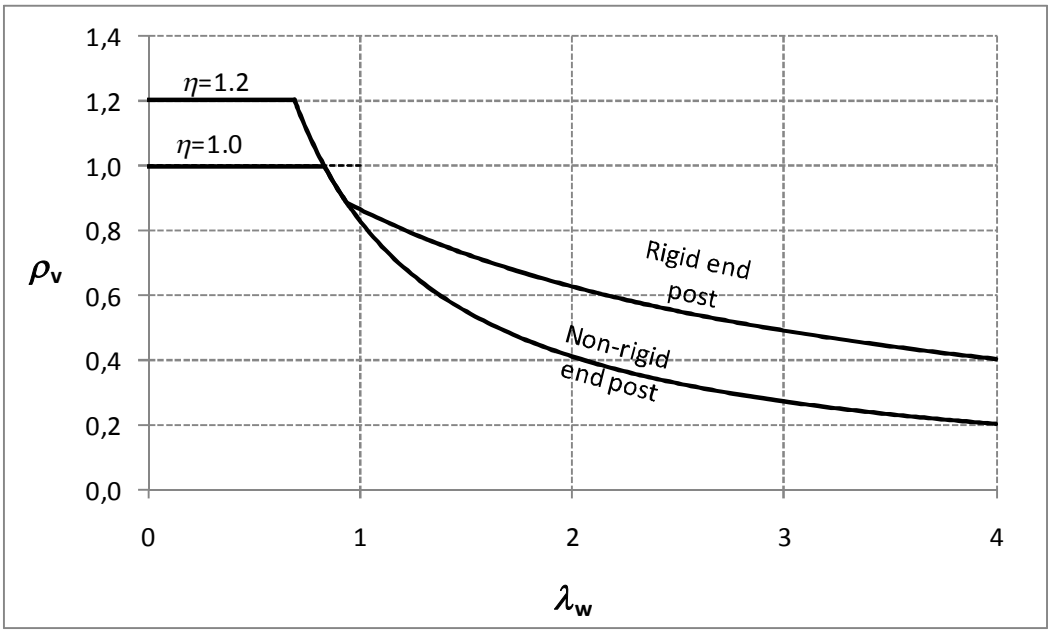

Figure 2.13. Contribution from the web according to EN 1999-1-1 [EN 1999-1-1, 2007].

The slenderness parameter λ_w for aluminium plate girders with web stiffeners only at supports is derived from:

$$\lambda_w = 0.35\frac{a}{t}\sqrt{\frac{f_o}{E}} \tag{2.50}$$

For aluminium plate girders with intermediate web stiffeners the slenderness parameter λ_w is:

$$\lambda_w = \frac{0.81}{\sqrt{k_\tau}}\frac{a}{t}\sqrt{\frac{f_o}{E}} \tag{2.51}$$

The contribution from the flanges $V_{f,Rd}$ can be included in ultimate shear resistance as shown in Equation (2.52) if flange resistance is not completely utilized in resisting bending moment.

$$V_{f,Rd} = \frac{b_f t_f^2 f_{of}}{c\gamma_{M1}}\left(1-\left(\frac{M_{Ed}}{M_{f,Rd}}\right)^2\right) \tag{2.52}$$

where
- f_{of} is flange strength for overall yielding
- $c = a\left(0.08 + \frac{4.4 b_f t_f^2 f_{of}}{t h^2 f_{ow}}\right)$ (2.53)

The width b_f and the thickness t_f of the flange are taken (as with carbon steel) for the flange which provides the least axial resistance so that the maximum value for b_f is $15t_f$ on both sides of the web. The value of $M_{f,Rd}$ should be reduced as in the case of carbon steel (Eq. (2.47) using f_{of} instead of f_y) when an axial force is present.

2.3.4 Stainless steel

Historically, the design rules for stainless steel have been based on assumed analogies with carbon steel behaviour, with modifications made where necessary to fit with test results. [Real et al, 2007].

According to EN 1993-1-4 [EN 1993-1-4, 2006] the shear buckling resistance of a thin stainless steel plate is calculated according to EN 1993-1-5 [EN 1993-1-5, 2005] with modified χ_w, which is determined as follows:

$$\chi_w = \eta \qquad \text{for } \lambda_w \le \frac{0.6}{\eta} \tag{2.54}$$

$$\chi_w = 0.11 + \frac{0.64}{\lambda_w} - \frac{0.05}{\lambda_w^2} \qquad \text{for } \lambda_w > \frac{0.6}{\eta} \tag{2.55}$$

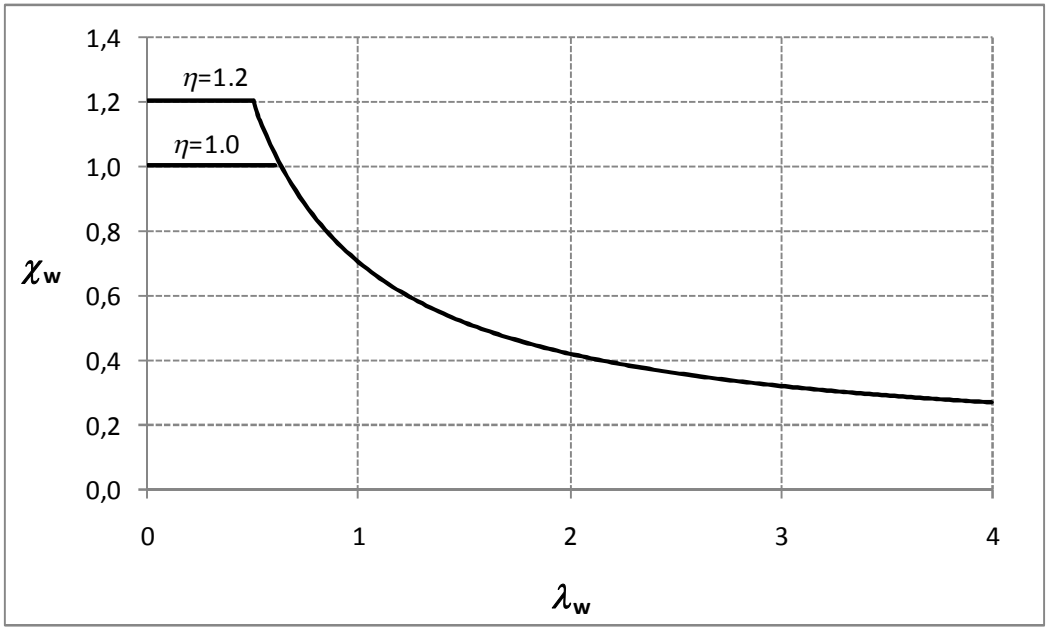

Figure 2.14. Contribution from the web according to EN 1993-1-4 [EN 1993-1-4, 2006].

The standard EN 1993-1-4 [EN 1993-1-4, 2006] recommends the value $\gamma_{M0} = 1.1$ as a partial factor in Equation (2.44). It should be noted that Equations (2.54) and (2.55) do

not consider a rigid or non-rigid condition. The slenderness parameter λ_w for stainless steel plates is calculated similarly as for carbon steel plates (Eq. (2.39)).

According to EN 1993-1-4 [EN 1993-1-4, 2006], the effect of the flanges may be included in ultimate shear resistance similarly as with carbon steel plates in EN 1993-1-5 [EN 1993-1-5, 2005] (Eq. (2.45)) but with c given by:

$$c = a\left(0.17 + \frac{3.5 b_f t_f^2 f_{yf}}{t h^2 f_{yw}}\right) \tag{2.56}$$

$$\frac{c}{a} \leq 0.65 \tag{2.57}$$

2.4 Comparisons between different methods

The different methods for predicting the shear resistance of thin metal plate presented in previous chapters are compared in the following. Figure 2.15 presents a comparison of theoretical shear buckling stress (Eq. (2.6)) and ultimate shear stress for carbon steel plates according to EN 1993-1-5 [EN 1993-1-5, 2005] (flanges ignored) and the tension field theory by Dubas [Dubas, Gehri, 1986] and Höglund [Höglund, 1972]. All shown relative ultimate shear stresses τ_u/τ_y are presented as a function of the slenderness parameter λ_w (Eq. (2.39)).

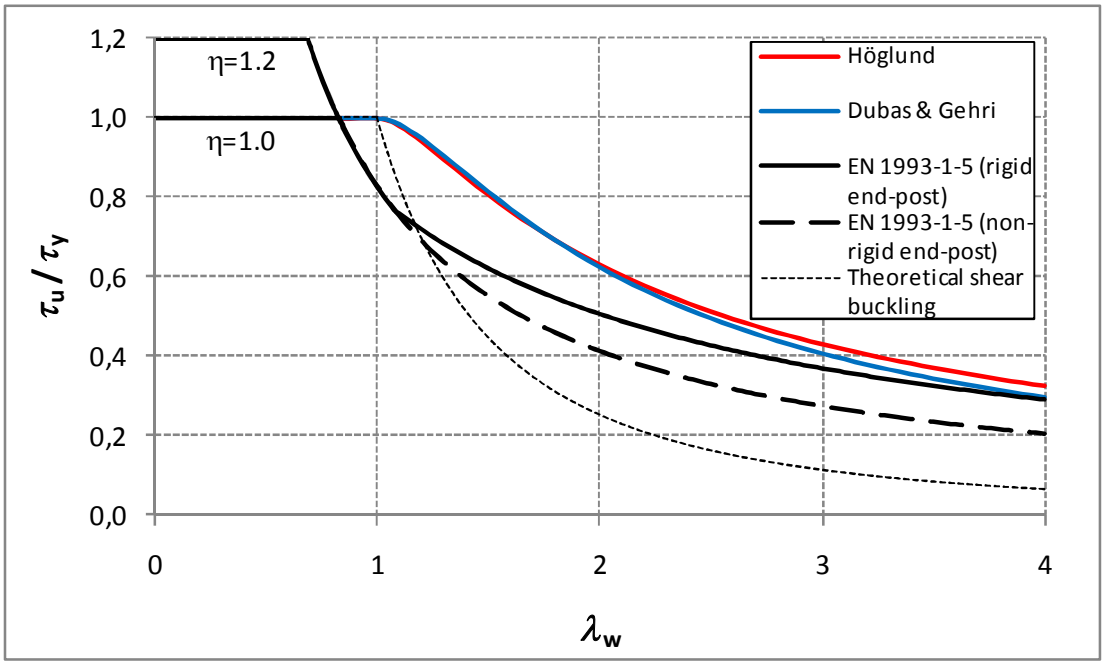

Figure 2.15. Comparison of different methods.

Figure 2.15 shows that the tension field theories of Dubas [Dubas, Gehri, 1986] and Höglund [Höglund, 1972] yield much the same results even though the approaches are

rather different. For the range covered in Figure 2.15 (λ_w=1−4), the rotated stress field theory gives, on average, 3.7 % higher resistances than the theory of Dubas. Reference [Alinia et al, 2011] compares the theories of Rockey [Rockey et al, 1978], Basler [Basler, 1962] and Höglund [Höglund, 1972] and standards: EN 1993-1-5 [EN 1993-1-5, 2005], AISC [AISC, 2005(a)] and AASHTO [AASHTO, 1994] for 30 slender web plates using FEM. According to Alinia et al, all the theories and standards, except EN 1993-1-5 overestimated the ultimate shear strength of web plate girders. From Figure 2.15 it can also be concluded that the post-buckling phase is a highly significant factor in ultimate shear resistance especially in the case of slender plates. Figure 2.16 also proves that by showing the contribution of post-buckling resistance τ_u - τ_{cr} according to the tension field theories by Höglund and Dubas and the design formulas of EN 1993-1-5 at slightly over 400 °C temperature meaning that η=1.

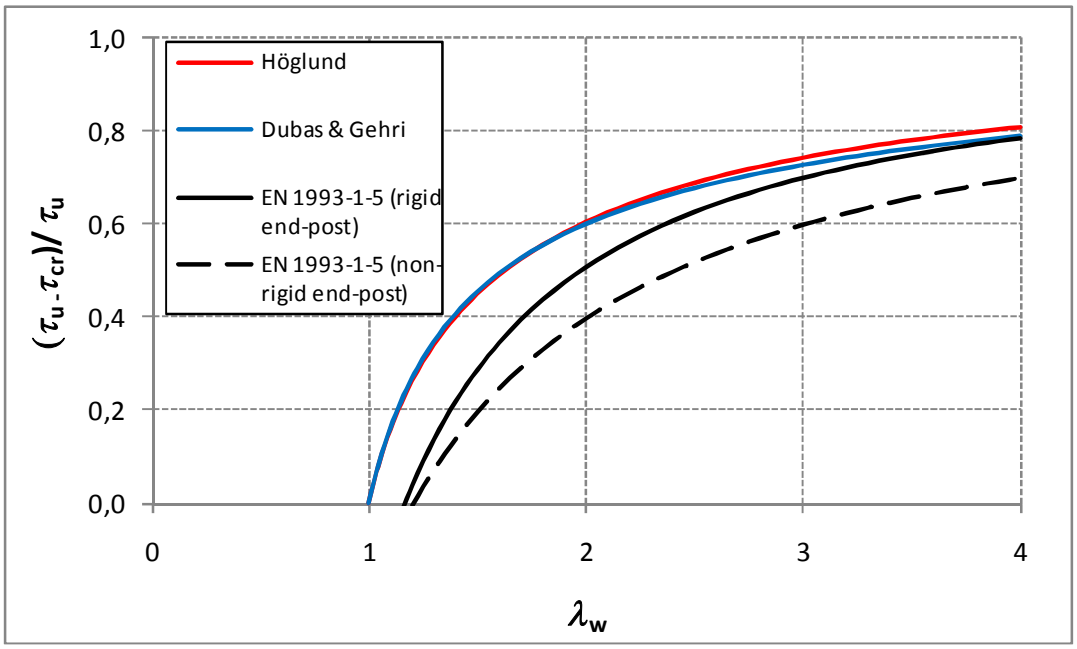

Figure 2.16. Contribution of post-buckling resistance to ultimate shear resistance.

Figure 2.16 shows, for example, that at web slenderness λ_w = 2, the contribution of post-buckling resistance to the ultimate shear resistance is approximately 40 % (non-rigid end-posts) or 50 % (rigid end-posts) according to EN 1993-1-5 [EN 1993-1-5, 2005] and 60 % according to the theories of Höglund [Höglund, 1972] and Dubas [Dubas, Gehri, 1986]. According to EN 1993-1-5, ultimate shear resistances are higher than theoretical shear buckling resistances when λ_w is approximately 1.2. However, Figure 2.16 illustrates clearly how the post-buckling behaviour of plates under shear loading is taken into account in EN 1993-1-5.

The contribution of shear buckling resistance is clearly higher according to Höglund [Höglund, 1972] than according to EN 1993-1-5 [EN 1993-1-5, 2005], even though the EN 1993-1-5 method is based on the theory of Höglund. That is because the EN 1993-1-

5 resistances are somewhat reduced compared to the theory of Höglund to allow for scatter in test results as a result of initial imperfections and plastic buckling [Höglund, 1997].

Figure 2.17 compares the design formulas of Eurocodes [EN 1993-1-5, 2005], [EN 1999-1-1, 2007] and [EN 1993-1-4, 2006] in the case of carbon steel, aluminium and stainless steel, respectively. The shear buckling factors (χ_w for carbon and stainless steel and ρ_v for aluminium) are presented as a function of the slenderness parameter λ_w. It should be noted that λ_w is calculated differently for aluminium plates for carbon and stainless steel plates (see Eqs. (2.39), (2.50) and (2.51)).

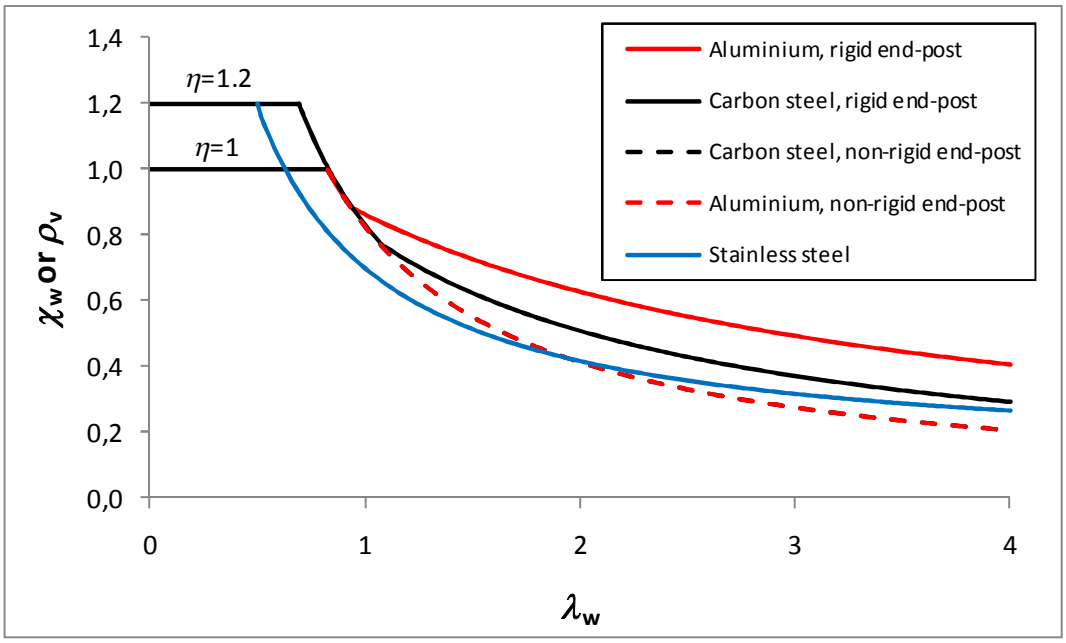

Figure 2.17. Shear buckling factors χ_w and ρ_w for carbon steel, aluminium and stainless steel according to Eurocodes.

Figure 2.17 shows that according to EN 1993-1-5 [EN 1993-1-5, 2005] and EN 1999-1-1 [EN 1999-1-1, 2007], the effect of the rigidity of end-posts is significantly higher for aluminium plates than for carbon steel plates. The values for non-rigid end-posts are the same in the case of carbon steel and aluminium. For stainless steel, χ_w starts to decrease at smaller slenderness ratios than in the case of carbon steel and aluminium due to non-linear material behaviour. According to EN 1993-1-4 [EN 1993-1-4, 2006], the rigidity of the end-post has no effect on χ_w.

Based on the analysis of this chapter, it can be concluded that post-buckling resistances that are in good agreement with test results can be obtained by quite different approaches (the tension field theories by Dubas [Dubas, Gehri, 1986] and Höglund [Höglund, 1972] considered in this study). Moreover, it can be said that post-buckling resistance is taken into account in the Eurocodes [EN 1993-1-5, 2005], [EN 1999-1-1,

2007] and [EN 1993-1-4, 2006] and that in the case of a slender plate, it has a significant effect on the ultimate shear resistance of the plate.

3 SHEAR RESISTANCE OF THIN METAL PLATE AT ELEVATED TEMPERATURES

When subjected to elevated temperatures, metal structures lose part of their loading capacity and stiffness. The shear resistance of a plate at elevated temperatures can be determined by reducing the material properties. Chapter 3.1 presents the reductions of material properties of carbon and stainless steel according to EN 1993-1-2 [EN 1993-1-2, 2005] and aluminium according to EN 1999-1-2 [EN 1999-1-2, 2007]. Chapter 3.2 presents the calculation procedure for shear resistance of thin metal plate at elevated temperatures according to EN 1993-1-2 and EN 1999-1-2. The test results [Vimonsatit, Tan, Qian, 2007] used as the benchmark case of this study are considered in Chapter 3.3 and Chapter 3.4 presents the temperature distributions from fire tests and FEM analysis on which the temperature distributions of this study are based.

3.1 Material properties at elevated temperatures

3.1.1 Carbon steel

According to EN 1993-1-2 [EN 1993-1-2, 2005], the strength and deformation properties of carbon steel should be obtained by using the reduction factors for elastic modulus, proportional limit and effective yield strength, which are presented as a function of steel temperature θ_a in Figure 3.1. The design strength of class 4 members (0.2 % proof strength) for carbon steel is also plotted [EN 1993-1-2, 2005]. The reduction factor $k_{i,\theta}$ of material property i at temperature θ is defined as follows:

$$k_{i,\theta} = \frac{i_\theta}{i_{amb}} \tag{3.1}$$

where
- i_θ is the value of the material property at elevated temperature and
- i_{amb} is the value of the material property at ambient temperature.

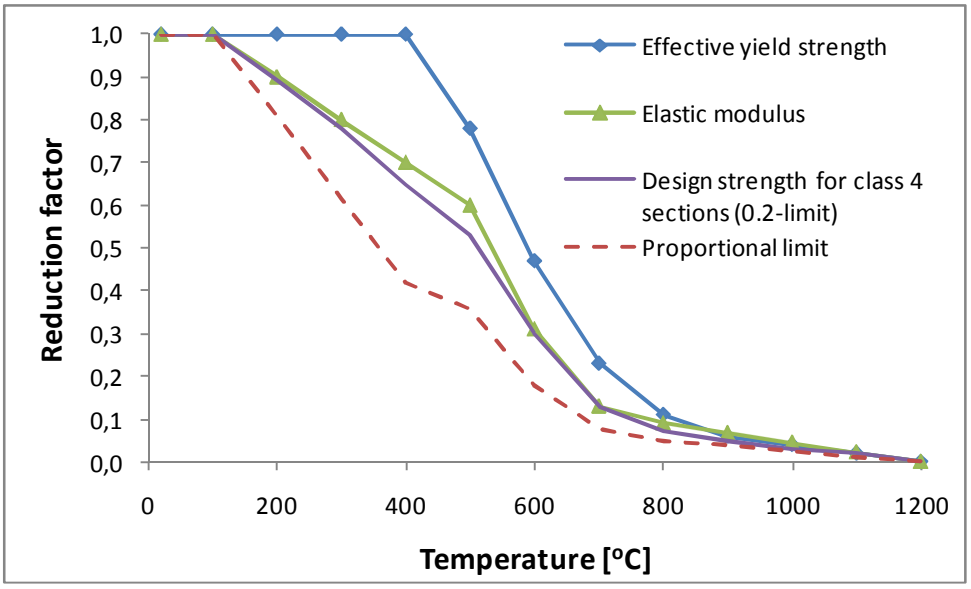

Figure 3.1. Reduction factors for carbon steel according to EN 1993-1-2 [EN 1993-1-2, 2005].

Based on the reduction factors presented above, the relationship between stresses and strains at elevated temperatures, required for example for numerical analysis, can be determined according to EN 1993-1-2 [EN 1993-1-2, 2005] (Fig. 3.2).

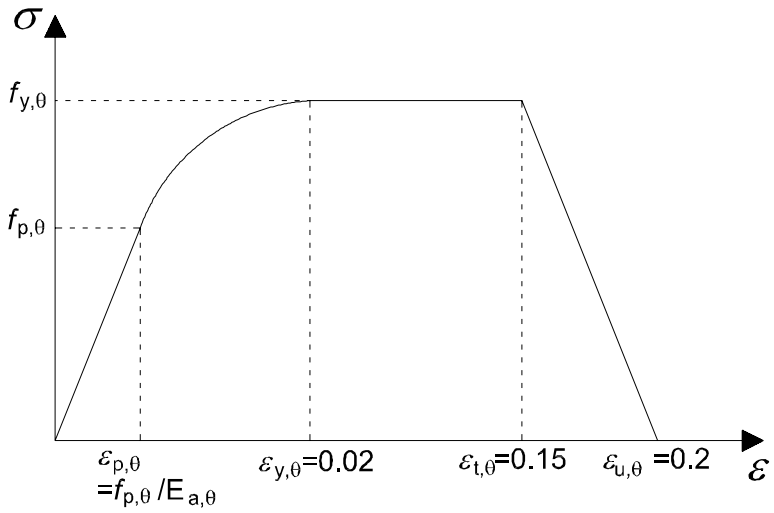

Figure 3.2. Principle of the stress-strain relationship of carbon steel at elevated temperatures according to EN 1993-1-2 [EN 1993-1-2, 2005].

The notations of Figure 3.2 are the following:

- $f_{y,\theta}$ is effective yield strength,
- $f_{p,\theta}$ is proportional limit,
- $E_{a,\theta}$ is slope of the linear elastic range,
- $\varepsilon_{p,\theta}$ is strain at the proportional limit,
- $\varepsilon_{y,\theta}$ is yield strain,

- $\varepsilon_{t,\theta}$ is limiting strain for yield strength, and
- $\varepsilon_{u,\theta}$ is ultimate strain.

The values of stresses between strains $\varepsilon_{p,\theta}$ and $\varepsilon_{y,\theta}$ are expressed as functions in EN 1993-1-2 [EN 1993-1-2, 2005]. The stress-strain curves for the benchmark case material according to EN 1993-1-2 at different elevated temperatures are shown in Figure 4.7.

3.1.2 Aluminium

Standard EN 1999-1-2 [EN 1999-1-2, 2007] gives 13 different reduction curves for 0.2 % proof strength of aluminium depending on the alloy and temper as shown in Figure 3.3. The lower limit may be used for alloys not covered by EN 1999-1-2, but listed in Table 3.2a and 3.2b of EN 1999-1-1 [EN 1999-1-1, 2007]. One reduction curve is given for elastic modulus.

This study considers alloy EN AW-5083-H111 (referred to as 5083-H111). According to Maljaars, it is one of the most common alloys used in structural applications in Europe [Maljaars, 2008]. For alloy 5083-O, the reduction curve for 0.2 % proof strength is given in EN 1999-1-2 but not for alloy 5083-H111, so the lower limit values should be used. However, Maljaars considers the reduction factors for alloy 5083-H111 to be the same as those for 5083-O, and the same assumption is made also in this study. It should be noted that no material model such as for carbon steel (Fig. 3.2) or stainless steel (Fig. 3.6) is given in EN 1999-1-2. The stress-strain curves for alloy 5083-H111 for the FEM analysis of this study are from the reference [Maljaars, 2008] (See Chapter 4.2.2).

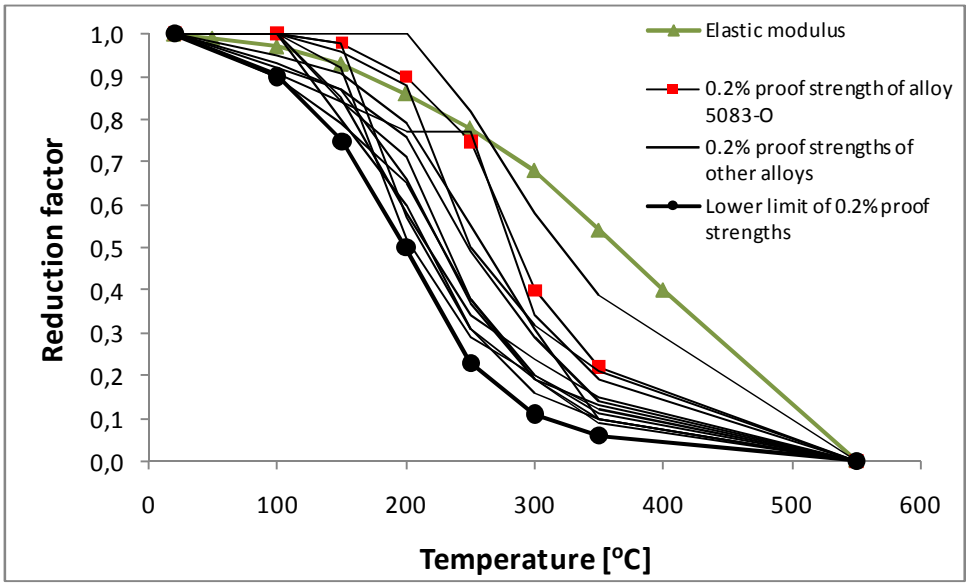

Figure 3.3. Reduction factors of elastic modulus and proof strengths for aluminium according to EN 1999-1-2 [EN 1999-1-2, 2007].

Figure 3.3 shows that the reduction factor of 0.2 % proof strength for aluminium depends significantly on the alloy. At the same temperature, the reduction factors of 0.2 % proof strength for alloy 5083-O are, on average, approximately 2.5 times higher than the lower limit values in the 100-350 °C range.

3.1.3 Stainless steel

The reduction factors of different stainless steel grades for elastic modulus, 0.2 % proof strength and tensile strength according to EN 1993-1-2 [EN 1993-1-2, 2005] are shown in Figures 3.4 and 3.5. This study considers grade 1.4301, which is commonly used in structural applications because it combines adequate corrosion resistance and strength with relative economy [Estrada et al, 2007].

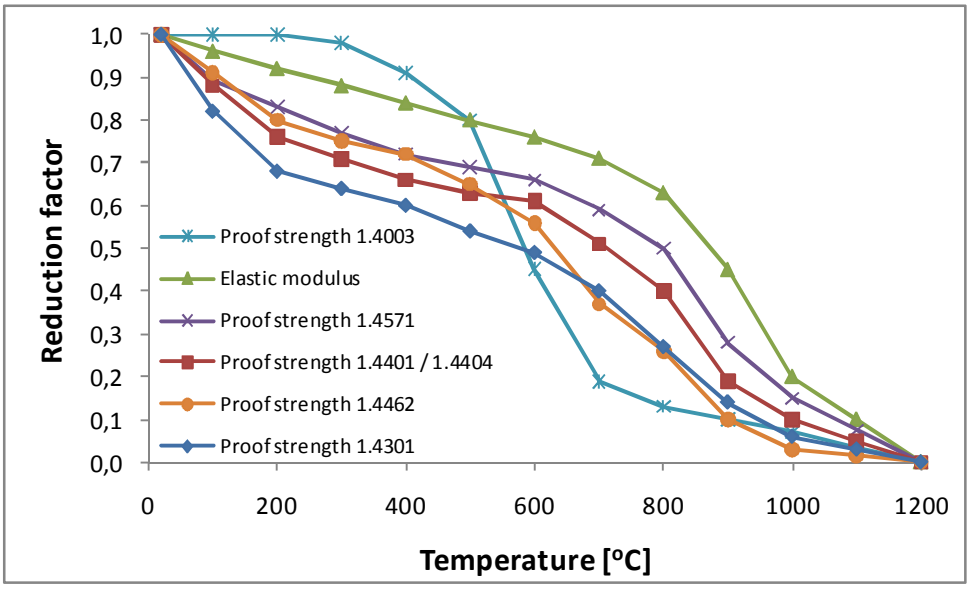

Figure 3.4. Reduction factors of elastic modulus and proof strength for stainless steel according to EN 1993-1-2 [EN 1993-1-2, 2005].

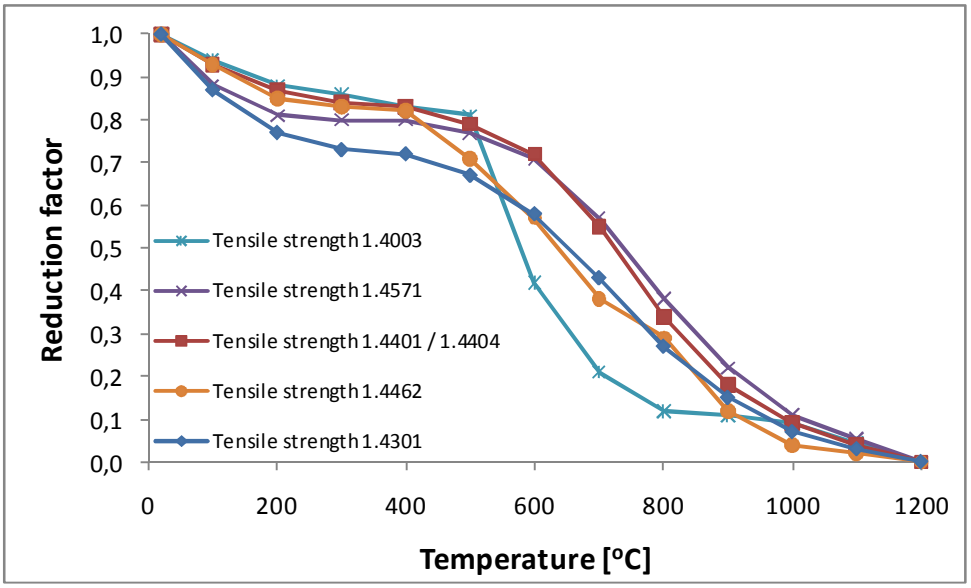

Figure 3.5. Reduction factors of tensile strength for stainless steel according to EN 1993-1-2 [EN 1993-1-2, 2005].

Figures 3.4 and 3.5 reveal that the reductions factors of proof strength and tensile strength for stainless steel are significantly different for different grades.

Figure 3.6 presents the principle of the formulation of the stress-strain relationship for stainless steel at elevated temperatures according to EN 1993-1-2 [EN 1993-1-2, 2005].

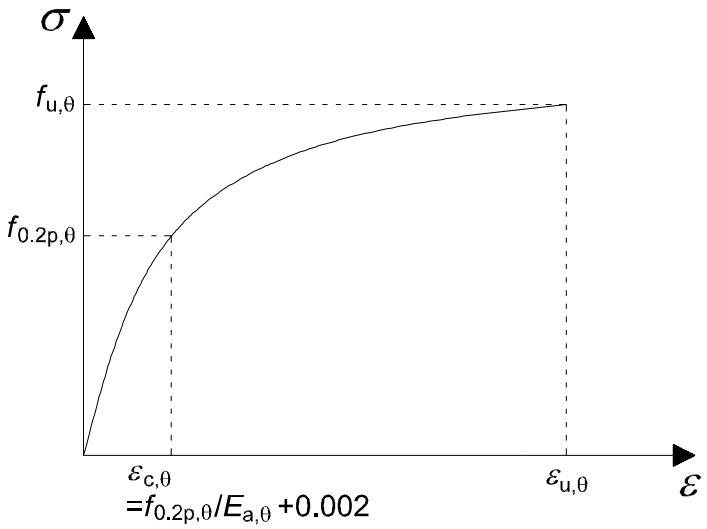

Figure 3.6. Principle of stress-strain relationship for stainless steel at elevated temperatures according to EN 1993-1-2 [EN 1993-1-2, 2005].

The notations of Figure 3.6 are the following:

- $f_{u,\theta}$ is tensile strength,
- $f_{0.2p,\theta}$ is the proof strength at 0.2 % plastic strain,
- $\varepsilon_{c,\theta}$ is the total strain at proof strength, and
- $\varepsilon_{u,\theta}$ is the ultimate strain.

Unlike in the case of carbon steel, the relationship of stresses and strains is not linear in any range at elevated temperatures. The functions for the stresses as a function of strains are given in EN 1993-1-2 [EN 1993-1-2, 2005]. Ultimate strain $\varepsilon_{u,\theta}$ also depends on temperature. The stress-strain curves of stainless steel grade 1.4301 according to EN 1993-1-2 at different elevated temperatures are shown in Figure 4.12.

3.1.4 Discussion on material models

Two types of test methods are commonly used in resistance tests for metals at elevated temperatures [Outinen et al, 2001]: the transient-state and steady-state methods. The steady-state method, which is a lot simpler, involves heating the specimen to the specified temperature and then conducting the mechanical test. The transient-state test method, which seems to give more realistic results [Outinen et al, 2001], involves subjecting the specimen to a constant load and a constant temperature rise. The temperatures and strains are measured during the test (left-hand side of Fig. 3.7), and the results are converted into stress-strain curves (right-hand side of Fig. 3.7).

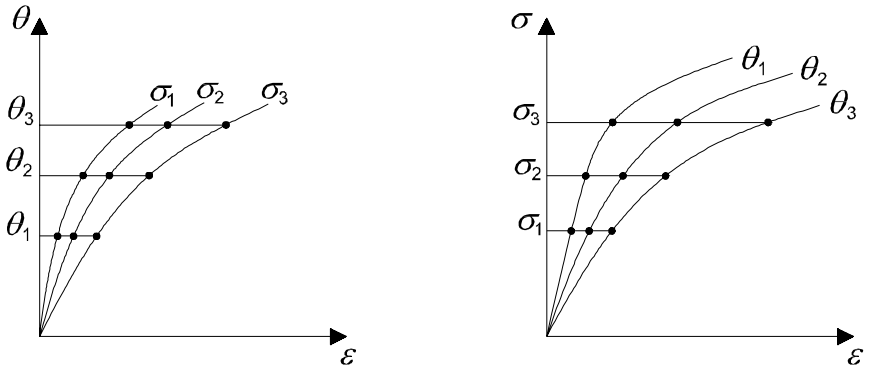

Figure 3.7. Determination of stress-strain curves (right) from transient-state test results (left).

Reference [Outinen et al, 2001] shows that the behaviour of the tested carbon steel specimen is significantly different depending on the test method. Strains at the same stress are clearly higher in the case of a transient-state test than in a steady-state test. Moreover, it can be said that the model based on transient-state test results is closer to

the EN 1993-1-2 [EN 1993-1-2, 2005] curve, which is based on transient-state test results [Outinen et al, 2001].

The stress-strain relationships for carbon steel and stainless steel (Figs. 3.2 and 3.6) are valid for heating rates between 2 and 50 K/min [EN 1993-1-2, 2005]. Figure 3.8 shows the heating rate of the standard fire curve defined in Equation (3.2) [EN 1991-1-2, 2002] and the heating rates of 2 and 50 K/min. The heating rate of standard fire is obtained by deriving Equation (3.2).

$$\theta_g = 20 + 345\log_{10}(8T + 1) \tag{3.2}$$

where
- θ_g is gas temperature [°C],
- T is time [min].

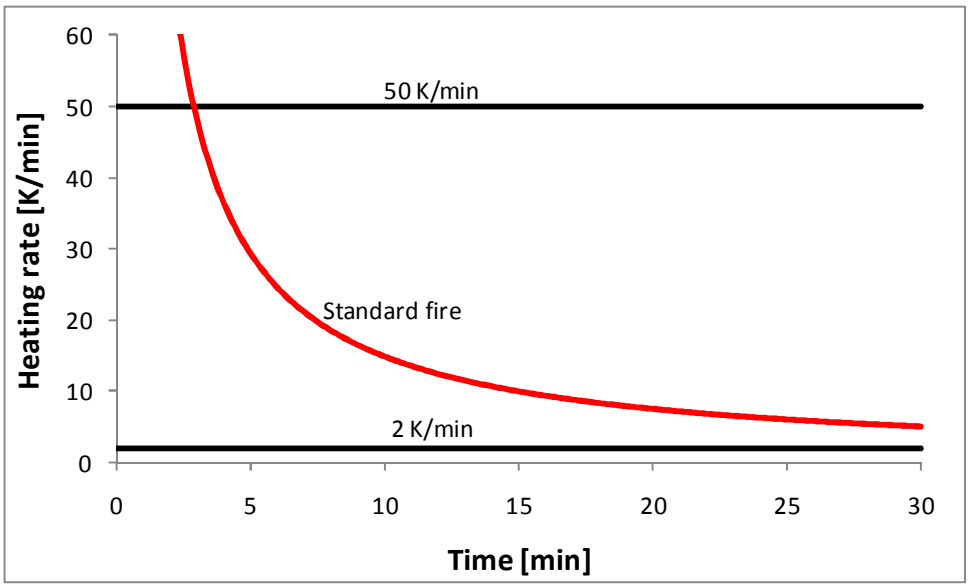

Figure 3.8. Heating rates of standard fire and 2 and 50 K/min.

Figure 3.8 shows that from the beginning to approximately three minutes, the heating rate of a standard fire curve is higher than 50 K/min, which is the maximum value given in EN 1993-1-2 [EN 1993-1-2, 2005] for use with the material model defined in Figures 3.2 and 3.6. According to Outinen, the effect of the heating rate is clear and should always be taken into account when carrying out material tests [Outinen, 2007]. In the numerical analyses of this study, it is assumed that the heating rates are in the 2–50 K/min range to justify the use of the material models of EN 1993-1-2 [EN 1993-1-2, 2005].

3.2 Shear resistance at elevated temperatures according to Eurocodes

According to Eurocodes [EN 1993-1-2, 2005] and [EN 1999-1-2, 2007], the design shear resistance $V_{\mathrm{fi,t,Rd}}$ of class 4 carbon steel and all stainless steel and aluminium cross-sections at elevated temperatures can be derived from the following equation:

$$V_{fi,t,Rd} = k_{p0.2,\theta,web} V_{Rd} \left[\gamma_{M0/1} / \gamma_{M,fi} \right] \tag{3.3}$$

where
- $k_{\mathrm{p0.2,\theta,web}}$ is the reduction factor for 0.2 % proof strength at the average temperature of the web plate (see Figs. 3.1, 3.3 and 3.4),
- V_{Rd} is design shear resistance at ambient temperature (see Chapter 2)
- $\gamma_{\mathrm{M0/1}}$ =1.00 for carbon steel, $\gamma_{\mathrm{M0/1}}$ = 1.10 for aluminium and stainless steel and $\gamma_{\mathrm{M,fi}}$ = 1.00 for all cases [EN 1993-1-1, 2005], [EN 1993-1-4, 2006], [EN 1999-1-2, 2007].

The design resistance of thick carbon steel plate (class 1, 2 and 3 cross-sections) at elevated temperatures is calculated using the reduction factor of yield strength $k_{\mathrm{y,\theta,web}}$ instead of $k_{\mathrm{p0.2,\theta,web}}$ [EN 1993–1–2, 2005] (see Fig. 3.1). In the case of aluminium and stainless steel, the reduction of 0.2 % proof strength is applied also when determining the shear resistance of thick plates [EN 1999-1-2, 2007], [EN 1993-1-2, 2005]. According to EN 1993-1-1 [EN 1993-1-1, 2005], the web of a bent carbon steel beam is a class 4 cross-section when $c/t > 124\varepsilon$ where c is the height of the straight portion of the web. At elevated temperatures, the classification of cross-sections is done with the reduced factor ε [EN 1993-1-2, 2005]:

$$\varepsilon = 0.85\sqrt{\frac{235}{f_y}} \tag{3.4}$$

In this study, all considered carbon steel plates are thin meaning that they are class 4 cross-sections.

3.3 Uniform temperature across the height of the plate

Test results are available for this case. The reference [Vimonsatit, Tan, Qian, 2007] presents test results and FEM calculations for 18 steel-plate girders loaded predominantly in shear at ambient (20 $^{\mathrm{o}}$C) and uniform elevated temperatures (400, 550

and 700 °C). The article by Tan and Qian deals with experimental and numerical investigation of thermally restrained plate girders loaded in shear at uniform elevated temperatures. Tan and Qian observed that ultimate shear resistance decreased significantly under a thermal restraint effect, involving axial force [Tan, Qian, 2007]. In this study, only pure shear is considered. Therefore, the results of the reference [Vimonsatit, Tan, Qian, 2007] are chosen as the benchmark case for this study.

The test series of the reference [Vimonsatit, Tan, Qian, 2007] were conducted for the five different web girders listed in Table 3.1. All panels were loaded at ambient temperature and at the elevated temperatures of 400, 550-565 and 700 °C, except for test panel TG1, which was loaded only at ambient temperature and 400 °C. The heating rate was 7 °C/min. The temperature distributions across the height of the web were very close to uniform. A steady-state test method (see Chapter 3.1.4) was applied as it was not possible for the electric furnace to achieve the standard fire curve presented in EN 1991-1-2 [EN 1991-1-2, 2002].

Table 3.1. Properties of the tested web girders from the reference [Vimonsatit, Tan, Qian, 2007].

	Web details						
Test panel	a [mm]	h [mm]	t [mm]	h/t	λ_w	E [GPa]	f_y [MPa]
TG1	139	139	6.1	22.8	0.25	197	342
TG2	181	181	8	22.6	0.24	205	332
TG3	305	305	2	152.5	1.51	200	287.8
TG4	305	305	2.7	113.0	1.01	200	232.8
TG5	305	305	1.5	203.3	2.17	200	332

Test specimens TG1 and TG2 were universal column sections and specimens TG3, TG4 and TG5 were fabricated from steel plates by welding the web and flange plates together using a longitudinal fillet. All specimens were designed so that the tested panels (Panel 1 and 2 in Fig. 3.9) would fail primarily due to shear force, not due to flexural failure caused by plastic hinge formation at midspan. Therefore, additional plates were welded onto the top and bottom flanges of the girders. Figure 3.9 shows the test girder configuration with test panel TG5 as reported in [Vimonsatit, Tan, Qian, 2007]. The specimens were allowed to move freely in the longitudinal direction during heating.

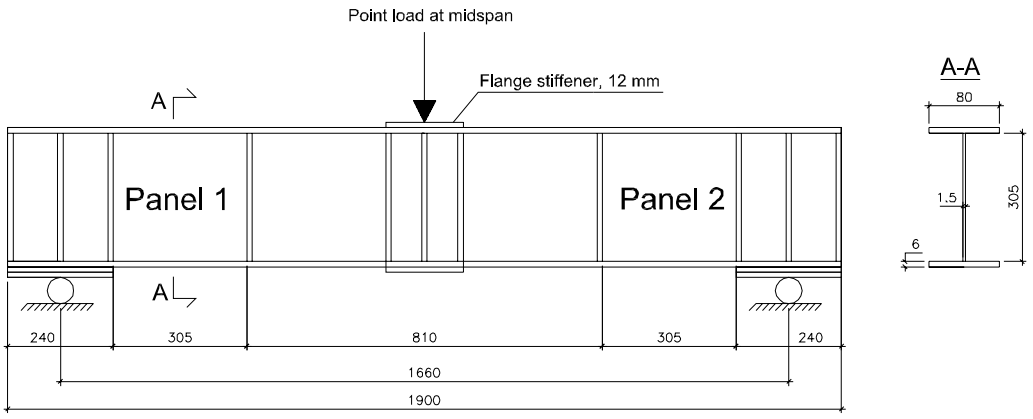

Figure 3.9. Test girder configuration with test panel TG5 as reported in [Vimonsatit, Tan, Qian, 2007].

The two most slender webs, TG3 (λ_w=1.51) and TG5 (λ_w=2.17), are considered in more detail in this study. In a previous work [Salminen, 2010], it was shown that the tested and calculated [EN 1993-1-2, 2005] resistances agreed well in the case of stocky webs (TG1 and TG2). Figure 3.10 presents the tested shear resistances at elevated temperatures divided by the ambient temperature shear resistance (V_{test} / $V_{EN,amb}$) for panels TG1 and TG2 according to EN 1993-1-5 [EN 1993-1-5, 2005]. The reduction factor curve for the effective yield strength according to EN 1993-1-2 is also plotted. For test panel TG4 (λ=1.01) the calculated results were clearly unconservative probably due to the reported problems in the tests [Vimonsatit, Tan, Qian, 2007].

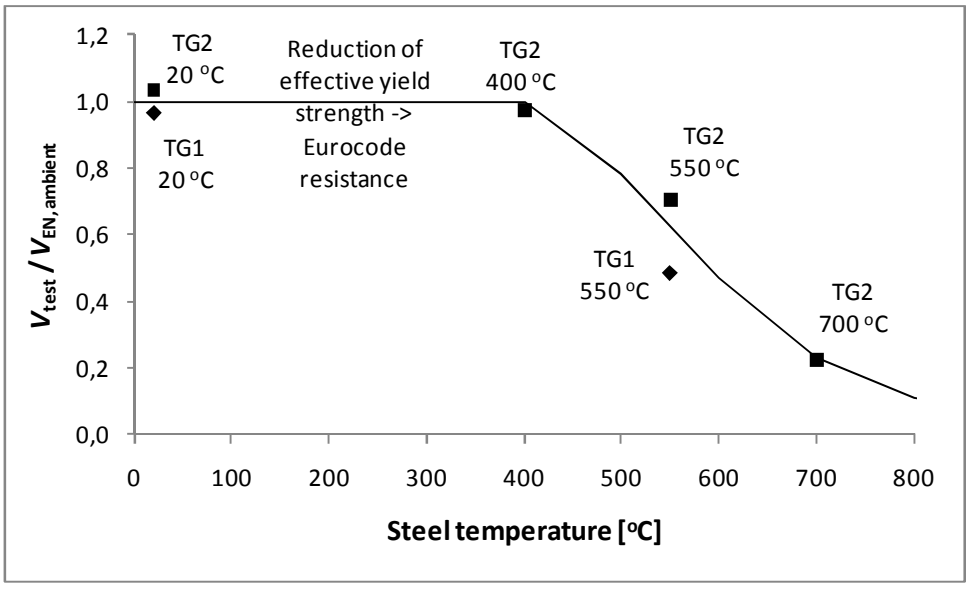

Figure 3.10. Tested shear resistances [Vimonsatit, Tan, Qian] compared to EN 1993-1-5 [EN 1993-1-5, 2005] and EN 1993-1-2 [EN 1993-1-2, 2005] resistances for stocky webs TG1 and TG2.

Table 3.2 presents the ultimate shear forces of the slender webs TG3 and TG5 from the tests ($V_{u,Test}$) and from the calculations with the analytical method ($V_{u,V}$) applied in [Vimonsatit, Tan, Qian, 2007], which is based on Rockey's theory [Rockey et al, 1978]. Moreover, the shear resistances are calculated according to Eurocodes ($V_{u,EN}$) [EN 1993-1-5, 2005], [EN 1993-1-2, 2005] so that the contribution from the flanges and the rigidity of the end posts are taken into account (see also Chapters 2.3 and 3.2). The width of the flange is 80 mm and thickness 6 mm for TG3 and TG5. The yield strengths of TG3 and TG5 flange materials are 274.5 and 277 N/mm^2, respectively [Vimonsatit, Tan, Qian, 2007].

Table 3.2 also presents the shear resistances calculated according to the tension field theories by Dubas ($V_{u,D}$) [Dubas, Gehri, 1986] and Höglund ($V_{u,H}$) [Höglund, 1972] (Eqs. (2.18) and (2.24), respectively) where material properties are reduced according to EN 1993-1-2 [EN 1993-1-2, 2005]. Yield strength is reduced based on the reduction factors of design strength for class 4 members.

Table 3.2. Ultimate shear forces.

[Vimonsatit, Tan, Qian, 2007]				This study		
Test panel	θ [°C]	$V_{u,Test}$ [kN]	$V_{u,V.}$ [kN]	$V_{u,EN}$ [kN]	$V_{u,D}$ [kN]	$V_{u,H}$ [kN]
TG3-1	20	79.85	85.7	68.7	82.0	81.3
TG3-2	400	67.63	65.2	44.6	54.9	54.4
TG3-3	565	34.34	37.13	26.1	32.3	31.9
TG3-4	690	17.15	15.7	10.1	12.1	12.0
TG5-1	20	59.6	69.28	49.5	50.5	51.4
TG5-2	400	46.4	53.17	32.2	34.2	34.6
TG5-3	550	28.6	32.39	20.6	22.0	22.3
TG5-4	700	10.16	11.48	6.4	6.6	6.7

Figures 3.11 and 3.12 present the results of Table 3.2 graphically for tested panels TG3 and TG5, respectively.

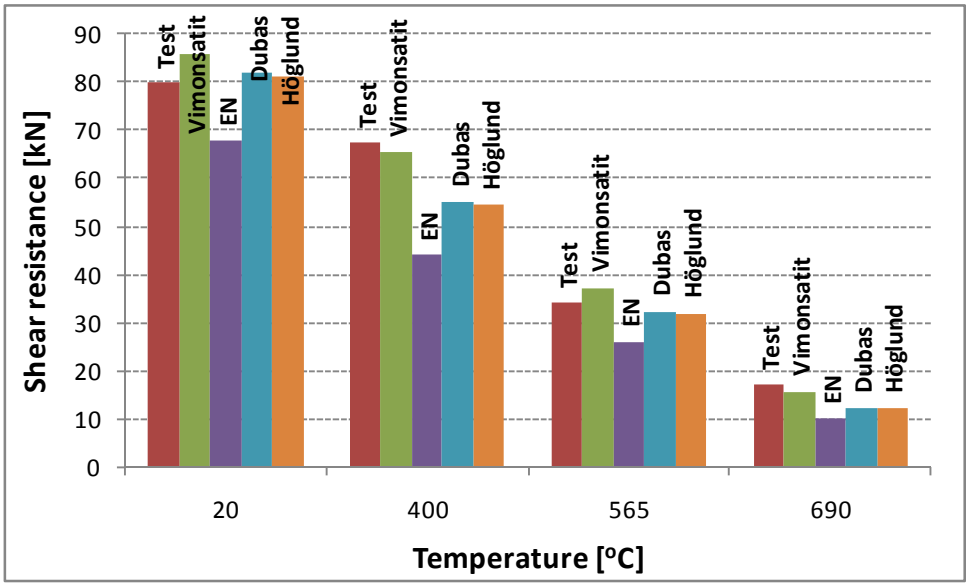

Figure 3.11. Tested shear resistances compared to Eurocodes and different theories in the case of TG3.

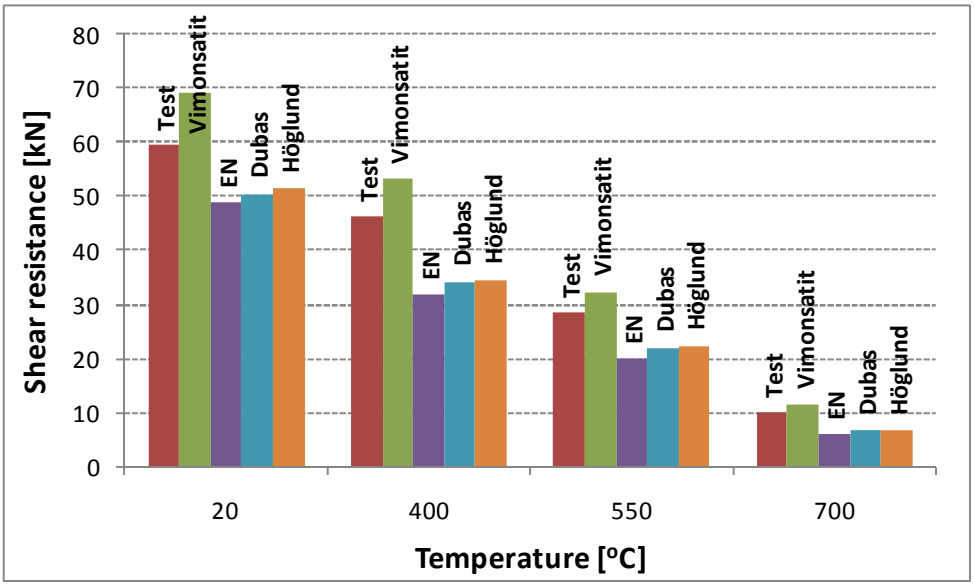

Figure 3.12. Tested shear resistances compared to Eurocodes and different theories in the case of TG5.

Based on Table 3.2 and Figures 3.11 and 3.12, it can be concluded that the analytical model presented in [Vimonsatit, Tan, Qian, 2007] gave results that were in quite good agreement with the tests but in some cases (TG5 at 20, 400 and 550 ^{o}C) the results were more than 10 % on the unsafe side.

Resistances calculated according to the Eurocodes [EN 1993-1-5, 2005], [EN 1993-1-2, 2005] were in all considered cases lower than the corresponding resistances from tests. The tension field theories of Dubas [Dubas, Gehri, 1986] and Höglund [Höglund, 1972] with EN 1993-1-2 reductions also gave resistances that were in most cases on the safe

side compared to test results. On average, the calculated resistances at elevated temperatures according to Eurocodes, Dubas' and Höglund's theory were 52, 32 and 31 % on the safe side, respectively.

All calculated Eurocode resistances for slender webs were more conservative at 690–700 ^{o}C than at ambient and other elevated temperatures. The possible reason for that is that Vimonsatit, Tan and Qian performed steady-state tests while the material model of EN 1993-1-2 [EN 1993-1-2, 2005] is based on transient test results.

3.4 Non-uniform temperature across the height of the plate

The temperature across the web height may vary in many different ways. The temperature distributions used in this study are motivated by fire tests results on a typical slim floor hat beam [Teräsnormikortti N:o 21/2009, 2009], an all-metal sandwich panel [Heinisuo, Ylihärsilä, 2006] and thermal analyses of an all-metal sandwich panel by FEM [Salminen, 2010], [Ala-Outinen et al, 2006].

Figure 3.13 shows the dimensions of the tested hat beams [Teräsnormikortti N:o 21/2009, 2009]. Three thicknesses of the lower flange (t_{lf}) were considered (10, 15 and 30 mm). The gas temperatures (below the beam) of the tests followed the standard temperature-time curve (Eq. (3.2)) [EN 1991-1-2, 2002] leading to temperature distributions shown as a function of the relative height co-ordinate (y/h) in Figure 3.14. The hat beams were embedded in concrete slabs to simulate an actual slim floor construction.

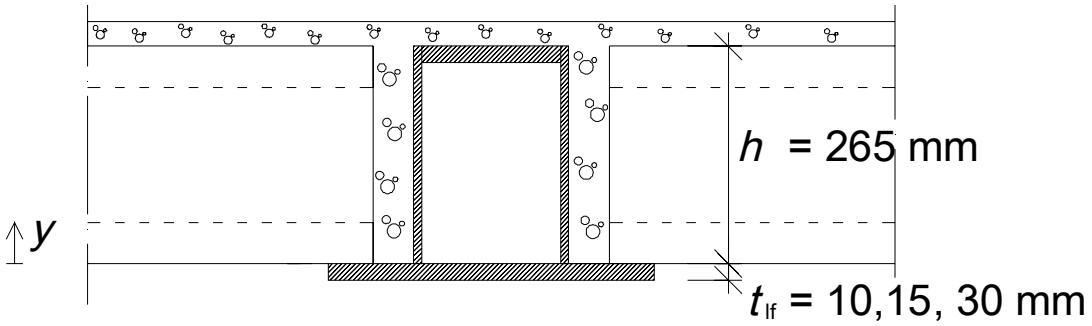

Figure 3.13. Hat beam dimensions.

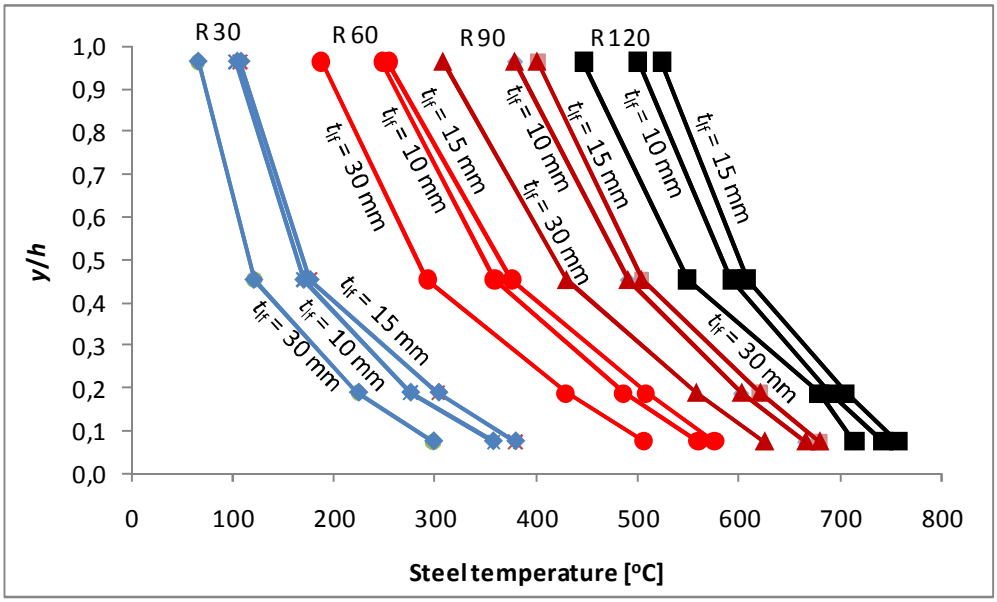

Figure 3.14. Measured temperature distributions of webs of slim floor hat beams from the reference [Teräsnormikortti 21/2009, 2009].

In a previous work [Salminen, 2010], the temperature distributions of an all-metal sandwich panel, which had no insulation inside, were calculated numerically using COMSOL Multiphysics software [COMSOL, 2008]. The FEM model was verified by comparing its results to temperatures from tests [Heinisuo, Ylihärsilä, 2006]. The results from the tests and analysis showed that the temperature distributions across the height of the web were highly non-uniform (Fig. 3.15). Thermal and mechanical FEM calculations on a similar panel with insulation can be found from the reference [Ala-Outinen et al, 2006].

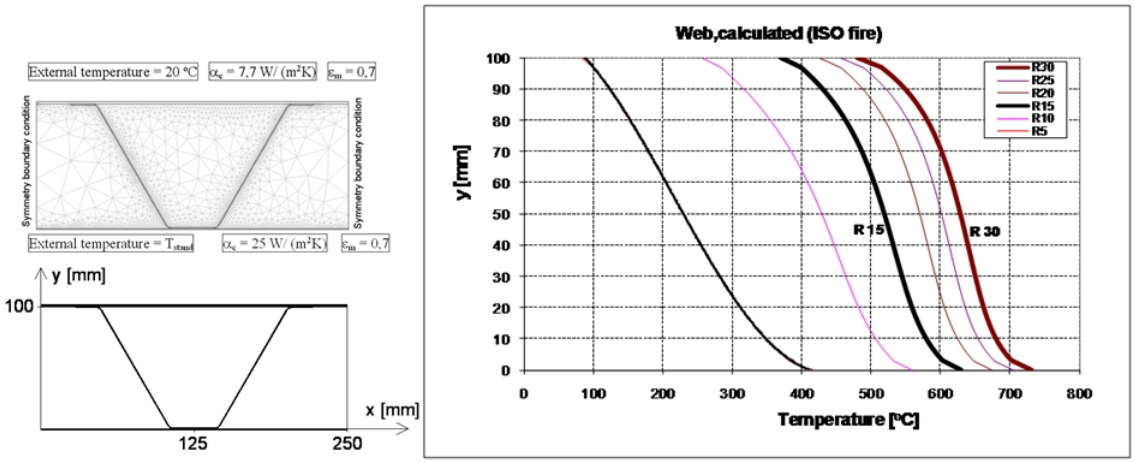

Figure 3.15. Calculated temperature distributions across non-insulated all-metal sandwich panel [Salminen, 2010].

The problem in this case is the definition of the right temperature and the reduction factors. In Eurocodes [EN 1993-1-2, 2005], [EN 1999-1-2, 2007], the average

temperature and 0.2 % proof strength is used in the reduction of ambient temperature shear resistance (see Eq. (3.3)). In Chapter 1, it was shown that numerous failure theories for ultimate shear resistance of thin plate are proposed at ambient temperatures. Therefore, the idea of proposing a tension field theory for non-uniform elevated temperatures is rejected and the strategy of finding a reliable way to reduce ambient temperature resistance is employed.

The buckling phase was studied in reference [Salminen, 2010], and it was shown that when a reduction factor based on the average temperature of the plate at non-uniform elevated temperatures is used, the results are almost always clearly on the unsafe side compared to FEM analysis. Moreover, a graphical design method intended to predict the shear buckling load of a thin metal plate at non-uniform elevated temperatures was proposed. The results from the method agreed well with those from FEM simulations and were on the safe side in most cases. The method proposed in [Salminen, 2010] is presented and utilised with a method intended to predict the ultimate shear resistance in Chapter 5.1.

4 FEM ANALYSES

The numerical analyses of this study were conducted using ABAQUS [ABAQUS, 2010] FEM software. Metal (carbon steel, aluminium and stainless steel) plates of different properties were considered at ambient, uniform elevated and non-uniform elevated temperatures. Chapter 4.1 presents all considered cases including the properties of the plates and temperature distributions. Chapter 4.2 describes the modelling of the benchmark case, for which test results [Vimonsatit, Tan, Qian, 2007] at ambient and uniform elevated temperatures are available. The main differences with the other cases (e.g. different aspect ratio, aluminium and stainless steel plates) are also pointed out. Chapter 4.3 provides a convergence study and sensitivity analysis considering the meshing and imperfections. All results of the numerical modelling are shown in Chapter 4.4, and finally a discussion of the obtained results is presented in Chapter 4.5.

4.1 Considered cases

This chapter presents all the calculated cases of this study. Properties of all considered plates are shown in Chapter 4.1.1 and temperature distributions in Chapter 4.1.2. Ambient temperature resistances were also calculated for each plate. Moreover, resistances at uniform elevated temperatures were calculated for some plates including the benchmark case.

4.1.1 Properties of the plates

All the considered plates are shown in Tables 4.1−4.2. A total of 12 carbon steel- (PL1−PL12), two aluminium plates made of alloy 5083-H111/5083-O (PLa1 and PLa2) and two stainless steel (grade 1.4301) plates (PLs1 and PLs2) were considered. All plates were selected so that elastic shear buckling preceded yielding at ambient temperature (theoretically $\lambda > 1$). Table 4.1 shows the properties of the carbon steel plates which were first considered in reference [Salminen, Heinisuo, 2011(b)]. These eight square plates include so-called benchmark cases (PL2 and PL7) for which test results at ambient and at uniform elevated temperatures are available [Vimonsatit, Tan, Qian, 2007]. More specific analyses were performed in the case of these plates.

Table 4.1. Properties of the carbon steel plates analysed in reference [Salminen, Heinisuo, 2011(b)] (benchmark cases in bold).

Plate	Boundaries	Geometry (a x h x t) [mm]	f_y [N/mm^2]	E [N/mm^2]	h/t	λ
PL1	Simple	305 x 305 x 1	355	210 000	305	3.28
PL2	**Simple**	**305 x 305 x 1.5**	**332**	**200 000**	**203**	**2.17**
PL3	Simple	305 x 305 x 2	355	210 000	153	1.64
PL4	Simple	305 x 305 x 1	235	210 000	305	2.67
PL5	Simple	305 x 305 x 1.5	235	210 000	203	1.78
PL6	Clamped	305 x 305 x 1	355	210 000	305	2.63
PL7	**Clamped**	**305 x 305 x 1.5**	**332**	**200 000**	**203**	**1.73**
PL8	Clamped	305 x 305 x 1	235	210 000	305	2.14

Table 4.2 presents the plates considered first in this study. These plates also include aspect ratios, a/h = 0.5, 2 and 3 (PL10−PL12). Carbon steel grade S460 (PL9), aluminium (PLa1 and PLa2) and stainless steel (PLs1 and PLs2) plates were also considered. The slenderness parameters λ for aluminium plates were calculated using Equation (2.51) (intermediate web stiffeners).

Table 4.2. Properties of the plates analysed in this study.

Plate	Boundaries	Geometry (a x h x t) [mm]	f_y or f_o/f_u [N/mm^2]	E [N/mm^2]	h/t	λ
PL9	Simple	305 x 305 x 2	460	210 000	153	1.87
PL10	Simple	152.5 x 305 x 1	235	210 000	305	1.62
PL11	Simple	610 x 305 x 1	235	210 000	305	3.24
PL12	Simple	915 x 305 x 1	235	210 000	305	3.39
PLa1	Simple	305 x 305 x 1.5	125/275	70 000	203	2.28
PLa2	Simple	305 x 305 x 2	125/275	70 000	153	1.71
PLs1	Simple	305 x 305 x 1	210/520	200 000	305	2.59
PLs2	Simple	305 x 305 x 1.5	210/520	200 000	203	1.72

4.1.2 Temperature distributions

The shear resistances of the plates presented in Tables 4.1 and 4.2 were calculated at ambient temperature and at 18 different non-uniform temperatures. Moreover, some cases, including the benchmark case, were also calculated at uniform elevated temperatures.

Non-uniform temperature distributions across the plate height for carbon steel were: 100−300, 100−500, 100−700, 100−900, 200−500, 300−600, 400−700, 500−800 and 600−900 ^{o}C. The reductions in material properties of carbon steel, aluminium and stainless steel are totally different at elevated temperatures. Moreover, the material model of aluminium is based on test results [Maljaars, 2008], which were conducted at

up to 350 °C while in EN 1993-1-2 [EN 1993-1-2, 2005] the material models of carbon and stainless steel are presented up to 1200 °C. Therefore, different temperature distributions were applied in the case of each material. In the case of aluminium, the following temperature distributions were applied: 50−200, 50−250, 50−300, 50−350, 100−250, 125−275, 150−300, 175−325 and 200−350 °C. For stainless steel the distributions were: 100−400, 100−600, 100−800, 100−1000, 200−600, 300−700, 400−800, 500−900 and 600−1000 °C. All distributions were considered linear and non-linear (3rd order polynomial) so that the hottest temperature occurs at the lower edge of the plate as shown in Figure 4.1 and Equations (4.1) and (4.2). The temperature distributions were motivated by fire tests on hat beams [Teräsnormikortti 21/2009, 2009] and FEM analysis and fire tests on an all-metal sandwich panel [Salminen, 2010], [Heinisuo, Ylihärsilä, 2006]. Figures 4.2−4.4 show all the non-uniform temperature distributions applied in the FEM analyses. In addition, temperature distributions from [Salminen, 2010] were applied in the worked example of the calculation method presented in Chapter 5.1.2.

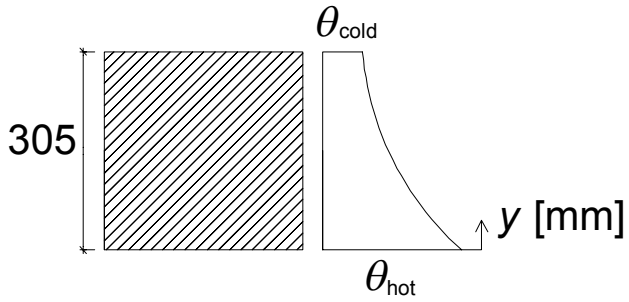

Figure 4.1. Temperature distributions.

Linear distribution: $$\theta(y) = \theta_{cold} + (1 - \frac{y}{305})(\theta_{hot} - \theta_{cold}) \quad (4.1)$$

Non-linear distribution: $$\theta(y) = \theta_{cold} + (1 - \frac{y}{305})^3(\theta_{hot} - \theta_{cold}) \quad (4.2)$$

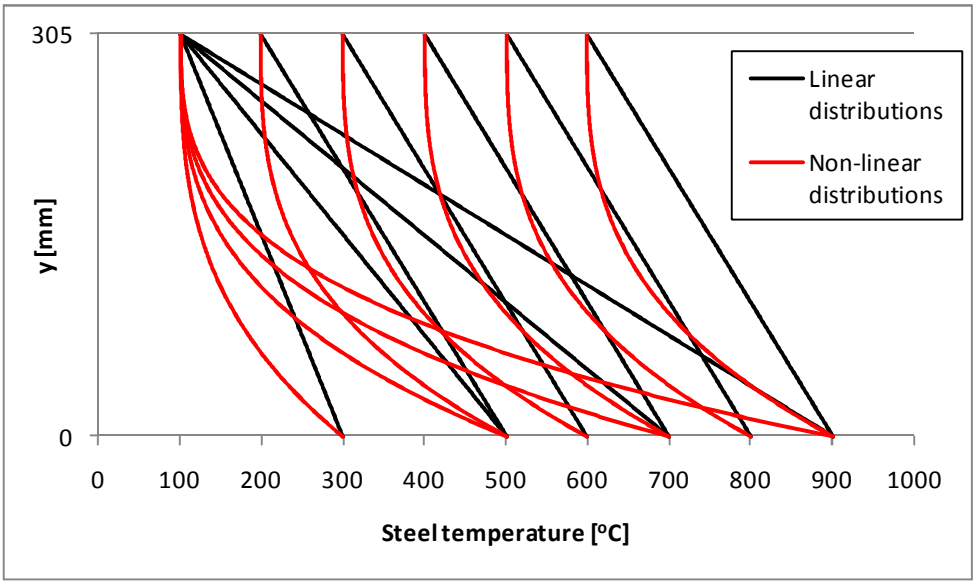

Figure 4.2. Temperature distributions of this study for carbon steel plates.

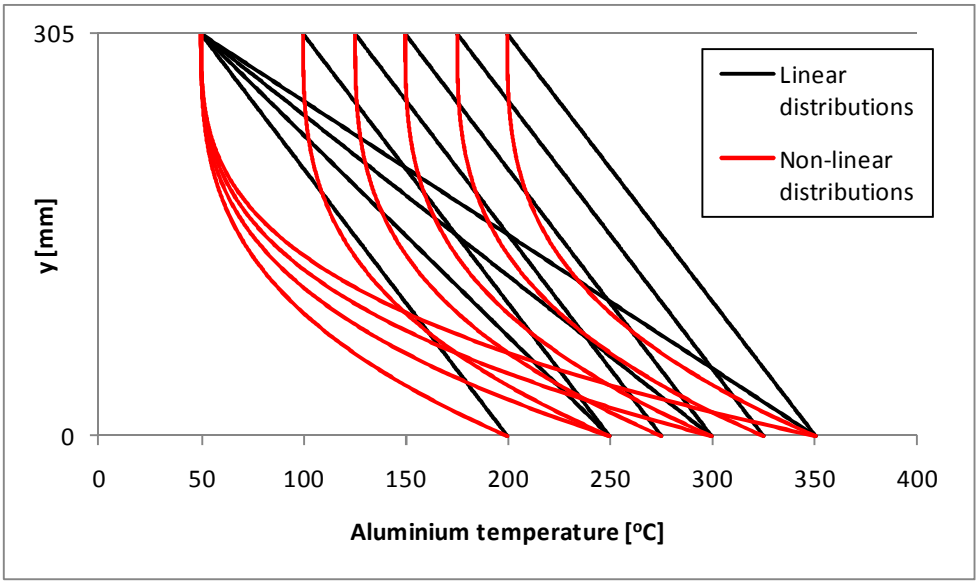

Figure 4.3. Temperature distributions of this study for aluminium plates.

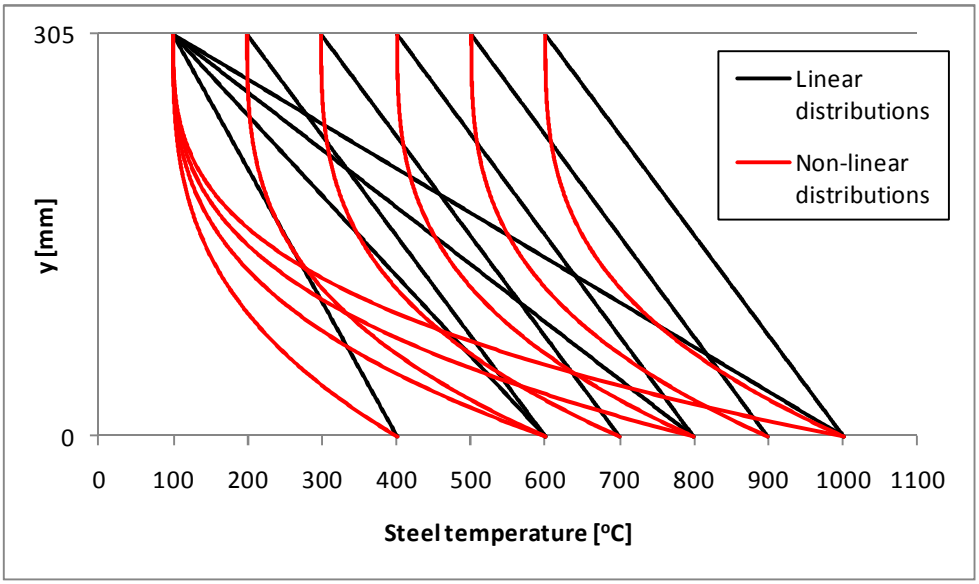

Figure 4.4. Temperature distributions of this study for stainless steel plates.

4.2 Modelling

The modelling of the benchmark cases (PL2 and PL7) [Vimonsatit, Tan, Qian, 2007] is described in Chapter 4.2.1. The procedure was the same for other plates of different properties and with plates made of aluminium and stainless steel. However, the differences in the modelling are pointed out where necessary (e.g. different aspect ratio), and the applied material models for aluminium and stainless steel are shown in Chapter 4.2.2. The modelling of the benchmark case is also shown in more detail in Appendix A

4.2.1 Benchmark case

The properties of the tested web girders (Chapter 3.3) [Vimonsatit, Tan, Qian, 2007] were the same as with plates PL2 and PL7. The only difference between modelled plates PL2 and PL7 was that PL2 was simply supported and PL7 was clamped. In the tests [Vimonsatit, Tan, Qian, 2007] the web was welded between flanges and vertical stiffeners. The nominal distance between the flanges and the vertical stiffeners was 305 mm. The yield strength (332 N/mm^2) and elastic modulus (200 000 N/mm^2) of the web material were measured in the tests. The test results are considered in more detail in Chapter 3.3.

The dimensions (a x h x t) of the benchmark case plates were 305 x 305 x 1.5 mm^3. Boundary conditions are shown in Tables 4.3 and 4.4 (see also Fig. 4.5). Uniformly distributed stress of 1 kN/(t x h) was applied on the edges of the plate as shown in Figure 4.6. The stress was then multiplied by the load proportionality factor, which gives the maximum shear load of the plate in kN. Uniformly applied shear loads have

been applied also in other recent studies concerning ultimate shear resistance of thin plates [Alinia et al, 2009], [Lee et al, 2008], [Estrada et al, 2007], [Yoo, Lee, 2006].

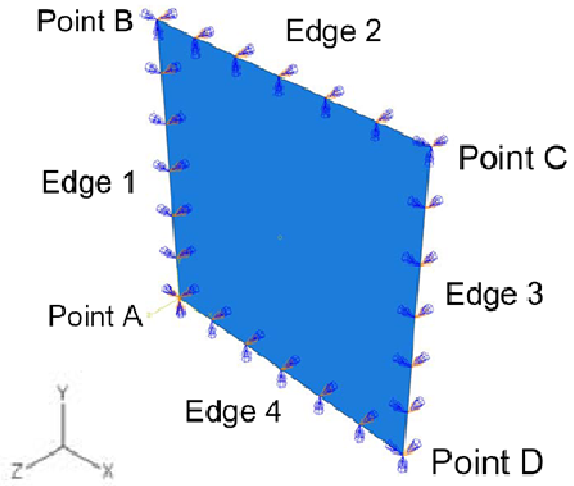

Figure 4.5. Boundaries and co-ordinate system of modelled plates [Salminen, 2010].

Table 4.3. Boundary conditions for simply supported plates (0 – not constrained, 1 – constrained).

Location	u_x	u_y	u_z	ROTx	ROTy	ROTz
Point A	1	1	1	1	1	1
Points B, C and D	0	0	1	1	1	1
Edges 1 and 3	0	0	1	1	0	1
Edges 2 and 4	0	0	1	0	1	1

Table 4.4. Boundary conditions for clamped plates (0 – not constrained, 1− constrained).

Location	u_x	u_y	u_z	ROTx	ROTy	ROTz
Point A	1	1	1	1	1	1
Points B, C and D	0	0	1	1	1	1
Edges 1 and 3	0	0	1	1	1	1
Edges 2 and 4	0	0	1	1	1	1

Similar boundary conditions have also been used in other studies concerning shear buckling and post-buckling of plates, such as [Yoo, Lee, 2006], [Alinia et al, 2009].

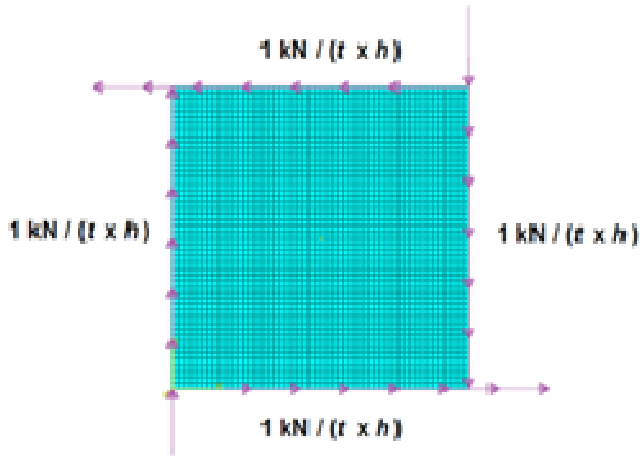

Figure 4.6. Applied loading and mesh (50 elements along the edges).

Non-linear behaviour of carbon steel material at elevated temperatures was taken into account according to EN 1993-1-2 [EN 1993-1-2, 2005] as shown in Figure 4.7. The obtained results are therefore valid for heating rates between 2 and 50 K/min [EN 1993-1-2, 2005]. In the tests [Vimonsatit, Tan, Qian, 2007] the heating rate was 7 K/min. Stress-strain relationships were inputted in ABAQUS every 50 ^{o}C and linear interpolation was used between these temperatures. It should be noted that creep strain is implicitly introduced in this stress-related strain [EN 1993-1-2, 2005]. True stresses (σ_{true}) and logarithmic strains ($\varepsilon_{ln,pl}$) were calculated and used in modelling as given in Equations (4.3) and (4.4). The initial value of the elastic modulus E was reduced according to EN 1993-1-2 [EN 1993-1-2, 2005] (Fig. 3.1). ABAQUS [ABAQUS, 2010] uses the value of elastic modulus until the proportional limit is reached. The Poisson's ratio ν is supposed to be 0.3 also at elevated temperatures.

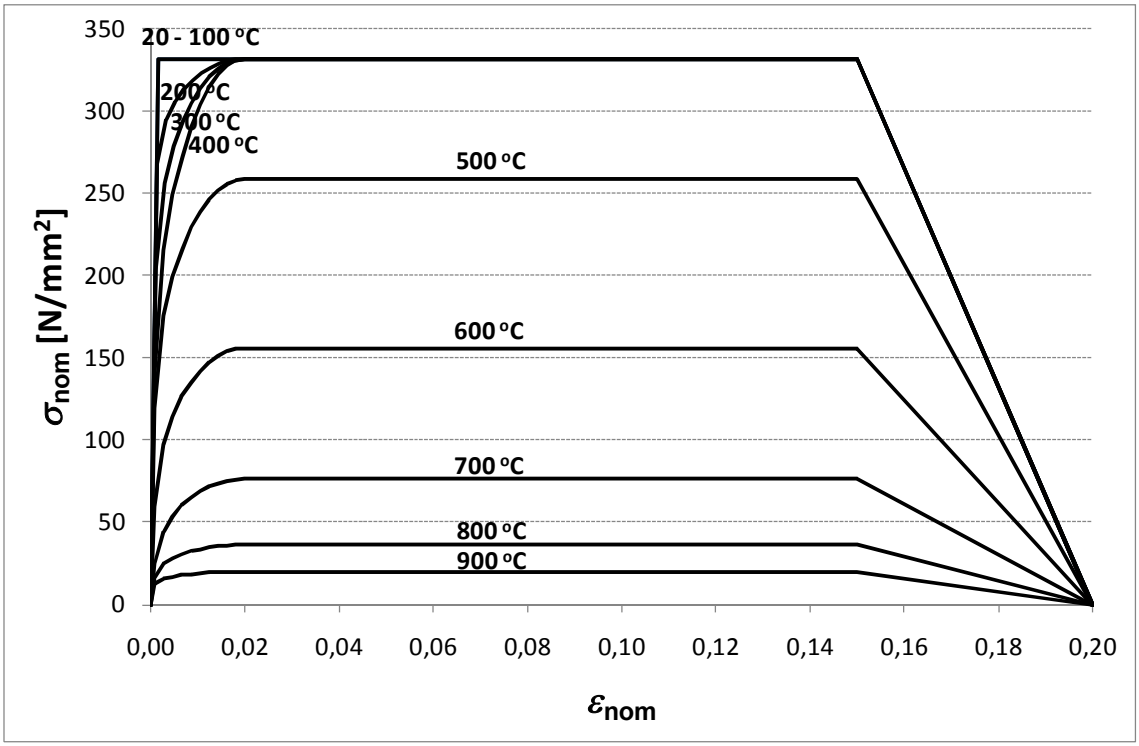

Figure 4.7. Stress-strain formulation according to EN 1993-1-2 [EN 1993-1-2, 2005] for the benchmark case (f_y = 332 N/mm^2).

$$\sigma_{true} = \sigma_{nom}(1 + \varepsilon_{nom}) \tag{4.3}$$

$$\varepsilon_{\ln, pl} = \ln(1 + \varepsilon_{nom}) - \frac{\sigma_{true}}{E} \tag{4.4}$$

Each edge of plate PL2 (and PL7) consisted of 50 nodes of four-node reduced-integration quadrilateral shell elements, coded as S4R in ABAQUS. These elements are capable of modelling elastic, plastic and large-strain behaviours and can simulate both membrane and flexural behaviours. The elements have three rotational and three translational degrees of freedom per node. Element S4R uses thick shell theory as shell thickness increases and becomes a Kirchhoff thin shell element as thickness decreases ($t < h/15$, the cases of this study) and transverse shear deformation becomes very small [ABAQUS, 2010]. The same element of ABAQUS and a corresponding one of other softwares has been used in other recent studies on the buckling and post-buckling behaviour of plates [Habashi, Alinia, 2009], [Alinia et al, 2009(a)], [Yoo, Lee, 2006], [Kaitila, 2004]. Plates with aspect ratios a/h = 0.5, 2 and 3 consisted of 25 x 50, 100 x 50 and 150 x 50 elements, respectively. In reference [Habashi, Alinia, 2009], 30 x 30 elements were the minimum requirement for the square plate in the analysis of thin unstiffened steel plate shear walls (SPSWs) when using the same software and elements at ambient temperature. Similar conclusions concerning mesh refinement have also been drawn in other studies related to shear buckling and shear resistance of thin metal plates, such as [Yoo, Lee, 2006], [Alinia et al, 2008], [Alinia et al, 2009(a)].

Newton-Raphson method and its modifications are often used in non-linear FEM analysis. However, it fails to trace the non-linear equilibrium path through the limit point because in the vicinity of the limit point (shear buckling in this case), the tangent matrix becomes singular and the iteration process diverges. Therefore, arc-length control (modified Riks method) was used as an incrementation procedure. In this method, the load increment for each load step is considered as an unknown and it is solved as a part of the solution [Reddy, 2004]. Thus, the modified Riks method is a displacement based procedure which allows for the decrease in the applied load, unloading and softening [Alinia, 2010]. The sizes of the initial, minimum and maximum increments were made appropriate for each case so that the displacement–shear force curve was smooth, which required approximately 15−30 increments depending on the temperature distribution until the maximum shear resistance was reached (see e.g. Figs. 4.28−4.30).

Initial imperfections were needed so that the tension field effect could occur. The three lowest eigenmodes from the linear buckling analysis were combined so that the maximum magnitude at the midpoint of the plate was $h/100$ (= 3.05 mm in all cases) as shown in Figure 4.8 (aspect ratio a/h=1, simply supported plate). The eigenmodes 1−3 for simply supported plates with aspect ratios 0.5, 2 and 3 are shown in Figure 4.9. The quantity $h/100$ is the maximum allowed imperfection after fabrication of the sheet according to EN 1090-2 [EN 1090-2, 2005]. The eigenmodes were calculated at ambient temperature separately for each considered case using the same boundary conditions, elements and mesh as in the calculation of ultimate shear resistance.

	Eigenmode 1	Eigenmode 2	Eigenmode 3
	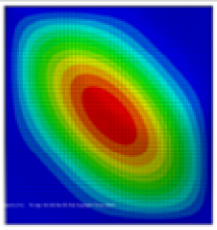	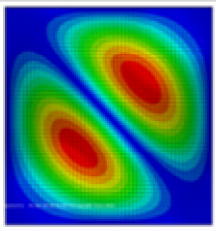	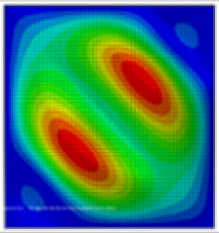
Maximum magnitude [mm]	2.4132	0.7 x h/200 = 1.0675	0.7 x 2.4132 = 1.6892
Magnitude at the midpoint of the plate [mm] (2.4132 + 0.6368 = 3.05)	2.4132	0	0.6368

Figure 4.8. Superimposition of the eigenmodes for initial imperfections [Salminen, Heinisuo, 2011(a)].

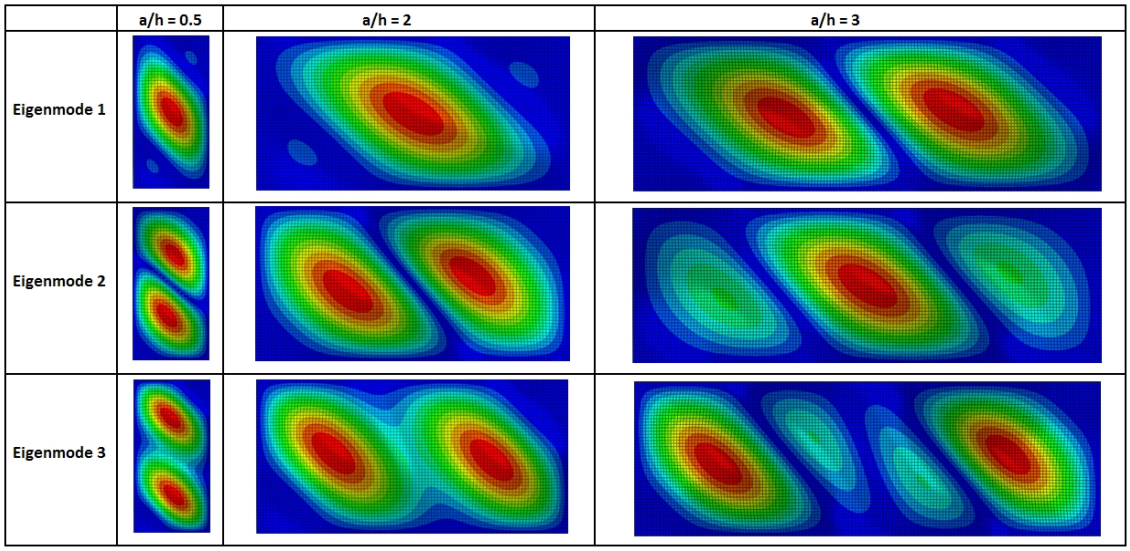

Figure 4.9. Eigenmodes applied in the imperfections for aspect ratios 0.5, 2 and 3.

Temperature distributions were given as a predefined field across the plate before loading. Movements in the x- and y-direction were prevented only at point A (see Fig. 4.5) to allow thermal elongation, which was taken into account according to EN 1993-1-2 [EN 1993-1-2, 2005].

4.2.2 Aluminium and stainless steel plates

The FEM model used for carbon steel plates was also applied to aluminium and stainless steel plates. The only differences between them were the material models. Thermal expansion was not taken into account in the cases of aluminium and stainless steel because it was observed to have no effect on the results for carbon steel plates.

Standard EN 1999-1-2 [EN 1999-1-2, 2007] does not include a similar stress-strain relationship for aluminium at elevated temperatures as is found for carbon- and stainless steel in EN 1993-1-2 [EN 1993-1-2, 2005] (Figs. 3.2 and 3.6). The material model for the aluminium plates considered in this study was taken from the dissertation of Maljaars [Maljaars, 2008]. It is based on test results on conventional flat tensile test specimens made of alloy 5083-H111 (f_o = 125 N/mm^2 and f_u = 275 N/mm^2 according to EN 1999-1-1 [EN 1999-1-1, 2007]). The uniaxial steady state tests were conducted at temperatures of 20, 200, 250, 300 and 350 ^oC and the stress-strain curves, which take creep implicitly into account were derived for constant heating rates corresponding to 30, 60, 90 and 120 minutes [Maljaars, 2008] (see also Chapter 3.1.4). The curve corresponding to a 30 minute constant heating rate was chosen for this study. The design curves at elevated temperatures are given in [Maljaars, 2008] up to strain ε = 0.015. In modeling, stress is assumed subsquently to remain the same until ε = 0.3 and to decrease then to zero. Chapter 4.4.3 shows the strain values when the maximum force at elevated temperatures is reached to prove that strains are relatively small at that stage.

It should be noted that the relative values $f_{0.2,\theta} / f_{0.2}$ in EN 1999-1-2 [EN 1999-1-2, 2007] are based on steady state tests [Maljaars, 2008]. According to Maljaars, the reductions of 0.2 % proof strength $k_{o,\theta}$ in EN 1999-1-2 [EN 1999-1-2, 2007] at elevated temperatures are unsafe for alloy 5083-H111. It should be noted that the dissertation of Maljaars considers the reduction factors of alloy 5083-H111 the same as those of 5083-O even though EN 1999-1-2 [EN 1999-1-2, 2007] does not include reduction factors $k_{o,\theta}$ for alloy 5083-H111, which means that the lower limit values should be used (see Fig. 3.3). The lower limit values of EN 1999-1-2 [EN 1999-1-2, 2007] are on the safe side compared to the reduction factors $k_{o,\theta}$ from tests conducted in [Maljaars, 2008]. The material model used for aluminium in this study is shown in Figure 4.10 and the corresponding reduction factors of 0.2 % proof strengths $k_{o,\theta}$ and the lower limit values according to EN 1999-1-2 [EN 1999-1-2, 2007] are presented in Figure 4.11.

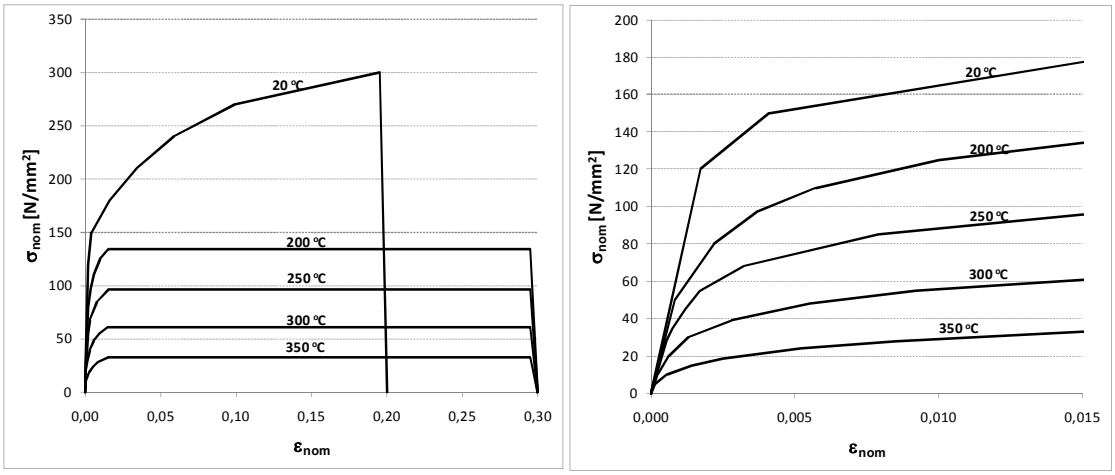

Figure 4.10. Stress-strain formulation for aluminium plates PLa1 and PLa2 (large strains at left and small strains at right).

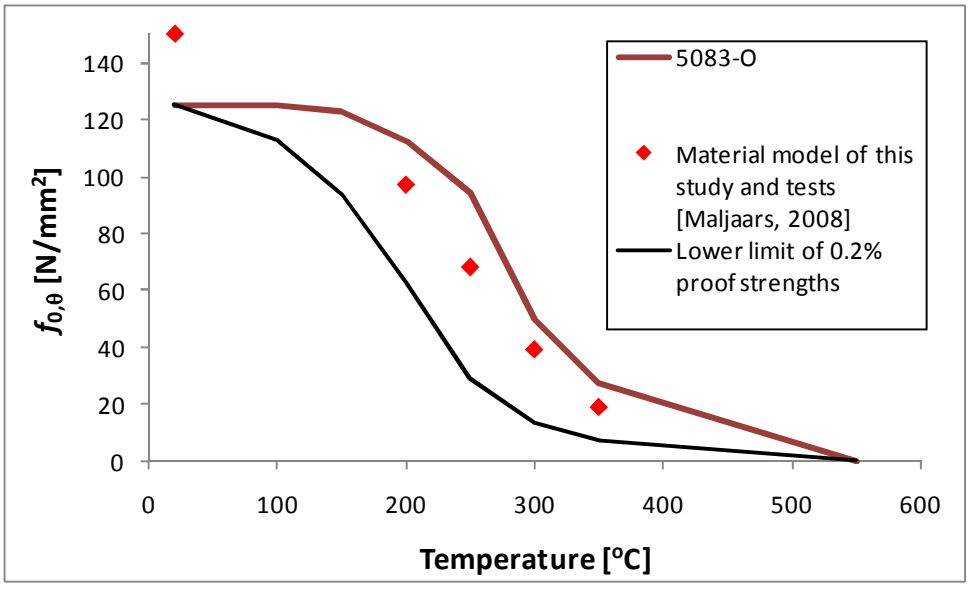

Figure 4.11. 0.2% proof strengths of material model applied in this study and EN 1999-1-2 [EN 1999-1-2, 2007] (alloy 5083-O and lower limit).

The stress-strain relationship for stainless steel at elevated temperatures is taken from Figure C.1 of EN 1993-1-2 [EN 1993-1-2, 2005]. Figure 4.12 shows the applied material model for stainless steel plates PLs1 and PLs2 (grade 1.4301, f_y = 210 N/mm^2, f_u = 520 N/mm^2).

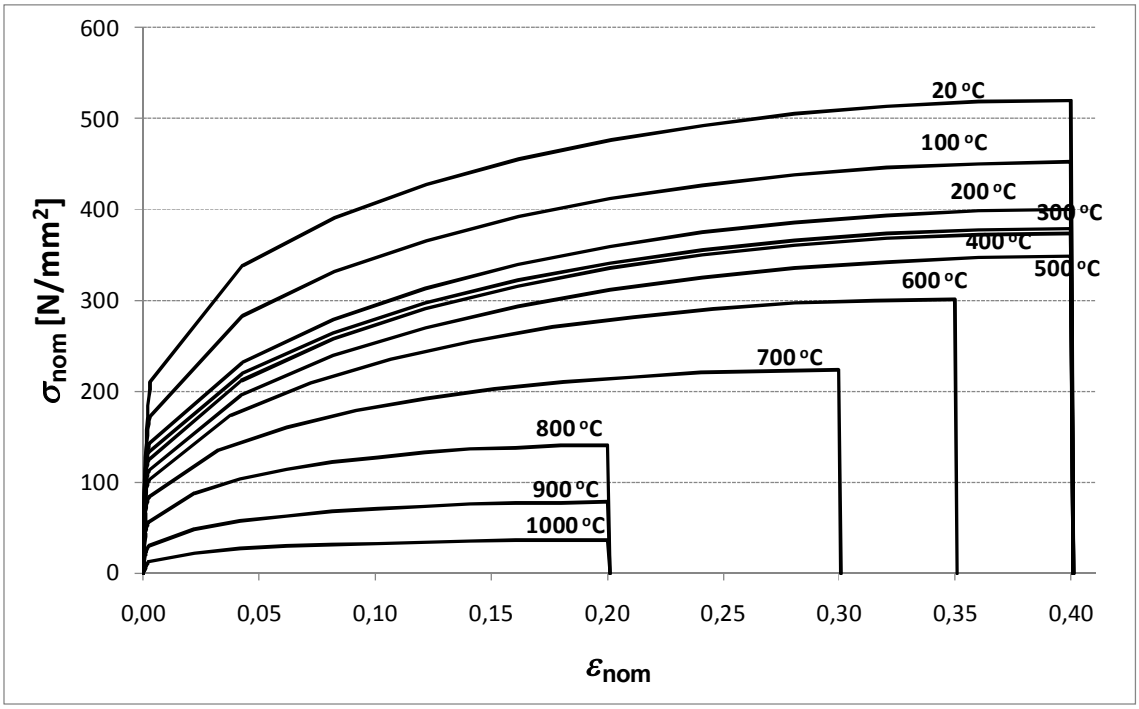

Figure 4.12. Stress-strain formulation according to EN 1993-1-2 [EN 1993-1-2, 2005] for stainless steel plates PLs1 and PLs2 (f_y = 210 N/mm^2, f_u = 520 N/mm^2).

Stress-strain relationships for stainless steel were inputted in ABAQUS every 50 °C and true stresses σ_{true} and logarithmic strains $\varepsilon_{ln,pl}$ were calculated for aluminium and stainless steel as shown in Equations (4.3) and (4.4) and used in modelling as in the case of carbon steel. The initial values of elastic modulus E were reduced for aluminium and stainless steel according to EN 1999-1-2 [EN 1999-1-2, 2007] and EN 1993-1-2 [EN 1993-1-2, 2005], respectively (Figs. 3.3 and 3.4). It should be noted that only four stress–strain curves at elevated temperatures were inputted in ABAQUS in the case of aluminium (20 for stainless steel). ABAQUS interpolates the values between the curves linearly, which may cause slight inaccuracy in the analysis of aluminium plates, especially when temperature is between 20 and 200 °C. However, when strains are less than 0.015, the right-hand side of Figure 4.10 indicates that linear interpolation between the stress-strain curves in this case describes the behaviour of aluminium relatively accurately. For example, the 250 °C curve represents closely the average values of curves 200 °C and 300 °C.

4.3 Convergence study and sensitivity analysis

The effect of mesh size on shear buckling and ultimate shear resistance is studied in Chapter 4.3.1, and a sensitivity analysis considering the effect of initial imperfections on ultimate shear resistance is presented in Chapter 4.3.2. The analyses were conducted at ambient as well as uniform and non-uniform elevated temperatures. The first FEM calculations of this study [Salminen, Heinisuo, 2010] were conducted using a bilinear material model instead of the accurate model of EN 1993-1-2 [EN 1993-1-2, 2005] (Fig. 4.7). The effect of the material model could therefore been studied with carbon steel plate PL2 at non-uniform elevated temperatures. The results of the comparison are presented in Chapter 4.4.4.

4.3.1 Meshing

Shear buckling analyses were used only for initial imperfections in this study. However, a brief convergence study to determine the suitable element mesh for shear buckling analysis was conducted for benchmark case PL2. Figure 4.13 presents the calculated eigenvalues $V_{cr,FEM}$ for benchmark case PL2 at ambient temperature as a function of used number of edge elements. The calculated values are compared to the theoretical shear buckling load (18.68 kN), which is calculated using Equations (2.5)−(2.8).

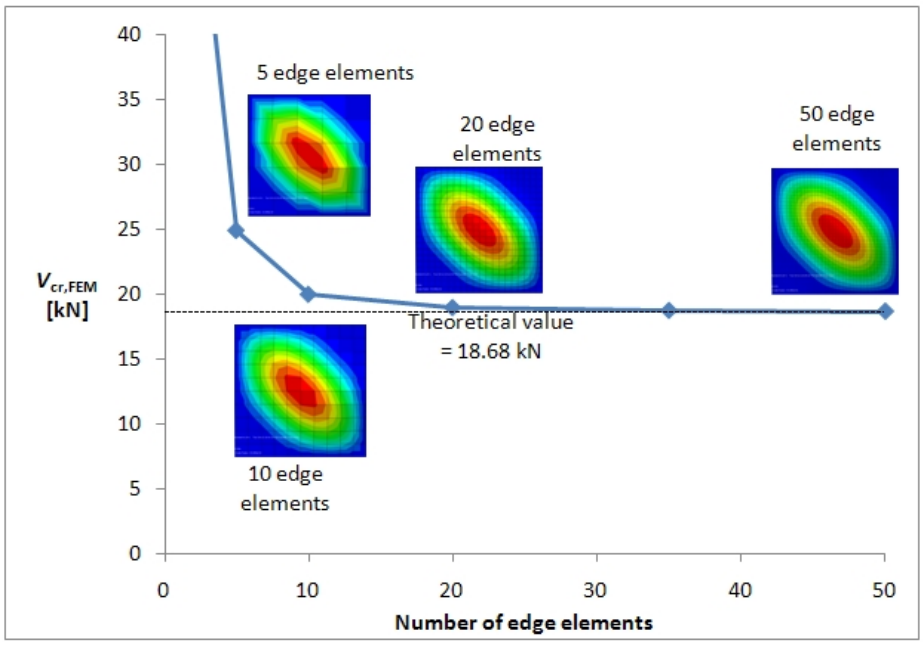

Figure 4.13. Convergence study for determining the number of edge elements (PL2, ambient temperature).

Figure 4.13 shows that in this case the shear buckling load from FEM analysis is very close to the theoretical value (Eq. (2.5)) when the model contains at least 20 edge elements. However, 50 edge elements were used in the calculation, because the

calculation time was rather short also there. Figure 4.14 presents the errors in the three first eigenvalues at ambient temperature (left) and a linear 100−900 °C (right) temperature distribution. It is assumed that FEM calculation gives an accurate result always when 50 edge elements are used.

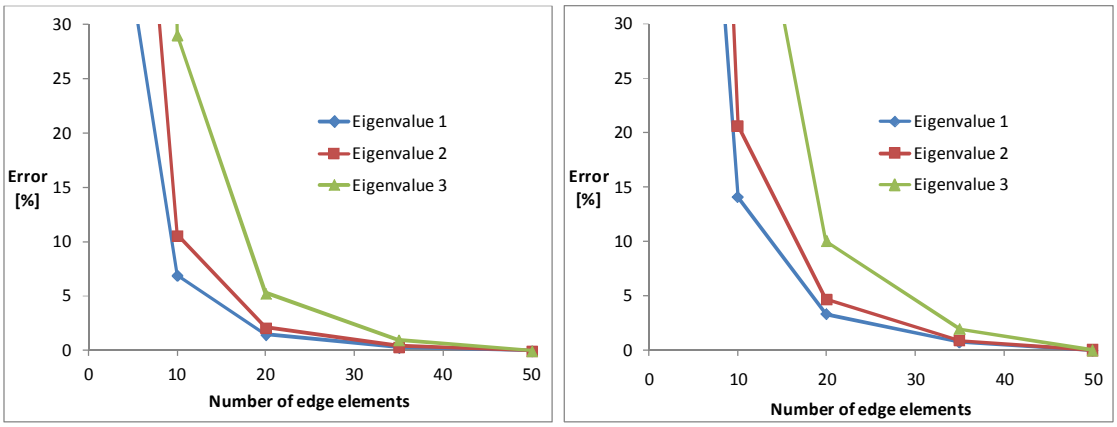

Figure 4.14. Percentage errors in shear buckling resistance at ambient (left) and elevated 100−900 °C (right) temperatures.

Ultimate shear resistances obtained with different meshes are compared in Figure 4.15. It should be noted that the initial imperfections were calculated for each case separately with the same meshing in order to apply the displacements for nodes. In this comparison, it is also assumed that FEM calculation gives an accurate result in each case when using 50 edge elements. Figure 4.16 illustrates the tension field at ambient temperature with different discretization of meshes.

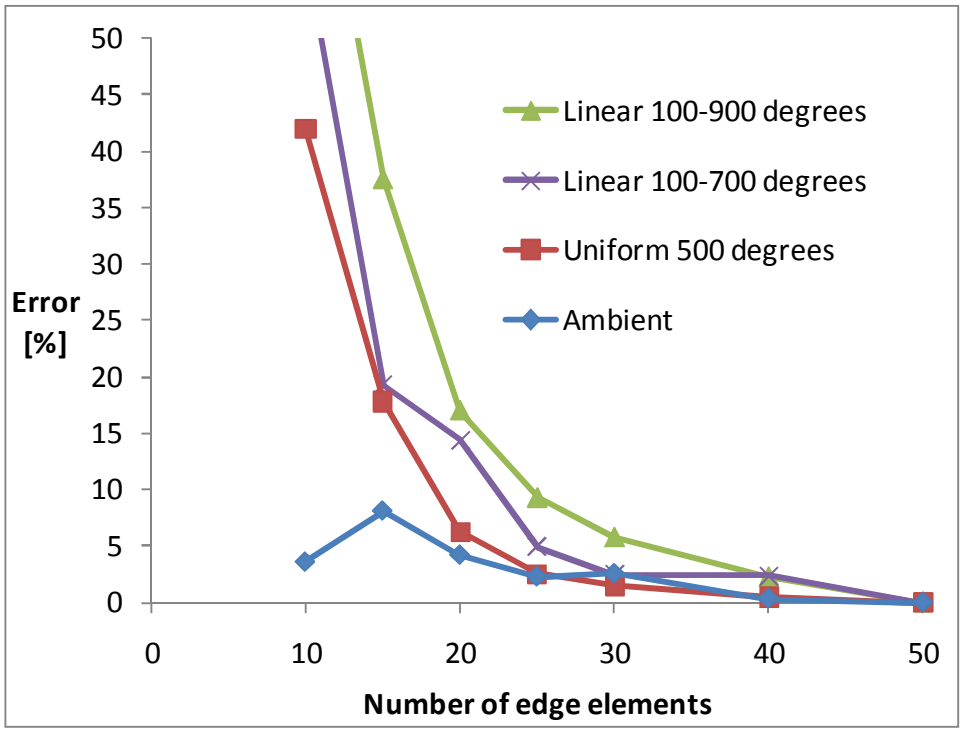

Figure 4.15. Percentage errors in ultimate shear resistance.

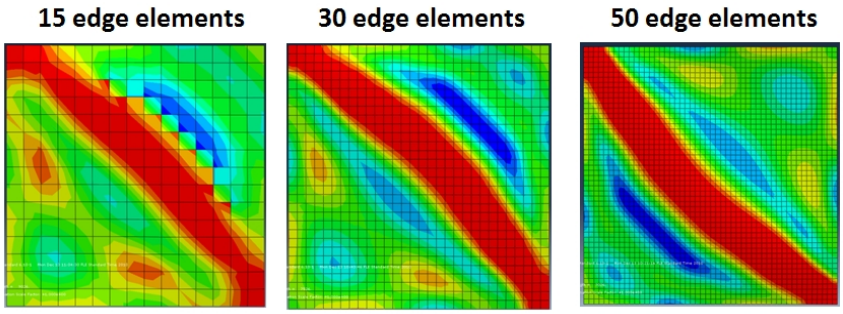

Figure 4.16. Tension fields at ambient temperature.

Based on Figures 4.14 and 4.15, it can be said that a denser element mesh is needed at elevated than at ambient temperatures to get accurate results. Moreover, it can be seen that too few elements leads to overestimated resistance. When the number of edge elements was at least 40 in this case, the results were very close. In this comparison, the most sensitive case for meshing was ultimate shear resistance at a linear temperature distribution of 100−900 ^{o}C. One hundred edge elements were used also in this case. The ultimate shear resistances with 50 and 100 edge elements were 4.00 and 3.81 kN, respectively. Moreover, the effect of the element type was tested at the linear temperature distribution of 100−900 ^{o}C. The calculated shear resistance using element type S4 of ABAQUS and 50 x 50 mesh was 3.94 kN (1.5 % smaller than with element type S4R). Element type S4 is a fully integrated, finite-membrane-strain shell element and has four integration locations per element compared with one for S4R, which makes the element computationally more expensive than S4R [ABAQUS, 2010].

It can be concluded that in this case the applied mesh (50x50 elements for a square plate) and element type S4R produce relatively accurate results within reasonable computer time. Figures 4.15 and 4.16 show that the post-buckling behaviour of the plate can also be modelled using a relatively coarse mesh, but the results may be inaccurate especially at elevated temperatures. The shapes of the tension fields shown in Figure 4.16 are clearly different for various meshes due to slightly different initial imperfections.

4.3.2 Initial imperfections

In order to find the worst possible imperfection, which yields the lowest resistance of the structure, a series of analyses need to be performed on a large range of possible imperfections. According to the results of the optimization approach by Kristanic and Korelc, it is difficult to characterize certain structures with certain types of imperfections because every change in thickness, geometry or loading conditions may change the worst imperfection significantly [Kristanic, Korelc, 2008]. It should be noted that Kristanic and Korelc performed their calculations for a compressed cantilever structure, a bended thin-walled T- and I-beam and a compressed cylinder. The paper by

Pavlovcic et al presents an initial geometric imperfection study on the shear resistance of longitudinally stiffened panels [Pavlovcic et al, 2007]. Based on their research, shear capacity has only limited sensitivity to any kind of imperfection shape variation with amplitude at the allowable fabrication tolerances (6.9 % reduction at the most compared to "perfect" structure). According to Pavlovcic et al, in the case of longitudinally stiffened panels, the imperfection direction, the critical buckling mode and different combinations of imperfections have to be tested for research purposes. For design purposes this study can be very limited [Pavlovcic et al, 2007].

In this study all final results were calculated using $h/100$ [EN 1090-2, 2005] as the magnitude and the shape presented in Figure 4.8 and 4.9 as the initial imperfection. The effects of the magnitude and shape of the given imperfection on the most slender carbon steel plate PL1 (λ = 3.28) were also studied briefly. Figures 4.17–4.19 illustrate the behaviour of PL1 at ambient and elevated temperatures at different magnitudes for the initial imperfection. The shape of the imperfection is the same as specified in Figure 4.8. Moreover, Figures 4.17–4.19 show the theoretical shear buckling resistances, calculated using Equations (2.5)–(2.8) and ultimate shear resistances for the plate alone according to EN 1993-1-5 [EN 1993-1-5, 2005] and EN 1993-1-2 [EN 1993-1-2, 2005] (Eqs. (2.44) and (3.3)). The theoretical shear buckling resistance at a non-uniform (linear 100–900 ^{o}C) temperature distribution in Figure 4.19 was calculated using the method presented in reference [Salminen, 2010] (see Chapter 5.1).

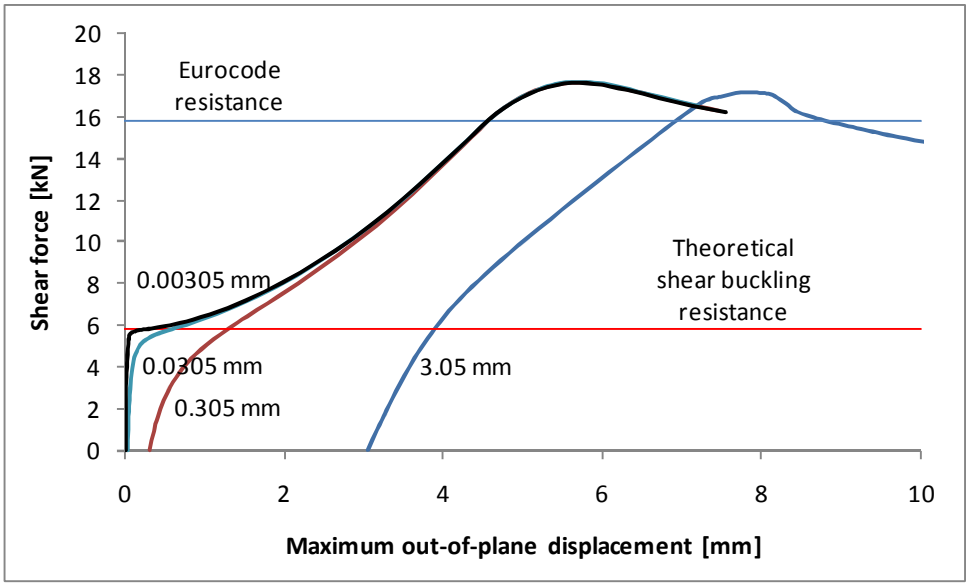

Figure 4.17. Effect of the magnitude of initial imperfection at ambient temperature.

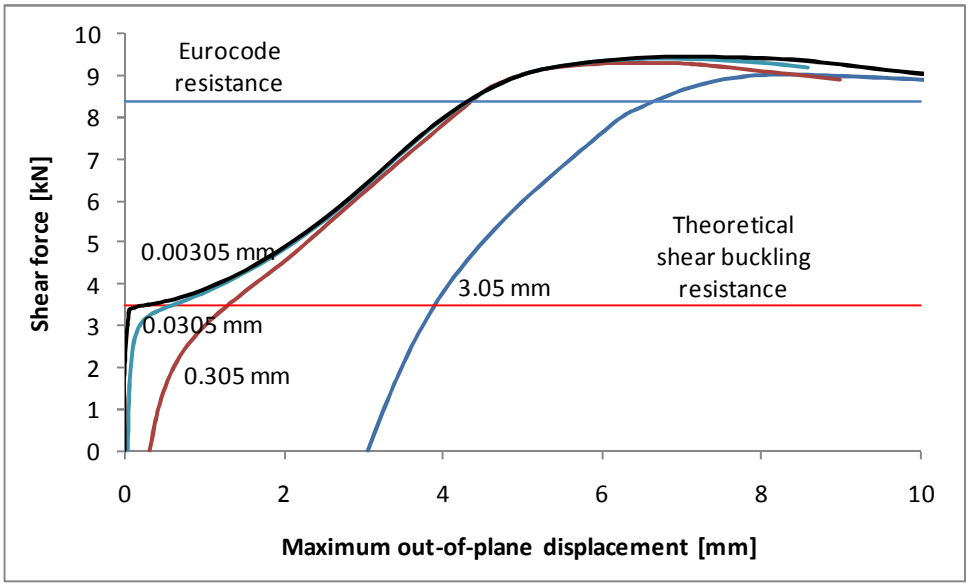

Figure 4.18. Effect of the magnitude of initial imperfection at 500 °C.

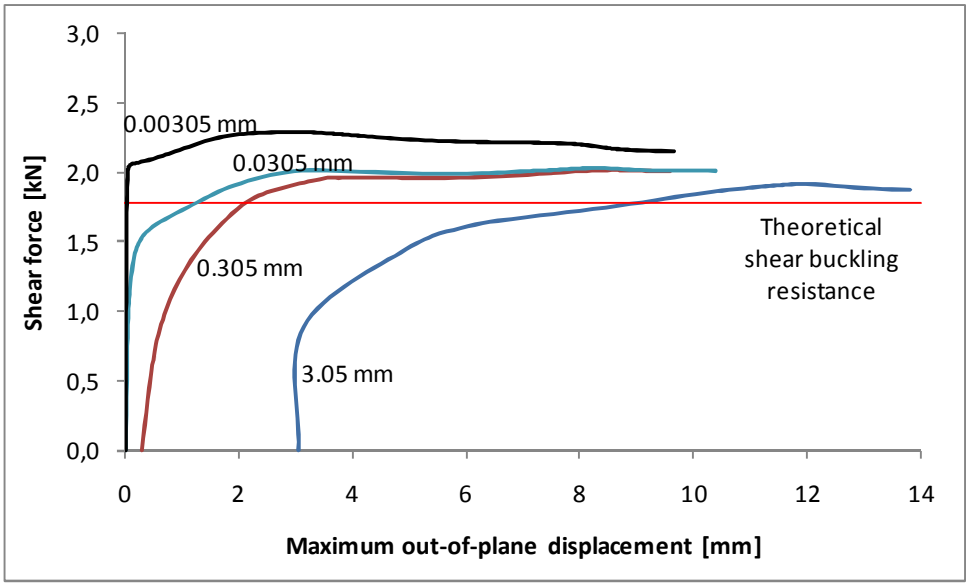

Figure 4.19. Effect of the magnitude of initial imperfection in case of a linear 100–900 °C temperature distribution.

From Figures 4.17–4.19 it can be determined that shear resistance is not considerably dependent on the magnitude of the initial imperfection at ambient and uniform 500 °C temperature. At a linear 100–900 °C temperature distribution the effect is clear. The differences in ultimate shear resistances calculated using the smallest imperfection (h/100 000 = 0.00305 mm) and the largest imperfection (h/100 = 3.05 mm) at ambient temperature, 500 °C and a linear 100–900 °C distribution were 2.5, 4.6 and 19.2 %, respectively. It can also be determined that the shear buckling phase is detectable only when the magnitude of the imperfection is very small (< h/1000 in this case). Moreover, it can be seen that the resistances according to EN 1993-1-5 [EN 1993-1-5, 2005] and

EN 1993-1-2 [EN 1993-1-2, 2005] correlate well with those from FEM in the case of ambient and at 500 °C temperatures but at a linear 100–900 °C distribution the Eurocode resistance (8.38 kN, see also Eq. (3.3)), which is calculated based on the average temperature of the plate, 500 °C is clearly on the unsafe side compared to resistances from numerical analysis. The shear buckling resistance calculated by the method proposed in reference [Salminen, 2010] is on the safe side compared to the result of the FEM calculation at a temperature distribution of 100–900 °C. The contribution of the post-buckling resistance decreases clearly in these cases compared to ambient temperature. Changes in plate behaviour at elevated temperatures are described in more detail in Chapters 4.4.3 and 4.4.4.

Based on the imperfection magnitude analysis presented in Figures 4.17–4.19, it can be concluded that the magnitude of the initial imperfection does not have a significant effect on ultimate shear resistance at ambient and uniform elevated temperatures, but at the studied non-uniform elevated temperature (Fig. 4.19) its effect is clear. Furthermore, the analysis shows that the resistances calculated with the applied magnitude (h/100) were in each case smaller than those obtained using smaller magnitudes (h/1 000, h/10 000 and h/100 000).

The effect of the shape of the imperfection was studied by applying the eight first positive and negative eigenmodes from ambient temperature analyses individually as imperfections of the most slender carbon steel plate PL1 (λ = 3.28) at ambient, uniform 500 °C and linear 100–900 °C temperatures. The magnitude of the imperfection was in each case 3.05 mm. Here, a negative eigenmode means that the shear stresses shown in Figure 4.6 act in opposite directions in the shear buckling analysis. The ultimate shear resistances calculated in this sensitivity analysis (V_{sens}) were compared to the results calculated using the imperfection applied in the calculation of the final results of this study ($V_{applied}$). Figure 4.20 presents the values V_{sens} / $V_{applied}$ for the cases considered.

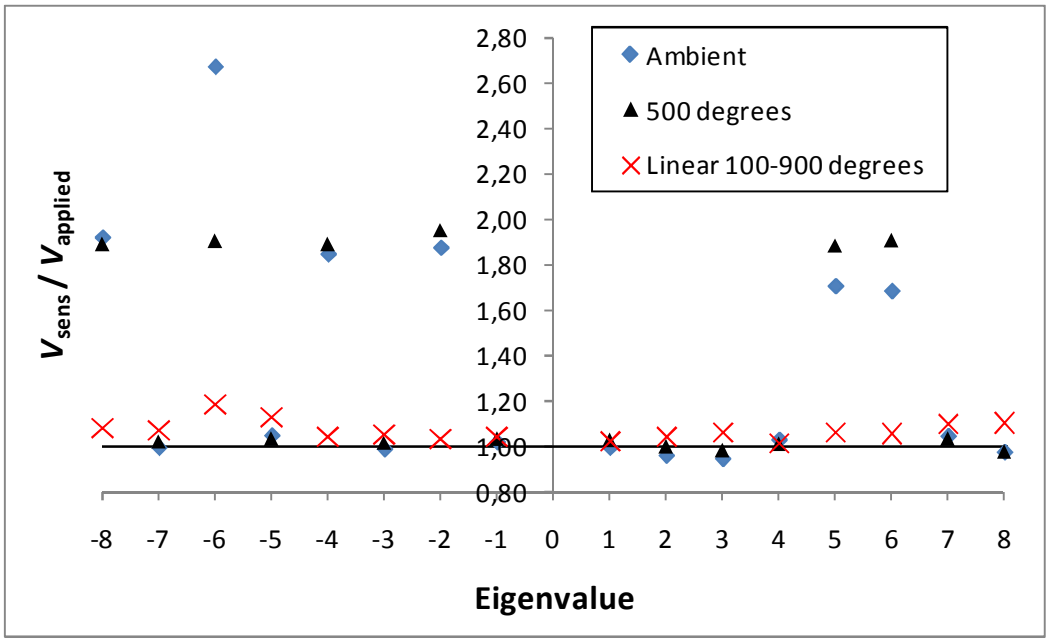

Figure 4.20. Ultimate shear resistances from sensitivity analysis compared to the basic case (Fig. 4.8).

Based on Figure 4.20, it can be said that ultimate shear resistance does not depend much on the shape of the initial imperfection in most cases, especially when using the lowest positive eigenmodes as an imperfection. However, it also appears that the resistances calculated using individual eigenmodes as imperfections were in some cases (especially at ambient and uniform 500 °C) significantly higher compared to results calculated using the imperfection defined in Figure 4.8. The smallest values for the ratio V_{sens} / $V_{applied}$ at ambient, uniform 500 °C and linear 100–900 °C temperatures were 0.94, 0.98 and 1.02, respectively. The ambient temperature result (0.94) is close to the 6.9 % reduction in the study of Pavlovcic et al [Pavlovcic et al, 2007]. It can be concluded that, especially at elevated temperatures, the imperfection applied in the calculation of the final results of this study (Fig. 4.8) gives results that are close to the minimum possible value for the resistance when using a rather arbitrary eigenmode as the imperfection.

However, it should be noted that in some cases shear resistance may increase significantly due to the applied imperfection. That happens especially when using negative eigenmodes, but such behaviour may occur also with positive eigenmodes. Figures 4.21 and 4.22 illustrate the behaviour of the considered plate at ambient and elevated temperatures when using different eigenmodes as an imperfection. Figure 4.21 considers the three lowest positive eigemodes and Figure 4.22 the positive eigenmodes 5, 6 and the negative eigenmode 2, which increase the shear resistance of the plate significantly compared to the basic case. In the imperfection graphs, red colour indicates the greatest out-of-plane displacement, in the tension field graphs at ambient and 500 °C the greatest von Mises stress, and at 100–900 °C the yielded regions. Figure 4.21

reveals that at a 100–900 °C temperature distribution the post-buckling behaviour of the considered plate is rather limited. The tension field graphs and yielded regions are plotted at the stage where maximum resistance is reached.

IMPERFECTION	TENSION FIELD, AMBIENT ($V_{applied}$ = 17.20 kN)	TENSION FIELD, 500 °C ($V_{applied}$ = 9.04 kN)	YIELDED REGIONS, 100-900 °C ($V_{applied}$ = 1.92 kN)
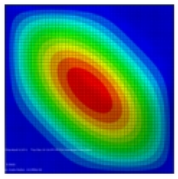 Eigenmode 1 (V_{cr} = 5.82 kN)	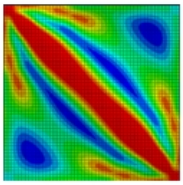 V_{ult} = 17.08 kN	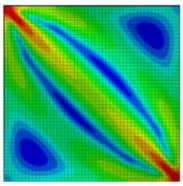 V_{ult} = 9.32 kN	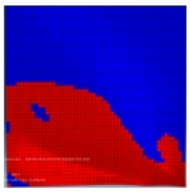 V_{ult} = 1.96 kN
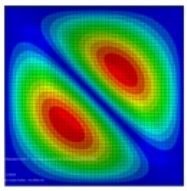 Eigenmode 2 (V_{cr} = 7.21 kN)	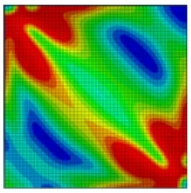 V_{ult} = 16.48 kN	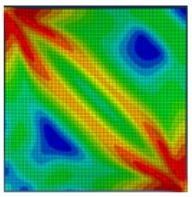 V_{ult} = 9.07 kN	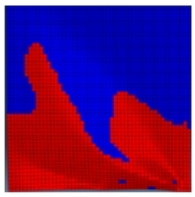 V_{ult} = 2.00 kN
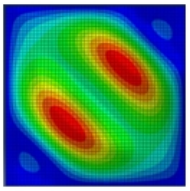 Eigenmode 3 (V_{cr} = 15.57 kN)	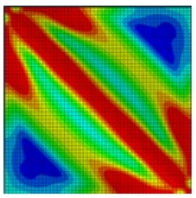 V_{ult} = 16.24 kN	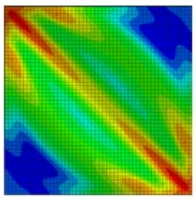 V_{ult} = 8.92 kN	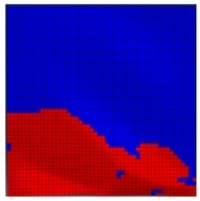 V_{ult} = 2.04 kN

Figure 4.21. Tension fields and yielded regions with eigenmodes 1–3 as imperfections.

Figure 4.21 shows that the shape of the tension field and the yielded regions clearly depend on the applied imperfection. However, in the case of the three lowest positive eigenmodes, the resistances were nearly the same at ambient as well as elevated temperatures.

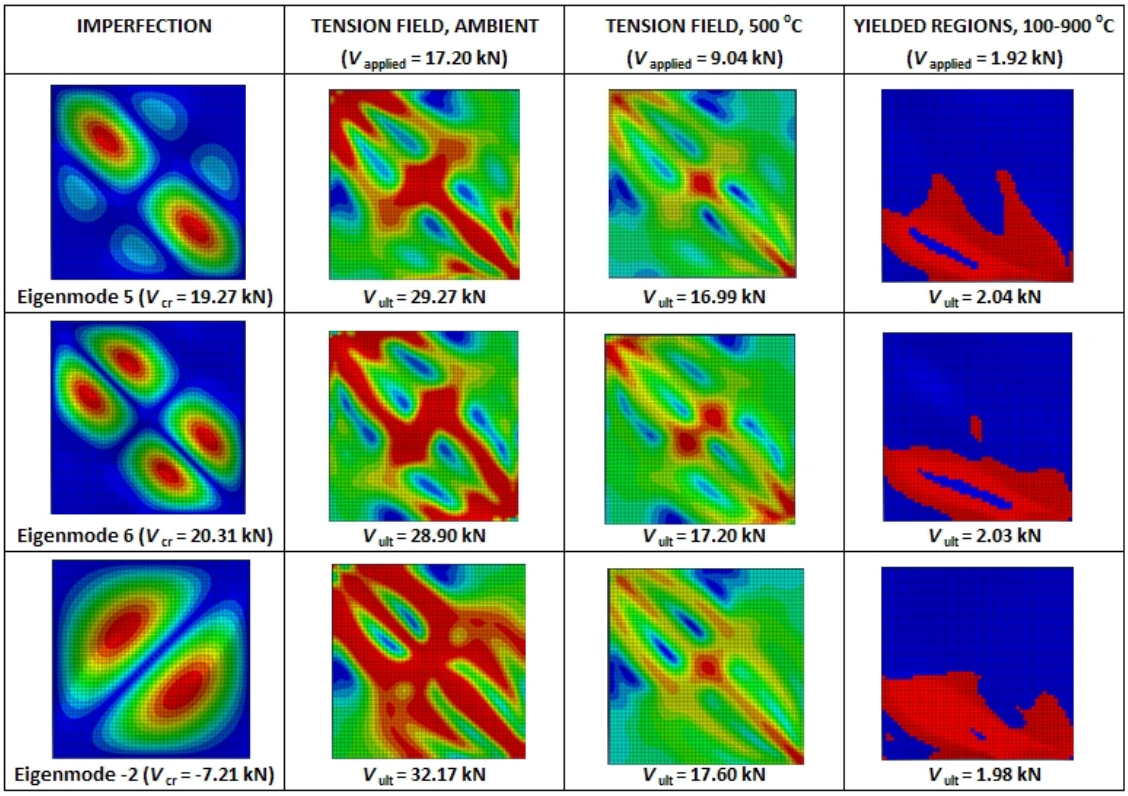

Figure 4.22. Tension fields and yielded regions with eigenmodes 5, 6 and -2 as imperfections.

Figure 4.22 (especially the ambient temperature tension field graphs) reveals that eigenmodes 5, 6 and -2 act like stiffeners and, therefore, increase shear resistance. The same observation can also be drawn from Figure 4.23 which shows all the imperfections which yielded to significantly higher resistances than in the other cases. The "stiffeners" formed by the imperfection are marked with red lines.

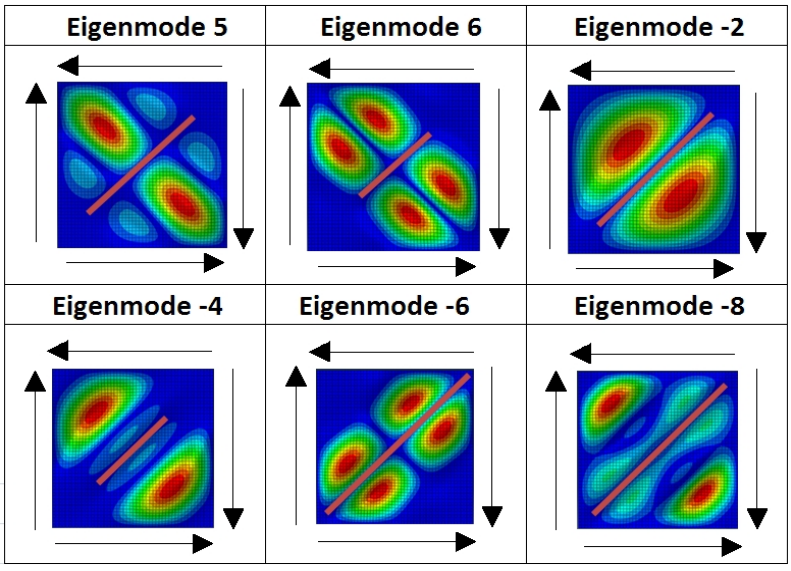

Figure 4.23. Imperfections that yielded significantly higher resistances.

It appears from Figure 4.23 that all the considered imperfections that yielded significantly higher resistances were antisymmetric with respect to the diagonal in the direction where the principal compressive stresses occur (red line in Fig. 4.23). Thus, it can be concluded that when calculating shear resistance, the applied imperfection(s) should be symmetric with respect to this direction when $a/h = 1$. Moreover, if the loading conditions are changed during the analysis, the validity of the applied imperfections should be reassessed.

4.4 Results

4.4.1 Results at ambient temperature

Tables 4.5 and 4.6 present the maximum shear loads for all considered plates at ambient temperature based on EN 1993-1-5 [EN 1993-1-5, 2005], EN 1993-1-4 [EN 1993-1-4, 2006], EN 1999-1-1 [EN 1999-1-1, 2007] and FEM calculations. FEM calculations were performed for plates PL1–PL8 using two different initial imperfections (h/100 and h/100 000).

Table 4.5. Shear resistances of plates PL1–PL8 at ambient temperature [kN].

	PL1	PL2	PL3	PL4	PL5	PL6	PL7	PL8
FEM (h/100)	17.18	35.50	64.17	13.70	29.29	19.00	38.52	14.81
FEM (h/100 000)	17.54	35.18	66.31	14.00	30.50	20.01	41.30	15.98
EN 1993-1-5	15.82	33.59	63.27	12.87	28.96	19.76	41.97	16.08
FEM (h/100)/EN	1.09	1.06	1.01	1.06	1.01	0.96	0.92	0.92

Table 4.6. Shear resistances of plates PL9–PL12, PLa1, PLa2, PLs1 and PLs2 at ambient temperature [kN].

	PL9	PL10	PL11	PL12	PLa1	PLa2	PLs1	PLs2
FEM (h/100)	74.65	17.61	10.52	8.88	13.75	23.50	10.15	21.85
EN	72.02	21.21	10.60	10.13	10.94	19.45	11.77	23.42
FEM (h/100)/EN	1.04	0.83	0.99	0.88	1.26	1.21	0.86	0.93

Based on Table 4.5, FEM results at ambient temperature were not very sensitive to changes in the magnitude of the initial imperfection as shown also in Chapter 4.3. Compared to EN 1993-1-5 [EN 1993-1-5, 2005] resistances, the resistances of carbon steel plates were slightly higher in the case of simply supported plates and slightly lower in the case of clamped plates. The FEM resistances of carbon steel plates PL10 (a/h = 0.5) and PL12 (a/h = 3) were clearly lower than EN 1993-1-5 resistances.

FEM resistances of aluminium plates PLa1 and PLa2 were clearly higher than those calculated according to EN 1999-1-1 [EN 1999-1-1, 2007] while FEM resistances for stainless steel plates (PLs1 and PLs2) were lower than the resistances according to EN

1993-1-4 [EN 1993-1-4, 2006]. It should be noted that in the case of aluminium, the applied values for 0.2 % proof strengths f_o were 150 N/mm^2 in FEM analysis (from test results [Maljaars, 2008]) and 125 N/mm^2 (EN 1999-1-1, Table 3.2a) in the calculation of EN 1999-1-1 resistance, which explains the differences in the resistances in the case of aluminium plates.

4.4.2 Benchmark case

Test results for a beam web loaded primarily in shear at ambient (20 ^{o}C) and uniform elevated temperatures (400 ^{o}C, 550 ^{o}C and 700 ^{o}C) [Vimonsatit, Tan, Qian, 2007] were used as benchmark cases in FEM simulations. The results of the test series are shown in more detail in Chapter 3.3. The properties of the tested web girders were the same as those of plates PL2 and PL7 (see Table 4.1). The only difference between PL2 and PL7 was that PL2 was simply supported and PL7 was clamped. The reference [Salminen, 2010] shows that almost all test results of reference [Vimonsatit, Tan, Qian] were on the safe side compared to EN 1993-1-2 [EN 1993-1-2, 2005] except for one test specimen, which they reported having had some problems with during the execution of the tests [Vimonsatit, Tan, Qian, 2007]. The tested web girder (PL2 and PL7) was selected as a benchmark case because it was the most slender one (h/t = 203).

Maximum shear loads from the tests and according to Eurocodes [EN 1993-1-5, 2005], [EN 1993-1-2, 2005] and FEM calculations [Salminen, Heinisuo, 2011(a)] are shown in Table 4.7. The EN 1993-1-5 resistances were calculated for the plate alone in the case of PL2 and PL7. The effect of flanges and end-posts was taken into account in the case of PL7,fl,ep when calculating the EN 1993-1-5 resistances. In FEM calculation the effect of flanges and end-posts was neglected. Figure 4.24 compares the calculated resistances (V_i) to test values (V_{test}).

Table 4.7. Comparison of shear resistances [kN].

Temperature [^{o}C]	Test result	Eurocodes (PL2)	Eurocodes (PL7)	Eurocodes (PL7,fl,ep)	FEM (PL2)	FEM (PL7)
20	59.6	33.59	41.97	55.69	35.50	40.46
400	46.4	21.83	27.28	36.20	22.42	26.30
550	28.6	13.94	17.42	23.11	14.26	16.59
700	10.16	4.37	5.46	7.24	4.68	5.60

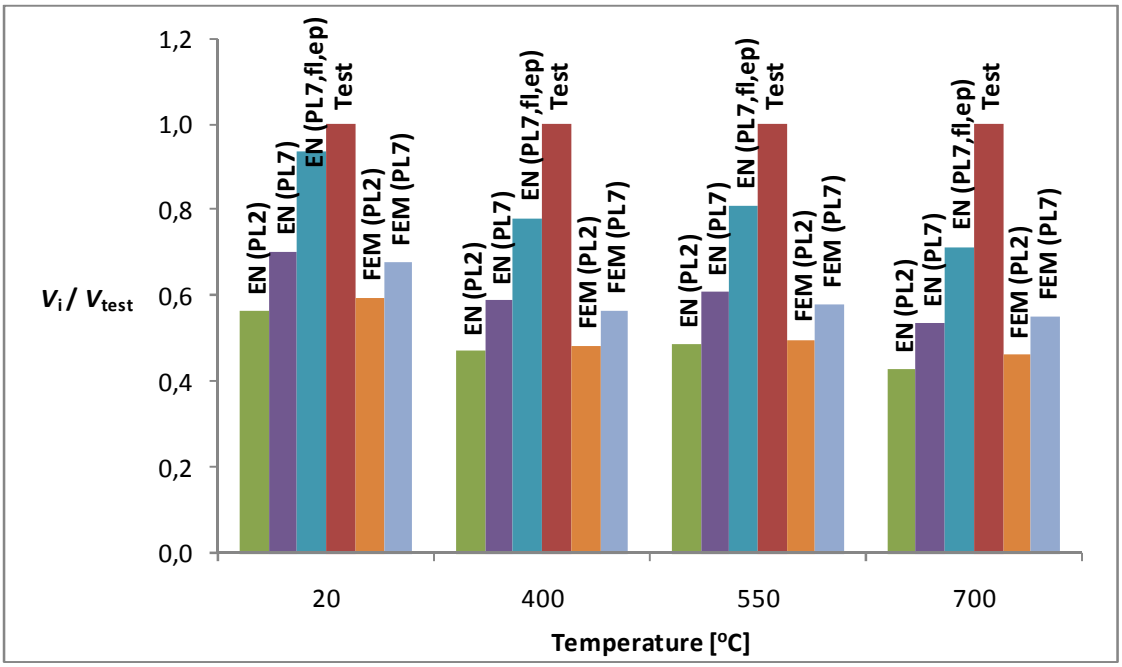

Figure 4.24. Comparison of shear resistances.

Table 4.7 and Figure 4.24 show that Eurocode resistances for the plate alone correlate quite well with the resistances from FEM analysis. Yet, all calculated resistances were clearly smaller than those from the tests. The Eurocode resistances were on average 19 % smaller than those from the tests assuming a clamped-plate web and considering the effect of the flanges according to EN 1993-1-5 [EN 1993-1-5, 2005]. The calculated resistances for clamped plates (PL7) were on average 25 % higher according to EN 1993-1-5 [EN 1993-1-5, 2005] and 17 % higher according to FEM calculations compared to simply supported plates (PL2). Moreover, when including the contribution of the flanges to the calculation according to EN 1993-1-5 (PL7,fl,ep), the resistances increased on average 33 %. Supporting structures seem to have a significant effect on shear resistance at ambient and elevated temperatures. That has been observed also in other recent studies [Vimonsatit, Tan, Ting, 2007], [Salminen, 2010]. Nevertheless, based on the benchmark case it can be concluded that the FEM model is reliable in analysing the behaviour of an isolated plate at elevated temperatures.

4.4.3 Other results at uniform elevated temperatures

The behaviour of plates PL1, PL3, PLa1, PLa2, PLs1 and PLs2 was studied at uniform elevated temperatures (at 100–700 °C for PL1, PL3, PLs1, PLs2 and 200–350 °C in the case of PLa1 and PLa2) in order to observe how plate behaviour changes at elevated temperatures. In the cases considered next, an initial imperfection of h/100 000 is applied in order to observe the contributions of shear buckling and tension field resistances separately. The calculated resistances at uniform elevated temperatures are presented in Tables 4.8–4.10. The shear force corresponding to the first increment

where maximum out-of-plane displacement of the plate was more than 0.1 mm (see also Figs. 4.28–4.30) was taken as the critical shear force V_{cr}.

Table 4.8. Calculated shear buckling and ultimate shear resistances of carbon steel plates PL1 and PL3 at uniform elevated temperatures.

	PL1		PL3	
Temperature [°C]	V_{cr} [kN]	V_{ult} [kN]	V_{cr} [kN]	V_{ult} [kN]
20-100	5.73	17.62	47.58	66.76
200	5.40	15.63	41.41	58.01
300	4.57	13.47	38.07	49.31
400	3.99	11.47	33.31	40.97
500	3.42	9.37	28.55	33.58
600	1.85	5.24	14.31	18.62
700	0.77	2.43	6.18	8.60

Table 4.9. Calculated shear buckling and ultimate shear resistances of aluminium plates PLa1 and PLa2 at uniform elevated temperatures.

	PLa1		PLa2	
Temperature [°C]	V_{cr} [kN]	V_{ult} [kN]	V_{cr} [kN]	V_{ult} [kN]
20	6.40	13.83	15.27	23.97
200	5.52	9.49	13.32	16.12
250	5.03	7.12	12.22	13.52
300	3.49	4.49	7.30	7.97
350	2.25	2.39	4.24	4.75

Table 4.10. Calculated shear buckling and ultimate shear resistances of stainless steel plates PLs1 and PLs2 at uniform elevated temperatures.

	PLs1		PLs2	
Temperature [°C]	V_{cr} [kN]	V_{ult} [kN]	V_{cr} [kN]	V_{ult} [kN]
20	5.36	10.45	14.89	22.41
100	5.22	9.31	14.46	20.03
200	5.04	8.29	13.48	17.91
300	4.82	7.83	13.14	16.92
400	4.55	7.37	12.88	15.97
500	4.35	6.71	11.58	14.52
600	4.15	6.15	10.85	13.32
700	3.86	5.16	9.56	11.26

The calculated shear buckling resistances V_{cr} of the considered plates at ambient temperature agreed well with the theoretical values (Eqs. (2.5)–(2.8)) if the plate was slender enough. The values $V_{cr,FEM}$ / $V_{cr,theoretical}$ for plates PL1, PL3, PLa1, PLa2, PLs1

and PLs2 were 0.99, 1.02, 0.98, 0.99, 0.97 and 0.80, respectively. In the case of stainless steel plate PLs2, theoretical shear buckling resistance was clearly higher than the critical shear buckling resistance from FEM because the material model of stainless steel is highly non-linear also at ambient temperature. Moreover, plate PLs2 was thicker than PLs1 leading to higher stresses and yielding of the material before theoretical V_{cr} was reached which means that the classical formulas (Eqs. (2.5)–(2.8)) do not apply.

The calculated ultimate shear resistances of carbon steel plates PL1 and PL3 at 20–100 ^{o}C might be slightly different than the ambient temperature results presented in Table 4.5 because the sizes of the increments were changed for each case separately and were not exactly the same in all analyses. However, the differences between the results were 0.7 % at the most. Figures 4.25–4.27 present the calculated reduction factors of shear buckling and ultimate shear resistances, $V_{cr,fi}$ / $V_{cr,ambient}$ and $V_{ult,fi}$ / $V_{ult,ambient}$ as a function of temperature. Moreover, the reduction factors of elastic modulus and design yield strength for class 4 members (0.2 % proof strengths) according to EN 1993-1-2 [EN 1993-1-2, 2005] and EN 1999-1-2 [EN 1999-1-2, 2007] are plotted.

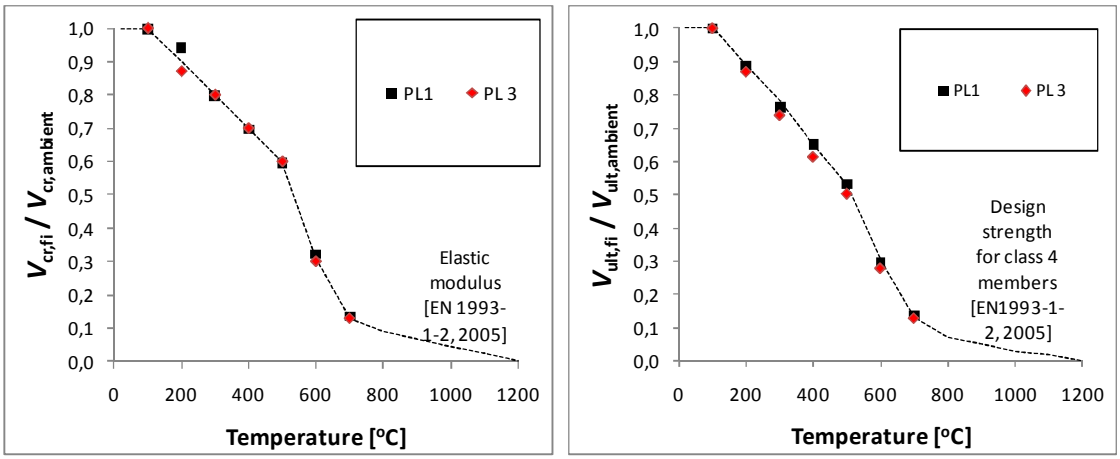

Figure 4.25. Reduction factors for shear buckling (left) and ultimate shear resistance (right) for plates PL1 and PL3 (carbon steel).

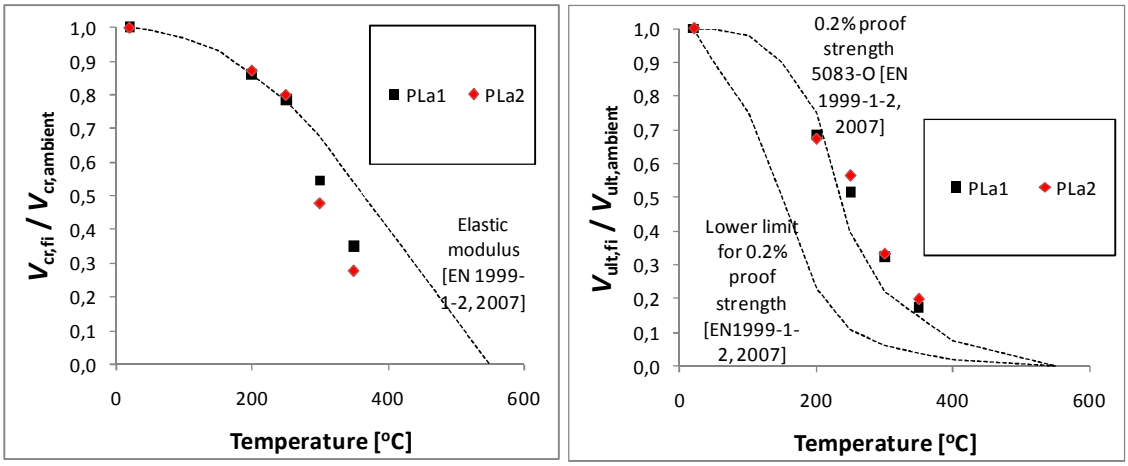

Figure 4.26. Reduction factors for shear buckling (left) and ultimate shear resistance (right) for plates PLa1 and PLa2 (aluminium).

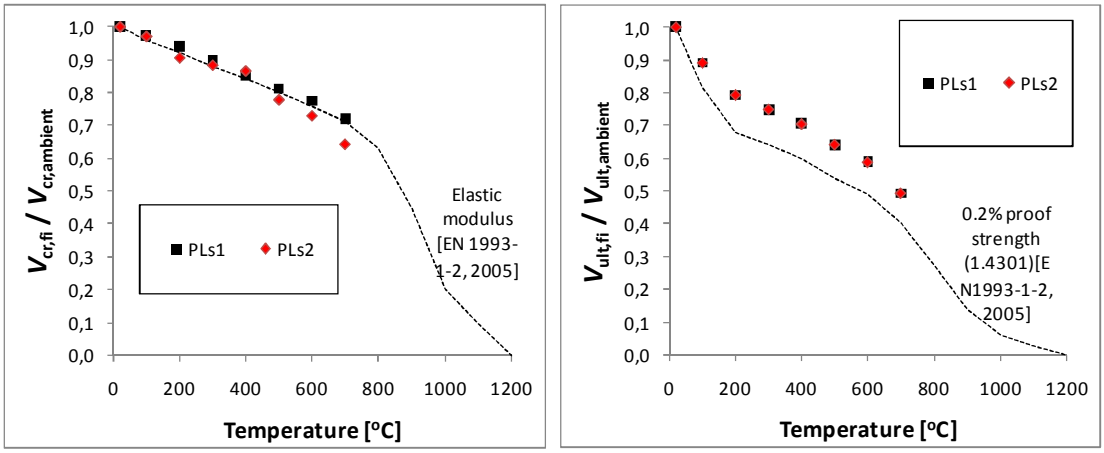

Figure 4.27. Reduction factors for shear buckling (left) and ultimate shear resistance (right) for plates PLs1 and PLs2 (stainless steel).

Figures 4.25–4.27 reveal that at uniform elevated temperatures the reduction factors for critical shear force V_{cr} obtained by FEM are close to the reduction factors for elastic modulus according to EN 1993-1-2 [EN 1993-1-2, 2005] in the case of carbon and stainless steel. The calculated reduction factors for V_{cr} in the case of aluminium plates were clearly lower than the reductions of elastic modulus according to EN 1999-1-2 [EN 1999-1-2, 2007] at temperatures 300 and 350 °C. The reason is that in the applied material model (Fig. 4.10) the proportional limit at those temperatures is very low, even compared to stainless steel. The reduction factors of ultimate shear resistance from FEM analysis correlated well with the design strength of class 4 members in the case of carbon steel. The calculated reduction factors for V_{ult} in the case of aluminium were close to the reduction factors for 0.2 % proof stress defined in EN 1999-1-2 [EN 1999-1-2, 2007] for alloy 5083-O, but clearly higher than those of the lower limit. In the case of stainless steel, the reduction factors from FEM analysis were clearly higher than the reduction factors for design strength according to EN 1993-1-2 [EN 1993-1-2, 2005]. However, it should be noted that the calculated ambient temperature resistances of

stainless steel plates PLs1 and PLs2 were smaller than those according to EN 1993-1-4 [EN 1993-1-4, 2006].

Figures 4.28–4.30 illustrate the behaviour of plates PL1, PLa1 and PLs1 at uniform elevated temperatures.

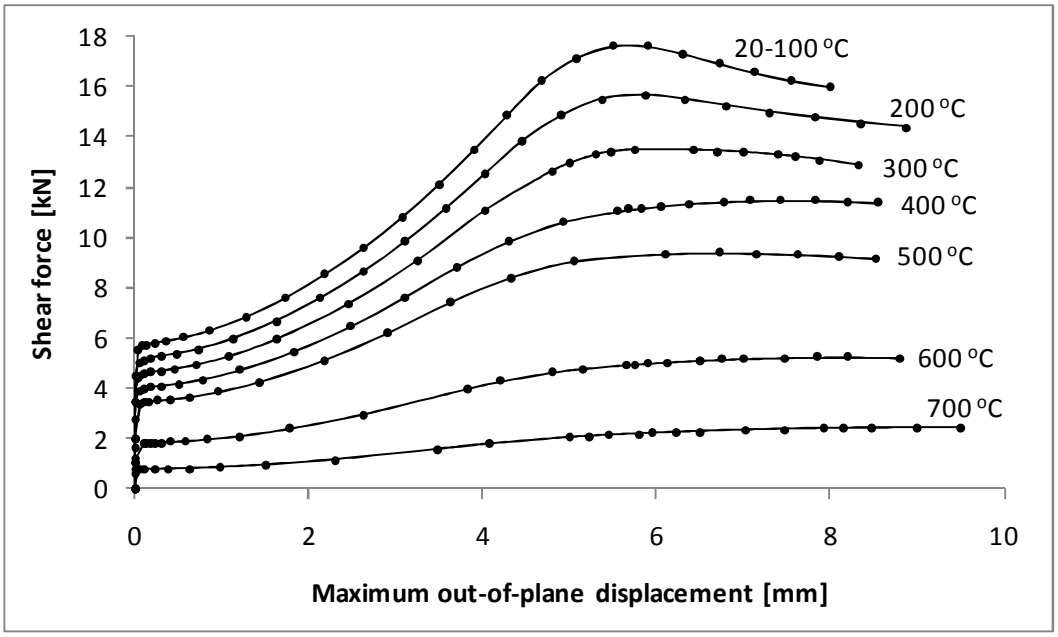

Figure 4.28. Behaviour of plate PL1 at different uniform temperatures.

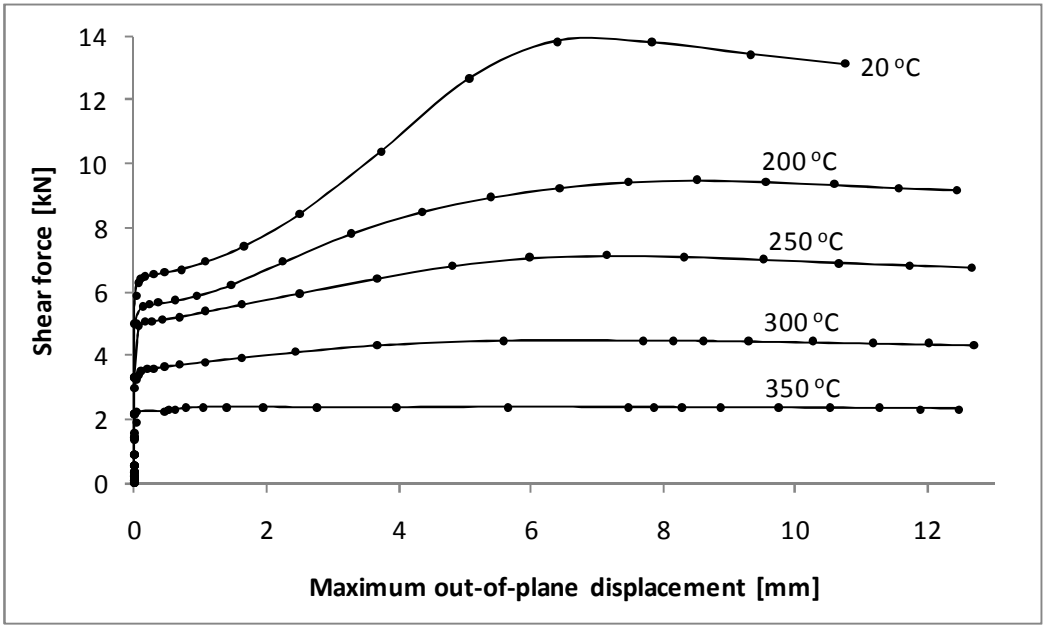

Figure 4.29. Behaviour of plate PLa1 at different uniform temperatures.

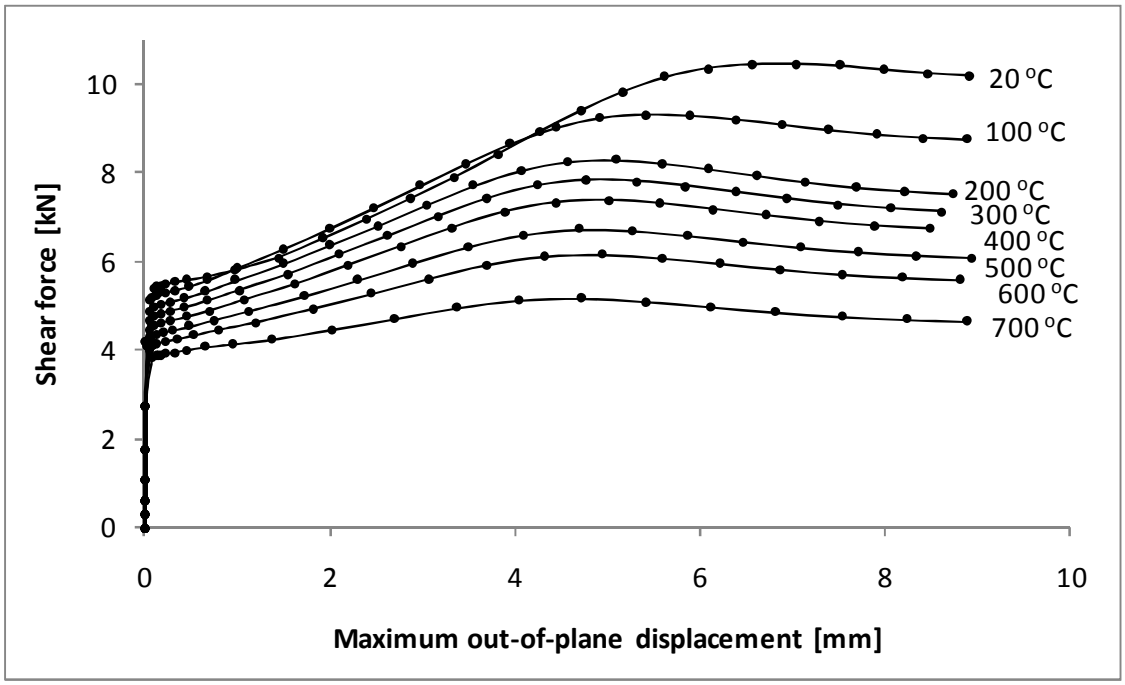

Figure 4.30. Behaviour of plate PLs1 at different uniform temperatures.

Figure 4.30 reveals that the maximum out-of-plane displacements of plate PLs1 when maximum shear force is applied are clearly smaller at elevated temperatures than at 20 °C (see e.g. curves at ambient and at 100 °C).

Figure 4.31 presents the yielded regions of plate PL1 when maximum shear force is reached. It should be noted that at elevated temperatures yielding starts at relatively low stresses due to increased material non-linearity (see Fig. 4.7).

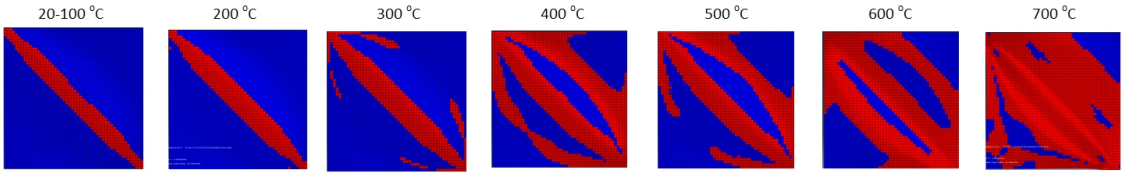

Figure 4.31. Yielded regions of plate PL1 at different uniform temperatures.

Tables 4.8–4.10 and Figures 4.28–4.30 clearly show that the tension field effect occurs also at elevated temperatures. However, the relative contribution of the post-buckling resistance V_{pb} (= V_{ult} - V_{cr}) to ultimate shear resistance V_{ult} decreases in most of the cases. Figure 4.32 shows the ratios V_{pb} / V_{ult} for all considered cases.

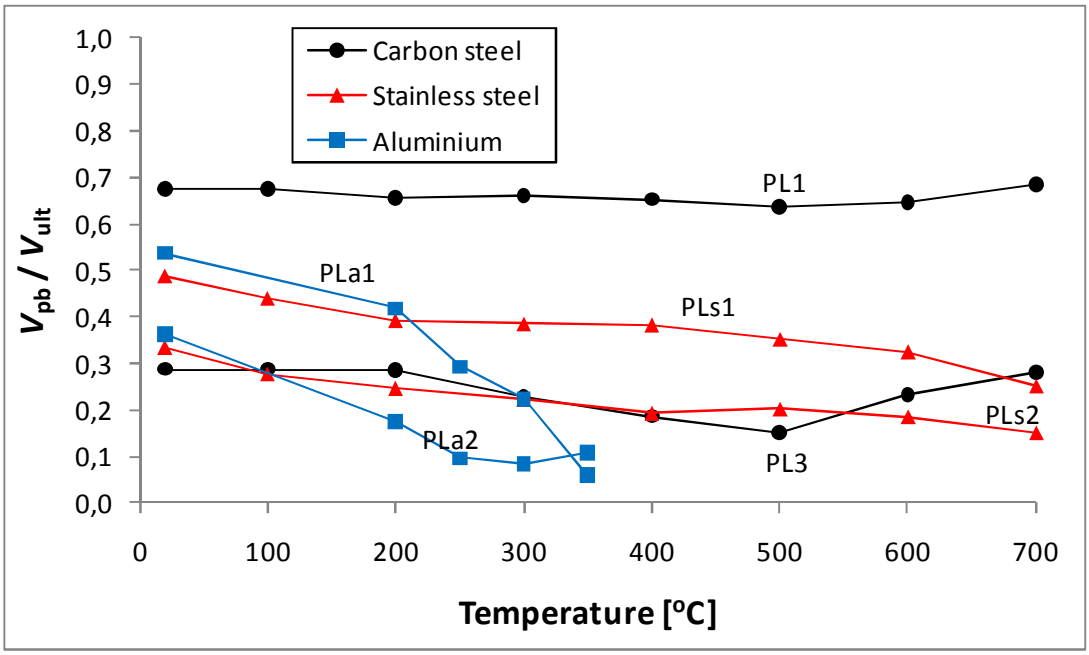

Figure 4.32. Ratios V_{pb} / V_{ult} at ambient and uniform elevated temperatures.

Figure 4.32 reveals that the relative contributions of shear buckling and post buckling resistances at uniform elevated temperatures are close to ambient temperature values in the case of carbon steel. The relative contribution of post-buckling resistance decreases at uniform elevated temperatures in the case of stainless steel, and especially in the case of aluminium. This effect can be explained by the difference in the reduction factors of the material properties of the considered materials. The reduction factors for 0.2 % proof strengths and elastic modulus are quite close to each other at the same temperature in the case of carbon steel (see Fig. 3.1), but in the case of aluminium (Fig. 3.3) and stainless steel (Fig 3.4), the reduction factors for 0.2 % proof strengths are clearly smaller than those of elastic modulus at the same temperature. The reduction of elastic modulus is related to shear buckling resistance (Eq. (2.6)) and the reduction of 0.2 % proof strength is related to ultimate shear resistance (Eqs. (3.3)). Figure 4.33 shows the ratios $k_{0.2,\theta}$ / $k_{E,\theta}$ (dashed lines) as a function of a temperature for all considered materials according to EN 1993-1-2 [EN 1993-1-2, 2005] and EN 1999-1-2 [EN 1999-1-2, 2007]. Moreover, the calculated contributions of post-buckling resistance V_{pb} / V_{ult} at elevated temperatures are compared to the corresponding value at ambient temperature $V_{pb,ambient}$ / $V_{ult,ambient}$.

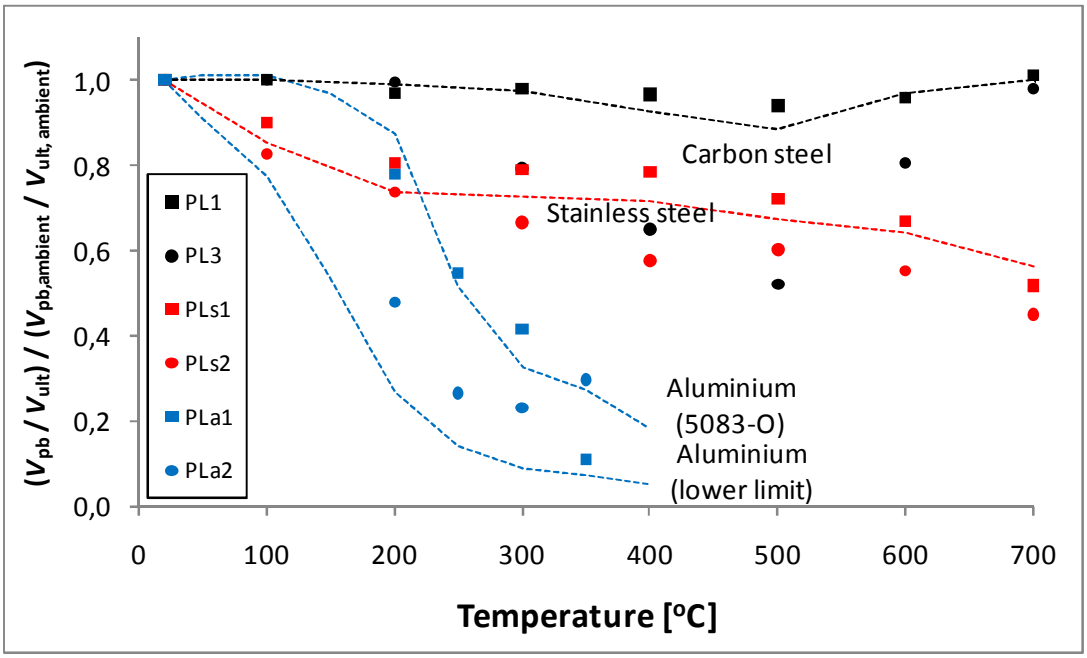

Figure 4.33. Ratios $k_{0.2,\theta}$ / $k_{E,\theta}$ (dashed lines) and (V_{pb} / V_{ult}) / ($V_{pb,ambient}$ / $V_{ult,ambient}$) as a function of temperature.

Figure 4.33 shows that the relative contribution of post-buckling resistance at uniform elevated temperatures depends clearly on the ratio $k_{0.2,\theta}$ / $k_{E,\theta}$. It can be concluded that if the reduction factor for 0.2 % proof strength is smaller than the reduction factor for elastic modulus at the same temperature, then the relative contribution of post-buckling resistance is smaller at the considered temperature than at ambient temperature.

The material model for aluminium was taken from the dissertation of Maljaars [Maljaars, 2008] where the design curves were derived up to strain $\varepsilon = 0.015$. For larger strains, in FEM modelling, the stress was assumed to remain the same as at $\varepsilon = 0.015$ before decreasing to zero at $\varepsilon = 0.3$. Table 4.11 shows the maximum principal strains of aluminium plates PLa1 and PLa2 when the ultimate shear resistance of the plate is reached.

Table 4.11. Maximum principal strains of plates PLa1 and PLa2 when the ultimate shear resistance is reached.

	20 °C	200 °C	250 °C	300 °C	350 °C
PLa1	0.0113	0.0126	0.0079	0.0088	0.0007
PLa2	0.0076	0.0104	0.0024	0.0014	0.0014

Table 4.11 shows that in the case of each considered aluminium plate the maximum principal strains at the ultimate shear resistance were smaller than 0.015. Thus, it can be concluded that the material model applied to aluminium was reliable in this case.

4.4.4 Results at non-uniform elevated temperatures

Tables 4.12–4.14 present the calculated reduction factors k_{FEM} defined in Equation (4.5).

$$k_{FEM} = \frac{V_{fi,R,FEM}}{V_{amb,R,FEM}} \tag{4.5}$$

where
- $V_{fi,R,FEM}$ is shear resistance at elevated temperature and
- $V_{amb,R,FEM}$ is shear resistance at ambient temperature.

Table 4.12 presents the results for carbon steel plates PL1–PL8, Table 4.13 for carbon steel plates PL9–PL12 and Table 4.14 for aluminium plates PLa1 and PLa2 as well as stainless steel plates PLs1 and PLs2. The properties of all considered plates are shown in Chapter 4.1.1 and the non-uniform temperature distributions in Chapter 4.1.2. The results of Table 4.12 were first presented in reference [Salminen, Heinisuo, 2011(b)].

Table 4.12. Calculated reduction factors $k_{FEM} = V_{fi,R,FEM} / V_{amb,R,FEM}$ for carbon steel plates PL1–PL8.

Temperature distribution [°C]	PL1	PL2	PL3	PL4	PL5	PL6	PL7	PL8
100–300 linear	0.836	0.831	0.828	0.809	0.804	0.827	0.829	0.804
100–500 linear	0.657	0.657	0.662	0.620	0.623	0.656	0.666	0.627
100–700 linear	0.319	0.320	0.319	0.301	0.301	0.308	0.330	0.298
100–900 linear	0.112	0.113	0.111	0.106	0.105	0.113	0.117	0.110
200–500 linear	0.631	0.630	0.633	0.596	0.597	0.633	0.637	0.602
300–600 linear	0.443	0.442	0.444	0.418	0.416	0.437	0.450	0.419
400–700 linear	0.244	0.245	0.243	0.230	0.230	0.238	0.248	0.228
500–800 linear	0.124	0.123	0.122	0.116	0.115	0.120	0.124	0.115
600–900 linear	0.070	0.069	0.067	0.066	0.064	0.065	0.070	0.061
100–300 non-linear	0.881	0.877	0.877	0.859	0.855	0.872	0.879	0.856
100–500 non-linear	0.753	0.755	0.763	0.718	0.721	0.749	0.766	0.722
100–700 non-linear	0.473	0.481	0.485	0.452	0.458	0.472	0.514	0.460
100–900 non-linear	0.231	0.222	0.195	0.213	0.180	0.216	0.226	0.214
200–500 non-linear	0.705	0.710	0.714	0.672	0.675	0.706	0.719	0.677
300–600 non-linear	0.540	0.538	0.545	0.509	0.509	0.536	0.560	0.517
400–700 non-linear	0.341	0.343	0.340	0.323	0.323	0.332	0.356	0.321
500–800 non-linear	0.181	0.185	0.185	0.172	0.174	0.177	0.189	0.172
600–900 non-linear	0.096	0.096	0.095	0.091	0.090	0.093	0.098	0.090

Table 4.13. Calculated reduction factors $k_{FEM} = V_{fi,R,FEM} / V_{amb,R,FEM}$ for carbon steel plates PL9–PL12.

Temperature distribution [°C]	PL9	PL10	PL11	PL12
100–300 linear	0.852	0.839	0.838	0.823
100–500 linear	0.688	0.662	0.640	0.636
100–700 linear	0.334	0.286	0.310	0.312
100–900 linear	0.116	0.101	0.128	0.137
200–500 linear	0.660	0.641	0.613	0.611
300–600 linear	0.463	0.434	0.428	0.422
400–700 linear	0.255	0.228	0.232	0.233
500–800 linear	0.128	0.116	0.119	0.122
600–900 linear	0.071	0.066	0.068	0.070
100–300 non-linear	0.898	0.880	0.890	0.864
100–500 non-linear	0.785	0.754	0.737	0.720
100–700 non-linear	0.501	0.430	0.468	0.464
100–900 non-linear	0.206	0.191	0.258	0.269
200–500 non-linear	0.739	0.713	0.690	0.673
300–600 non-linear	0.567	0.523	0.523	0.507
400–700 non-linear	0.356	0.311	0.327	0.320
500–800 non-linear	0.191	0.164	0.182	0.182
600–900 non-linear	0.099	0.089	0.097	0.096

Table 4.14. Calculated reduction factors $k_{FEM} = V_{fi,R,FEM} / V_{amb,R,FEM}$ for aluminium plates PLa1, PLa2 and stainless steel plates PLs1, PLs2.

Temperature distribution [°C]	PLa1	PLa2	Temperature distribution [°C]	PLs1	PLs2
50–200 linear	0.783	0.783	100–400 linear	0.752	0.733
50–250 linear	0.667	0.668	100–600 linear	0.667	0.645
50–300 linear	0.523	0.519	100–800 linear	0.510	0.498
50–350 linear	0.370	0.366	100–1000 linear	0.252	0.258
100–250 linear	0.641	0.641	200–600 linear	0.602	0.633
125–275 linear	0.554	0.551	300–700 linear	0.537	0.558
150–300 linear	0.465	0.460	400–800 linear	0.459	0.437
175–325 linear	0.378	0.375	500–900 linear	0.314	0.303
200–350 linear	0.293	0.290	600–1000 linear	0.180	0.184
50–200 non-linear	0.836	0.838	100–400 non-linear	0.781	0.763
50–250 non-linear	0.762	0.768	100–600 non-linear	0.718	0.694
50–300 non-linear	0.660	0.655	100–800 non-linear	0.614	0.603
50–350 non-linear	0.525	0.526	100–1000 non-linear	0.407	0.416
100–250 non-linear	0.721	0.725	200–600 non-linear	0.624	0.671
125–275 non-linear	0.643	0.644	300–700 non-linear	0.567	0.611
150–300 non-linear	0.564	0.560	400–800 non-linear	0.535	0.515
175–325 non-linear	0.480	0.475	500–900 non-linear	0.413	0.402
200–350 non-linear	0.391	0.387	600–1000 non-linear	0.260	0.263

Figures 4.34 and 4.44 present the upper and lower limit as well as the average value for the calculated reduction factor at the same temperature distribution. Carbon steel plates PL1–PL12 were considered in this comparison. Figure 4.34 shows the linear and Figure 4.35 the non-linear temperature distributions. Table 4.14 shows that the reduction factors of two aluminium and two stainless steel plates were close to each other in all cases.

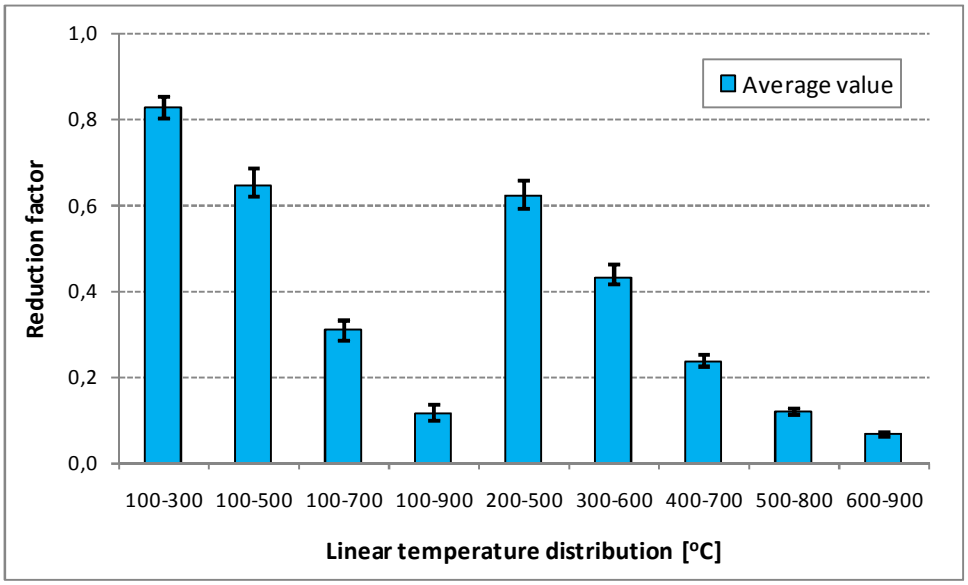

Figure 4.34. Average values, upper and lower limits of reduction factors (carbon steel plates PL1–PL12, linear temperature distributions).

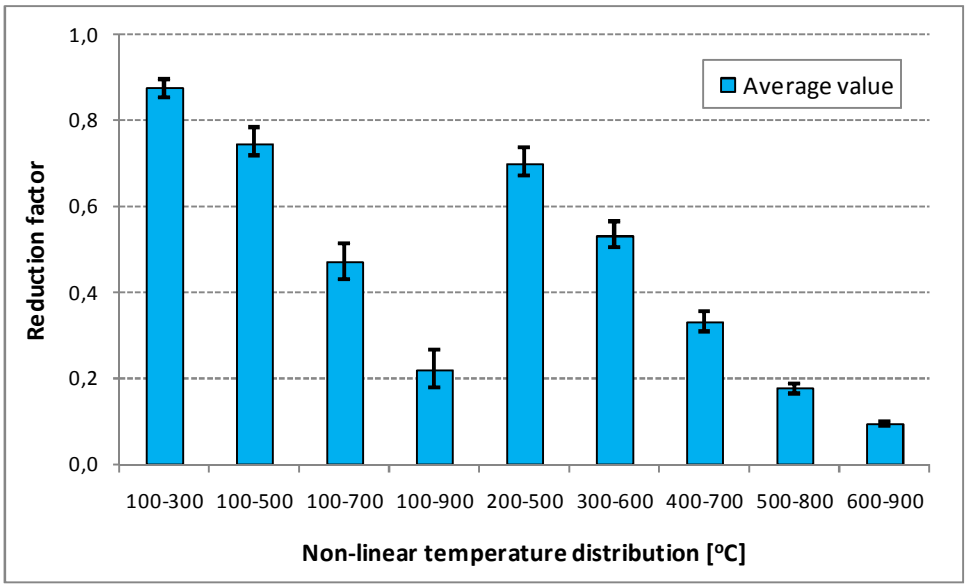

Figure 4.35. Average values, upper and lower limits of reduction factors (carbon steel plates PL1–PL12, non-linear temperature distributions).

Figures 4.34 and 4.35 reveal that the reduction factors k_{FEM} of carbon steel plates PL1–PL12 were close to each other at the same temperature distribution in most cases.

Deviations in the reduction factors were slightly higher in the case of non-linear temperature distributions. The effects of thickness, yield strength, boundary conditions and aspect ratio are considered in detail later in this chapter.

Figures 4.36–4.40 present the behaviour of the most slender plate of each considered material (PL1, PLa1 and PLs1) at four linear non-uniform elevated temperatures. The final results of this study were calculated using an initial imperfection of $h/100$. However, the following shear force–displacement graphs were plotted also for initial imperfections of $h/100\ 000$ (dashed lines) in order to observe the contributions of the shear buckling and tension field phases. Figures 4.37 and 4.38 show the yielded regions of carbon steel plate PL1 at ambient and at four linear non-uniform elevated temperatures when maximum shear force is applied. The yielded regions were not plotted in the case of aluminium and stainless steel plates because yielding starts at relatively low stresses with them compared to carbon steel.

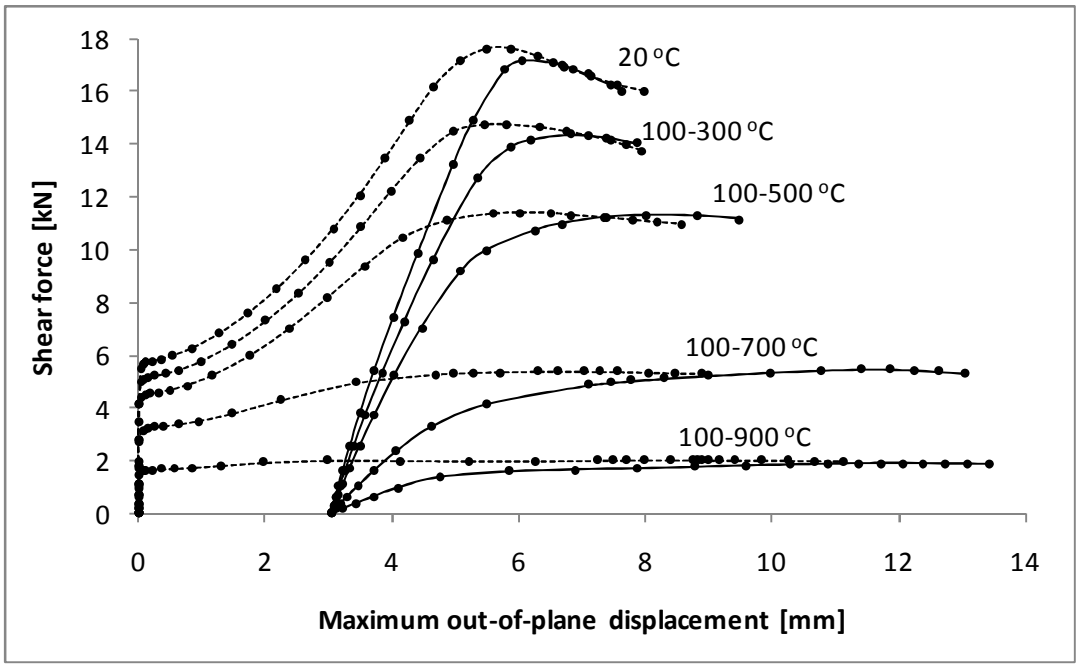

Figure 4.36. Behaviour of carbon steel plate PL1 at ambient and linear non-uniform elevated temperatures.

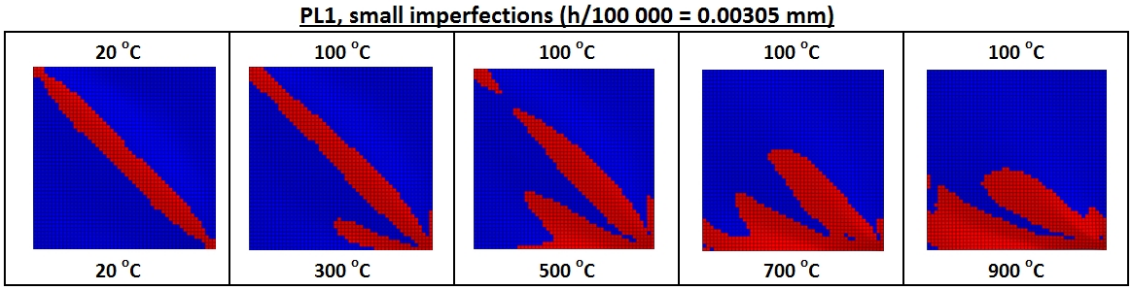

Figure 4.37. Yielded regions of carbon steel plate PL1 at linear non-uniform elevated temperatures (small imperfections).

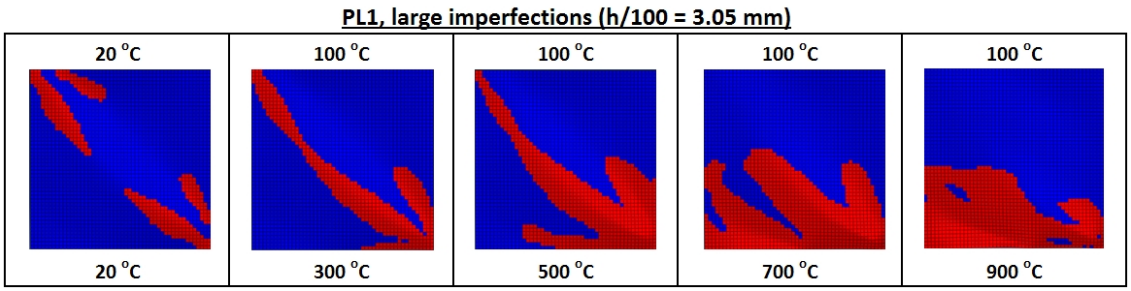

Figure 4.38. Yielded regions of carbon steel plate PL1 at linear non-uniform elevated temperatures (large imperfections).

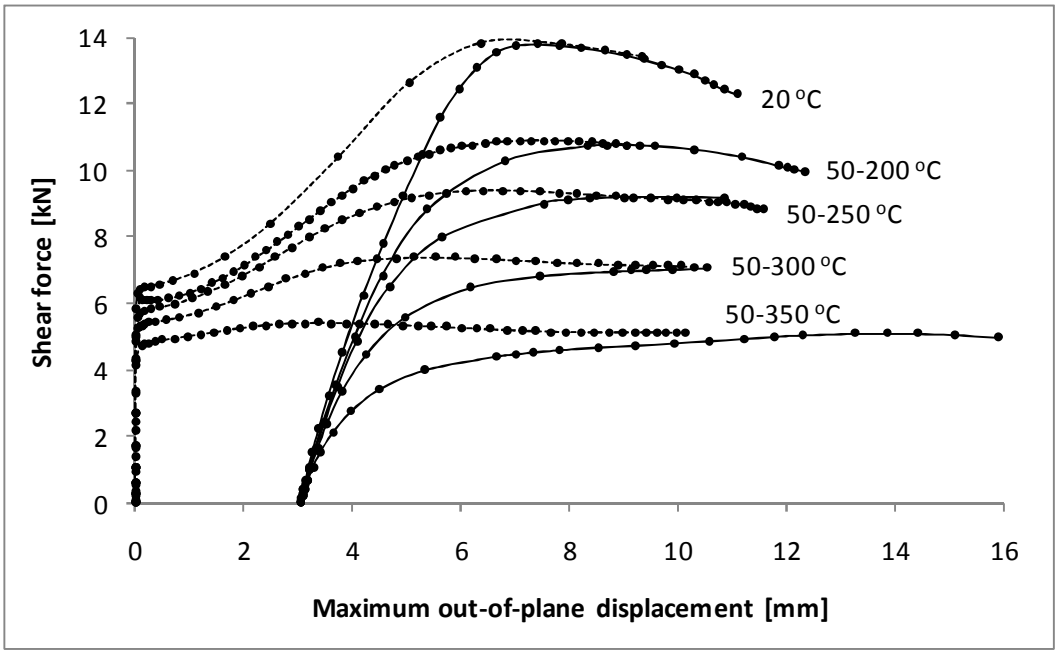

Figure 4.39. Behaviour of aluminium plate PLa1 at ambient and linear non-uniform elevated temperatures.

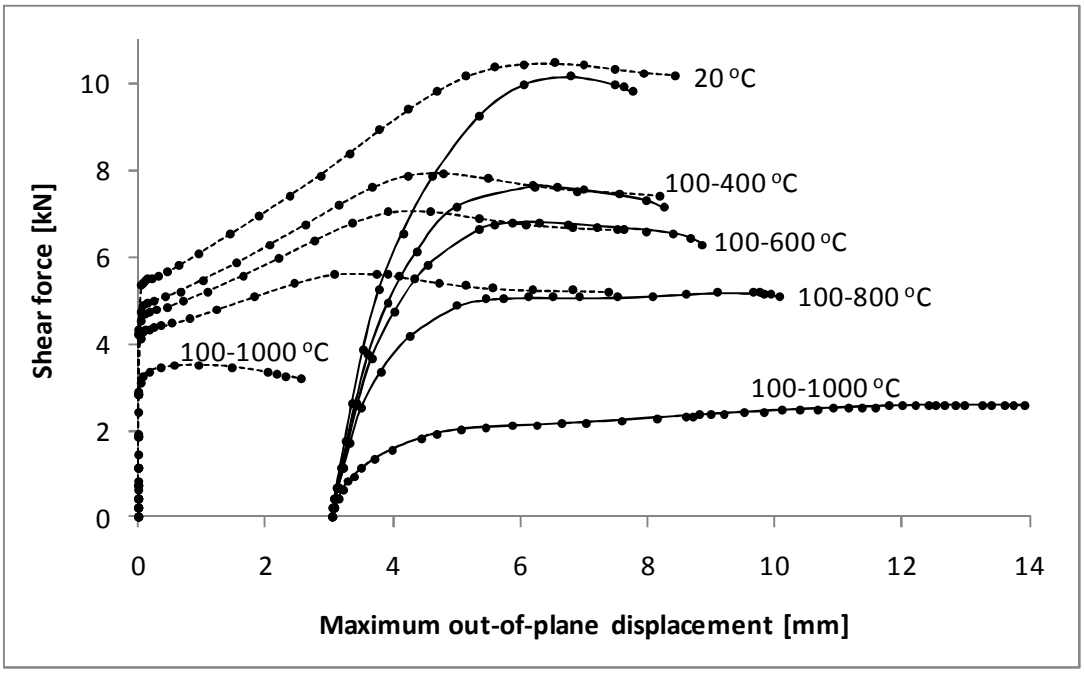

Figure 4.40. Behaviour of stainless steel plate PLs1 at ambient and linear non-uniform elevated temperatures.

Based on Figures 4.36–4.40 it can be said that the shear buckling and tension field phases are evident also at non-uniform elevated temperatures even though the contribution of post-buckling resistance to ultimate shear resistance decreases clearly when the hottest temperature of the plate increases. It can also be seen that the shear buckling phase is undetectable if the initial imperfection is 3.05 mm in this case. Figures 4.37 and 4.38 reveal that when the hottest temperature of the plate rises, most of the yielding occurs in the lower (hotter) part of the plate. A comparison of Figures 4.37 and 4.38 reveals that the shape of the tension field is clearly dependent on initial imperfection. Based on Figures 4.36–4.40, it can be concluded that the behaviour of thin metal plate is significantly different at non-uniform elevated temperatures than at ambient temperature.

Tables 4.15–4.17 present the calculated values for shear buckling resistance V_{cr} and ultimate shear resistance V_{ult} when using h/100 000 as the magnitude of the initial imperfection in FEM analyses. Moreover, ultimate shear resistances are compared to those obtained using an imperfection of h/100, and shear buckling resistances are compared to those calculated using the method presented in reference [Salminen, 2010] ($V_{cr,[Salminen,\ 2010]}$). The critical shear strength at ambient temperature in this case is calculated using classical Equations (2.5)–(2.8), and the resulting value is reduced at elevated temperatures using method f presented in [Salminen, 2010]. As in the previous analyses, the shear force corresponding to the first increment where maximum out-of-plane displacement was more than 0.1 mm was used as the critical shear force V_{cr}.

Table 4.15. Comparison of critical- and ultimate shear forces on carbon steel plate PL1.

	$V_{cr,h/100000}$ [kN]	$V_{ult,h/100000}$ [kN]	$V_{cr,[Salminen, 2010]}$ [kN]	$V_{cr,h/100000}$ / $V_{cr,[Salminen, 2010]}$	$V_{ult,h/100000}$ / $V_{ult,h/100}$
20 °C	5.73	17.62	5.81	0.99	1.03
Lin. 100–300 °C	5.10	14.75	5.04	1.01	1.03
Lin. 100–500 °C	4.49	11.42	4.26	1.05	1.01
Lin. 100–700 °C	3.24	5.39	2.96	1.09	0.98
Lin. 100–900 °C	1.65	2.03	1.78	0.93	1.06

Table 4.16. Comparison of critical- and ultimate shear forces on aluminium plate PLa1.

	$V_{cr,h/100000}$ [kN]	$V_{ult,h/100000}$ [kN]	$V_{cr,[Salminen, 2010]}$ [kN]	$V_{cr,h/100000}$ / $V_{cr,[Salminen, 2010]}$	$V_{ult,h/100000}$ / $V_{ult,h/100}$
20 °C	6.40	13.83	6.54	0.98	1.00
Lin. 50–200 °C	6.12	10.90	6.00	1.02	1.01
Lin. 50–250 °C	5.72	9.40	5.69	1.01	1.02
Lin. 50–300 °C	5.35	7.39	5.32	1.01	1.02
Lin. 50–350 °C	4.73	5.42	4.86	0.97	1.06

Table 4.17. Comparison of critical- and ultimate shear forces on stainless steel plate PLs1.

	$V_{cr,h/100000}$ [kN]	$V_{ult,h/100000}$ [kN]	$V_{cr,[Salminen, 2010]}$ [kN]	$V_{cr,h/100000}$ / $V_{cr,[Salminen, 2010]}$	$V_{ult,h/100000}$ / $V_{ult,h/100}$
20 °C	5.44	10.45	5.54	0.98	1.03
Lin. 100–400 °C	4.93	7.92	4.88	1.01	1.04
Lin. 100–600 °C	4.64	7.05	4.58	1.01	1.04
Lin. 100–800 °C	4.30	5.61	4.23	1.02	1.08
Lin. 100–1000 °C	3.36	3.49	3.47	0.97	1.36

Tables 4.15–4.17 and Figures 4.36–4.40 show clearly the decrease in the contribution of post-buckling resistance. Moreover, they reveal that the graphical method presented in [Salminen, 2010] predicted the shear buckling resistance of the plates accurately in the cases considered. Comparison of the ultimate shear resistances calculated using imperfections $h/100$ and $h/100\,000$ reveals that the effect of the magnitude of the imperfection was quite small in most cases. However, in one case (PLs1, 100–1000 °C) the effect of the magnitude was significant.

Figure 4.41 shows the yielded regions of plates PL10, PL11 and PL12 (a/h = 0.5, 2 and 3, respectively) at ambient temperature and at linear distributions 100–300, 100–500, 100–700, 100–900 °C.

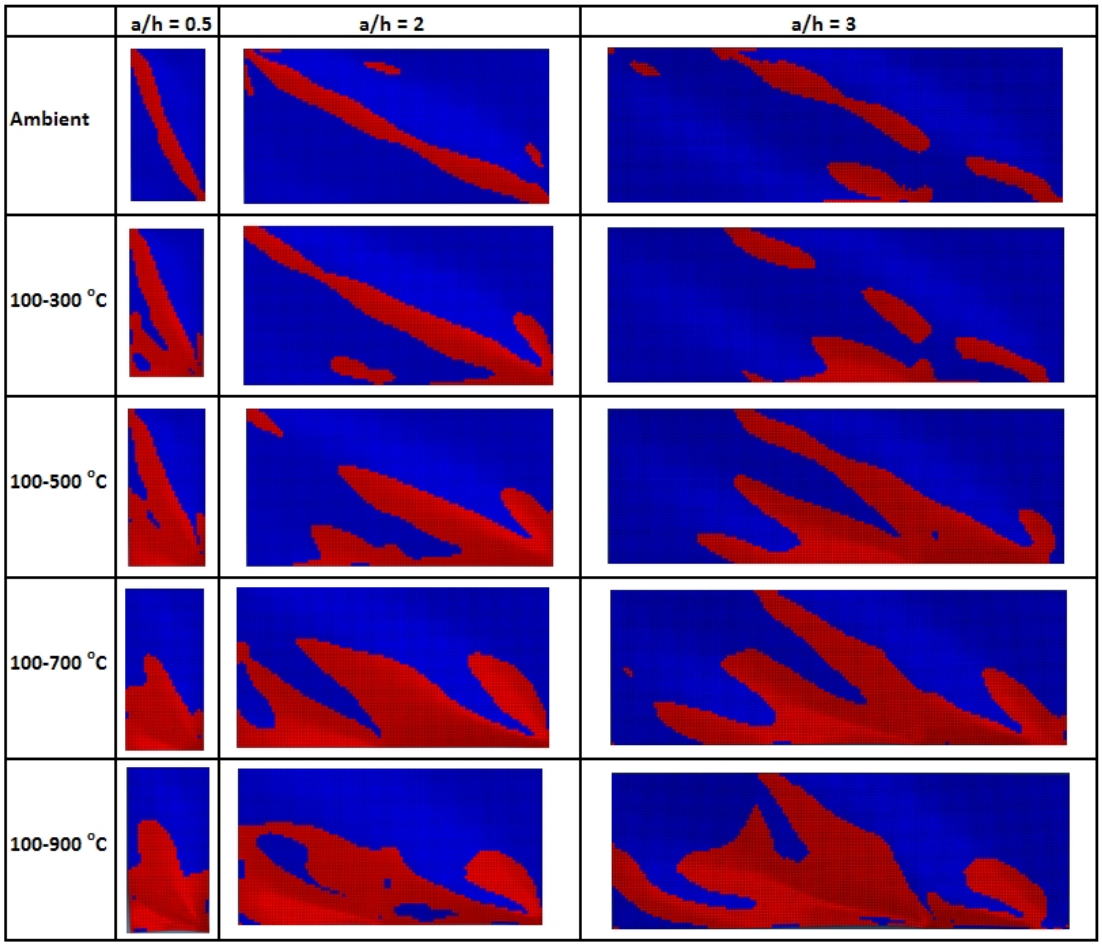

Figure 4.41. Yielded regions of plates PL10–PL12 at ambient and non-uniform elevated temperatures.

Figure 4.41 shows that the tension field does not form from corner to corner when a/h = 3 even at ambient temperature.

The reduction factors for carbon steel plates representing different cases are compared in Figures 4.42–4.48. The effects of thickness, yield strength, boundary conditions and aspect ratio are considered.

Figures 4.42 and 4.43 show the effect of yield strengths ($k_{FEM,355}$ / $k_{FEM,235}$) and ($k_{FEM,460}$ / $k_{FEM,355}$) on the calculated reduction factors for plates PL1, PL3, PL4, PL6, PL8 and PL9 as a function of the hottest temperature of the plate. All other properties, except strength, were the same for plates PL1 and PL4, PL6 and PL8, and PL3 and PL9.

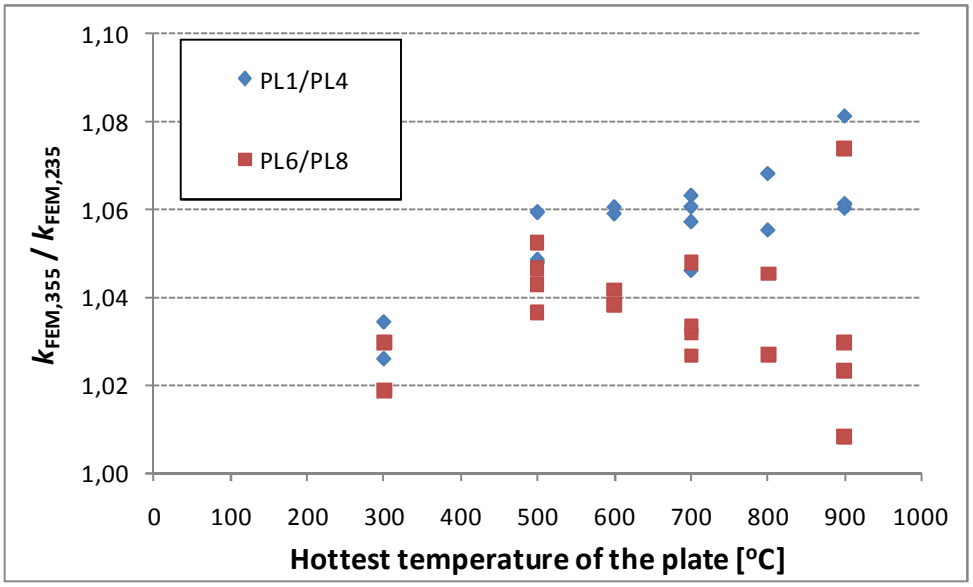

Figure 4.42. Effect of yield strength on reduction factors for plates PL1/PL4 and PL6/PL8.

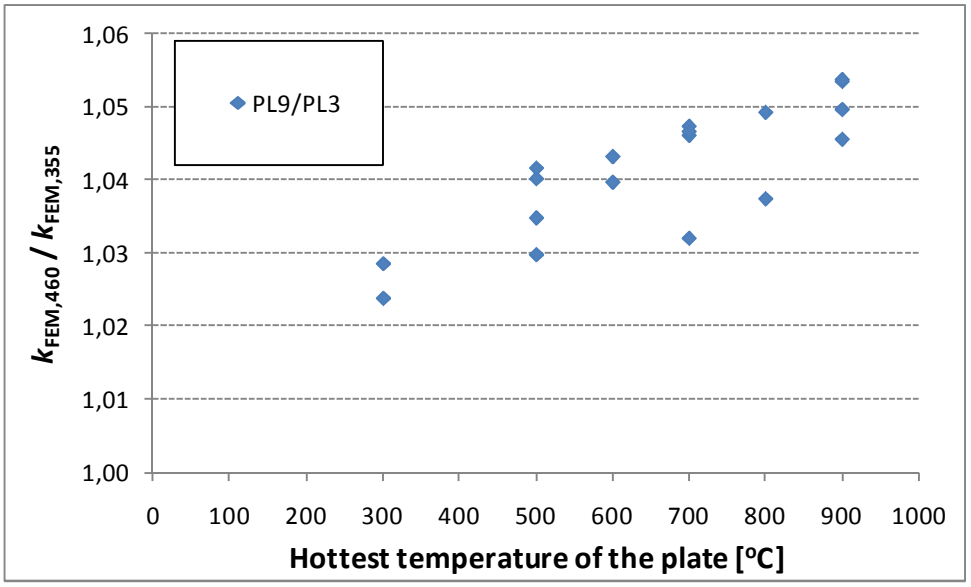

Figure 4.43. Effect of yield strength on reduction factors for plates PL9 and PL3.

The reduction factors for plates PL1 and PL6 (f_y = 355 N/mm^2) were in each case higher (on average 4.6 %) than those for plates PL4 and PL8 (f_y = 235 N/mm^2). The same conclusion can be drawn for plates PL3 and PL9. The reduction factors for PL9 (f_y = 460 N/mm^2) were on average 4.1 % higher than those for PL3 (f_y = 355 N/mm^2).

The effect of the thickness of the plate was studied for carbon steel plates PL1–PL2 and PL4–PL5. Plates PL1 and PL2 as well as PL4 and PL5 have the same properties except that PL2 and PL5 are thicker than PL1 and PL4 and the yield strengths of PL1 and PL2 are slightly different (f_y = 355 and 332 N/mm^2). The effect of the thickness ($k_{FEM,1.5mm}/k_{FEM,1mm}$) of the plate is presented graphically in Figure 4.44. It should be

noted that at a non-linear 100–900 °C distribution the ratio $k_{FEM,1.5mm}/k_{FEM,1mm}$ of plates PL5 and PL4 was 0.84 (not shown in Fig. 4.44).

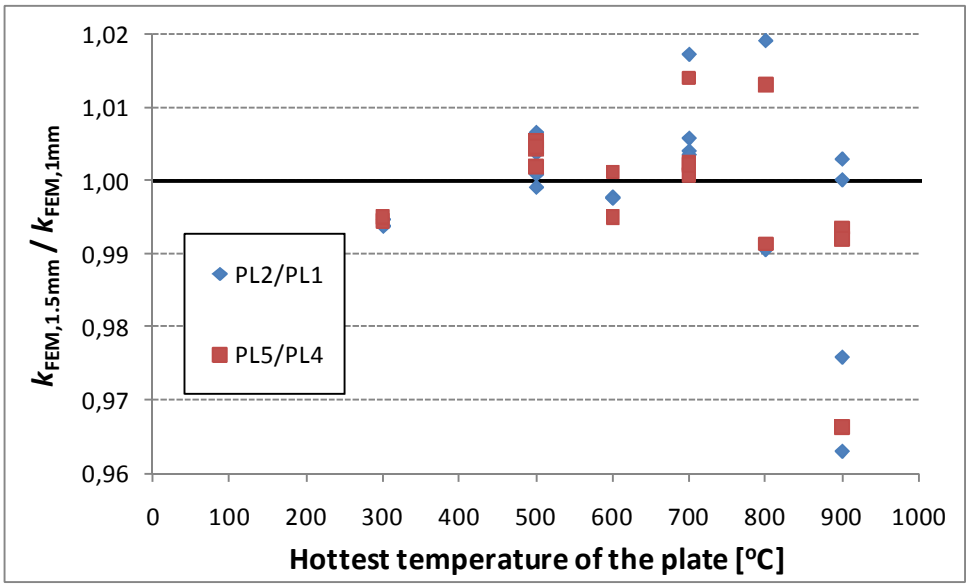

Figure 4.44. Effect of the thickness of the plate on reduction factors (carbon steel).

Figure 4.44 shows that reduction factors were approximately the same for plates of different thicknesses (except for the non-linear 100–900 °C distribution). In some cases the reduction factors for more slender plates were slightly higher and in some cases slightly lower. Therefore, no connection between the slenderness of plate and reduction factor could be established.

The effect of boundary conditions was studied in the cases of PL1 and PL6, PL2 and PL7 as well as PL4 and PL8. The properties of the plates were the same, except that plates PL1, PL2 and PL4 were simply supported (ss) and plates PL6, PL7 and PL8 were clamped (cl). Figure 4.45 presents the effect of the boundary conditions in the cases considered.

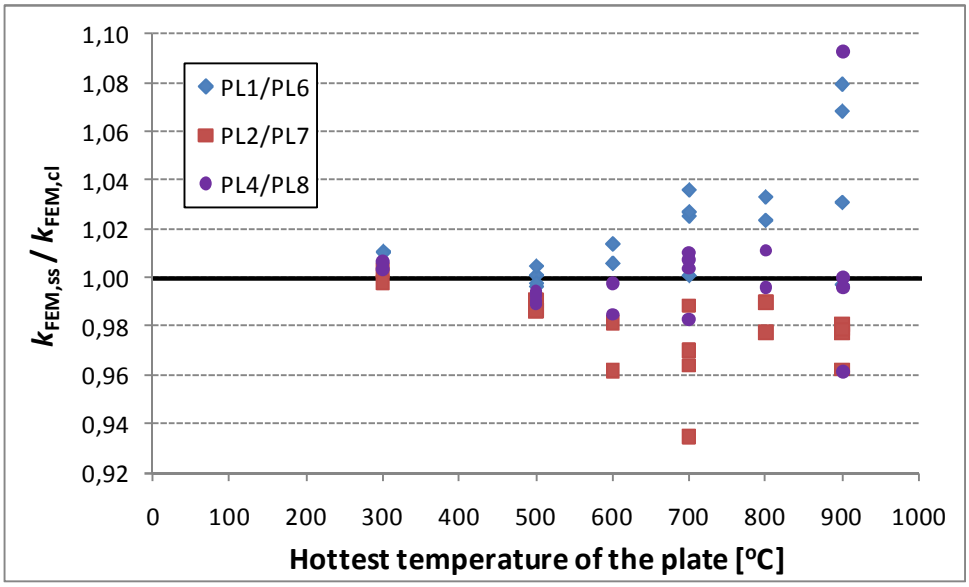

Figure 4.45. Effect of boundary conditions of plate on reduction factors.

Figure 4.45 reveals that reduction factors for simply supported plates were, on average, approximately the same as for clamped plates, but in the case of PL1 and PL6 the reduction factors for the simply supported plate were higher and in the case of PL2 and PL7 lower than those for clamped plates.

The effect of the aspect ratio (a/h) was studied in the cases of PL10, PL4, PL11 and PL12. The properties of PL10, PL4, PL11 and PL12 were the same, except for the aspect ratios which were 0.5, 1, 2 and 3, respectively. Figure 4.46 presents the effect of the aspect ratio in the cases considered. The reduction factors obtained from cases where a/h = 0.5, 2 and 3 are compared to the case where a/h = 1.

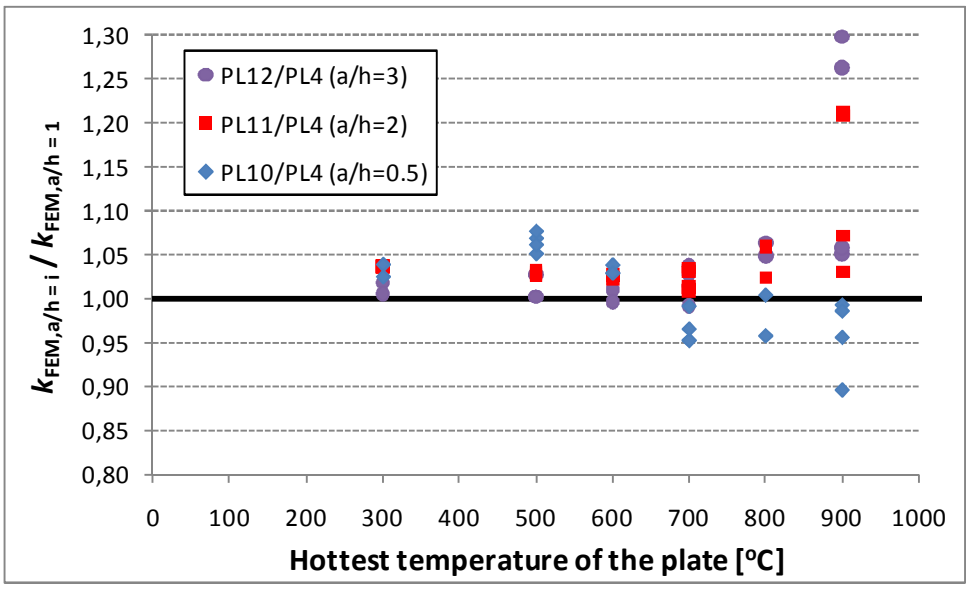

Figure 4.46. Effect of aspect ratio of plate on reduction factors.

The reduction factors for PL10 (a/h = 0.5) were, on average, approximately the same as those for PL4 (a/h = 1). However, in the cases where the maximum temperature of the plate was less than 700 °C, they were slightly higher while in the cases where the maximum temperature was at least 700 °C they were lower compared to PL4. The reduction factors for plates PL11 (a/h = 2) and PL12 (a/h = 3) were, on average, approximately 5 % higher than those for PL4 (a/h = 1). Especially at the temperature distribution of 100–900 °C the difference was significant.

Only two aluminium and stainless steel plates were considered in this comparison. The reduction factors for them are compared in Figures 4.47 and 4.48. The only difference between the cases is that plates PLa2 and PLs2 are thicker compared to plates PLa1 and PLs1.

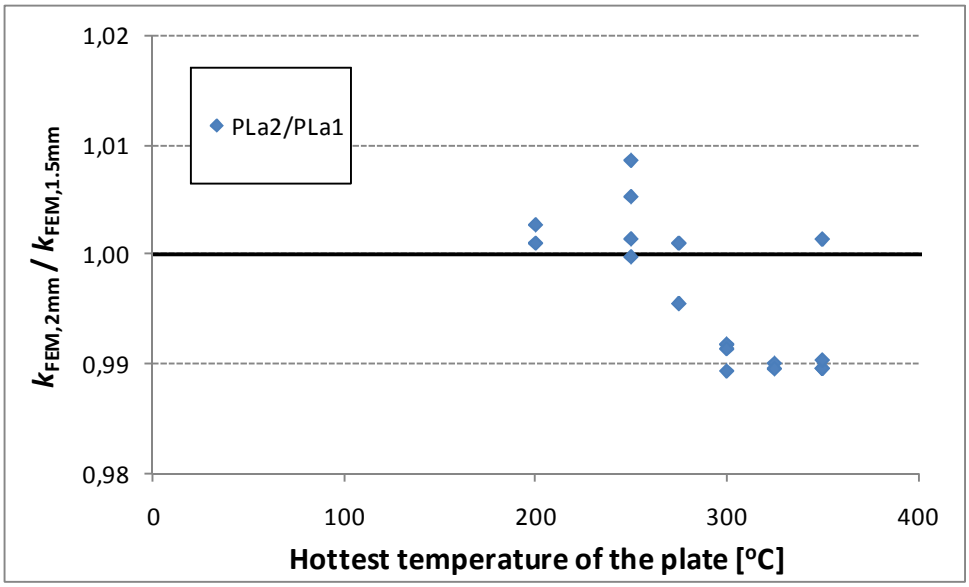

Figure 4.47. Effect of thickness of plate on reduction factors (aluminium).

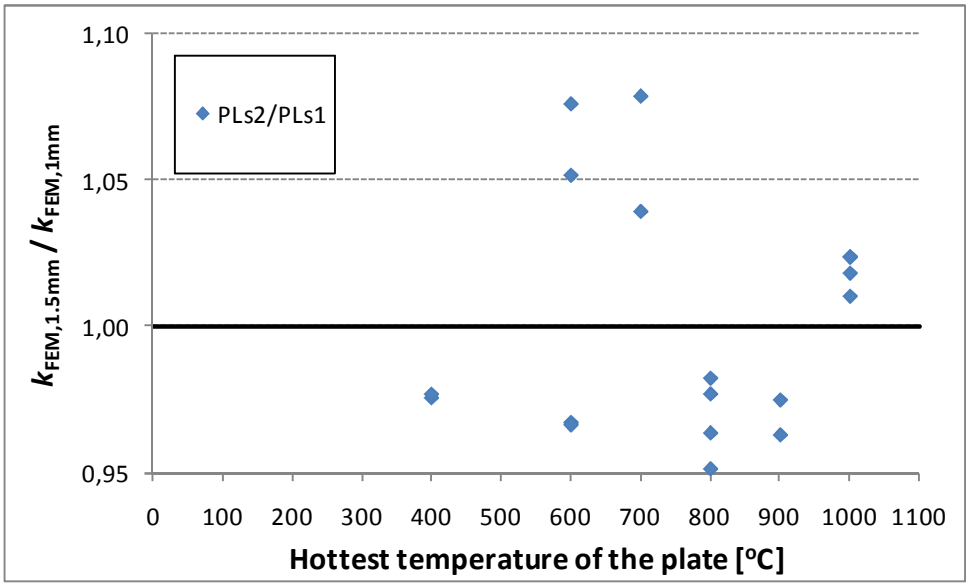

Figure 4.48. Effect of thickness of plate on reduction factors (stainless steel).

Figures 4.47 and 4.48 show that in some cases the reduction factors for PLa1 and PLs1 were higher and in some cases lower compared to those for PLa2 and PLs2. On average, the reduction factors for plates PLa1 and PLa2 as well as PLs1 and PLs2 were approximately the same. However, they also show that the scattering of the reduction factors in the case of stainless steel was clearly greater than in similar comparisons of the reduction factors for aluminium and carbon steel plates (Figs. 4.44 and 4.47).

Based on Tables 4.12–4.14 and Figures 4.42–4.48, it can be concluded that no connection between thickness or boundary conditions and reduction factor exists. The calculated reduction factors were independent of these properties in most cases, especially when the hottest temperature of the plate was no more than 600 °C. Based on Figures 4.42 and 4.43, it can be said that the calculated reduction factors were dependent on the yield strength of the plate; in every case they were higher for higher grade steel. Furthermore, the aspect ratio a/h also had a clear effect on the results; on average, the reduction factors were higher for higher aspect ratios.

The first FEM calculations of this research dealing with ultimate shear resistance [Salminen, Heinisuo, 2010] were conducted for carbon steel plate PL2 using a bilinear material model instead of the accurate model of EN 1993-1-2 [EN 1993-1-2, 2005] (Fig. 4.7). Figure 4.49 illustrates the differences between the material models at 400, 500, 600 and 700 °C. The effect of the material models was therefore studied for carbon steel plate PL2 at non-uniform elevated temperatures. The results of this comparison are presented in Tables 4.18 and 4.19.

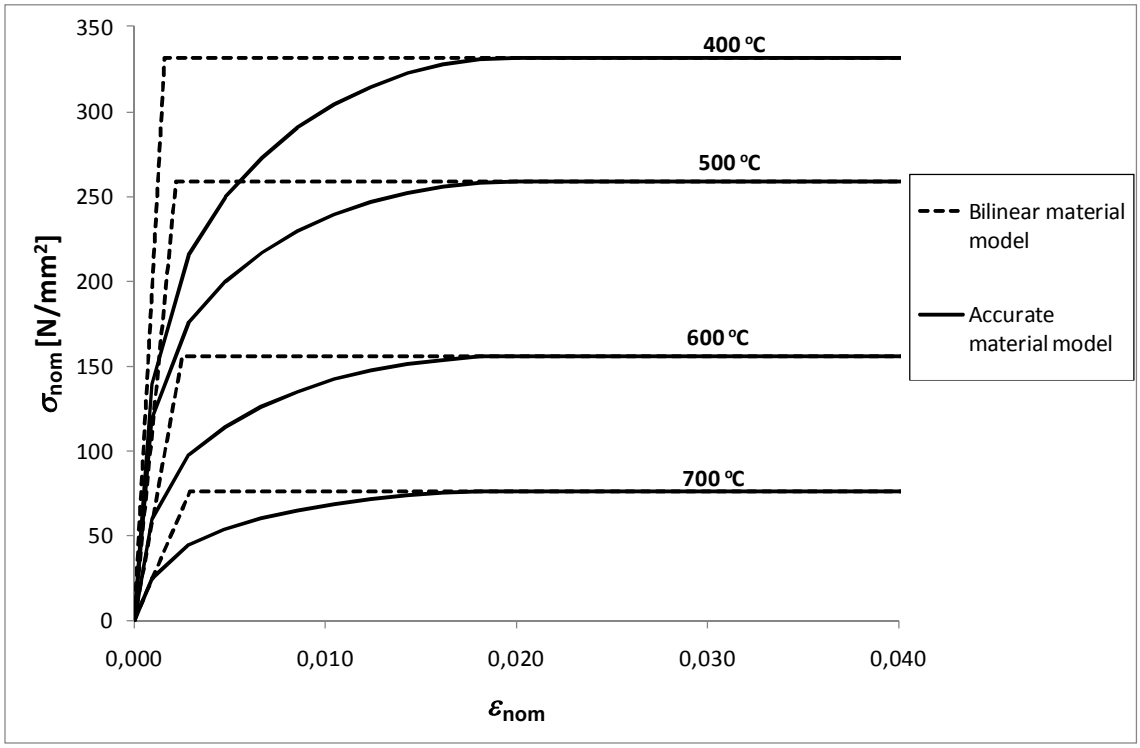

Figure 4.49. Difference between bilinear and accurate material models at elevated temperatures (PL2).

Table 4.18. Shear resistances of carbon steel plate PL2 using different material models (linear temperature distributions) [kN].

	100–300 °C	100–500 °C	100–700 °C	100–900 °C	200–500 °C	300–600 °C	400–700 °C	500–800 °C	600–900 °C
Accurate	29.51	23.33	11.37	4.00	22.38	15.69	8.71	4.36	2.44
Bilinear	33.69	29.46	13.27	4.61	28.48	19.95	10.53	5.18	3.02
Acc/Bil	0.88	0.79	0.86	0.87	0.79	0.79	0.83	0.84	0.81

Table 4.19. Shear resistances of carbon steel plate PL2 using different material models (non-linear temperature distributions) [kN].

	100–300 °C	100–500 °C	100–700 °C	100–900 °C	200–500 °C	300–600 °C	400–700 °C	500–800 °C	600–900 °C
Accurate	31.12	26.82	17.07	7.88	25.19	19.11	12.18	6.55	3.41
Bilinear	34.59	32.58	20.42	8.29	31.14	23.97	14.74	7.49	3.90
Acc/Bil	0.90	0.82	0.84	0.95	0.81	0.80	0.83	0.87	0.87

The resistances calculated using a bilinear material model were, on average, 16 % on the unsafe side compared to those obtained using the accurate material model shown in Figure 4.7. Based on the comparison presented in Tables 4.18 and 4.19, it is obvious that an accurate material model (Fig. 4.7) should be used in FEM analysis at elevated temperatures to obtain reliable results. The same conclusion can be drawn from the results shown in Figure 4.25, which indicates that a reduction based on 0.2 % proof

strength gives accurate results at uniform elevated temperatures. The problem with a bilinear material model is that the 0.2 % proof stresses are as high as the effective yield strength (see Fig. 4.49) while in reality they should be clearly lower.

Since the reduction factors shown in Tables 4.12–4.14 were somewhat independent on the thickness of the plate, one clearly thicker plate (PLT) was analysed in order to investigate if the reduction factors are completely independent on the thickness. A plate with same properties as PL1 (Table 4.1) except that t = 10 mm instead of 1 mm (λ = 0.33) was analysed at ambient temperature, uniform elevated temperatures of 400, 550 and 700 °C and at linear temperature distributions of 100–300, 100–500, 100–700 and 100–900 °C. Table 4.20 compares the resistances from FEM and according to EN 1993-1-5 [EN 1993-1-5, 2005] and EN 1993-1-2 [EN 1993-1-2, 2005] so that η = 1.0 (see Chapter 2.3).

Table 4.20. Shear resistances of thick plate PLT according to Eurocodes and FEM [kN].

	Temperature [°C]							
	20	400	550	700	100–300	100–500	100–700	100–900
EN	625.13	625.13	390.70	143.78	625.13	625.13	625.13	487.60
FEM	620.23	588.56	367.85	133.59	600.16	564.24	195.56	54.58
FEM/EN	0.99	0.94	0.94	0.93	0.96	0.90	0.31	0.11

Table 4.20 reveals that the resistances according to EN 1993-1-2 [EN 1993-1-2, 2005] are on unsafe side at elevated temperatures in the case of thick plate also. Especially at temperature distributions of 100–700 and 100–900 °C the Eurocode resistances were highly unconservative compared to those from FEM. Table 4.21 compares the reduction factors k_{FEM} (Eq. (4.5)) of plates PLT and PL1 at non-uniform elevated temperatures.

Table 4.21. Reduction factors k_{FEM} for PLT and PL1.

	Temperature distribution			
	100–300	100–500	100–700	100–900
PLT	0.968	0.910	0.315	0.088
PL1	0.836	0.657	0.319	0.112
PLT/PL1	1.16	1.39	0.99	0.79

Table 4.21 reveals that the reduction of shear resistance is different for thick plates than for thin plates at non-uniform elevated temperatures. The reduction factors of thick plate PLT were higher than those of PL1 at distributions of 100–300 and 100–500 °C and lower at distributions 100–700 °C and 100–900 °C. Thus, it can be concluded that even though the thickness of the plate did not have considerable effect on the reduction factors in the case of plates presented in Tables 4.12–4.14, the results of this study cannot be applied to thicker plates than considered in this study.

4.5 Discussion on the results of FEM analyses

The test results [Vimonsatit, Tan, Qian, 2007] for a beam web loaded in shear at ambient and uniform elevated temperatures were used as benchmark cases for FEM simulations. The comparison between tested and calculated resistances showed that the FEM model is reliable in analyzing the behaviour of an isolated plate at elevated temperatures.

Calculations at uniform elevated temperatures (Chapter 4.4.3) show that the ultimate shear resistance of thin metal plates at elevated temperatures can be reduced based on 0.2 % proof strength (see Figs. 4.25–4.27). According to EN 1993-1-2 [EN 1993-1-2, 2005] and EN 1999-1-2 [EN 1999-1-2, 2007], the reduction factor should be based on the average temperature of the plate in the case of a non-uniform temperature distribution. Figures 4.50–4.52 show all the reduction factors from numerical analyses at non-uniform temperature distributions (Tables 4.12–4.14) as a function of both the average and the hottest temperature of the plate. Moreover, the reduction factors for 0.2 % proof strengths according to EN 1993-1-2 [EN 1993-1-2, 2005] and EN 1999-1-2 [EN 1999-1-2, 2007] are plotted. Furthermore, an example is given in Figure 4.50 where the calculated reduction factor k_{FEM} for plate PL9 at the non-linear 300–600 °C temperature distribution was 0.567 and the average and hottest temperatures of the plate were 375 and 600 °C, respectively. Clearly in this case the reduction should be based on a temperature between the average and hottest temperature of the plate (approximately 480 °C) when using the 0.2 % proof strength curve of EN 1993-1-2 [EN 1993-1-2, 2005].

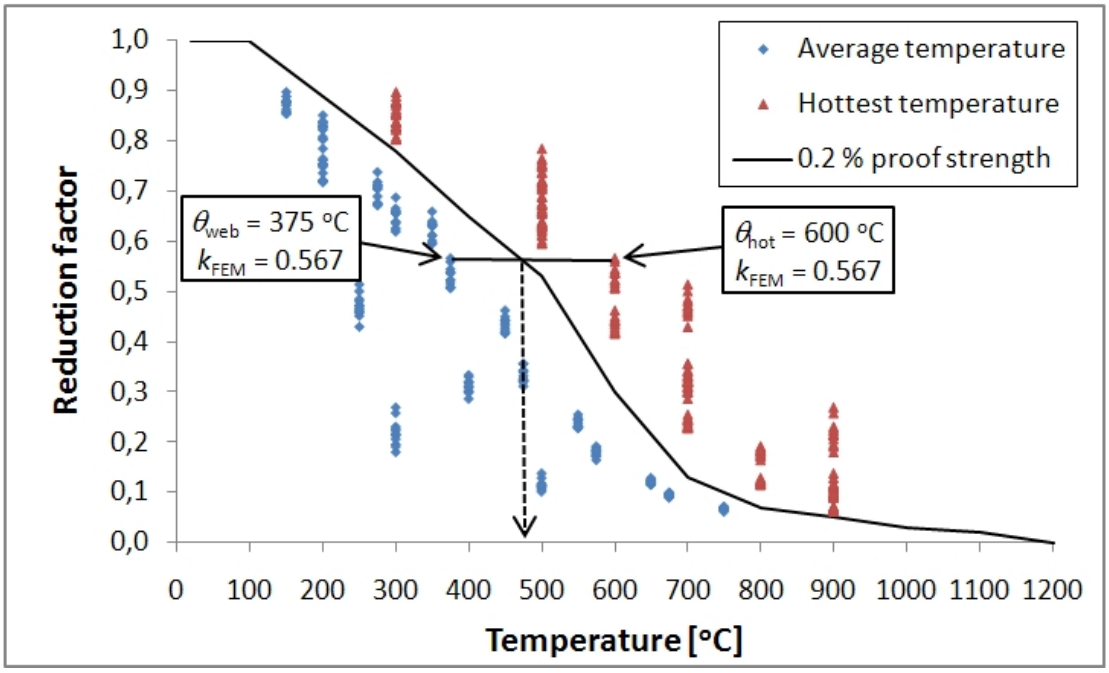

Figure 4.50. Reduction factors from numerical analyses as a function of average and hottest temperature of the plate (carbon steel).

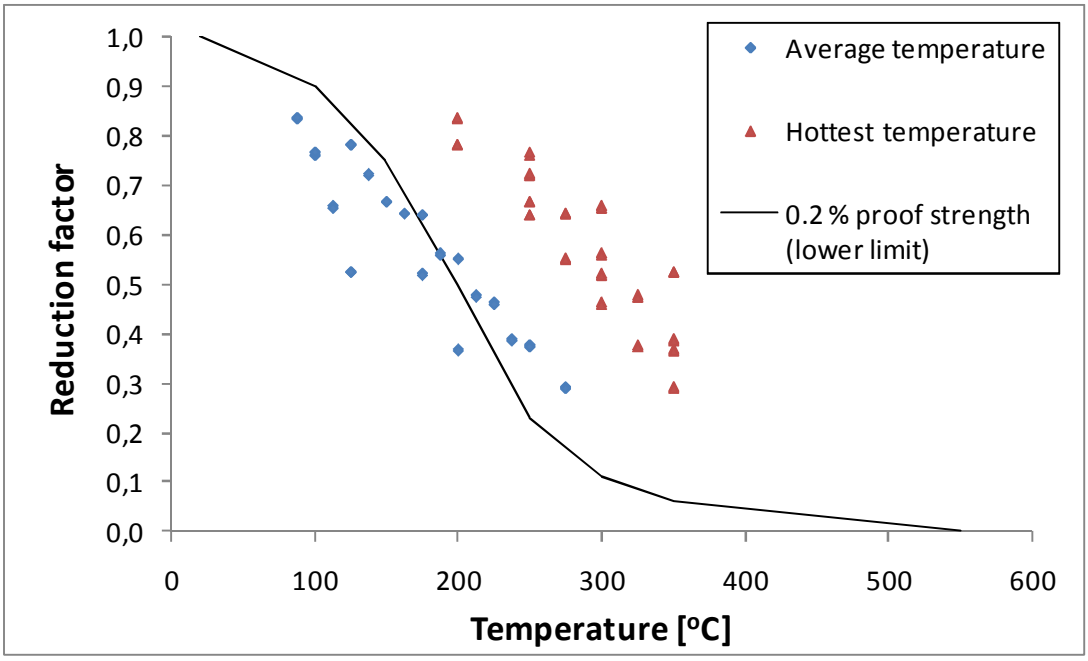

Figure 4.51. Reduction factors from numerical analyses as a function of average and hottest temperature of the plate (aluminium).

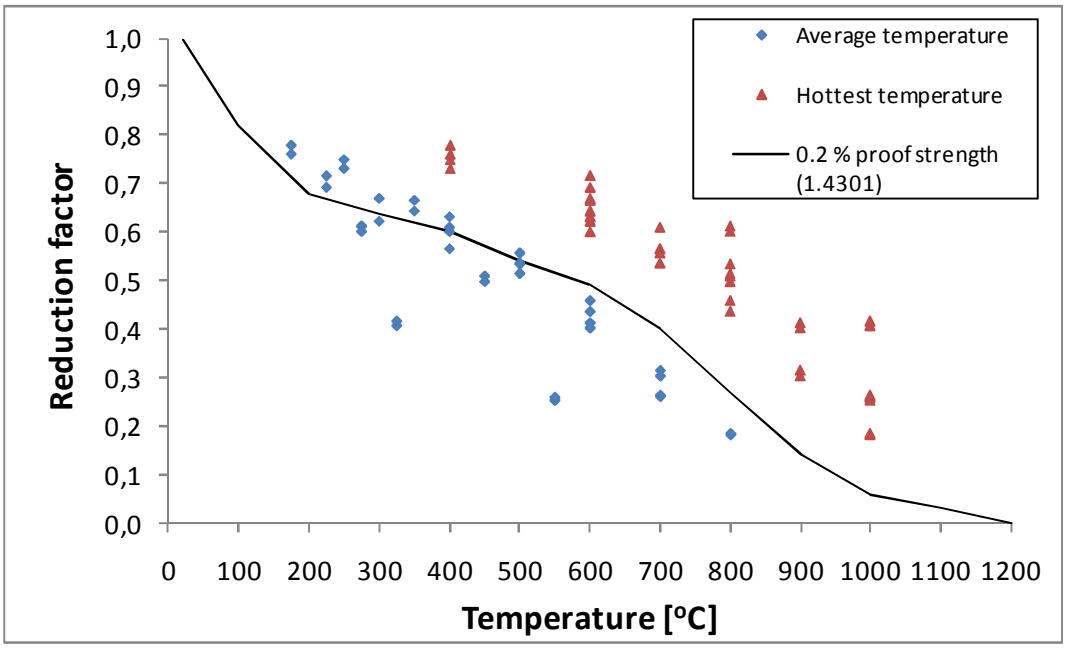

Figure 4.52. Reduction factors from numerical analyses as a function of average and hottest temperature of the plate (stainless steel).

Based on Figures 4.50–4.52, it can be said that if the temperature distribution across the plate is clearly non-uniform, there is no connection between the average temperature and the predicted reduction factor. Moreover, they show that all reduction factors based on average temperature were on the unsafe side compared to FEM results in the case of carbon steel. In the cases of aluminium and stainless steel, most of the reduction factors

based on average temperature were on the unsafe side. In all considered cases, the reductions based on the hottest temperature of the plate were on the safe side compared to FEM results. Therefore, it can be concluded that in most of the cases, the correct reduction factor should be based on a temperature between the average and the hottest temperature of the plate.

Figures 4.53–4.55 present the behaviour of plates PL1, PLa1 and PLs1 at uniform and non-uniform elevated temperatures when the average temperature of the plate θ_{web} is the same in both cases. All cases were calculated using small (h/100 000) initial imperfections. Some examples are given below:

Carbon steel plate PL1 (Fig. 4.53)

- Linear temperature distribution 100–500 °C (θ_{web} = 300 °C) compared to uniform 300 °C temperature,
- Linear temperature distribution 100–700 °C (θ_{web} = 400 °C) compared to uniform 400 °C temperature,
- Linear temperature distribution 100–900 °C (θ_{web} = 500 °C) compared to uniform 500 °C temperature.

Aluminium plate PLa1 (Fig. 4.54)

- Linear temperature distributions 50–350 °C and 125-275 °C (θ_{web} = 200 °C) compared to uniform 200 °C temperature,
- Linear temperature distribution 175–325 °C (θ_{web} = 250 °C) compared to uniform 250 °C temperature.

Stainless steel plate PLs1 (Fig. 4.55)

- Linear temperature distribution 100–600 °C (θ_{web} = 350 °C) compared to uniform 350 °C temperature,
- Linear temperature distribution 100–800 °C (θ_{web} = 450 °C) compared to uniform 450 °C temperature,
- Linear temperature distribution 100–1000 °C (θ_{web} = 550 °C) compared to uniform 550 °C temperature.

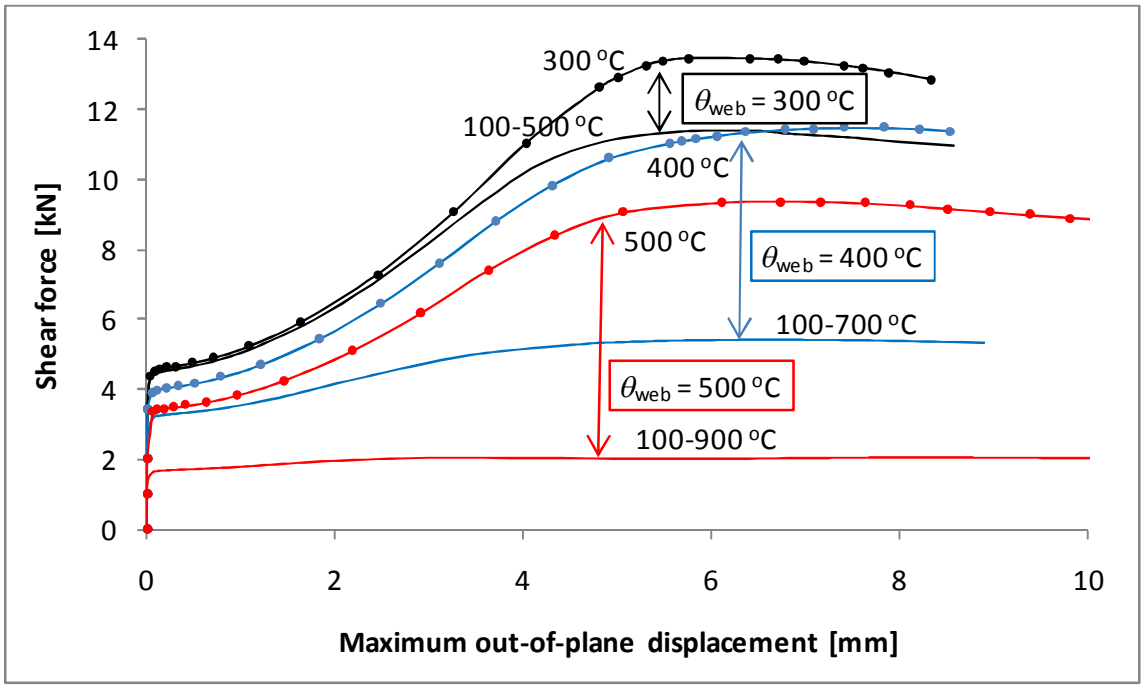

Figure 4.53. Behaviour of carbon steel plate PL1 at elevated temperatures with same average temperature.

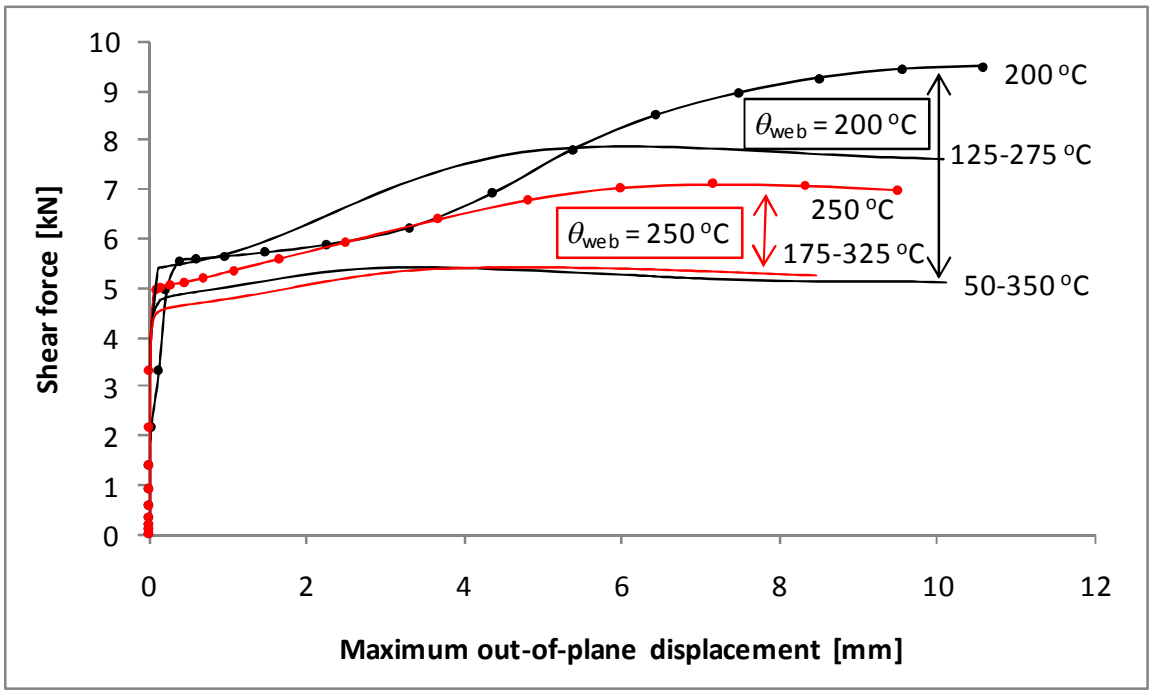

Figure 4.54. Behaviour of aluminium plate PLa1 at elevated temperatures with same average temperature.

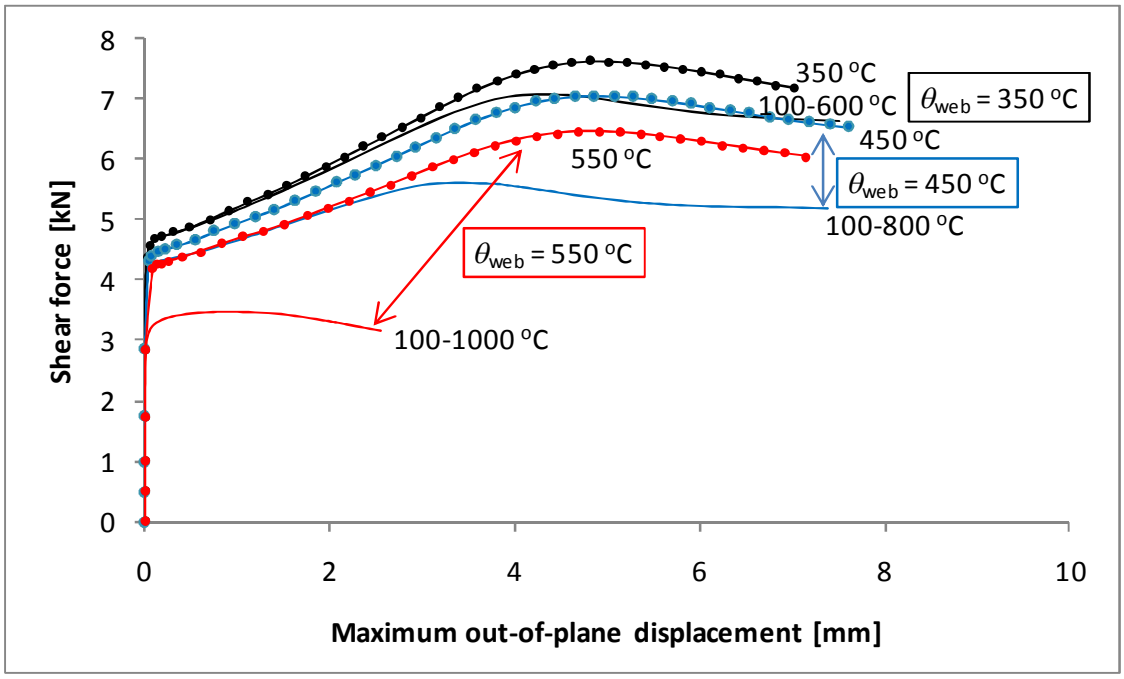

Figure 4.55. Behaviour of stainless steel plate PLs1 at elevated temperatures with same average temperature.

Figures 4.53–4.55 show that the behaviour of a plate at non-uniform elevated temperatures is significantly different from that of a plate at uniform elevated temperature, of the same magnitude as the average temperature of the non-uniform distribution. The wider the distribution, the wider were the differences in behaviour (see e.g. curves 100–900 °C compared to 500 °C in Fig. 4.53 or 100–1000 °C compared to 550 °C in Fig. 4.55). For aluminium the differences in behaviour were smaller due to the smaller temperature differences of the distributions.

It can be concluded that in the case of a clearly non-uniform temperature distribution, the use of average temperature for the whole plate does not yield accurate results. Moreover, it can be seen that the use of average temperature leads to too high resistances in the cases considered.

5 PROPOSED CALCULATION METHODS

As described in Chapters 1 and 2, numerous different tension field models have been developed in order to describe the behaviour of a thin plate under shear loading. However, no complete explanation for that phenomenon exists even at ambient temperature [Yoo, Lee, 2006]. At elevated temperatures metal material behaviour becomes highly non-linear (Figs. 4.7, 4.10 and 4.12) and the phenomenon becomes even more complex, especially when the temperature distribution across the plate is non-uniform. Thus, instead of trying to develop a tension field model for non-uniform elevated temperatures, the strategy was to reduce ambient temperature resistances by appropriate reduction factors.

Chapter 5.1 presents method of separation of shear and post-buckling (referred as method A), which was first considered in [Salminen, Heinisuo, 2011(a)]. Method A predicts the shear buckling ($V_{cr,fi}$) and post-buckling resistances ($V_{pb,fi}$) separately. It should be noted that most of the final shear resistances at non-uniform elevated temperatures of this study were calculated using an initial imperfection $h/100$ according to EN 1090-2 [EN 1090-2, 2008] which meant that shear buckling and post-buckling resistances cannot be seen separately. Thus, in a worked example for method A presented in Chapter 5.1.2, the resistances are calculated using an imperfection $h/100\,000$. Moreover, some of the cases in Chapter 4.4.4 were calculated with small imperfections. They are compared to the results yielded by method A in Chapter 5.1.3.

Chapter 5.2 proposes a method of reference temperature (referred as method B) which is a modification of the Eurocode [EN 1993-1-2, 2005] and [EN 1999-1-2, 2007] methods and intended only for determining ultimate shear resistance $V_{ult,fi}$. Method B is applied to carbon steel, aluminium and stainless steel in Chapters 5.2.2, 5.2.3 and 5.2.4, respectively. Chapter 5.2.5 presents a worked example that uses method B, and in Chapter 5.2.6 the results of this method are compared to all the calculated reduction factors at non-uniform elevated temperatures shown in Chapter 4.4.4. Finally, Chapter 5.3 discusses the proposed calculation methods.

5.1 Method of separation of shear and post-buckling (method A)

5.1.1 General

Method of separation of shear and post-buckling (referred as method A) is based on the assumption that the contribution of post-buckling resistance to ultimate shear resistance at elevated temperatures ($V_{pb,fi}$ / $V_{ult,fi}$) can be defined from the respective relationship at ambient temperature ($V_{pb,amb}$ / $V_{ult,amb}$) by reducing it by the ratio $k_{p0.2,\theta}$ / $k_{E,\theta}$ as shown in Equation (5.1). The equation is in relatively good agreement with calculated cases at uniform elevated temperatures as can be seen from Figure 4.33. The problem at non-uniform elevated temperatures is the definition of the temperatures on which reduction factors are based.

$$\frac{k_{p0.2,\theta}}{k_{E,\theta}} \frac{V_{pb,amb}}{V_{ult,amb}} = \frac{V_{pb,fi}}{V_{ult,fi}} \tag{5.1}$$

Shear buckling ($V_{cr,fi}$) and post-buckling resistances ($V_{pb,fi}$) at elevated temperatures are calculated separately in this method, and ultimate shear resistance $V_{ult,fi}$ is their sum, $V_{ult,fi} = V_{cr,fi} + V_{pb,fi}$. The contributions of shear buckling ($V_{cr,amb}$) and post-buckling resistances ($V_{pb,amb}$) at ambient temperature are needed in this method to calculate the corresponding resistances at elevated temperatures. They can be obtained by using the equations of Eurocodes [EN 1993-1-5, 2005], [EN 1993-1-4, 2006], [EN 1999-1-1, 2007] or by FEM analysis. Thus, method A can take two different forms, depending on how ambient temperature resistances are defined:

- Design method (A1): Ambient temperature resistances ($V_{cr,amb}$, $V_{pb,amb}$ and $V_{ult,amb}$) are calculated using the equations of Eurocodes, and
- Theoretical method (A2): Ambient temperature resistances are defined using FEM.

In EN 1993-1-5 [EN 1993-1-5, 2005] shear buckling and post-buckling resistances are not calculated separately even though the classical formulas (Eqs. (2.6)–(2.8)) for defining V_{cr} are applied in the calculation of the slenderness parameter λ. Only the contributions of web and flanges are calculated separately in EN 1993-1-5. The proposed method A assumes that plate behaviour is ideal meaning that both phases of the thin plate behaviour under shear loading (buckling and post-buckling) are evident. Therefore, Equations (2.5)–(2.8) are applied in the calculation of $V_{cr,amb}$ according to approach A1.

Method A is applicable only to slender plates where the proportional limit is not exceeded (even at elevated temperatures) as shear buckling occurs, because otherwise the method proposed in [Salminen, 2010] does not give reliable values for $V_{cr,fi}$. The ultimate shear resistance ($V_{ult,fi}$) of a plate at non-uniform elevated temperatures is calculated as follows:

$$V_{ult,fi} = V_{cr,fi} + V_{pb,fi} \tag{5.2}$$

Shear buckling resistance at elevated temperatures $V_{cr,fi}$ is obtained from Equation (5.3).

$$V_{cr,fi} = k_{E,\theta,A} V_{cr,amb} \tag{5.3}$$

where
- $k_{E,\theta,A}$ is the reduction factor for elastic modulus defined according to the method presented in [Salminen, 2010] (see Figs. 5.1 and 5.2), and
- $V_{cr,amb}$ is the shear buckling resistance of the plate at ambient temperature (Eqs. (2.5)–(2.10)) (A1) or from FEM analysis (A2).

The reduction factor $k_{E,\theta,A}$ is defined by connecting points $\begin{pmatrix} \theta_{mid} \\ k_{E,\theta}(\theta_{hot}) \end{pmatrix}$ and $\begin{pmatrix} 2\theta_{web} - \theta_{cold} \\ k_{E,\theta}(\theta_{cold}) \end{pmatrix}$ (blue points in Fig. 5.2) by a line in a drawing displaying the reduction curve of elastic modulus according to EN 1993-1-2 [EN 1993-1-2, 2005] for carbon and stainless steel or EN 1999-1-2 [EN 1999-1-2, 2007] for aluminium. The intersection of the drawn line and the reduction curve (red point in Fig. 5.2) indicates the reduction factor $k_{E,\theta,A}$ (and corresponding temperature θ_A) to be used [Salminen, 2010]. Use of this method is illustrated in Figures 5.1 and 5.2.

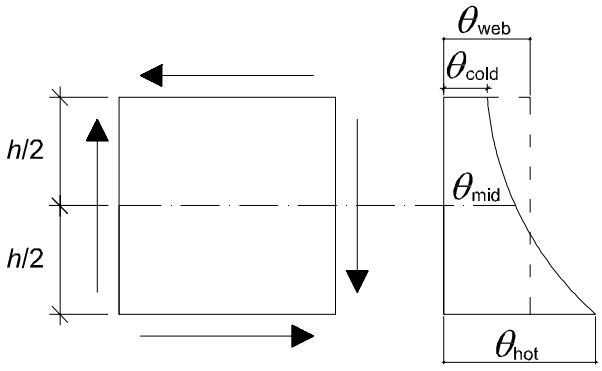

Figure 5.1. Temperatures needed to define reduction factor $k_{E,\theta,A}$.

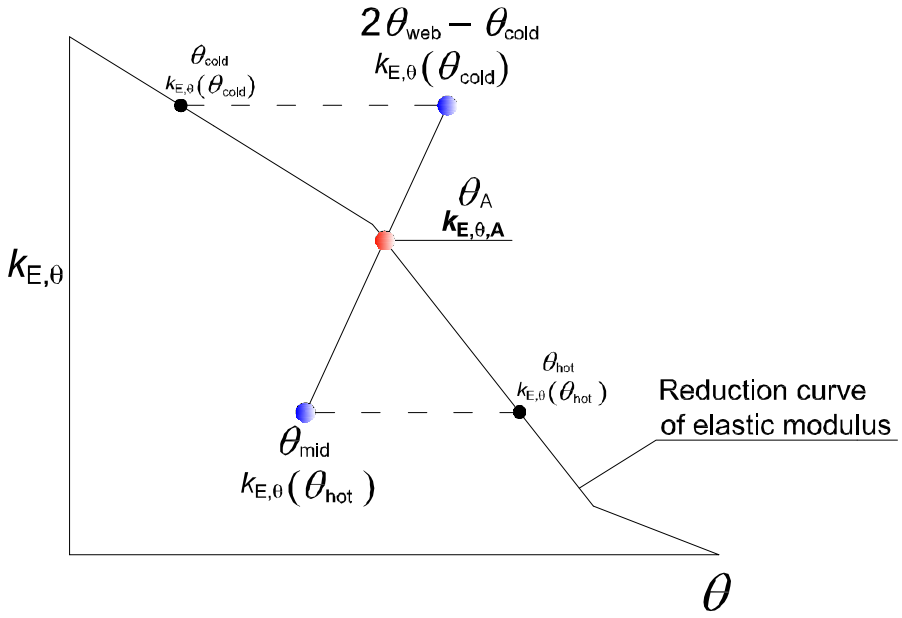

Figure 5.2. Method for defining reduction factor $k_{E,\theta,A}$.

The temperature and reduction factor notations of Figures 5.1 and 5.2 are as follows:

- θ_{web} is the average temperature of the plate [°C],
- θ_{cold} is the coldest temperature of the plate [°C],
- θ_{mid} is the temperature in the middle of the height of the plate [°C],
- θ_{hot} is the hottest temperature of the plate [°C],
- $k_{E,\theta}$ (θ_{cold}) is the reduction factor for elastic modulus at θ_{cold},
- $k_{E,\theta}$ (θ_{hot}) is the reduction factor for elastic modulus at θ_{hot},

Post-buckling resistance at non-uniform elevated temperatures $V_{pb,fi}$ is calculated as shown in Equation (5.4), which is derived from Equation (5.1). Shear buckling resistance at elevated temperatures is needed for this equation. Thus, $V_{cr,fi}$ must be calculated first as shown in Equation (5.3).

$$V_{pb,fi} = \frac{k_{p0.2,\theta,A} V_{pb,amb} V_{cr,fi}}{k_{E,\theta,A} V_{ult,amb} - k_{p0.2,\theta,A} V_{pb,amb}} \tag{5.4}$$

where

- $k_{p0.2,\theta,A}$ is the reduction factor for 0.2 % proof stress at temperature $\frac{\theta_{web} + \theta_{hot}}{2}$,
- $V_{pb,amb}$ is the post-buckling resistance at ambient temperature,
- $V_{cr,fi}$ is the shear buckling resistance at elevated temperatures as defined in Equation (5.3),

- $k_{E,\theta,A}$ is the reduction factor for elastic modulus as defined in Figure 5.2,
- $V_{ult,amb} = V_{cr,amb} + V_{pb,amb}$ is the ultimate shear resistance at ambient temperature.

Ultimate shear resistance at ambient temperature $V_{ult,amb}$ is calculated according to Eurocodes [EN 1993-1-5, 2005], [EN 1993-1-4, 2006], [EN 1999-1-1, 2007] (approach A1) or derived from non-linear FEM analysis (approach A2) while post-buckling resistance at ambient temperature $V_{pb,amb}$ is obtained from the following:

$$V_{pb,amb} = V_{ult,amb} - V_{cr,amb} \geq 0 \tag{5.5}$$

5.1.2 Worked example

The proposed method of separation of shear and post-buckling (method A) was applied to carbon steel plate PL1 and stainless steel plate PLs1 at non-uniform elevated temperatures. The mechanical FEM analyses of this worked example were conducted the same way as described in Chapter 4.2, except that the magnitude of the initial imperfection was $h/100\ 000$ instead of $h/100$ to ensure the visibility of the shear buckling phase. The properties of the considered plates are shown in Table 5.1. The most slender plates of each material (see Tables 4.1 and 4.2) were selected so that shear buckling would occur before the proportionality limit is exceeded. The results obtained using method A are compared to those from FEM analysis and those calculated according to Eurocodes [EN 1993-1-5, 2005], [EN 1993-1-4, 2006] and [EN 1993-1-2, 2005]. This worked example was first presented in [Salminen, Heinisuo, 2011(a)]. It should be noted that material safety factors are not considered in this worked example. They are assumed to be 1.0.

Table 5.1. Properties of the plates considered in the worked example.

Plate	Boundaries	Geometry (a x h) [mm]	f_y or f_o/f_u [N/mm^2]	E [N/mm^2]	h/t	λ
PL1	Simple	305 x 305 x 1	355	210 000	305	3.28
PLs1	Simple	305 x 305 x 1	210/520	200 000	305	2.59

The temperature distributions of this worked example are motivated by a thermal FEM analysis conducted for an all-metal sandwich panel [Salminen, 2010] (see also Fig. 3.15). The temperature distributions from the FEM analysis were rather close to linear and correspond to 5, 10, 15, 20, 25 and 30 minutes exposure to standard fire [EN 1991-1-2, 2002] in the case of the carbon steel all-metal sandwich panel analyzed in [Salminen, 2010]. The same temperature distributions were applied also to stainless steel plates.

The shear resistances of the plates shown in Table 5.1 will be calculated at ambient temperature, and at six linear temperature distributions: 80–420, 260–560, 370–630, 430–680, 460–700 and 480–730 °C. Figure 5.3 presents the applied temperature distributions as a function of the height coordinate *y* of the plate.

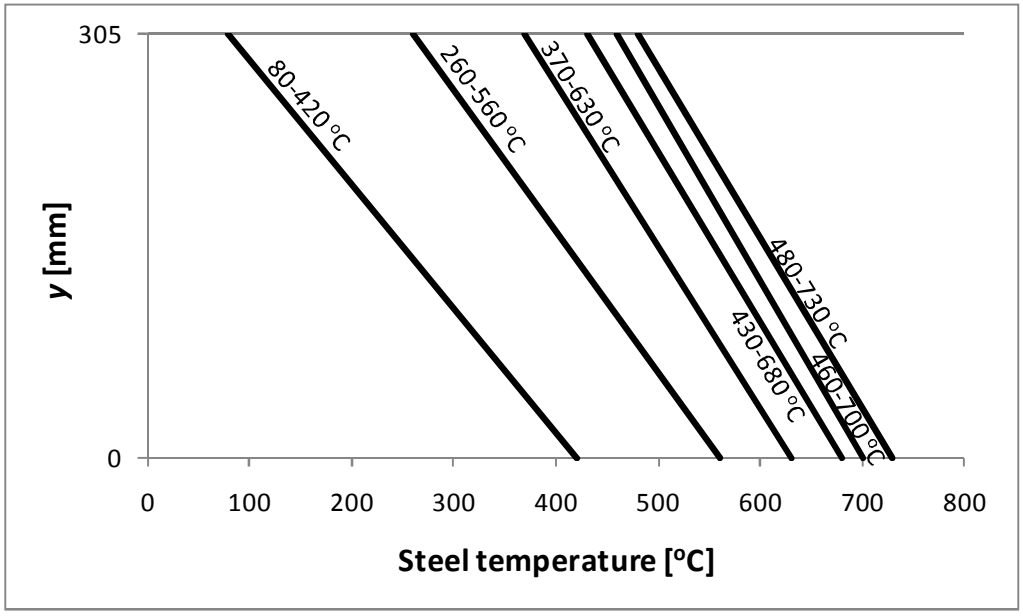

Figure 5.3. Temperature distributions of the worked example.

In the following, the shear resistance of carbon steel plate PL1 is calculated at the 480–730 °C temperature distribution by the hand-calculation method A1 where ambient temperature resistances are defined using the equations given in EN 1993-1-5 [EN 1993-1-5, 2005].

Calculation of shear buckling resistance

First, the shear buckling resistance $V_{\mathrm{cr,amb}}$ is calculated at ambient temperature using classical Equations (2.5)–(2.8), which are also found in EN 1993-1-5 [EN 1993-1-5, 2005]:

$$\tau_{cr} = 9.34\frac{\pi^2 210000}{12(1-0.3^2)}\left(\frac{1}{305}\right)^2 = 19.06 \text{ N/mm}^2 \tag{5.6}$$

$$V_{cr,amb} = 19.06 \cdot 1 \cdot 305 = \underline{5.81 \text{ kN}} \tag{5.7}$$

The following temperatures and reduction factors are needed for the graphical method shown in Figure 5.2:

- $\theta_{\mathrm{web}} = 605$ °C,
- $\theta_{\mathrm{cold}} = 480$ °C,

- θ_{mid} = 605 °C,
- θ_{hot} = 730 °C,
- $k_{E,\theta}$ (θ_{cold}) = 0.620 according to EN 1993-1-2 [EN 1993-1-2, 2005] and
- $k_{E,\theta}$ (θ_{hot}) = 0.118 according to EN 1993-1-2 [EN 1993-1-2, 2005].

Figure 5.4 shows how the reduction factor $k_{E,\theta,A}$ for shear buckling is determined in this case (see also Fig. 5.2).

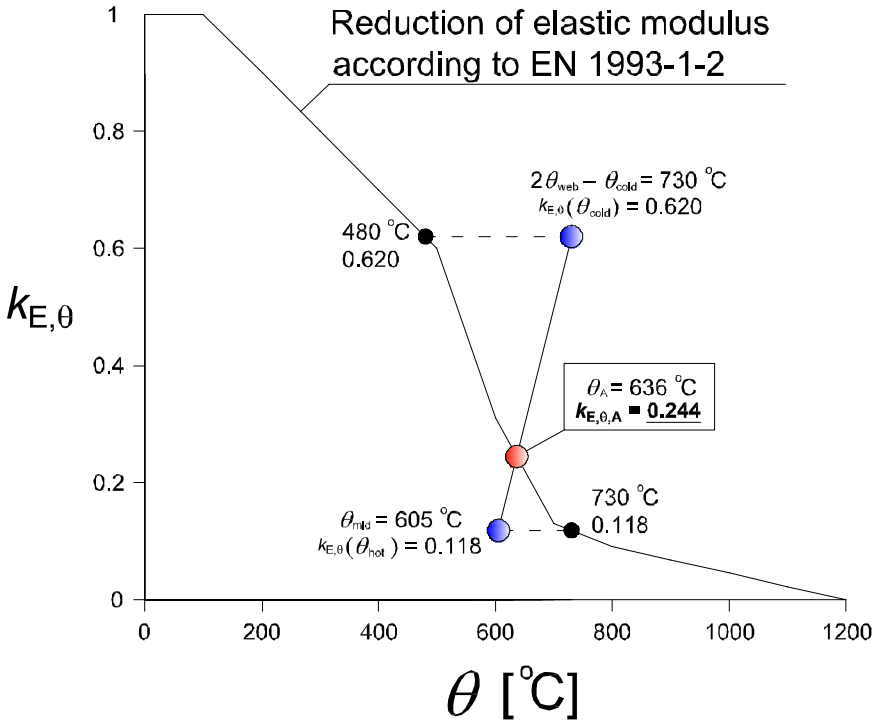

Figure 5.4. Determining the reduction factor $k_{E,\theta,A}$ for carbon steel plate PL1 at 480–730 °C temperature distribution.

Figure 5.4 shows that reduction factor $k_{E,\theta,A}$ = 0.244 in this case. The shear buckling resistance of plate PL1 at 480–730 °C temperatures is then obtained from the following:

$$V_{cr,fi} = k_{E,\theta,A} \cdot V_{cr,amb} = 0.244 \cdot 5.81 \text{ kN} = \underline{1.42 \text{ kN}} \qquad (5.8)$$

Calculation of post-buckling resistance

The post-buckling resistance of plate PL1 at 480–730 °C temperatures is determined using Equation (5.4). The following data is needed in the calculation:

- $k_{p0.2,\theta,A} = k_{p0.2,\theta}\left(\frac{605^{o}C + 730^{o}C}{2}\right) = k_{p0.2,\theta}$ (668 °C) = 0.185

- $V_{ult,amb}$ = 15.82 kN according to EN 1993-1-5 [EN 1993-1-5, 2005]
- $V_{pb,amb} = V_{ult,amb} - V_{cr,amb}$ = 15.82 kN – 5.81 kN = 10.01 kN
- $V_{cr,fi}$ = 1.42 kN (see Eq. (5.8),
- $k_{E,\theta,A}$ = 0.244 (see Fig. 5.4)

When inputting the above values into Equation (5.4), the post-buckling resistance at elevated temperatures is calculated as follows (in kN):

$$V_{pb,fi} = \frac{0.185 \cdot 10.01 \cdot 1.42}{0.244 \cdot 15.82 - 0.185 \cdot 10.01} = \underline{1.31 \text{ kN}} \qquad (5.9)$$

Calculation of ultimate shear resistance

Ultimate shear resistance is the sum of the shear buckling and post-buckling resistances as defined in Equation (5.2):

$$V_{ult,fi} = V_{cr,fi} + V_{pb,fi} = 1.42 \text{ kN} + 1.31 \text{ kN} = \underline{2.73 \text{ kN}} \qquad (5.10)$$

Results

The calculated shear buckling (V_{cr}), post-buckling (V_{pb}) and ultimate shear resistances (V_{ult}) of plates PL1 and PLs1 at ambient and elevated temperatures are shown in Tables 5.2 and 5.3, respectively. Resistances from numerical analysis (FEM) are compared to those obtained using methods A1 and A2 and those calculated according to Eurocodes ($V_{ult,EN}$) [EN 1993-1-5], [EN 1993-1-4, 2006] and [EN 1993-1-2, 2005]. According to EN 1993-1-2 [EN 1993-1-2, 2005], shear resistance at ambient temperature is reduced by the reduction factor $k_{p0.2,\theta,web}$ which is based on the average temperature of the plate θ_{web}. Eurocode resistances were also calculated using the reduction factor $k_{p0.2,\theta,hot}$ based on the hottest temperature of the plate θ_{hot}. Eurocode resistances calculated using the average temperature of the plate are marked $V_{ult,EN}$ and those calculated using the maximum temperature of the plate are marked $V_{ult,EN}$*. In the FEM analysis, the shear force corresponding to the first increment where maximum out-of-plane displacement of the plate was more than 0.1 mm was used as the critical shear force V_{cr}.

Table 5.2. Calculated shear buckling, post-buckling and ultimate shear resistances of carbon steel plate PL1 [kN].

	Temperature distribution [°C]						
	20	80–420	260–560	370–630	430–680	460–700	480–730
$V_{cr,FEM}$	5.73	4.80	3.83	2.94	2.21	1.88	1.55
$V_{cr,A1}$	5.81	4.60	3.60	2.60	1.89	1.64	1.42
$V_{cr,A2}$	5.73	4.53	3.55	2.57	1.87	1.62	1.40
$V_{cr,FEM}$ / $V_{cr,A1}$	0.99	1.04	1.06	1.13	1.17	1.15	1.09
$V_{cr,FEM}$ / $V_{cr,A2}$	1.00	1.06	1.08	1.15	1.18	1.16	1.11
$V_{pb,FEM}$	11.89	8.20	5.37	3.34	2.28	1.91	1.55
$V_{pb,A1}$	10.01	6.55	4.57	3.02	2.09	1.78	1.31
$V_{pb,A2}$	11.89	7.61	5.25	3.45	2.37	2.02	1.47
$V_{pb,FEM}$ / $V_{pb,A1}$	1.19	1.25	1.17	1.10	1.09	1.07	1.18
$V_{pb,FEM}$ / $V_{pb,A2}$	1.00	1.08	1.02	0.97	0.96	0.95	1.06
$V_{ult,FEM}$	17.62	13.00	9.20	6.28	4.49	3.79	3.10
$V_{ult,A1}$	15.82	11.14	8.17	5.63	3.98	3.42	2.73
$V_{ult,A2}$	17.62	12.14	8.80	6.01	4.24	3.63	2.87
$V_{ult,EN}$	15.82	13.21	10.09	8.38	6.38	5.47	4.61
$V_{ult,EN}$*	15.82	9.90	6.20	3.94	2.59	2.06	1.77
$V_{ult,FEM}$ / $V_{ult,A1}$	1.11	1.17	1.13	1.12	1.13	1.11	1.14
$V_{ult,FEM}$ / $V_{ult,A2}$	1.00	1.07	1.05	1.04	1.06	1.04	1.08
$V_{ult,FEM}$ / $V_{ult,EN}$	1.11	0.98	0.91	0.75	0.70	0.69	0.67
$V_{ult,FEM}$ / $V_{ult,EN}$*	1.11	1.31	1.48	1.59	1.73	1.84	1.75

Table 5.3. Calculated shear buckling, post-buckling and ultimate shear resistances of stainless steel plate PLs1 [kN].

	Temperature distribution [°C]						
	20	80–420	260–560	370–630	430–680	460–700	480–730
$V_{cr,FEM}$	5.45	4.90	4.54	4.34	4.20	4.19	4.13
$V_{cr,A1}$	5.54	4.86	4.52	4.33	4.21	4.14	4.06
$V_{cr,A2}$	5.45	4.79	4.45	4.26	4.14	4.08	3.99
$V_{cr,FEM}$ / $V_{cr,A1}$	0.98	1.01	1.00	1.00	1.00	1.01	1.02
$V_{cr,FEM}$ / $V_{cr,A2}$	1.00	1.02	1.02	1.02	1.01	1.03	1.03
$V_{pb,FEM}$	5.01	3.01	2.48	2.20	1.91	1.72	1.50
$V_{pb,A1}$	7.41	3.35	2.83	2.56	2.34	2.20	2.05
$V_{pb,A2}$	5.01	2.48	2.11	1.92	1.77	1.67	1.56
$V_{pb,FEM}$ / $V_{pb,A1}$	0.68	0.90	0.88	0.86	0.82	0.78	0.73
$V_{pb,FEM}$ / $V_{pb,A2}$	1.00	1.21	1.18	1.15	1.08	1.03	0.96
$V_{ult,FEM}$	10.46	7.91	7.02	6.54	6.11	5.91	5.63
$V_{ult,A1}$	12.95	8.22	7.35	6.89	6.55	6.35	6.11
$V_{ult,A2}$	10.46	7.27	6.56	6.18	5.91	5.75	5.55
$V_{ult,EN}$	12.95	8.55	7.69	6.99	6.64	6.47	6.29
$V_{ult,EN}$*	12.95	7.61	6.60	5.99	5.41	5.18	4.67
$V_{ult,FEM}$ / $V_{ult,A1}$	0.81	0.96	0.96	0.95	0.93	0.93	0.92
$V_{ult,FEM}$ / $V_{ult,A2}$	1.00	1.09	1.07	1.06	1.03	1.03	1.01
$V_{ult,FEM}$ / $V_{ult,EN}$	0.81	0.93	0.91	0.94	0.92	0.91	0.90
$V_{ult,FEM}$ / $V_{ult,EN}$*	0.81	1.04	1.06	1.09	1.13	1.14	1.20

The resistances presented in Tables 5.2 and 5.3 are shown graphically in Figures 5.5–5.10.

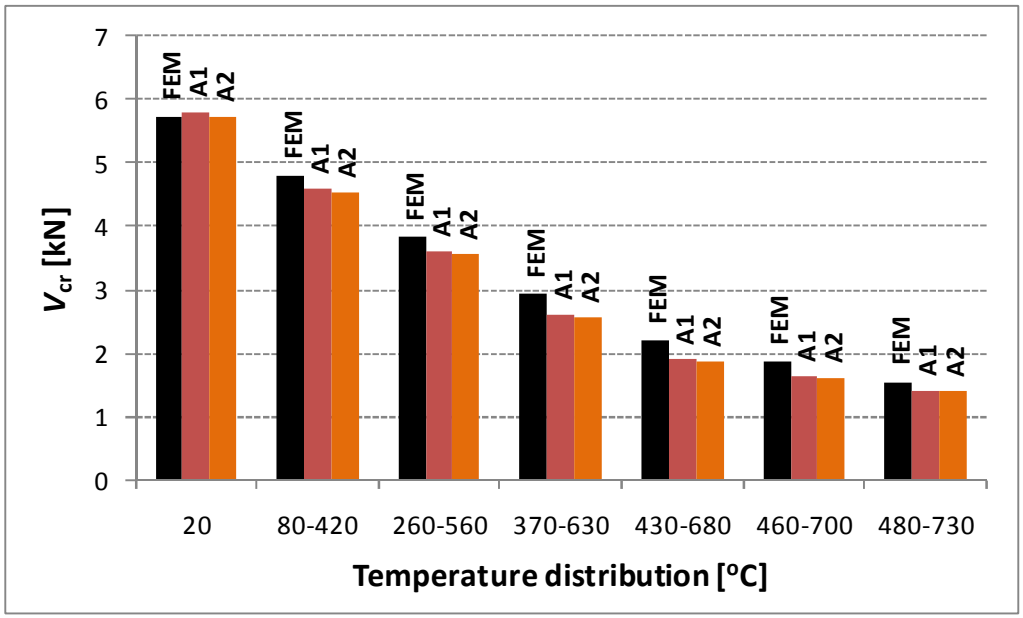

Figure 5.5. Shear buckling resistances V_{cr} of carbon steel plate PL1 from FEM and methods A1 and A2.

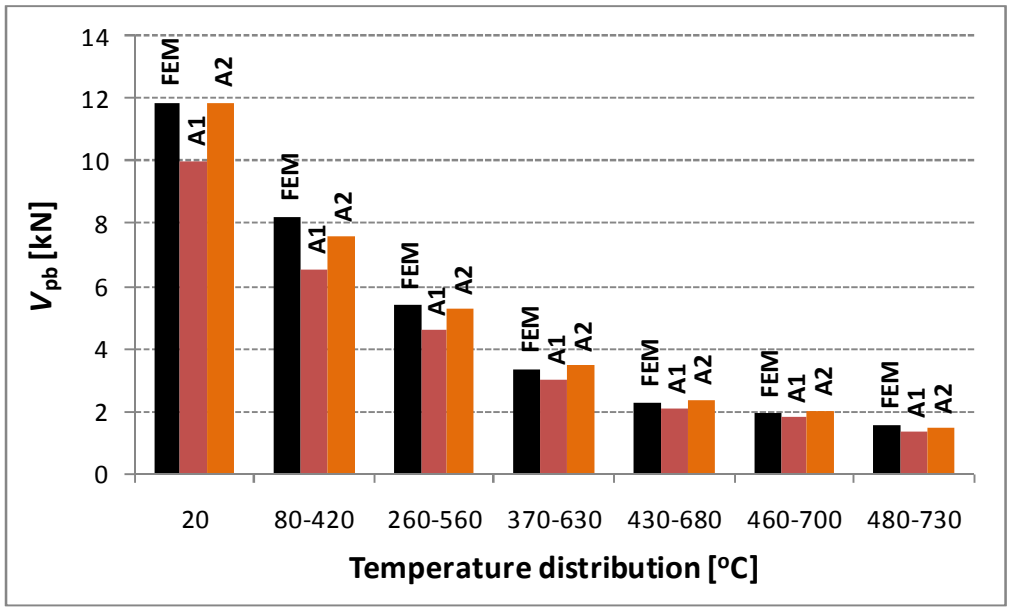

Figure 5.6. Post-buckling resistances V_{pb} of carbon steel plate PL1 from FEM and methods A1 and A2.

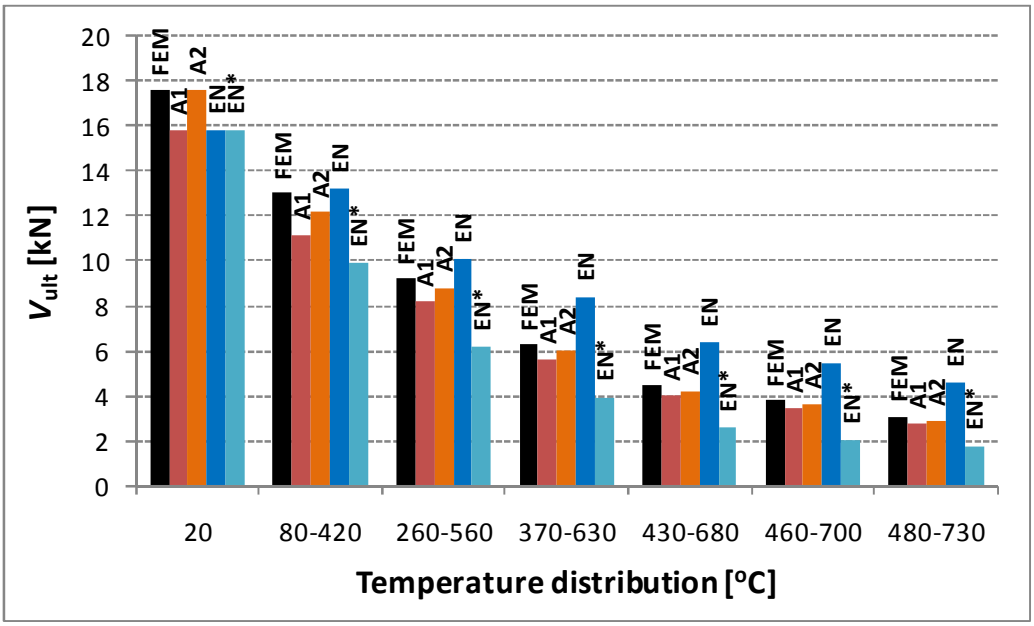

Figure 5.7. Ultimate shear resistances V_{ult} of carbon steel plate PL1 from FEM, methods A1 and A2 and Eurocodes.

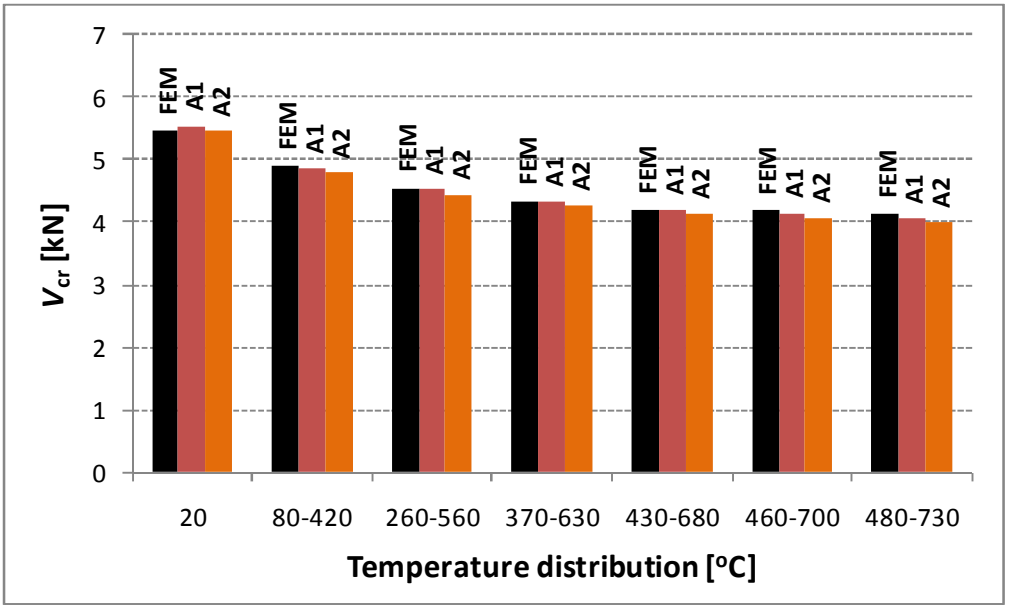

Figure 5.8. Shear buckling resistances V_{cr} of stainless steel plate PLs1 from FEM and method A.

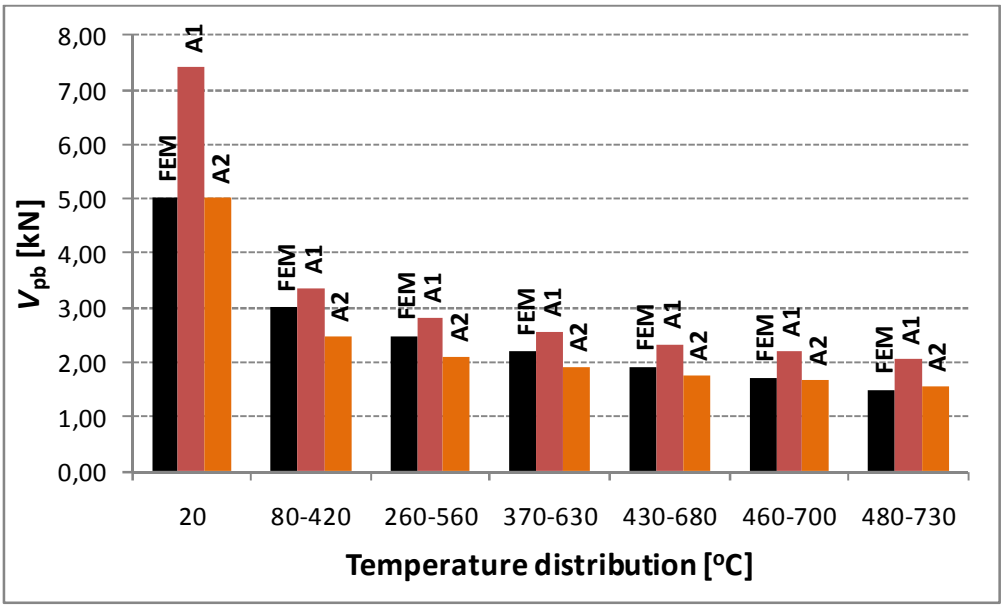

Figure 5.9. Post-buckling resistances V_{pb} of stainless steel plate PLs1 from FEM and methods A1 and A2.

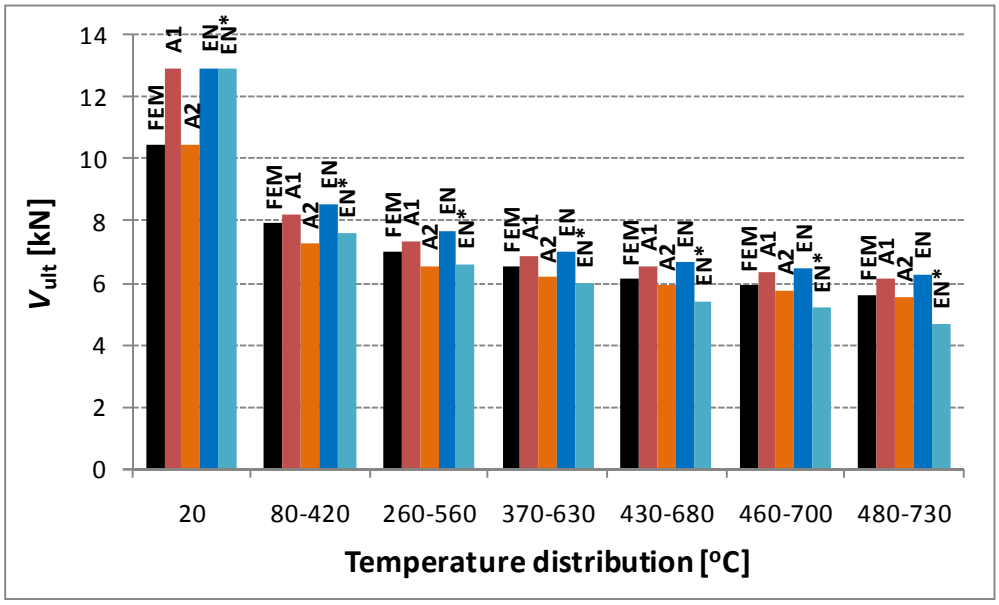

Figure 5.10. Ultimate shear resistances V_{ult} of stainless steel plate PLs1 from FEM, methods A1 and A2 and Eurocodes.

Based on Tables 5.2 and 5.3 and Figures 5.5–5.10, it can be said that the proposed method A (A1 and A2) predicts shear buckling resistances accurately in the considered cases, especially with stainless steel plate PLs1. In the case of post-buckling resistances, the scattering of the results was somewhat larger.

All ultimate shear resistances of carbon steel plate PL1 at elevated temperatures, calculated using method A, were on the safe side compared to FEM results. On average, they were 13 % on the safe side in the case of form A1 (design method) and 6 % with

form A2 (theoretical method). For stainless steel plate PLs1, ambient temperature resistance according to EN 1993-1-4 [EN 1993-1-4, 2006] was clearly higher than from FEM. Ultimate shear resistances of PLs1 calculated by form A1 were slightly higher than those from FEM analysis at elevated temperatures. All ultimate shear resistances of plate PLs1 at elevated temperatures calculated by form A2 were on the safe side compared to FEM resistances (on average by 5 %).

All ultimate shear resistances at elevated temperatures according to EN 1993-1-2 [EN 1993-1-2, 2005] were on the unsafe side compared to FEM resistances. For example, at the temperature distribution of 480–730 ^{o}C the EN 1993-1-2 resistances for plates PL1 and PLs1 were 33 % and 10 % on the unsafe side, respectively, compared to the resistances from numerical analysis. Thus, it is obvious that the use of average temperature in reduction leads to unconservative results. Moreover, it can be concluded that the use of maximum temperature instead of average temperature does not solve the problem; EN 1993-1-2 resistances calculated using reduction based on maximum temperature of the plate PL1 were, on average, 62 % on the safe side compared to resistances from FEM. For stainless steel plate PLs1, resistances calculated using maximum temperature of the plate were, on average, only 11 % on the safe side. However, it should be noted that ambient temperature resistance according to EN 1993-1-4 [EN 1993-1-4, 2006] (which is reduced at elevated temperatures) was 19 % higher than the corresponding resistance from FEM analysis. Moreover, resistances of PLs1 at elevated temperatures were clearly closer to the ambient temperature value than in the case of PL1 due to the material properties of stainless steel, which do not deteriorate as fast at elevated temperatures as those of carbon steel. Thus, it is expected that use of maximum temperature in the case of stainless steel plates leads to clearly conservative results at higher elevated temperatures, too. Higher elevated temperatures than those used in this worked example are considered in Chapter 5.1.3.

Figures 5.11 and 5.12 show the maximum out-of-plane displacements of plates PL1 and PLs1 as a function of applied shear force at ambient and the considered non-uniform elevated temperatures from FEM analysis.

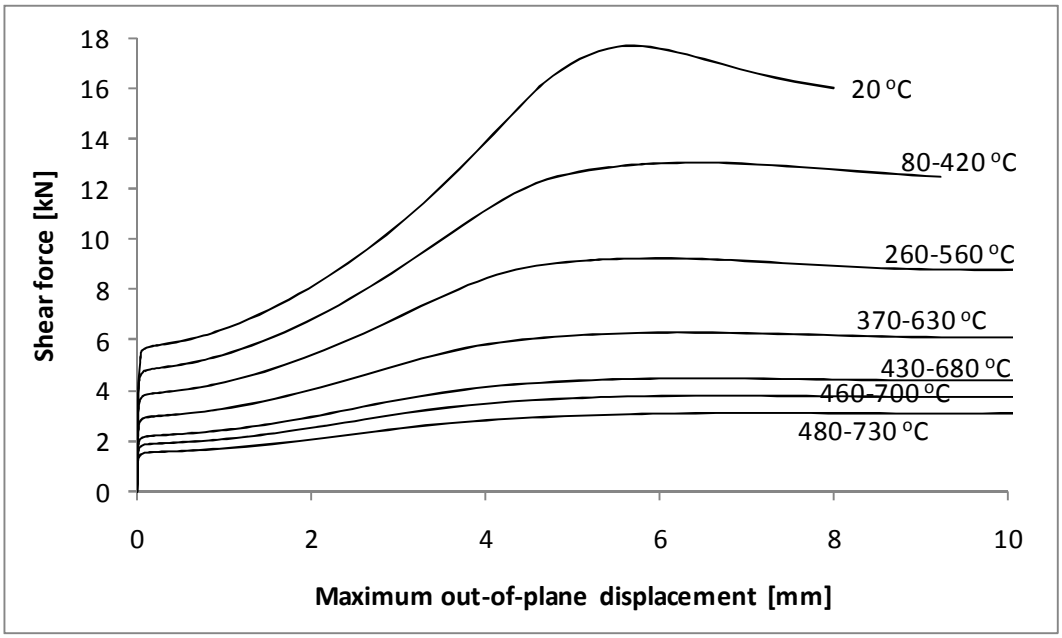

Figure 5.11. Behaviour of carbon steel plate PL1 at ambient and non-uniform elevated temperatures.

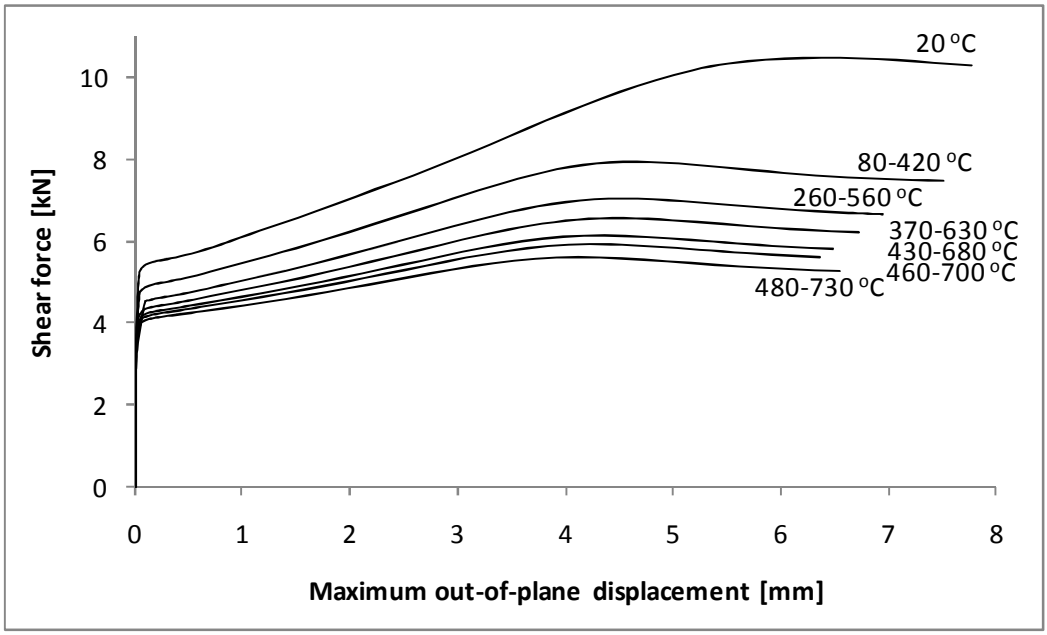

Figure 5.12. Behaviour of stainless steel plate PLs1 at ambient and non-uniform elevated temperatures.

Figures 5.11 and 5.12 show the ultimate shear resistance of carbon steel plate PL1 decreases more than the resistance of stainless steel plate PLs1 at the same elevated temperatures. From Figure 5.12 it can be observed how post-buckling resistance of plate PLs1 decreases more than the corresponding shear buckling resistance, which can be explained by the differences in the reductions of elastic modulus (related to shear buckling resistance) and 0.2 % proof strength (related to post-buckling resistance) (see also Fig. 3.4).

5.1.3 Comparison to other FEM results and Eurocodes

Even though the final results of this study were calculated using the magnitude $h/100$ for initial imperfections, some of the resistances for plates PL1, PLa1 and PLs1 were calculated using $h/100\ 000$ (Tables 4.15–4.17). Tables 5.4–5.6 and Figures 5.13–5.18 compare the resistances from numerical analysis to the corresponding resistances from method of separation of shear and post-buckling (method A) and from Eurocodes [EN 1993-1-5, 2005], [EN 1993-1-4, 2006], [EN 1999-1-1, 2007], [EN 1993-1-2, 2005] and [EN 1999-1-2, 2007]. All temperature distributions considered in the following are linear. Eurocode resistances were in this case also calculated using the reduction based on the hottest temperature of the plate (EN*).

Table 5.4. Calculated shear buckling, post-buckling and ultimate shear resistances of carbon steel plate PL1 [kN].

	Temperature distribution [°C]				
	20	100–300	100–500	100–700	100–900
$V_{cr,FEM}$	5.73	5.10	4.49	3.24	1.65
$V_{cr,A1}$	5.81	5.04	4.26	2.96	1.78
$V_{cr,A2}$	5.73	4.97	4.20	2.92	1.75
$V_{cr,FEM}$ / $V_{cr,A1}$	0.99	1.01	1.05	1.09	0.93
$V_{cr,FEM}$ / $V_{cr,A2}$	1.00	1.03	1.07	1.11	0.94
$V_{pb,FEM}$	11.89	9.65	6.93	2.15	0.38
$V_{pb,A1}$	10.01	7.86	5.45	3.14	0.65
$V_{pb,A2}$	11.89	9.22	6.26	3.56	0.70
$V_{pb,FEM}$ / $V_{pb,A1}$	1.19	1.23	1.27	0.68	0.58
$V_{pb,FEM}$ / $V_{pb,A2}$	1.00	1.05	1.11	0.60	0.54
$V_{ult,FEM}$	17.62	14.75	11.42	5.39	2.03
$V_{ult,A1}$	15.82	12.90	9.71	6.10	2.43
$V_{ult,A2}$	17.62	14.19	10.46	6.48	2.46
$V_{ult,EN}$	15.82	14.08	12.34	10.28	8.38
$V_{ult,EN}$*	15.82	12.34	8.38	2.06	0.79
$V_{ult,FEM}$ / $V_{ult,A1}$	1.11	1.14	1.18	0.88	0.83
$V_{ult,FEM}$ / $V_{ult,A2}$	1.00	1.04	1.09	0.83	0.83
$V_{ult,FEM}$ / $V_{ult,EN}$	1.11	1.05	0.93	0.52	0.24
$V_{ult,FEM}$ / $V_{ult,EN}$*	1.11	1.20	1.36	2.62	2.57

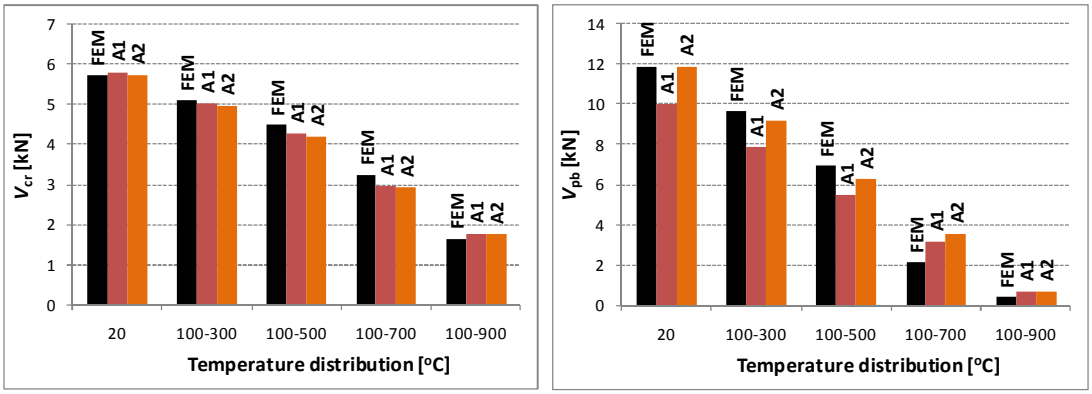

Figure 5.13. Shear buckling (V_{cr} at left) and post-buckling resistances, (V_{pb} at right) of carbon steel plate PL1 from FEM and methods A1 and A2.

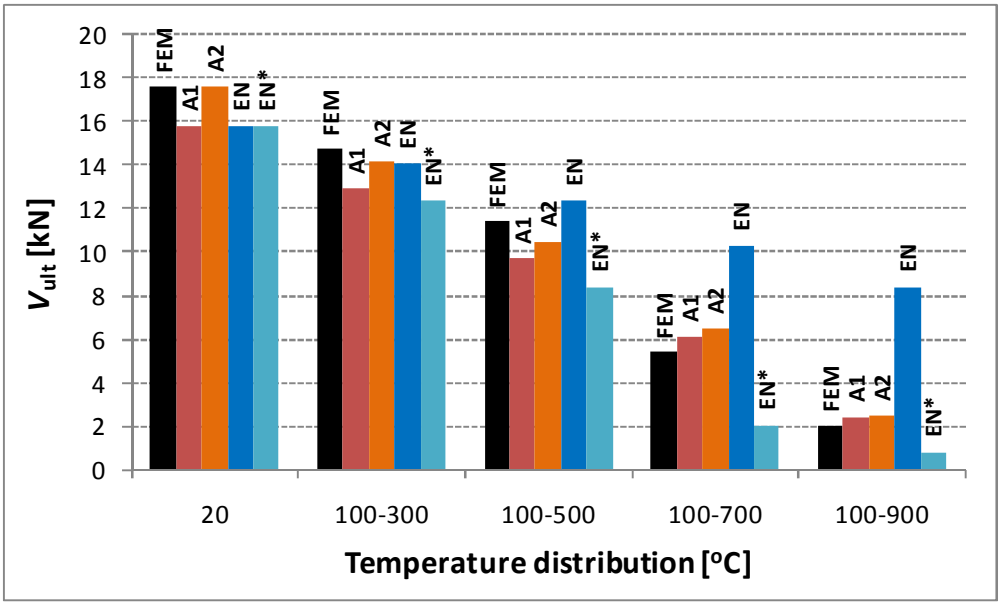

Figure 5.14. Ultimate shear resistances V_{ult} of carbon steel plate PL1 from FEM, methods A1 and A2 and Eurocodes.

Table 5.5. Calculated shear buckling, post-buckling and ultimate shear resistances of aluminium plate PLa1 [kN

	Temperature distribution [°C]				
	20	50–200	50–250	50–300	50–350
$V_{cr,FEM}$	6.40	6.12	5.72	5.35	4.73
$V_{cr,A1}$	6.54	6.00	5.69	5.32	4.86
$V_{cr,A2}$	6.40	5.88	5.57	5.21	4.76
$V_{cr,FEM}$ / $V_{cr,A1}$	0.98	1.02	1.01	1.01	0.97
$V_{cr,FEM}$ / $V_{cr,A2}$	1.00	1.04	1.03	1.03	0.99
$V_{pb,FEM}$	7.43	4.78	3.68	2.04	0.69
$V_{pb,A1}$	5.49	3.12	2.02	1.06	0.57
$V_{pb,A2}$	7.43	3.96	2.49	1.27	0.67
$V_{pb,FEM}$ / $V_{pb,A1}$	1.35	1.53	1.82	1.92	1.22
$V_{pb,FEM}$ / $V_{pb,A2}$	1.00	1.21	1.48	1.60	1.04
$V_{ult,FEM}$	13.83	10.90	9.40	7.39	5.42
$V_{ult,A1}$	12.03	9.12	7.71	6.38	5.43
$V_{ult,A2}$	13.83	9.83	8.06	6.48	5.42
$V_{ult,EN}$	12.03	9.93	9.03	7.52	6.02
$V_{ult,EN}$*	12.03	6.02	2.77	1.32	0.72
$V_{ult,FEM}$ / $V_{ult,A1}$	1.15	1.20	1.22	1.16	1.00
$V_{ult,FEM}$ / $V_{ult,A2}$	1.00	1.11	1.17	1.14	1.00
$V_{ult,FEM}$ / $V_{ult,EN}$	1.15	1.10	1.04	0.98	0.90
$V_{ult,FEM}$ / $V_{ult,EN}$*	1.15	1.81	3.40	5.58	7.51

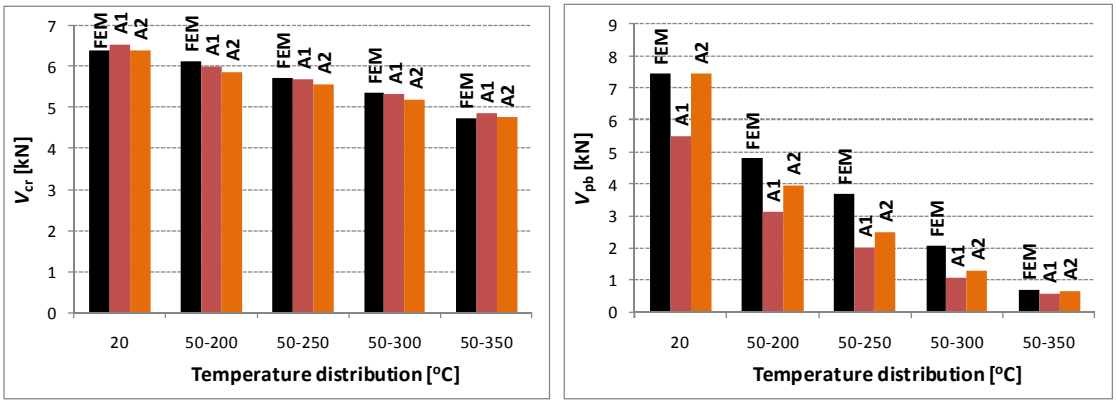

Figure 5.15. Shear buckling (V_{cr} at left) and post-buckling resistances (V_{pb} at right) of aluminium plate PLa1 from FEM and methods A1 and A2.

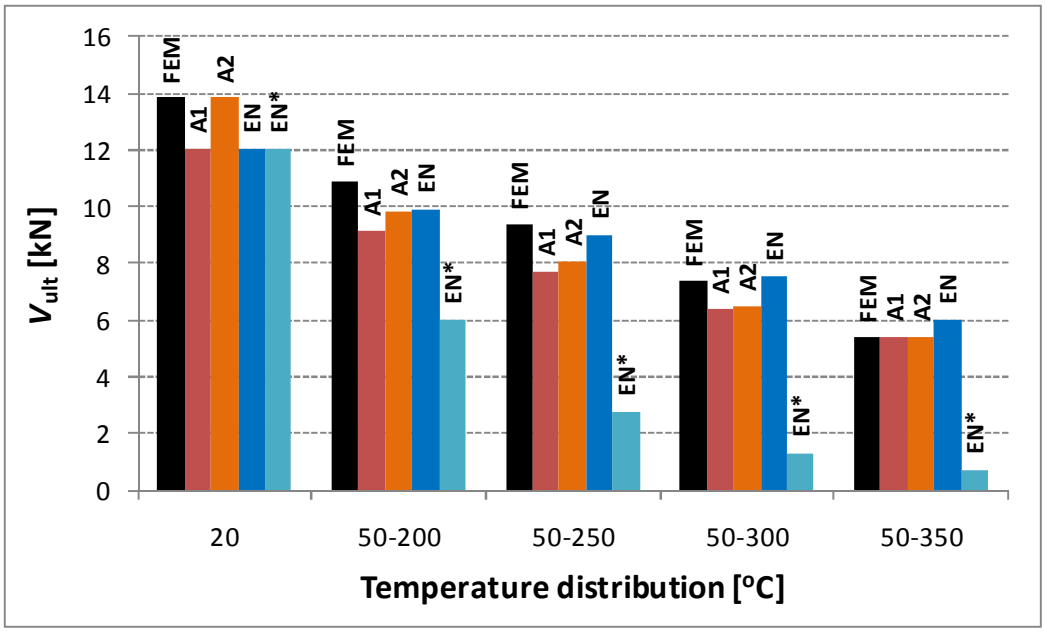

Figure 5.16. Ultimate shear resistances V_{ult} of aluminium plate PLa1 from FEM, methods A1 and A2 and Eurocodes.

Table 5.6. Calculated shear buckling, post-buckling and ultimate shear resistances of stainless steel plate PLs1 [kN].

	Temperature distribution [°C]				
	20	100–400	100–600	100–800	100–1000
$V_{cr,FEM}$	5.44	4.93	4.64	4.30	3.36
$V_{cr,A1}$	5.54	4.88	4.58	4.23	3.47
$V_{cr,A2}$	5.44	4.79	4.50	4.15	3.41
$V_{cr,FEM}$ / $V_{cr,A1}$	0.98	1.01	1.01	1.02	0.97
$V_{cr,FEM}$ / $V_{cr,A2}$	1.00	1.03	1.03	1.04	0.99
$V_{pb,FEM}$	5.01	2.99	2.41	1.31	0.13
$V_{pb,A1}$	7.41	3.39	2.86	2.28	1.33
$V_{pb,A2}$	5.01	2.50	2.13	1.73	1.03
$V_{pb,FEM}$ / $V_{pb,A1}$	0.68	0.88	0.84	0.57	0.10
$V_{pb,FEM}$ / $V_{pb,A2}$	1.00	1.20	1.13	0.76	0.13
$V_{ult,FEM}$	10.45	7.92	7.05	5.61	3.49
$V_{ult,A1}$	12.95	8.27	7.44	6.51	4.80
$V_{ult,A2}$	10.45	7.29	6.63	5.88	4.43
$V_{ult,EN}$	12.95	8.55	8.03	7.38	6.67
$V_{ult,EN}$*	12.95	7.77	6.35	3.50	0.78
$V_{ult,FEM}$ / $V_{ult,A1}$	0.81	0.96	0.95	0.86	0.73
$V_{ult,FEM}$ / $V_{ult,A2}$	1.00	1.09	1.06	0.95	0.79
$V_{ult,FEM}$ / $V_{ult,EN}$	0.81	0.93	0.88	0.76	0.52
$V_{ult,FEM}$ / $V_{ult,EN}$*	0.81	1.02	1.11	1.60	4.49

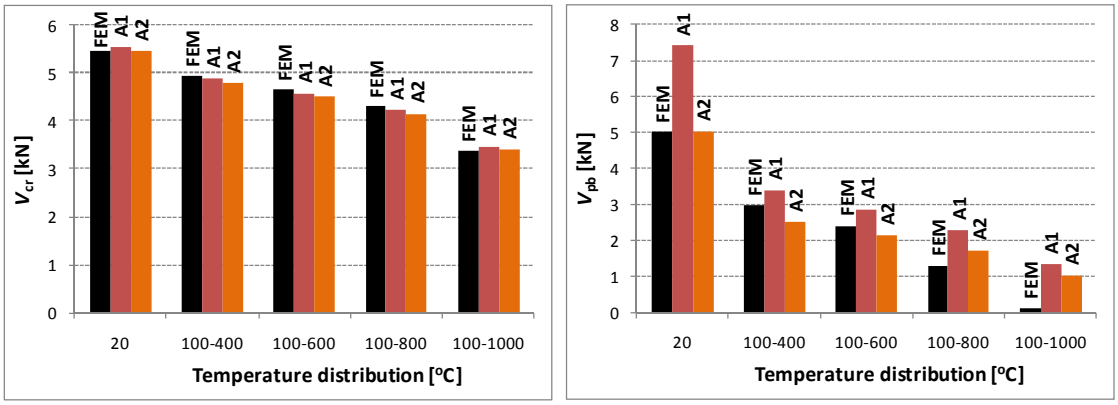

Figure 5.17. Shear buckling (V_{cr} at left) and post-buckling resistances (V_{pb} at right) of stainless steel plate PLs1 from FEM and methods A1 and A2.

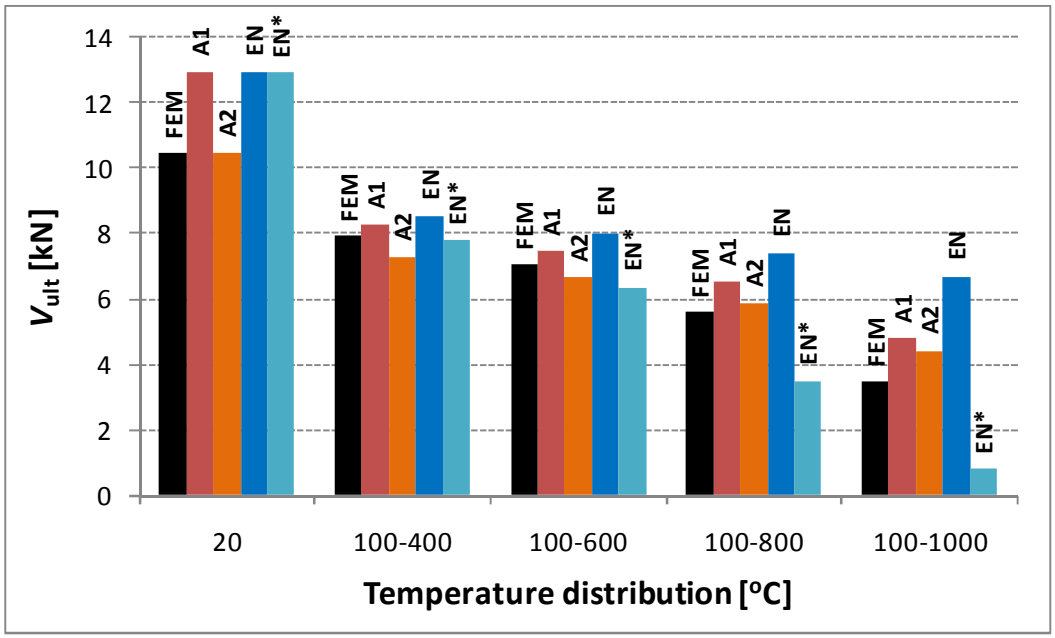

Figure 5.18. Ultimate shear resistances V_{ult} of stainless steel plate PLs1 from FEM, methods A1 and A2 and Eurocodes.

Based on Tables 5.4–5.6 and Figures 5.13–5.18, it can be concluded that the proposed method of separation of shear and post-buckling (method A) predicts shear buckling resistances quite accurately in all considered cases. All ratios $V_{cr,FEM}$ / $V_{cr,A}$ at elevated temperatures were in the range 0.93–1.09 with approach A1 (design method) and in the range 0.94–1.11 with approach A2 (theoretical method) in the considered cases.

The post-buckling resistances of carbon steel plate PL1 according to method A were on the safe side compared to FEM results at temperature distributions 100–300 and 100–500 °C and clearly on the unsafe side at distributions 100–700 and 100–900 °C. All post-buckling resistances at elevated temperatures according to method A for aluminium plate PLa1 were clearly on the safe side compared to resistances from numerical analysis. Especially the resistances calculated using approach A1 were highly

conservative (on average by 62 %). In the case of stainless steel plate PLs1, post-buckling resistances according to method A were relatively close to those from FEM at temperature distributions 100–400 and 100–600 °C, but at temperature distributions 100–800 and 100–1000 °C they were clearly unconservative.

The ultimate shear resistances of PL1 calculated using method A were on the safe side compared to FEM resistances at temperature distributions 100–300 and 100–500 °C and on the unsafe side at temperature distributions 100–700 and 100–900 °C. All ultimate shear resistances of aluminium plate PLa1 from method A were conservative compared to FEM results. Especially the resistances from approach A2 were relatively close to those from FEM. However, it should be noted that the temperature distributions applied to PLa1 were rather narrow due to the material data from test results [Maljaars, 2008] (see also Chapter 4.2.2). The ultimate shear resistances of stainless steel plate PLs1 from method A were relatively close to those from FEM at temperature distributions 100–400, 100–600 and 100–800 °C especially with approach A2. At the temperature distribution 100–1000 °C, the calculated resistances were clearly unconservative compared to FEM.

The ultimate shear resistances of carbon steel plate PL1 at elevated temperatures according to EN 1993-1-2 [EN 1993-1-2, 2005] were on the unsafe side compared to FEM resistances at temperature distributions 100–500, 100–700 and 100–900 °C. Especially at the elevated temperatures of 100–700 and 100–900 °C, the Eurocode resistances were significantly on the unsafe side (by 48 and 76 %, respectively).

The ultimate shear resistances of aluminium plate PLa1 according to EN 1999-1-2 [EN 1999-1-2, 2007] were on the safe side compared to FEM at elevated temperatures of 50–200 and 50–250 °C. At temperature distributions 50–300 and 50–350 °C, they were slightly unconservative. It should be noted that the ultimate shear resistance of PLa1 at ambient temperature is 15 % higher according to numerical analysis than based on the equations of EN 1999-1-1 [EN 1999-1-1, 2007]. In this case use of the maximum temperature of the plate in the reduction yielded resistances which were significantly conservative compared to FEM results (even 651 % on the safe side at 50–350 °C).

All ultimate shear resistances of stainless steel plate PLs1 at elevated temperatures based on EN 1993-1-2 [EN 1993-1-2, 2005] were on the unsafe side compared to FEM resistances. Especially at temperature distributions 100–800 and 100–1000 °C, the resistances were clearly unconservative (by 24 and 48 %, respectively). When using maximum temperature instead of average temperature in the reduction, the resistances were slightly on the safe side at temperature distributions 100–400 and 100–600 °C (by 2 and 11 %, respectively) and highly conservative at temperatures 100–800 and 100–1000 °C (by 60 and 349 %, respectively). It should be noted that at ambient

temperature, the ultimate shear resistance of stainless steel plate PLs1 based on the equations of EN 1993-1-4 [EN 1993-1-4, 2006], was 19 % higher than the corresponding resistance from FEM analysis.

5.2 Method of reference temperature (method B)

The idea of this method is to modify the Eurocode equations to make them applicable also to non-uniform temperature distributions. According to Eurocodes [EN 1993-1-2, 2005] and [EN 1999-1-2, 2007], the shear resistances of thin metal (carbon steel, aluminium and stainless steel) plates at elevated temperatures are calculated by reducing the shear resistance at ambient temperature V_{Rd} by the reduction factor of the design yield strength (0.2 % proof strength), $k_{p0.2,\theta,web}$ which is based on the average temperature of the plate θ_{web} (see also Eq. (3.3)).

Chapter 5.2.1 presents the theoretical background of the proposed method and equations for carbon steel, aluminium and stainless steel are given in Chapters 5.2.2, 5.2.3 and 5.2.4, respectively. Chapter 5.2.5 presents a worked example, where method of reference temperature (referred as method B) is applied to non-uniform elevated temperatures, and Chapter 5.2.6 finally compares the reduction factors obtained by using FEM, method B, EN 1993-1-2 [EN 1993-1-2] and EN 1999-1-2 [EN 1999-1-2, 2007].

5.2.1 Theory behind method of reference temperature

The proposed method is based on the reduction factors calculated in this study (Tables 4.12–4.14). Chapter 4.4.3 showed that in the case of a slender plate at uniform elevated temperature, reduction based on design yield strength (0.2 % proof strength) is justified (Figs. 4.25–4.27). Chapter 4.5 showed that at non-uniform elevated temperatures most reduction factors based on average temperature were on the unsafe side while all those based on the hottest temperature of the plate were on the safe side compared to FEM results (Figs. 4.50–4.52). Therefore, the correct reduction is based on a temperature between the average temperature θ_{web} and the hottest temperature θ_{hot} of the plate. Thus, a reference temperature θ_{ref} between θ_{web} and θ_{hot} is introduced. The basic idea of the proposed method is illustrated in Figure 5.19.

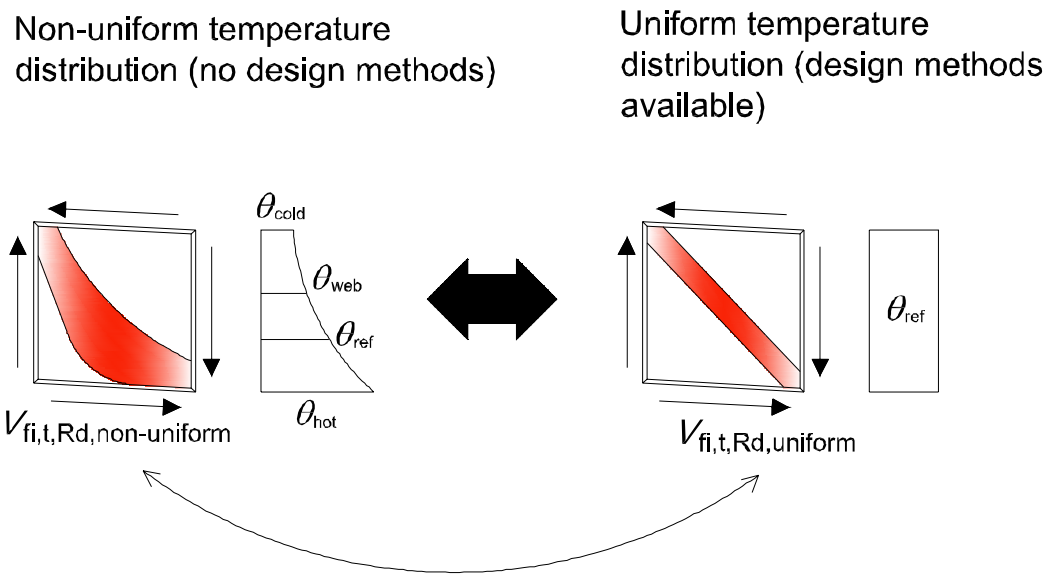

Figure 5.19. Basic idea of the proposed method.

Figure 5.19 shows that the basic idea of the proposed design method is to convert the non-uniform temperature distribution into a uniform temperature distribution so that the behaviour of the plates is close to each other. Thus, the major problem is then how to define θ_{ref}?

The idea of defining θ_{ref} based on the results from FEM analysis is explained below. In our example, carbon steel plates PL1–PL12 (see Tables 4.1 and 4.2) are studied at the linear 100–700 °C temperature distribution. Figure 5.20 shows the reduction curve of 0.2 % proof strength for carbon steel at elevated temperatures. The reduction factors corresponding to θ_{cold} = 100 °C, θ_{web} = 400 °C and θ_{hot} = 700 °C are indicated on the curve. Furthermore, the minimum ($k_{FEM,min}$), average ($k_{FEM,avg}$) and maximum ($k_{FEM,max}$) values of 12 reduction factors from FEM (Tables 4.12 and 4.13) and the corresponding temperatures from the reduction curve are shown. The rectangle, whose width is θ_{hot} - θ_{web} = 300 °C and height $k_{p0.2,\theta,web}$ - $k_{p0.2,\theta,hot}$ = 0.520, is scaled by factor d so that the intersection with the reduction curve is at the same point as the average value of the reduction factors from FEM. According to EN 1993-1-2 [EN 1993-1-2, 2005] and EN 1999-1-2 [EN 1999-1-2, 2007], the reduction should be based on the average temperature or in this formulation d = 1. When reduction is based on the hottest temperature d = 0.

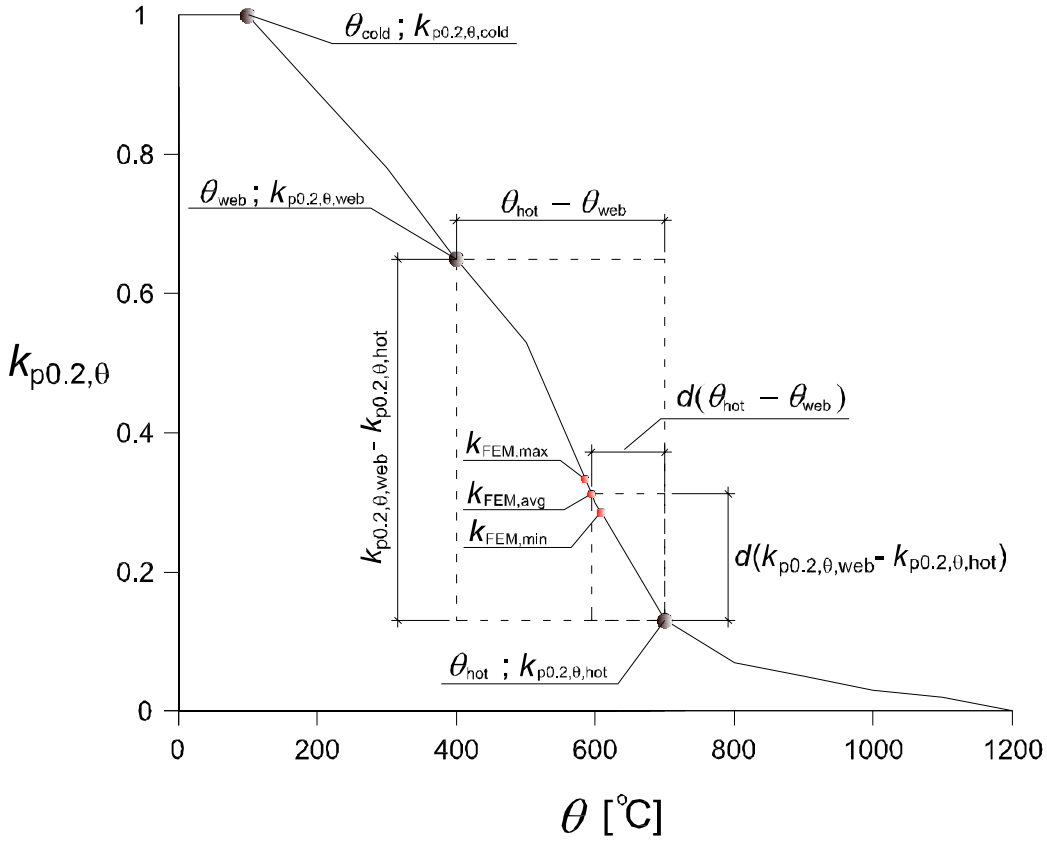

Figure 5.20. Definition of factor *d* required for method of reference temperature.

Factor *d* can be determined from Figure 5.20. Here, the value of *d*, which corresponds to the average reduction factor from FEM was 0.35. Factors *d* corresponding to the minimum and maximum reduction factors from FEM were here 0.31 and 0.39, respectively. It should be noted that in some cases the intersection between the scaled rectangle and the reduction curve occurs on the vertical side ($k_{FEM,min}$ in this case) and in some cases on the horizontal side ($k_{FEM,max}$ in this case) of the rectangle.

Factor *d* can be determined similarly for other temperature distributions, too. Table 5.7 shows factors *d* which correspond to the minimum (d_{min}), average (d_{avg}) and maximum (d_{max}) reduction factors from FEM for carbon steel plates at the considered linear temperature distributions.

Table 5.7. Factors *d* for carbon steel plates PL1–PL12 at linear temperature distributions.

	Linear temperature distribution [°C]								
	100-300	100-500	100-700	100-900	200-500	300-600	400-700	500-800	600-900
d_{min}	0.22	0.38	0.31	0.38	0.37	0.40	0.39	0.50	0.37
d_{avg}	0.43	0.50	0.35	0.43	0.52	0.47	0.43	0.55	0.57
d_{max}	0.66	0.65	0.39	0.51	0.72	0.56	0.49	0.65	0.68

Table 5.7 shows that the d_{min} values at the considered temperature distributions were on average 0.37. The value d = 0.33 was chosen as the basic value for the calculation method for carbon steel plates. The table also reveals that d_{min} = 0.22 at the 100–300 °C temperature distribution, which is clearly lower than 0.33. However, the error is not significant here because the reduction factors corresponding to the average and hottest temperatures are relatively high and close to each other ($k_{p0.2,\theta,web}$ = 0.890 and $k_{p0.2,\theta,hot}$ = 0.780). Thus, the so-called basic form of method B can be written as:

$$V_{ult,fi} = k_{p0.2,\theta,ref} V_{ult,amb} \le \left[k_{p0.2,\theta,hot} + 0.33(k_{p0.2,\theta,web} - k_{p0.2,\theta,hot})\right] \cdot V_{ult,amb} \qquad (5.11)$$

where • $\theta_{ref} = \theta_{hot} - 0.33(\theta_{hot} - \theta_{web})$

Table 5.7 shows that the average and maximum values of d were clearly higher than the minimum values. However, that variation can be controlled relatively accurately by introducing factors k_y (Eq. (5.15)) and k_a (Eq. (5.16)) which take into account the yield strength and aspect ratio of the plate, respectively. These factors are based on the analysis conducted in Chapter 4.4.4 (Figs. 4.42, 4.43 and 4.46).

When analyzing reduction factors at non-linear (3rd order) temperature distributions, it was observed that the value of d should be increased slightly (from 0.33 to 0.38) in order to get accurate results compared to those from FEM. Thus, the factor d_{add}, shown in Equation (5.12) and Figure 5.21, is added to the basic value d = 0.33 when temperature distribution is not linear.

$$d_{add} = 0.025\left(\frac{\theta_{hot} - \theta_{web}}{\theta_{web} - \theta_{cold}} - 1\right) \qquad (5.12)$$

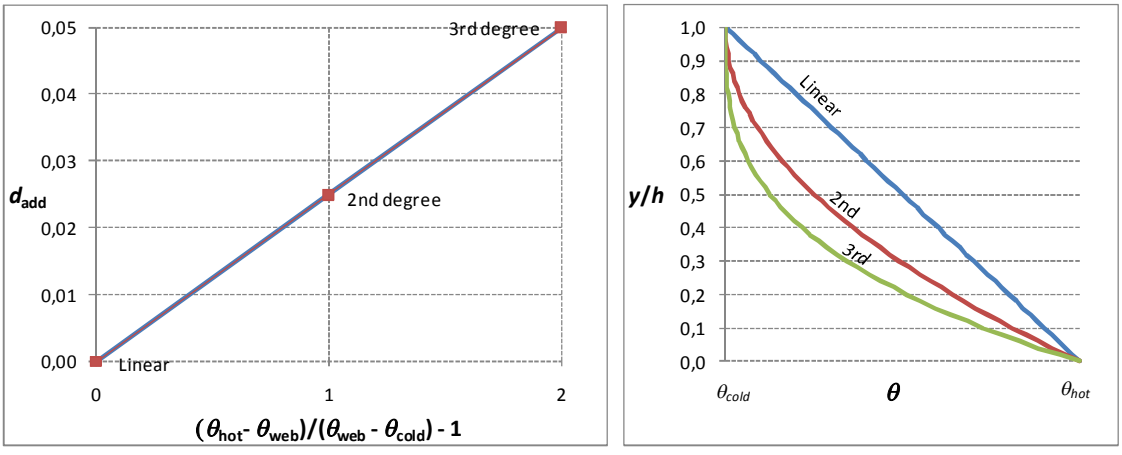

Figure 5.21. Factor d_{add} for different temperature distributions.

The values $(\theta_{hot} - \theta_{web})/(\theta_{web} - \theta_{cold})$-1 for linear, 2nd and 3rd degree temperature distributions are 0, 1 and 2, respectively meaning that the corresponding d-values are 0.33, 0.355 and 0.38, respectively.

Furthermore, when analyzing the results at non-linear temperature distributions, it was observed that in cases where the coldest temperature of the plate is relatively high, the results from Equation (5.11) were clearly conservative compared to those from FEM. Thus, a factor (k_d (≥1), see Eq. (5.17)) which takes into account the effect of the relatively high coldest temperature of the plate at non-linear temperature distributions is introduced. All the equations and factors for the considered materials are presented in Chapters 5.2.2–5.2.4. It should be noted that factor k_d depends on the reduction curve of 0.2 % proof strength and is thus different for each material.

The proposed method is formulated as close to the method of EN 1993-1-2 [EN 1993-1-2, 2005] as possible (see also Eq. (3.3)). The coldest and hottest temperatures of the plate are needed for the calculation in addition to the EN 1993-1-2 method.

Chapters 5.2.2, 5.2.3 and 5.2.4 present the proposed method of reference temperature (method B) in the case of carbon steel, aluminium and stainless steel, respectively.

5.2.2 Carbon steel

The following modified EN 1993-1-2 [EN 1993-1-2, 2005] equation is proposed for carbon steel:

$$V_{fi,t,Rd} = k_{p0.2,\theta,ref} V_{Rd} \le \left[k_{p0.2,\theta,hot} + d(k_{p0.2,\theta,web} - k_{p0.2,\theta,hot})\right] V_{Rd} \tag{5.13}$$

where

- $k_{p0.2,\theta,ref}$ is the reduction factor for the design yield strength of class 4 section according to EN 1993-1-2 [EN 1993-1-2, 2005] at steel temperature θ_{ref},
- V_{Rd} is design shear resistance at ambient temperature.
- $k_{p0.2,\theta,hot}$ is the reduction factor for the design yield strength of class 4 section at the hottest temperature of the plate θ_{hot},
- $k_{p0.2,\theta,web}$ is the reduction factor for the design yield strength of class 4 section at the average temperature of the plate θ_{web},
- $\theta_{ref} = \theta_{hot} - d(\theta_{hot} - \theta_{web})$

Coefficient d is obtained from:

$$d = k_y k_a k_d \left[0.33 + 0.025 \left(\frac{\theta_{hot} - \theta_{web}}{\theta_{web} - \theta_{cold}} - 1 \right) \right] \tag{5.14}$$

where the factors k_y, k_a and k_d are defined as given in Equations (5.15)–(5.17).

$$k_y = 1 + 0.00035 \left(f_y - 235 \right), \quad 1 \le k_y \le 1.06 \tag{5.15}$$

$$k_a = 0.9 + 0.1 \left(\frac{a}{h} \right), \quad 0.95 \le k_a \le 1.15 \tag{5.16}$$

$$k_d = 1 + \left(\frac{\theta_{hot} - \theta_{web}}{\theta_{web} - \theta_{cold}} - 1 \right) \left(\frac{\theta_{cold} - 200}{2000} \right), \quad 1 \le k_d \le 1.40 \tag{5.17}$$

where
- f_y is the yield strength of the plate at ambient temperature [N/mm^2],
- a is the distance between the stiffeners of the plate [mm],
- h is the height of the plate [mm] and
- θ_{cold} is the coldest temperature of the plate [^{o}C].

Coefficient d is $0.33 k_y k_a k_c$ in the case of a linear temperature distribution and $0.38 k_y k_a k_c$ in the case of a 3rd degree polynomial, which were the distributions applied in the FEM calculations. Factors depending on yield strength, aspect ratio and temperature distribution (k_y, k_a and k_d, respectively) are presented graphically in Figures 5.22 and 5.23. Factor k_d is plotted for linear, 2nd and 3rd degree temperature distributions when temperature distributions are defined as in Equations (4.1) and (4.2).

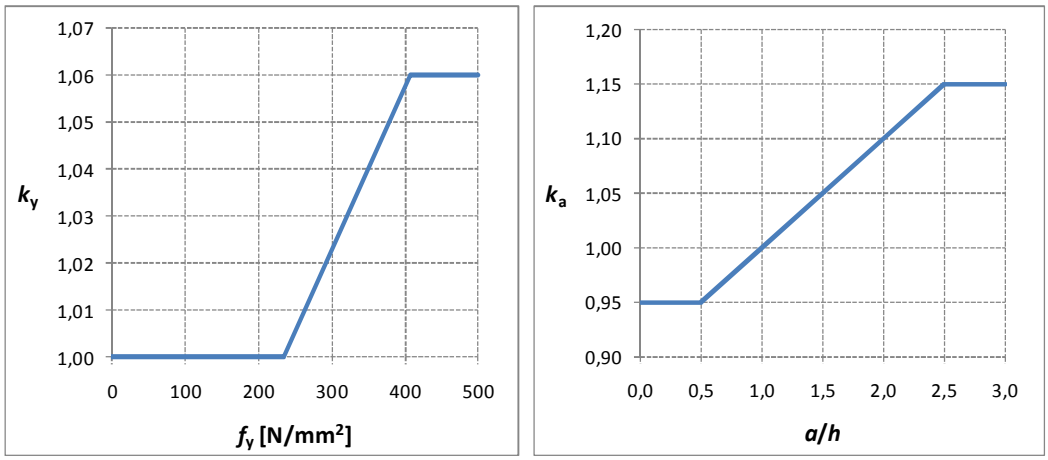

Figure 5.22. Factors k_y (left) and k_a (right).

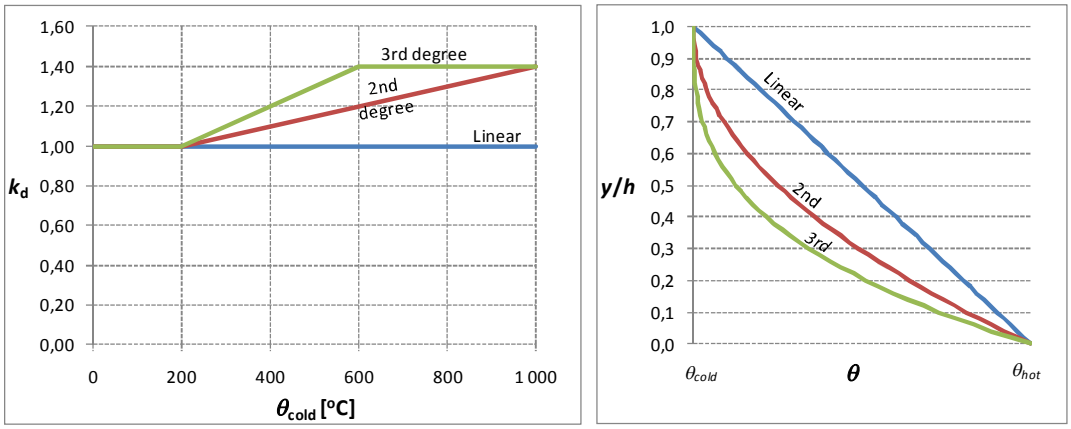

Figure 5.23. Factor k_d for different temperature distributions.

The basic idea of method B is the same for aluminium and stainless steel as for carbon steel. However, Equation (5.14) and factors k_d (Eq. (5.17)) had to be modified due to differences in material behaviour at elevated temperatures.

5.2.3 Aluminium

The material model applied in FEM to aluminium at elevated temperatures is based on the tests conducted in the dissertation of Maljaars [Maljaars, 2008]. According to Maljaars [Maljaars, 2008], the properties of the tested aluminium alloy 5083-H111 at elevated temperatures are close to those of alloy 5083-O. EN 1999-1-2 [EN 1999-1-2, 2007] gives the reduction of 0.2 % proof strength for alloy 5083-O, but for alloy 5083-H111 there is no such curve meaning that the lower limit values are to be used. This study showed that the reductions in shear strength of aluminium plates PLa1 and PLa2 at uniform elevated temperatures were very close to the reduction curve of 0.2 % proof strength of 5083-O and much higher than the lower limit values (see Fig. 4.26). Thus, it is more realistic to use here the reductions of 0.2 % proof strength based on alloy 5083-O than the lower limit values. The shear resistance of an aluminium plate can be derived from Equations (5.18)–(5.21). Equations (5.18) and (5.20) are the same as those for carbon steel (except for the factor γ_0) while Equations (5.19) and (5.21) have been modified.

$$V_{fi,t,Rd} = k_{p0.2,\theta,ref} V_{Rd} \gamma_0 \le \left[k_{p0.2,\theta,hot} + d(k_{p0.2,\theta,web} - k_{p0.2,\theta,hot}) \right] V_{Rd} \gamma_0 \tag{5.18}$$

The material factor $\gamma_0 = 1.1$ for aluminium [EN 1999-1-1, 2007] and coefficient d is obtained from:

$$d = k_a k_d \left[0.1 + 0.025 \left(\frac{\theta_{hot} - \theta_{web}}{\theta_{web} - \theta_{cold}} - 1 \right) \right] \tag{5.19}$$

where $$k_a = 0.9 + 0.1\left(\frac{a}{h}\right), \quad 0.95 \le k_a \le 1.15 \tag{5.20}$$

$$k_d = 1 + 0.006 \cdot (\theta_{hot} - 275), \; k_d \ge 1 \tag{5.21}$$

5.2.4 Stainless steel

In the case of stainless steel, Equations (5.22) and (5.24) are the same as those for carbon steel (except for the factor γ_0) while Equations (5.23) and (5.25) have been modified.

$$V_{fi,t,Rd} = k_{p0.2,\theta,ref} V_{Rd} \gamma_0 \le \left[k_{p0.2,\theta,hot} + d(k_{p0.2,\theta,web} - k_{p0.2,\theta,hot})\right] V_{Rd} \gamma_0 \tag{5.22}$$

The material factor $\gamma_0 = 1.1$ for stainless steel and coefficient d is obtained from:

$$d = k_a k_d \left[0.55 + 0.025\left(\frac{\theta_{hot} - \theta_{web}}{\theta_{web} - \theta_{cold}} - 1\right)\right] \tag{5.23}$$

where $$k_a = 0.9 + 0.1\left(\frac{a}{h}\right), \quad 0.95 \le k_a \le 1.15 \tag{5.24}$$

$$k_d = 1 - 0.005(\theta_{web} - \theta_{cold} - 400), \quad k_d \le 1 \tag{5.25}$$

5.2.5 Worked example

The shear resistance of carbon steel plate PL1 (properties shown in Table 5.1) is defined at ambient temperature and at the linear 100–700 °C temperature distribution below. Ambient temperature resistance is calculated according to EN 1993-1-5 [EN 1993-1-5, 2005] and resistance at the 100–700 °C temperature distribution is defined according to EN 1993-1-2 [EN 1993-1-2, 2005] and the proposed method of reference temperature (method B).

Calculation of shear resistance at ambient temperature according to EN 1993-1-5

The following data is needed for the calculation:

- h = 305 mm
- a = 305 mm
  $\rightarrow k_\tau$ = 9.34 (see Eq. (2.7))
- t = 1 mm
- f_y = 355 N/mm^2
- γ_{M1} = 1.00 [EN 1993-1-1, 2005]
- ν = 0.3 [EN 1993-1-1, 2005]

The critical shear stress τ_{cr}, the slenderness parameter λ and factor χ_w, which takes the slenderness into account, are needed in the calculation. They are defined as follows (in N and mm) (see also Eqs. (2.6), (2.39) and Table 2.4):

$$\tau_{cr} = 9.34 \frac{\pi^2 210000}{12(1-0.3^2)} \left(\frac{1}{305} \right)^2 = 19.06 \text{ N/mm}^2 \tag{5.26}$$

$$\lambda = 0.76 \sqrt{\frac{355}{19.06}} = 3.28 \tag{5.27}$$

$$\chi_w = \frac{0.83}{3.28} = 0.253 \tag{5.28}$$

Here, the effect of the flanges is ignored and ultimate shear resistance $V_{ult,amb}$ equals the contribution of the web $V_{bw,Rd}$ defined in EN 1993-1-5 [EN 1993-1-5, 2005] (Eq. (2.44)). The ultimate shear resistance of the plate is calculated in this case as follows:

$$V_{ult,amb} = \frac{0.253 \cdot 355 \cdot 305 \cdot 1}{\sqrt{3}} = \underline{15.82 \text{ kN}} \tag{5.29}$$

Shear resistance at the linear temperature distribution 100–700 °C according to EN 1993-1-2

The average temperature (θ_{web}) of the plate is here 400 °C and the corresponding reduction factor $k_{p0.2,\theta,web}$ = 0.65 [EN 1993-1-2, 2005] (see also Fig. 3.1). The shear

resistance at the linear temperature distribution 100–700 °C is calculated according to EN 1993-1-2 [EN 1993-1-2, 2005] as follows:

$$V_{ult,fi,EN} = 0.65 \cdot 15.82 = \underline{10.28 \text{ kN}} \tag{5.30}$$

The safe solution is to use the reduction based on the maximum temperature (700 °C) which yields to the reduction factor $k_{p0.2,\theta,hot} = 0.13$ and resistance 2.06 kN.

Shear resistance at the linear temperature distribution 100–700 °C according to method of reference temperature (method B)

The following data is needed for the calculation (see also Chapter 5.2.2):

- $\theta_{cold} = 100$ °C
- $\theta_{hot} = 700$ °C
- $\theta_{web} = 400$ °C
- $k_{p0.2,\theta,hot} = 0.13$ [EN 1993-1-2, 2005]
- $k_{p0.2,\theta,web} = 0.65$ [EN 1993-1-2, 2005]

Factors k_y, k_a and k_d are defined here as follows (see also Equations (5.15)–(5.17)):

$$k_y = 1 + 0.00035 \cdot (355 - 235) = 1.042 \tag{5.31}$$

$$k_a = 0.9 + 0.1\left(\frac{305}{305}\right) = 1 \tag{5.32}$$

$$k_d = 1 + \left(\frac{700-400}{400-100} - 1\right)\left(\frac{100-200}{2000}\right) = 0.95 \rightarrow$$

$$1 \le k_d \le 1.40 \rightarrow k_d = 1 \tag{5.33}$$

Next, coefficient d is obtained as shown in Equation (5.14):

$$d = 1.042 \cdot 1 \cdot 1\left[0.33 + 0.025\left(\frac{700-400}{400-100} - 1\right)\right] = 0.344 \tag{5.34}$$

Then, reference temperature θ_{ref} can be calculated from the following:

$$\theta_{ref} = \theta_{hot} - d \cdot (\theta_{hot} - \theta_{web}) = 700 - 0.344 \cdot (700 - 400) = 597\ ^{o}\text{C} \tag{5.35}$$

In this case reduction factor $k_{p0.2,\theta,ref}$ is 0.307, and shear resistance at elevated temperatures is calculated as follows:

$$V_{fi,t,Rd} = 0.307 \cdot 15.82 = \underline{4.86\ \text{kN}} \tag{5.36}$$

Equation (5.13) requires that shear resistance at elevated temperatures is not higher than the following value:

$$V_{fi,t,Rd} \leq \left[0.13 + 0.344 \cdot (0.65 - 0.13)\right] \cdot 15.82 = 4.89\ \text{kN} \tag{5.37}$$

The condition (Eq. (5.37)) is satisfied in this case. Thus, the shear resistance of plate PL1 at the linear 100–700 °C distribution is 4.86 kN according to method B.

Table 5.8 shows all the calculated resistances of the plate considered in this worked example. The resistances based on different temperatures, $V_i = V(\theta_{web} = 400\ ^{o}\text{C})$, $V(\theta_{hot} = 700\ ^{o}\text{C})$ and $V(\theta_{ref} = 597\ ^{o}\text{C})$, are compared to the FEM resistance at 100–700 °C (see Tables 4.5 and 4.12).

Table 5.8. Shear resistances at 100–700 °C using reductions based on different temperatures.

		Reduction based on temperature		
	FEM	θ_{web} (= 400 °C)	θ_{hot} (= 700 °C)	θ_{ref} (= 597 °C)
$V_{fi,t,Rd}$ [kN]	5.05	10.28	2.06	4.86
V_{FEM} / V_i		0.49	2.45	1.04

Table 5.8 shows that the if the shear resistance at 100–700 °C is calculated using the reduction based on average temperature of the plate, the result is 51 % on the unsafe side compared to the FEM result. Use of reduction based on the hottest temperature of the plate yields a highly conservative resistance result (145 % on the safe side) in this case. When using reduction based on the reference temperature θ_{ref} = 597 °C, the shear resistance is very close to the value obtained from numerical analysis.

Figure 5.24 shows the shear force-maximum out-of-plane displacement curves for the considered plate from FEM at the 100–700 °C temperature distribution and at uniform 400 °C (average temperature θ_{web}), 700 °C (hottest temperature θ_{hot}) and 597 °C (reference temperature θ_{ref}). The curves were calculated using small (h/100 000) and large (h/100) imperfections in order to observe the ideal and more realistic behaviour of the plate. FEM resistances were calculated as described in Chapter 4.2.

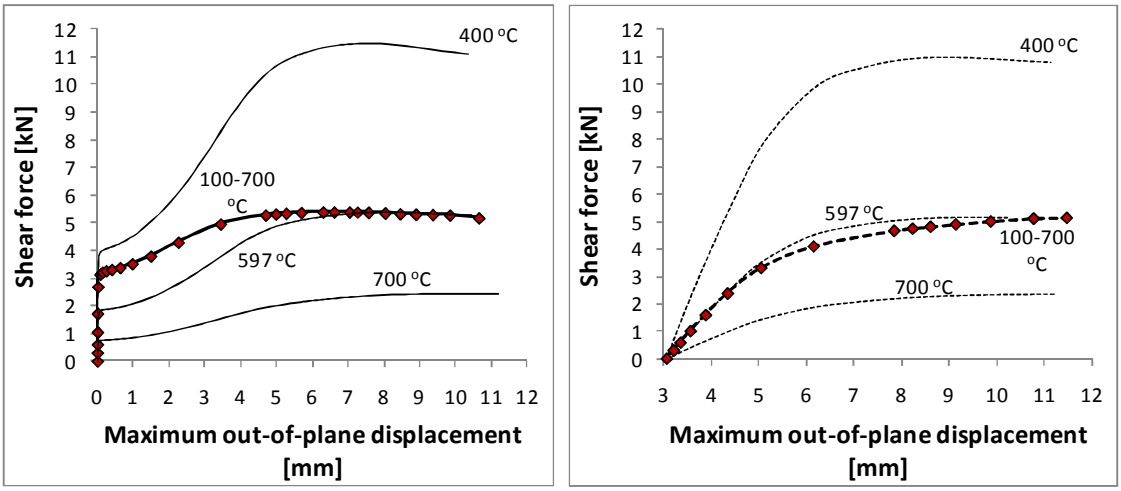

Figure 5.24. Behaviour of carbon steel plate PL1 at considered elevated temperatures with small (left) and large (right) imperfections.

Figure 5.24 shows clearly that the behaviour of the plate at the 100–700 °C temperature distribution is very different from the behaviour of the same plate at uniform 400 or 700 °C. It also reveals that with small imperfections, shear buckling occurs at a clearly lower load at uniform θ_{ref} = 597 °C than at the 100–700 °C distribution, even though the ultimate shear resistances are nearly the same in both cases. However, when large imperfections are used in the analysis, the behaviour of the plate at the actual temperature distribution (100–700 °C) and the reference temperature (θ_{ref} = 597 °C) is very similar, which was the basic idea behind this method as illustrated in Figure 5.19.

5.2.6 Comparison to the FEM results and Eurocodes

This chapter compares all the reduction factors at non-uniform elevated temperatures from the FEM analysis presented in Chapter 4.4.4 (Tables 4.12–4.14) to the reduction factors obtained by the Eurocodes and the proposed method of reference temperature (method B). Carbon steel, aluminium and stainless steel plates are considered in Chapters 5.2.6.1, 5.2.6.2 and 5.2.6.3, respectively. It is emphasized that, the reduction factors $k = V_{ult,fi} / V_{ult,amb}$ (not resistances) given by each method are compared, which means that the Eurocode [EN 1993-1-1, 2005], [EN 1993-1-4, 2006] and [EN 1999-1-1, 2007] resistances at ambient temperature are assumed to be correct. Moreover, the material factors γ_M are assumed to be 1. The ambient temperature resistances from FEM and Eurocodes are considered in Chapter 4.4.1.

5.2.6.1 Carbon steel plates PL1-PL12

Tables 5.9 and 5.10 present all the calculated reduction factors according to method of reference temperature (method B) for carbon steel plates. Plates with the same yield strength (PL1, PL3, PL6 - S355, PL2, PL7 - S332, PL4, PL5 - S235 and PL9 - S460)

and aspect ratio a/h (PL10 – a/h = 0.5, PL1–PL9 – a/h = 1, PL11 – a/h = 2 and PL12 – a/h = 3) are considered in the same column in Tables 5.9 and 5.10 because the calculated reduction factors according to method B were the same for them (see Eqs. (5.13)–(5.16)). Moreover, the reduction factors according to Eurocodes [EN 1993-1-2, 2005] are shown. According to the Eurocodes, the reduction factor of 0.2 % proof strength is based on the average temperature of the plate θ_{web}. The Eurocode reduction factors based on the hottest temperature of the plate θ_{hot} are also shown (EN*) for comparison. The range of the reduction factors obtained from FEM analysis for all 12 plates is also shown.

Table 5.9. Reduction factors $V_{ult,fi}$ / $V_{ult,amb}$ according to method B, EN 1993-1-2 [EN 1993-1-2, 2005] and FEM (carbon steel plates, linear temperature distributions).

	Method B							EN	EN*	FEM
Temperature distribution [°C]	PL1, PL3, PL6	PL2, PL7 S332	PL4, PL5, PL8	PL9	PL10	PL11	PL12	All	All	All
100–300	0.818	0.818	0.816	0.818	0.814	0.820	0.822	0.890	0.780	0.804–0.852
100–500	0.613	0.612	0.609	0.614	0.605	0.617	0.621	0.780	0.530	0.620–0.688
100–700	0.307	0.305	0.298	0.311	0.290	0.319	0.327	0.650	0.130	0.286–0.334
100–900	0.093	0.092	0.089	0.094	0.085	0.097	0.101	0.530	0.050	0.101–0.137
200–500	0.592	0.591	0.589	0.593	0.586	0.595	0.598	0.715	0.530	0.596–0.660
300–600	0.400	0.399	0.396	0.401	0.391	0.405	0.410	0.590	0.300	0.416–0.463
400–700	0.218	0.217	0.214	0.219	0.210	0.223	0.227	0.415	0.130	0.228–0.255
500–800	0.101	0.101	0.100	0.101	0.098	0.103	0.104	0.215	0.070	0.115–0.128
600–900	0.060	0.060	0.060	0.060	0.059	0.061	0.061	0.100	0.050	0.061–0.071

Table 5.10. Reduction factors $V_{ult,fi}$ / $V_{ult,amb}$ according to method B, EN 1993-1-2 [EN 1993-1-2, 2005] and FEM (carbon steel plates, non-linear temperature distributions).

	Method B							EN	EN*	FEM
Temperature distribution [°C]	PL1, PL3, PL6	PL2, PL7	PL4, PL5, PL8	PL9	PL10	PL11	PL12	All	All	All
100–300	0.845	0.845	0.843	0.846	0.840	0.849	0.852	0.945	0.780	0.855–0.898
100–500	0.673	0.671	0.667	0.675	0.660	0.680	0.687	0.890	0.530	0.718–0.785
100–700	0.409	0.407	0.398	0.414	0.385	0.425	0.438	0.835	0.130	0.430–0.514
100–900	0.194	0.191	0.178	0.201	0.158	0.216	0.236	0.780	0.050	0.180–0.269
200–500	0.637	0.636	0.633	0.639	0.627	0.643	0.648	0.808	0.530	0.672–0.739
300–600	0.467	0.465	0.460	0.469	0.452	0.476	0.484	0.683	0.300	0.507–0.567
400–700	0.316	0.314	0.306	0.320	0.296	0.330	0.341	0.560	0.130	0.311–0.356
500–800	0.157	0.155	0.149	0.160	0.140	0.168	0.177	0.358	0.070	0.164–0.191
600–900	0.085	0.084	0.082	0.086	0.078	0.089	0.093	0.173	0.050	0.089–0.099

Tables 5.9 and 5.10 show that the reduction factors according to method of reference temperature (method B) are relatively close to each other for different plates in most

cases. They also reveal that the reduction factors based on average temperature (EN) are in all cases higher than those from method B and FEM. On the other hand, the reduction factors based on hottest temperature are in all cases clearly lower than those from method B and numerical analysis.

Tables 5.11 and 5.12 compare the reduction factors from FEM ($k_{FEM} = V_{ult,fi,FEM} / V_{ult,amb,FEM}$) to those from method B (Tables 5.9 and 5.10) and EN 1993-1-2 [EN 1993-1-2, 2005] using the ratio k_{FEM} / k_i (i = method B, EN and EN*). When the ratio k_{FEM} / k_i is more than one, the reduction factor is on the safe side compared to the FEM analysis.

Tables 5.11 and 5.12 show the minimum, average and maximum values of ratio k_{FEM} / k_i for plates PL1–PL12 at all considered temperature distributions from method B and EN 1993-1-2 [EN 1993-1-2, 2005] (based on average and maximum temperatures of the plate).

Table 5.11. Ratios k_{FEM} / k_i from method B and EN 1993-1-2 (carbon steel plates PL1–PL12, linear temperature distributions).

	Method B			EN			EN*		
Temperature distribution [°C]	min.	avg.	max.	min.	avg.	max.	min.	avg.	max.
100–300	0.98	1.01	1.04	0.90	0.93	0.96	1.03	1.06	1.09
100–500	1.02	1.06	1.12	0.79	0.83	0.88	1.17	1.23	1.30
100–700	0.95	1.02	1.08	0.44	0.48	0.51	2.20	2.40	2.57
100–900	1.18	1.24	1.36	0.19	0.22	0.26	2.02	2.28	2.75
200–500	1.01	1.05	1.11	0.83	0.87	0.92	1.12	1.18	1.25
300–600	1.03	1.09	1.15	0.71	0.74	0.78	1.39	1.45	1.54
400–700	1.03	1.09	1.16	0.55	0.57	0.61	1.75	1.83	1.96
500–800	1.15	1.19	1.26	0.53	0.56	0.60	1.64	1.72	1.83
600–900	1.01	1.12	1.17	0.61	0.67	0.71	1.22	1.35	1.41
All	0.95	1.10	1.36	0.19	0.65	0.96	1.03	1.61	2.75

Table 5.12. Ratios k_{FEM} / k_i from method B and EN 1993-1-2 (carbon steel plates PL1–PL12, non-linear temperature distributions).

	Method B			EN			EN*		
Temperature distribution [°C]	min.	avg.	max.	min.	avg.	max.	min.	avg.	max.
100–300	1.01	1.03	1.06	0.90	0.92	0.95	1.10	1.12	1.15
100–500	1.05	1.11	1.16	0.81	0.84	0.88	1.36	1.41	1.48
100–700	1.06	1.16	1.26	0.51	0.56	0.62	3.31	3.63	3.96
100–900	1.01	1.14	1.21	0.23	0.28	0.35	3.60	4.37	5.38
200–500	1.04	1.10	1.16	0.83	0.87	0.91	1.27	1.32	1.39
300–600	1.05	1.14	1.21	0.74	0.78	0.83	1.69	1.77	1.89
400–700	0.94	1.06	1.13	0.56	0.59	0.64	2.39	2.56	2.74
500–800	1.03	1.15	1.21	0.46	0.50	0.54	2.34	2.56	2.73
600–900	1.03	1.12	1.16	0.52	0.55	0.58	1.78	1.88	1.99
All	0.94	1.11	1.26	0.23	0.65	0.95	1.10	2.29	5.38

Figure 5.25 shows the ratios k_{FEM} / k_i for all 216 studied cases (12 carbon steel plates x 18 temperature distributions) as a function of the hottest temperature of the plate. Linear trendlines are also given in the following figures.

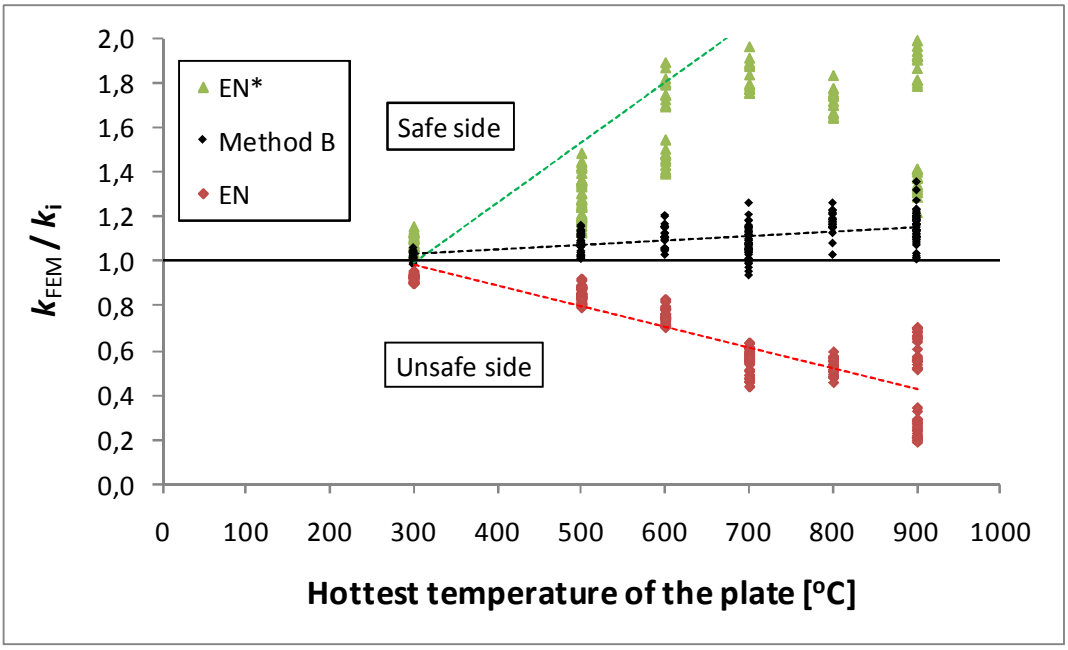

Figure 5.25. Reduction factors from FEM divided by reduction factors from method B and EN 1993-1-2 [EN 1993-1-2, 2005] (carbon steel plates PL1–PL12).

Figure 5.25 shows that method B gave in most cases results, which were on the safe side compared to numerical analysis of carbon steel plates PL1–PL12. The reduction factors obtained using average temperature of the plate (EN) were clearly on the unsafe side

compared to FEM results, especially when the hottest temperature of the plate was more than 500 °C. On the other hand, the reduction factors based on the hottest temperature of the plate were highly conservative, especially in cases where $\theta_{hot} > 300$ °C. It should be noted that in some cases the reduction factors based on the hottest temperature of the plate were even 438 % on the safe side meaning that $k_{FEM} / k_i = 5.38$. Figure 5.25 shows the cases where $k_{FEM} / k_i = 2$ at the most. Based on Tables 5.11 and 5.12 and Figure 5.25, it can be concluded that method of reference temperature (method B) is a reliable way to predict the shear resistance of a thin carbon steel plate at non-uniform elevated temperatures.

In the following, the effects of temperature distributions and the properties of plates on the accuracy of method B are studied. The following cases are considered:

- Temperature distribution (linear/non-linear, Fig. 5.26)
- Thickness of the plate (t = 1, 1.5 and 2 mm, Fig 5.27)
- Slenderness ratio ($\lambda \leq 1.87$, $2.14 \leq \lambda \leq 2.67$ and $\lambda \geq 3.24$, Fig. 5.28)
- Yield strength (f_y = 235, 332, 355 and 460 N/mm^2, Fig. 5.29)
- Boundary conditions (simply supported, clamped, Fig 5.30)
- Aspect ratio (a/h = 0.5, 1, 2, 3, Fig. 5.31)

The effect of plate thickness was considered because the height of all analyzed plates was the same (305 mm), and it was easy to divide the plates into three groups (t = 1, 1.5 and 2 mm). However, the effect of slenderness ratio λ was also studied by using three groups ($\lambda \leq 1.87$, $2.14 \leq \lambda \leq 2.67$ and $\lambda \geq 3.24$).

Figure 5.26 shows all the calculated values k_{FEM}/k_B for linear and non-linear temperature distributions as a function of the hottest temperature of the plate.

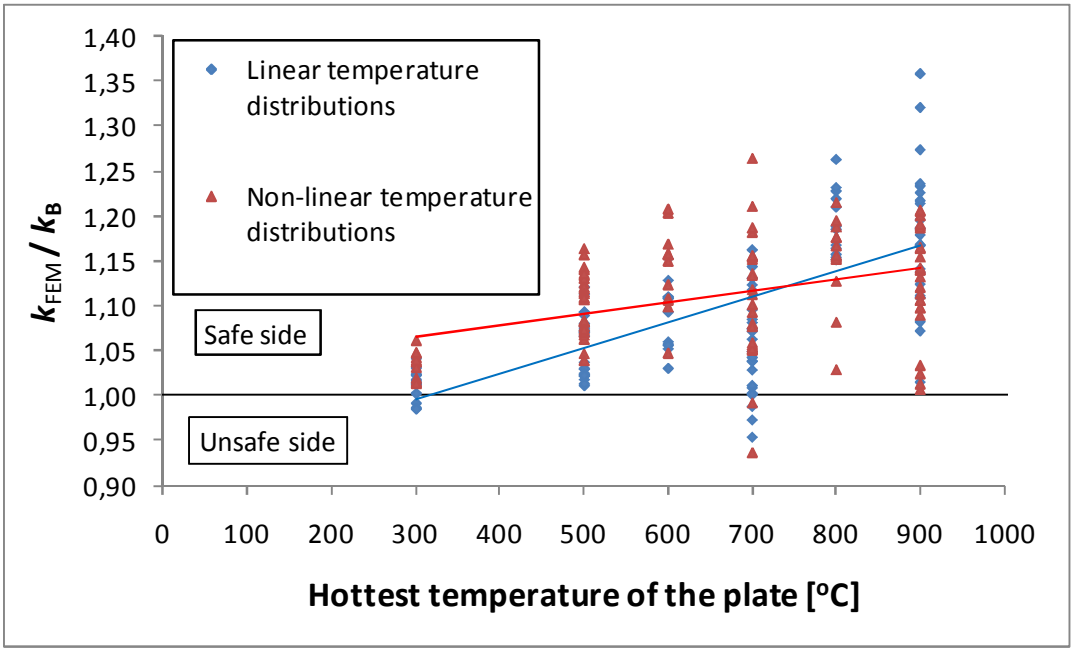

Figure 5.26. The effect of temperature distribution on the accuracy of method B (carbon steel plates PL1–PL12).

Figure 5.26 shows that the scattering of the values k_{FEM}/k_B was slightly higher in the case of linear than non-linear temperature distributions. However, it should be noted that also the scale of the reduction factors k_{FEM} was larger in the case of linear temperature distributions than at non-linear distributions. On average, the reduction factors from method B were 10 % on the safe side in the case of linear temperature distributions and 11 % in the case of non-linear temperature distributions. The corresponding standard deviations were 0.081 and 0.061, respectively.

Figure 5.27 shows the ratios k_{FEM}/k_B for carbon steel plates of different thicknesses and Figure 5.28 for different slendernesses. Plates were divided into three groups depending on the slenderness ratio λ defined in Equation (2.39).

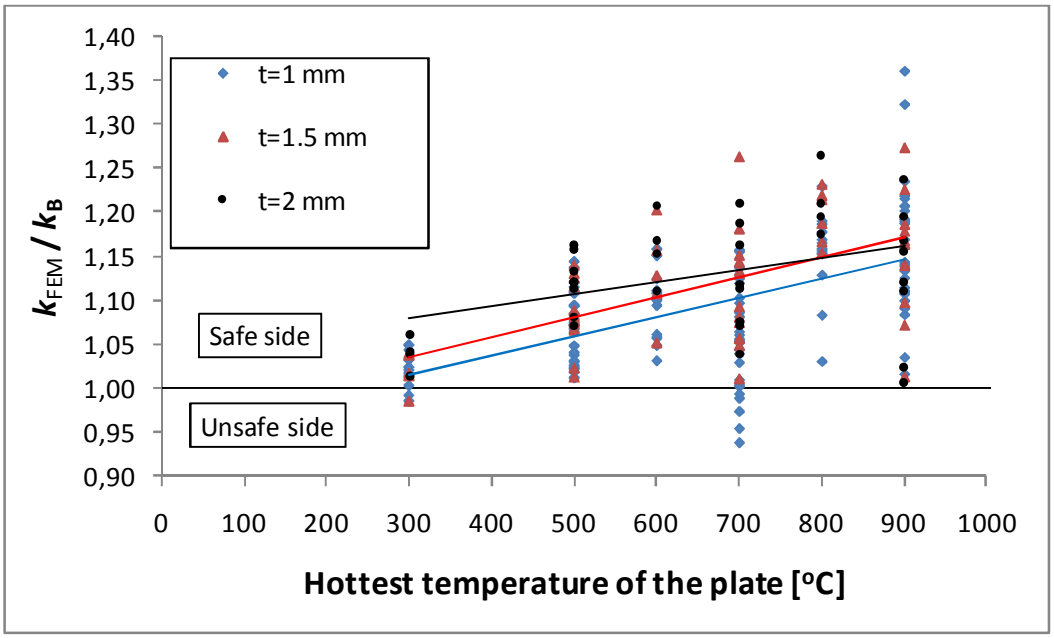

Figure 5.27. The effect of thickness of the plate on the accuracy of method B (carbon steel plates PL1–PL12).

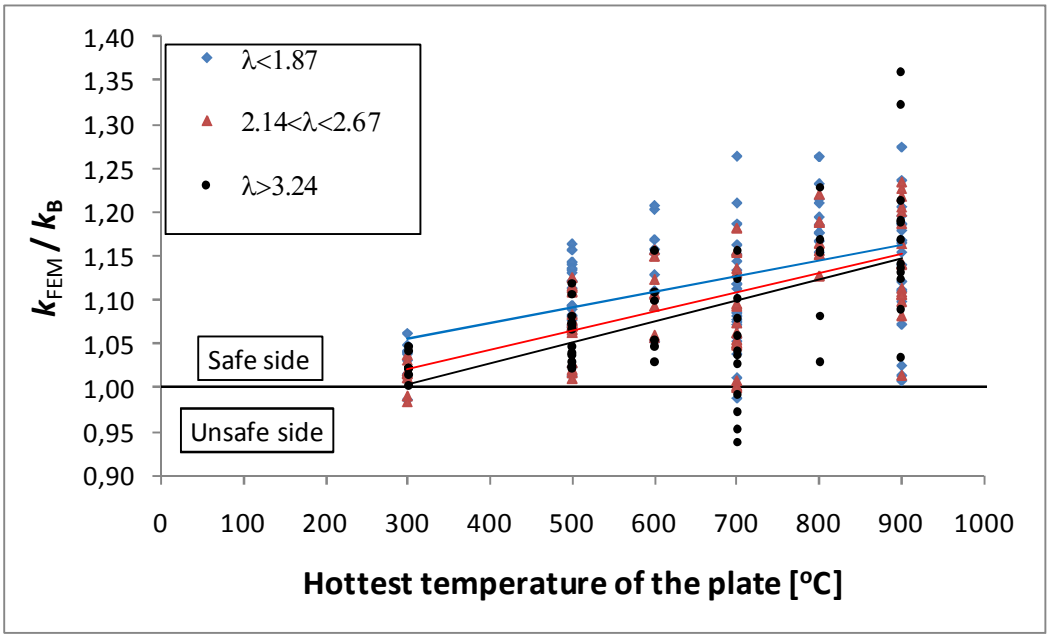

Figure 5.28. The effect of slenderness ratio of the plate on the accuracy of method B (carbon steel plates PL1–PL12).

Based on Figures 5.27 and 5.28, it can be said that the results of method B are slightly safer for thicker plates or plates with a lower slenderness ratio compared to FEM results. The reductions from method B for carbon steel plates of thicknesses 1, 1.5 and 2 mm were on the safe side, on average by 9, 12 and 13 %, respectively, and the corresponding standard deviations were 0.072, 0.071 and 0.066, respectively. However, it should be noted that PL12 was also among the most slender plates for which the scattering of the ratios k_{FEM}/k_B was the largest.

Figure 5.29 shows the effect of yield strength on the accuracy of method B. In Chapter 4.4.4 it was shown that reduction factors were somewhat dependent on yield strength (Figs. 4.42 and 4.43), which is taken into account in method B by the factor k_y (Eq. (5.15)).

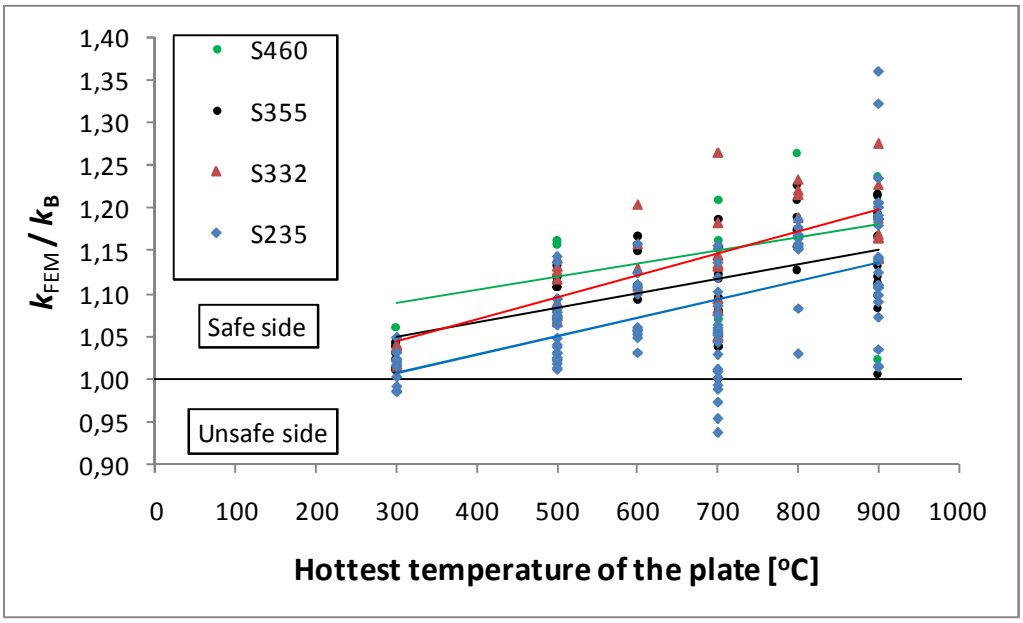

Figure 5.29. The effect of yield strength on the accuracy of method B (carbon steel plates PL1–PL12).

Figure 5.29 shows that the reduction factors from method B were slightly more conservative for carbon steel grades S332 and S460 than for grades S235 and S355. It should be noted that only two plates of grade S332 and one plate of grade S460 were analyzed. Compared to FEM results, the reductions from method B for carbon steel grades S235, S332, S355 and S460 were on the safe side, on average by 8, 14, 11 and 15 % and the corresponding standard deviations were 0.073, 0.067, 0.059 and 0.066, respectively.

Figure 5.30 shows the effect of the boundary conditions on the ratio k_{FEM}/k_B. Nine simply supported and three clamped carbon steel plates were analyzed in this study.

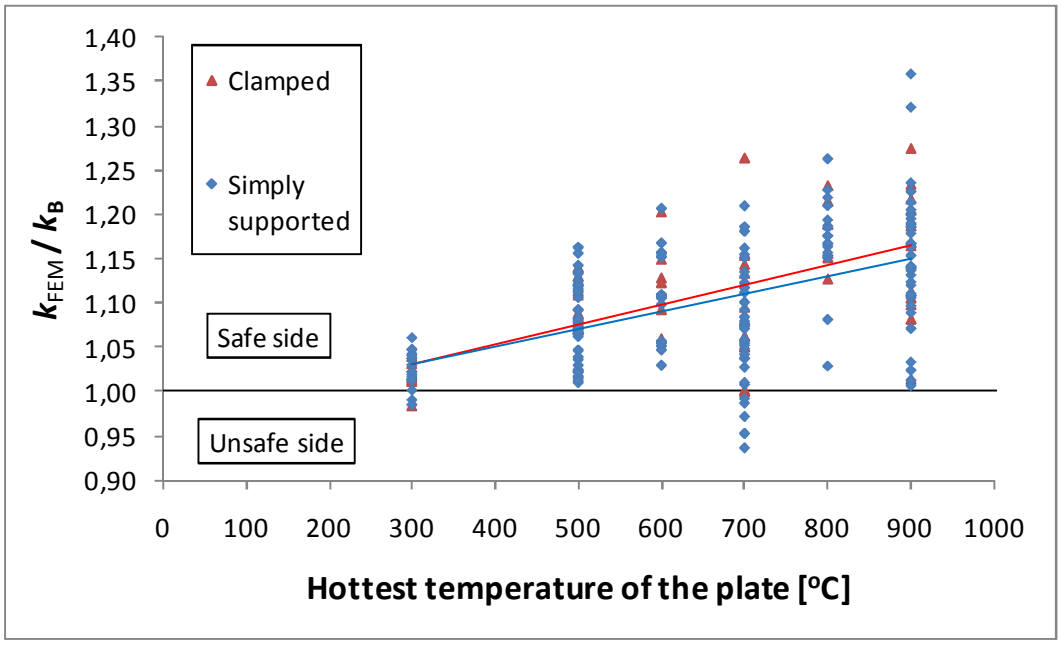

Figure 5.30. The effect of boundary conditions on the accuracy of method B (carbon steel plates PL1–PL12).

Figure 5.30 shows that the ratios k_{FEM}/k_B were approximately the same for simply supported and clamped plates. The same observation that boundary conditions do not affect on the reduction factor can also be drawn from Figure 4.45. On average, the reduction factors from method B were 10 % on the safe side in the case of simply supported plates and 11 % in the case of clamped plates. Standard deviations were 0.072 in both cases.

Figure 5.31 shows the ratios k_{FEM}/k_B for carbon steel plates with different aspect ratios a/h. Only one plate of aspect ratios 0.5, 2 and 3 was considered. The other nine analyzed carbon steel plates had an aspect ratio $a/h = 1$. Factor k_A (Eq. (5.16)) takes the aspect ratio into account in method B.

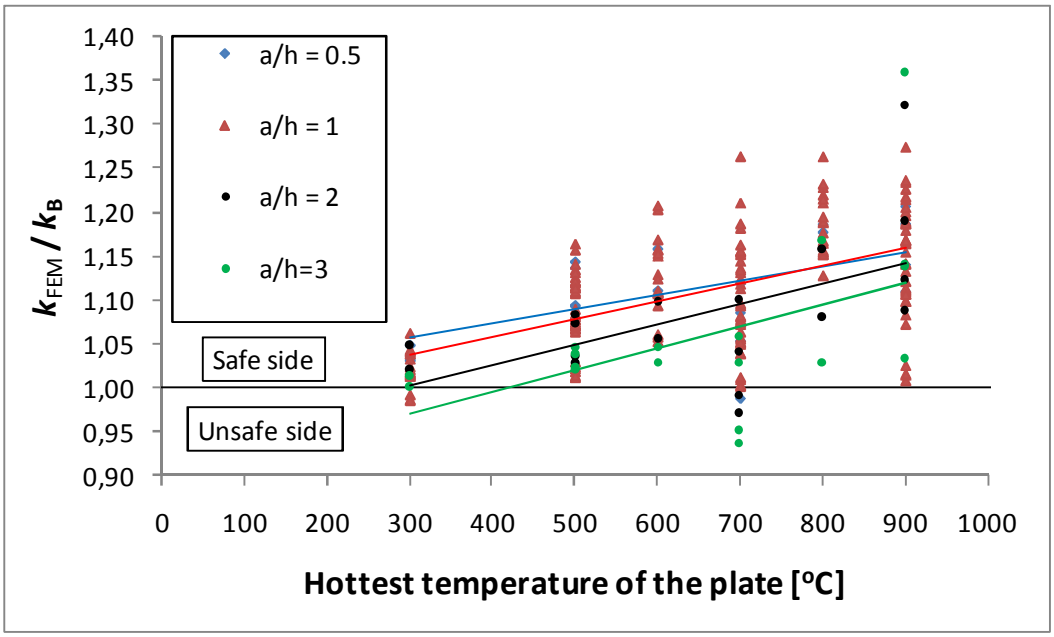

Figure 5.31. The effect of aspect ratio on the accuracy of method B (carbon steel plates PL1–PL12).

Figure 5.31 shows that the scattering of the k_{FEM}/k_B ratios was higher for aspect ratios a/h = 0.5, 2 and especially 3 than for a/h = 1. At linear 100–700 °C and non-linear 400–700 °C temperature distributions, the reduction factors for plate PL12 (a/h = 3) from method B were on the unsafe side by 5 and 6 %, respectively. On the other hand, the reduction factor for PL12 at linear 100–900 °C temperatures was 36 % on the safe side, which was the most conservative result of all considered cases. Overall, compared to the FEM results, the reductions from method B for aspect ratios a/h = 0.5, 1, 2 and 3 were on the safe side, on average by 11, 11, 8 and 6 %, and the corresponding standard deviations were 0.059, 0.067, 0.080 and 0.095, respectively.

Figures 5.26–5.31 show that method B gives reliable results for carbon steel plates with different yield strengths, thicknesses, slenderness ratios, boundary conditions and aspect ratios at different types of temperature distributions. Largest scattering of the ratios k_{FEM}/k_B occurred in the case of PL12 (a/h = 3). However, the reduction factors from method B were at the most 36 % conservative and 6 % on the unsafe side in the 216 considered cases of carbon steel plates. On average, method B gave results that were 10 % more conservative compared to FEM results.

5.2.6.2 Aluminium plates PLa1 and PLa2

Tables 5.13 and 5.14 show the reduction factors for aluminium plates PLa1 and PLa2 at the considered non-uniform elevated temperatures according to method of reference temperature (method B), EN 1999-1-2 [EN 1999-1-2, 2007] (based on the average temperature of the plate, "EN") and FEM analysis. The reduction factors based on the

hottest temperature of the plate are also shown (EN*) as in the case of carbon steel plates. It should be noted that the reduction factors according to method B and EN 1993-1-2 were based on the 0.2 % proof strength curve of alloy 5083-O (see also Chapter 4.2.2). The properties of the two analyzed aluminium plates PLa1 and PLa2 were the same, except for their thicknesses which were 1.5 and 2 mm, respectively. Thus, the reduction factors from method B were also the same for both plates at the same temperature distribution.

Table 5.13. Reduction factors according to method B, EN 1999-1-2 [EN 1999-1-2, 2007] and FEM (aluminium plates, linear temperature distributions).

Temperature distribution [°C]	B	EN	EN*	FEM (PLa1)	FEM (PLa2)
50–200	0.909	0.990	0.900	0.783	0.783
50–250	0.773	0.980	0.750	0.667	0.668
50–300	0.462	0.940	0.400	0.523	0.519
50–350	0.298	0.900	0.220	0.370	0.366
100–250	0.769	0.940	0.750	0.641	0.641
125–275	0.608	0.900	0.575	0.554	0.551
150–300	0.449	0.825	0.400	0.465	0.460
175–325	0.345	0.750	0.310	0.378	0.375
200–350	0.259	0.575	0.220	0.293	0.290

Table 5.14. Reduction factors according to method B, EN 1999-1-2 [EN 1999-1-2, 2007] and FEM (aluminium plates, non-linear temperature distributions).

Temperature distribution [°C]	B	EN	EN*	FEM (PLa1)	FEM (PLa2)
50–200	0.915	1.000	0.900	0.836	0.838
50–250	0.788	1.000	0.750	0.762	0.768
50–300	0.503	0.995	0.400	0.660	0.655
50–350	0.387	0.990	0.220	0.525	0.526
100–250	0.785	0.985	0.750	0.721	0.725
125–275	0.633	0.960	0.575	0.643	0.644
150–300	0.490	0.920	0.400	0.564	0.560
175–325	0.389	0.863	0.310	0.480	0.475
200–350	0.308	0.788	0.220	0.391	0.387

Tables 5.15 and 5.16 show the ratios k_{FEM} / k_i (i = method B, EN and EN*) for plates PLa1 and PLa2 at all considered temperature distributions according to method B and EN 1993-1-2 [EN 1993-1-2, 2005] (using average as well as maximum temperature of the plate). When the ratio k_{FEM} / k_i is more than one, the reduction factor is on the safe side compared to the FEM analysis.

Table 5.15. Ratios k_{FEM} / k_i from method B and EN 1999-1-2 (aluminium plates PLa1 and PLa2, linear temperature distributions).

	Method B		EN		EN*	
Temperature distribution [°C]	PLa1	PLa2	PLa1	PLa2	PLa1	PLa2
50–200	0.86	0.86	0.79	0.79	0.87	0.87
50–250	0.86	0.86	0.68	0.68	0.89	0.89
50–300	1.13	1.12	0.56	0.55	1.31	1.30
50–350	1.24	1.23	0.41	0.41	1.68	1.67
100–250	0.83	0.83	0.68	0.68	0.86	0.85
125–275	0.91	0.91	0.62	0.61	0.96	0.96
150–300	1.04	1.03	0.56	0.56	1.16	1.15
175–325	1.10	1.09	0.50	0.50	1.22	1.21
200–350	1.13	1.12	0.51	0.51	1.33	1.32
Min.	0.83	0.83	0.41	0.41	0.86	0.85
Avg.	1.01	1.01	0.59	0.59	1.14	1.14
Max.	1.24	1.23	0.79	0.79	1.33	1.32

Table 5.16. Ratios k_{FEM} / k_i from method B and EN 1999-1-2 (aluminium plates PLa1 and PLa2, non-linear temperature distributions).

	Method B		EN		EN*	
Temperature distribution [°C]	PLa1	PLa2	PLa1	PLa2	PLa1	PLa2
50–200	0.91	0.92	0.84	0.84	0.93	0.93
50–250	0.97	0.98	0.76	0.77	1.02	1.02
50–300	1.31	1.30	0.66	0.66	1.65	1.64
50–350	1.36	1.36	0.53	0.53	2.39	2.39
100–250	0.92	0.92	0.73	0.74	0.96	0.97
125–275	1.02	1.02	0.67	0.67	1.12	1.12
150–300	1.15	1.14	0.61	0.61	1.41	1.40
175–325	1.23	1.22	0.56	0.55	1.55	1.53
200–350	1.27	1.26	0.50	0.49	1.78	1.76
Min.	0.91	0.92	0.50	0.49	0.93	0.93
Avg.	1.13	1.12	0.65	0.65	1.42	1.42
Max.	1.36	1.36	0.84	0.84	2.39	2.39

Figure 5.32 shows the ratios k_{FEM} / k_i for all 36 studied cases (2 aluminium plates x 18 temperature distributions) as a function of the hottest temperature of the plate.

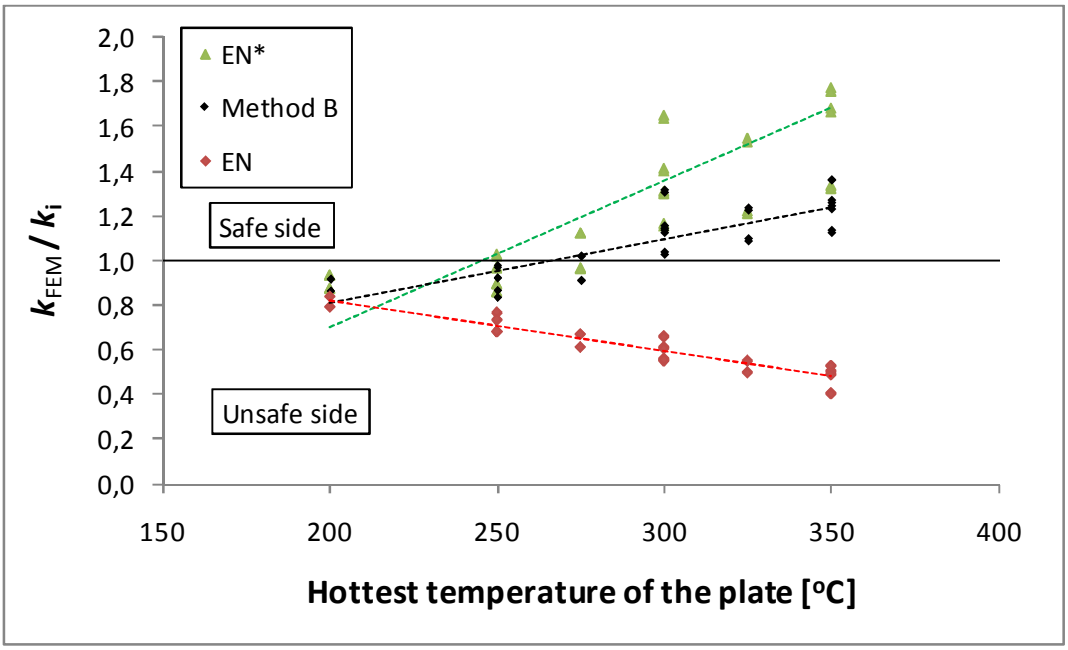

Figure 5.32. Reduction factors from FEM divided by reduction factors from method B and EN 1999-1-2 [EN 1999-1-2, 2007] (aluminium plates PLa1 and PLa2).

Figure 5.32 shows that method B gave results, which were on the safe side compared to numerical analysis when the hottest temperature of the plate was more than 275 °C. When the hottest temperature of the plate did not exceed 275 °C, the results from method B were unconservative. The scattering of the ratios k_{FEM} / k_i with method B was clearly higher with aluminium plates than with carbon steel plates.

The reduction factors obtained using the average temperature of the plate (EN) were also in this case clearly on the unsafe side compared to FEM results, especially when the hottest temperature of the plate exceeded 250 °C. On the other hand, the reduction factors based on the hottest temperature of the plate were conservative in cases where θ_{hot} > 275 °C. It should be noted that in some cases even the reduction factor based on the hottest temperature was unconservative compared to FEM possibly because the reduction curve was adopted from EN 1999-1-2 [EN 1999-1-2, 2007] and the material model from [Maljaars, 2008].

Based on Tables 5.15 and 5.16 and Figure 5.32, it can be concluded that method B gives more reliable results on the shear resistance of a thin aluminium plate at non-uniform elevated temperatures than methods (EN) and (EN*). However, the results that method B gave for aluminium were not as good as they were for carbon steel.

Figure 5.33 shows all the calculated values k_{FEM}/k_B for linear and non-linear temperature distributions as a function of a hottest temperature of the plate.

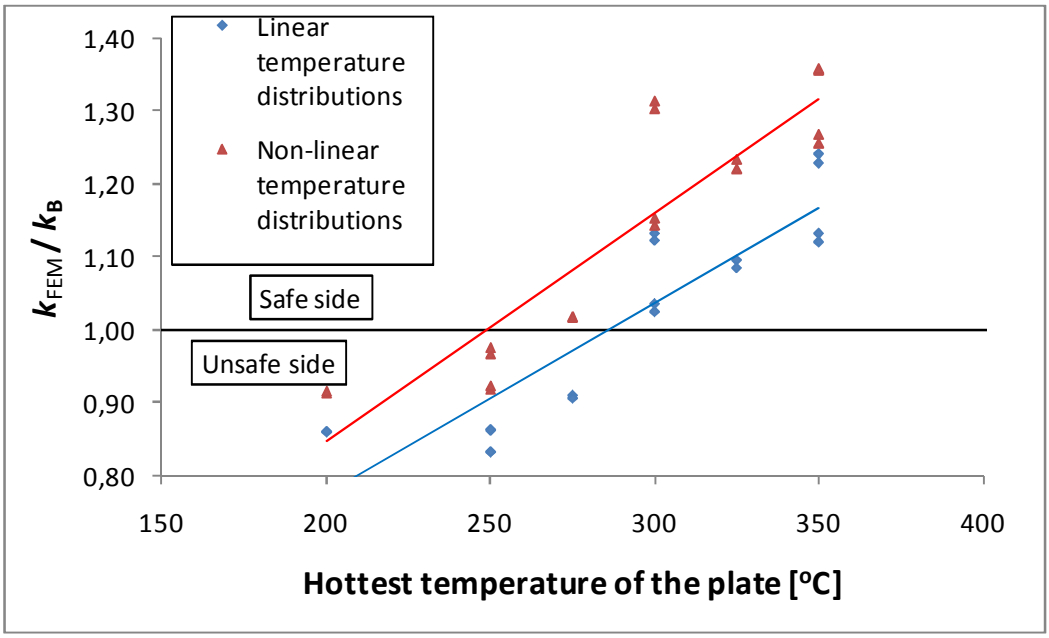

Figure 5.33. The effect of temperature distribution on the accuracy of method B (aluminium plates PLa1 and PLa2).

Figure 5.33 shows that the values k_{FEM}/k_B were slightly higher in the case of non-linear than linear temperature distributions. On average, the reduction factors from method B were 1 % on the safe side in the case of linear temperature distributions and 12 % in the case of non-linear temperature distributions. The corresponding standard deviations were 0.141 and 0.167, respectively.

Figure 5.34 presents the ratios k_{FEM}/k_B for the two considered plates as a function of the hottest temperature of the plate.

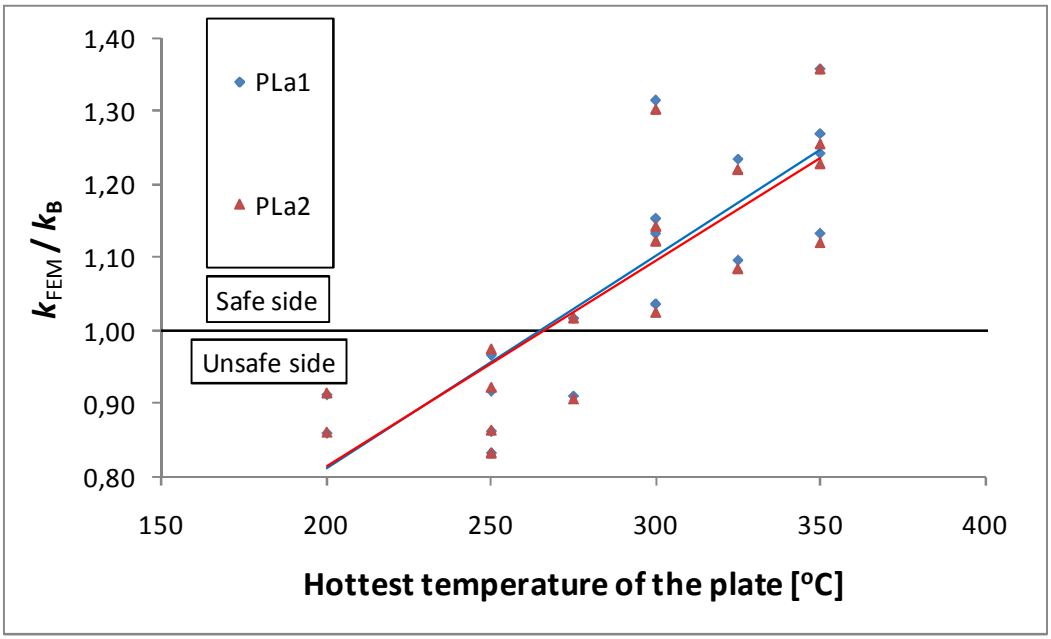

Figure 5.34. The effect of thickness of the plate on the accuracy of method B (aluminium plates PLa1 and PLa2).

Figure 5.34 shows that the ratios k_{FEM}/k_B were approximately the same for both plates. On average, the reduction factors from method B were 7 % on the safe side for PLa1 (t = 1.5 mm) and 6 % for PLa2 (t = 2 mm). The corresponding standard deviations were 0.168 and 0.164, respectively.

5.2.6.3 Stainless steel plates PLs1 and PLs2

Tables 5.17 and 5.18 show the reduction factors for stainless steel plates PLs1 and PLs2 at the considered non-uniform elevated temperatures according to method of reference temperature (method B), EN 1999-1-2 [EN 1999-1-2, 2007] (based on the average temperature of the plate, "EN") and FEM analysis. The reduction factors based on the hottest temperature of the plate are also shown (EN*) as in the case of carbon steel and aluminium plates. The properties of the two analyzed stainless steel plates PLs1 and PLs2 were the same, except that their thicknesses were 1 and 1.5 mm, respectively. Thus, the reduction factors from method B were also the same for both plates at the same temperature distribution.

Table 5.17. Reduction factors according to method B, EN 1993-1-2 [EN 1993-1-2, 2005] and FEM (stainless steel plates, linear temperature distributions).

Temperature distribution [°C]	B	EN	EN*	FEM (PLs1)	FEM (PLs2)
100–400	0.633	0.660	0.600	0.752	0.733
100–600	0.562	0.620	0.490	0.667	0.645
100–800	0.435	0.570	0.270	0.510	0.498
100–1000	0.248	0.515	0.060	0.252	0.258
200–600	0.546	0.600	0.490	0.602	0.633
300–700	0.477	0.540	0.400	0.537	0.558
400–800	0.391	0.490	0.270	0.459	0.437
500–900	0.283	0.400	0.140	0.314	0.303
600–1000	0.153	0.270	0.060	0.180	0.184

Table 5.18. Reduction factors according to method B, EN 1993-1-2 [EN 1993-1-2, 2005] and FEM (stainless steel plates, non-linear temperature distributions).

Temperature distribution [°C]	B	EN	EN*	FEM (PLs1)	FEM (PLs2)
100–400	0.654	0.715	0.600	0.781	0.763
100–600	0.598	0.670	0.490	0.718	0.694
100–800	0.498	0.650	0.270	0.614	0.603
100–1000	0.402	0.630	0.060	0.407	0.416
200–600	0.580	0.640	0.490	0.624	0.671
300–700	0.520	0.600	0.400	0.567	0.611
400–800	0.432	0.540	0.270	0.535	0.515
500–900	0.350	0.490	0.140	0.413	0.402
600–1000	0.244	0.400	0.060	0.260	0.263

Tables 5.19 and 5.20 show the ratios k_{FEM} / k_i (i = method B, EN and EN*) for plates PLs1 and PLs2 at all considered temperature distributions according to method B and EN 1993-1-2 [EN 1993-1-2, 2005] (using average as well as maximum temperature of the plate). When the ratio k_{FEM} / k_i is more than one, the reduction factor is on the safe side compared to FEM analysis.

Table 5.19. Ratios k_{FEM} / k_i from method B and EN 1993-1-2 (stainless steel plates PLs1 and PLs2, linear temperature distributions).

	Method B		EN		EN*	
Temperature distribution [°C]	PLs1	PLs2	PLs1	PLs2	PLs1	PLs2
100–400	1.19	1.16	1.14	1.11	1.25	1.22
100–600	1.19	1.15	1.08	1.04	1.36	1.32
100–800	1.17	1.15	0.90	0.87	1.89	1.85
100–1000	1.02	1.04	0.49	0.50	4.20	4.30
200–600	1.10	1.16	1.00	1.05	1.23	1.29
300–700	1.13	1.17	0.99	1.03	1.34	1.39
400–800	1.17	1.12	0.94	0.89	1.70	1.62
500–900	1.11	1.07	0.79	0.76	2.24	2.16
600–1000	1.18	1.20	0.67	0.68	3.00	3.06
Min.	1.02	1.04	0.49	0.50	1.23	1.22
Avg.	1.14	1.13	0.89	0.88	2.03	2.02
Max.	1.19	1.20	1.14	1.11	4.20	4.30

Table 5.20. Ratios k_{FEM} / k_i from method B and EN 1993-1-2 (stainless steel plates PLs1 and PLs2, non-linear temperature distributions).

	Method B		EN		EN*	
Temperature distribution [°C]	PLs1	PLs2	PLs1	PLs2	PLs1	PLs2
100–400	1.19	1.17	1.09	1.07	1.30	1.27
100–600	1.20	1.16	1.07	1.04	1.47	1.42
100–800	1.23	1.21	0.94	0.93	2.27	2.23
100–1000	1.01	1.04	0.65	0.66	6.78	6.94
200–600	1.08	1.16	0.97	1.05	1.27	1.37
300–700	1.09	1.17	0.94	1.02	1.42	1.53
400–800	1.24	1.19	0.99	0.95	1.98	1.91
500–900	1.18	1.15	0.84	0.82	2.95	2.87
600–1000	1.07	1.08	0.65	0.66	4.33	4.38
Min.	1.01	1.04	0.65	0.66	1.27	1.27
Avg.	1.14	1.15	0.91	0.91	2.64	2.66
Max.	1.24	1.21	1.09	1.07	6.78	6.94

Figure 5.35 shows the ratios k_{FEM} / k_i for all 36 studied cases (2 aluminium plates x 18 temperature distributions) as a function of the hottest temperature of the plate.

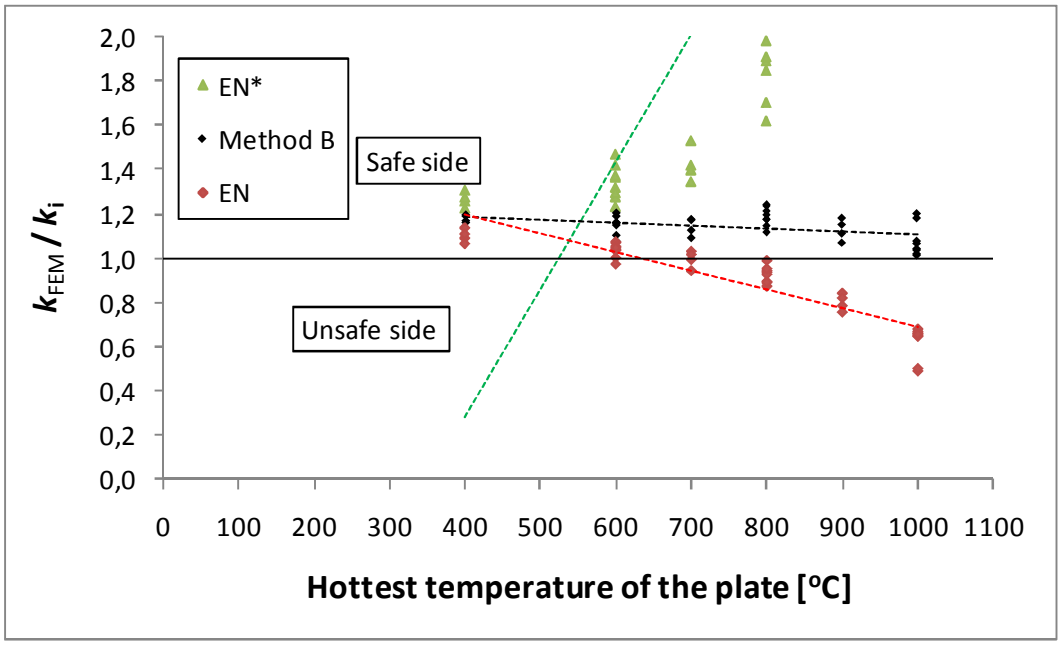

Figure 5.35. Reduction factors from FEM divided by reduction factors from method B and Eurocodes (using average and maximum temperature).

Figure 5.35 shows that the results from method B were conservative in every case compared to FEM analysis. The reduction factors obtained by using the average temperature of the plate (EN) were also mostly on the safe side when the hottest temperature did not exceed 600 °C. When the hottest temperature of the plate exceeded 600 °C, use of reduction based on average temperature yielded unconservative results. The reduction factors based on the hottest temperature of the plate (EN*) were highly conservative in all considered cases. It should be noted that in some cases reduction factors based on the hottest temperature of the plate were as much as 594 % on the safe side meaning that $k_{FEM} / k_i = 6.94$. Figure 5.35 shows the cases where $k_{FEM} / k_i = 2$ at the most. Based on Tables 5.19 and 5.20 and Figure 5.35, it can be concluded that method B is a reliable way to predict the shear resistance of a thin stainless steel (grade 1.4301) plate at non-uniform elevated temperatures.

Figure 5.36 shows all the calculated values k_{FEM}/k_B for linear and non-linear temperature distributions as a function of the hottest temperature of the plate.

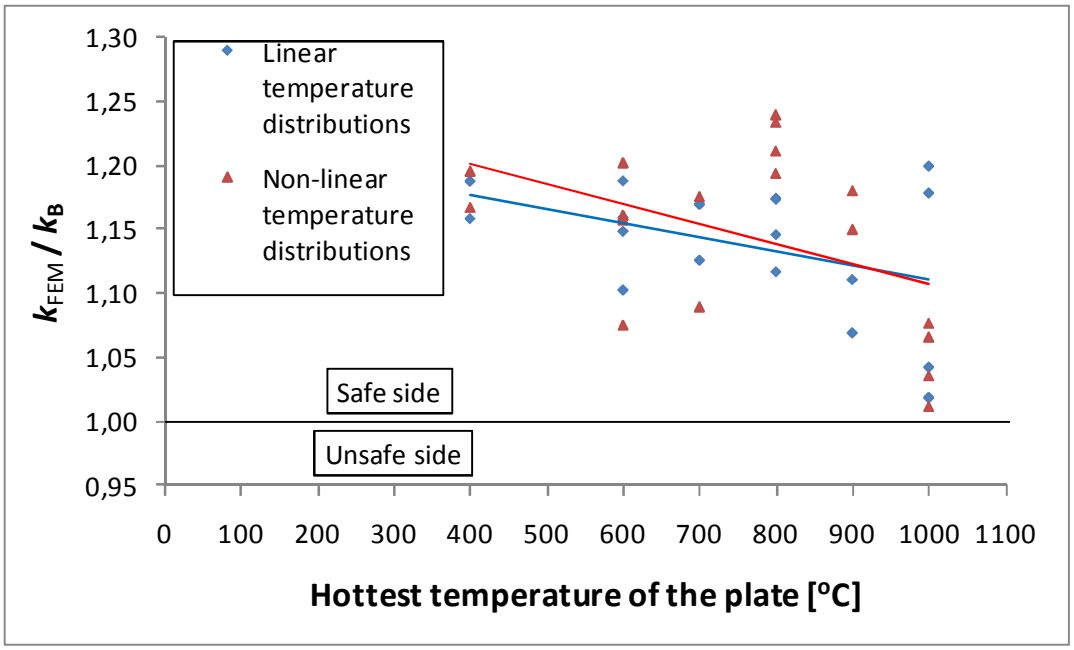

Figure 5.36. Reduction factors from FEM divided by reduction factors from method B.

Figure 5.36 shows that the scattering of the values k_{FEM}/k_B was slightly higher in the case of non-linear than linear temperature distributions. On average, the reduction factors from method B were 14 % on the safe side in the case of linear temperature distributions and 15 % in the case of non-linear temperature distributions. The corresponding standard deviations were 0.052 and 0.069, respectively.

Figure 5.37 presents the ratios k_{FEM}/k_B for the two considered plates as a function of the hottest temperature of the plate.

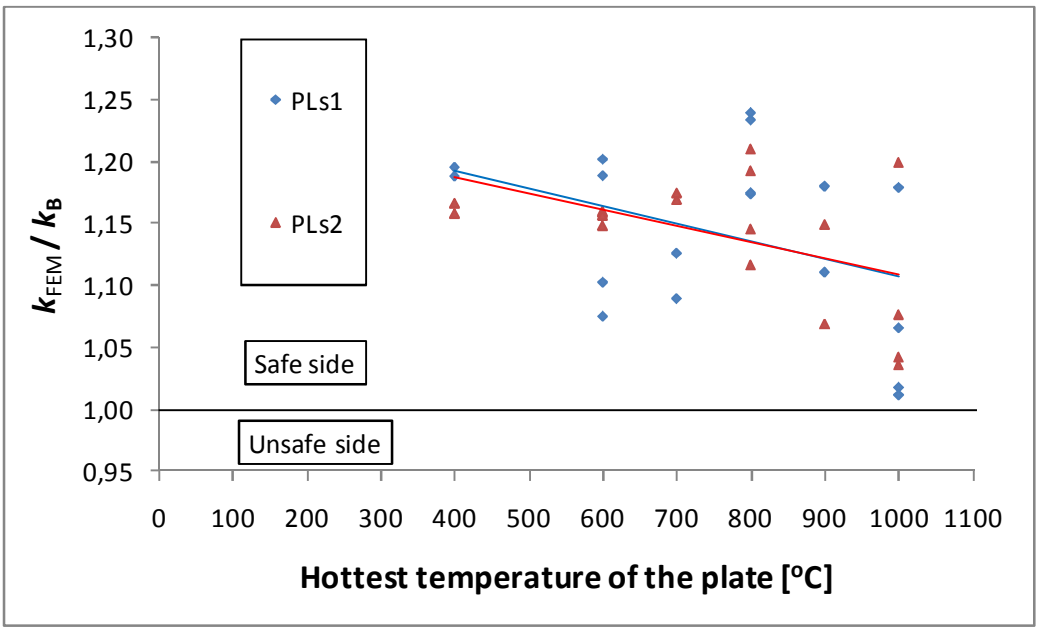

Figure 5.37. Reduction factors from FEM divided by reduction factors from method B.

Figure 5.37 shows that the ratios k_{FEM}/k_B were approximately the same for both plates. On average, the reduction factors from method B were 14 % on the safe side for PLa1 (t = 1 mm) and PLa2 (t = 1.5 mm). The corresponding standard deviations were 0.069 and 0.052, respectively.

5.3 Discussion

Two methods for predicting the shear resistance of a thin metal plate at non-uniform elevated temperatures were proposed: method of separation of shear and post-buckling (method A, Chapter 5.1) and method of reference temperature (method B, Chapter 5.2). The advantages and weaknesses of both methods are summarized in the following:

Method of separation of shear and post-buckling (method A)

This method predicts shear buckling and post-buckling resistances separately. It is based on the assumption that the contribution of post-buckling resistance to ultimate shear resistance at elevated temperatures can be defined from the respective relationship at ambient temperature. Shear buckling and post-buckling resistances at ambient temperatures may be determined by Eurocode [EN 1993-1-5, 2005], [EN 1999-1-1, 2007], [EN 1993-1-4, 2006] equations (A1) or FEM analysis (A2), which means that method A consists of two approaches.

Method A gave reliable results for the considered carbon and stainless steel plates in the worked example (Chapter 5.1.2) when the difference between the hottest and coldest temperature did not exceed 340 ^{o}C and the hottest temperature was 730 ^{o}C at the most. In the other considered cases where the temperature distributions were wider and the hottest temperature was higher (Chapter 5.1.3), there was more scattering in the results, and in some cases the results from method A were clearly unconservative compared to FEM results.

Moreover, method A is applicable only to very thin plates when the proportionality limit is not exceeded even at elevated temperatures as shear buckling occurs, so that shear buckling resistance can be calculated accurately. It is difficult to define the limit slenderness analytically because the proportionality limit depends on material temperature. The plates PL1 and PLs1 analyzed in the worked example were thin enough (λ=3.28 and 2.59, respectively) at the considered temperature distributions, but, for example, plate PLs2 was too thick (λ=1.72) even at ambient temperature and its shear buckling resistance according to classical formulas (Eqs. (2.5)–(2.8)) was clearly higher than the respective value from FEM analysis.

In order to be able calculate shear buckling and post-buckling resistances according to method A, the corresponding values at ambient temperature should be known. In EN

1993-1-5 [EN 1993-1-5, 2005] the resistances are not calculated separately. However, they can be obtained by using the classical Equations (2.5)–(2.10) which are also applied in EN 1993-1-5 when calculating the slenderness parameter. Alternatively, the contribution of shear buckling and post-buckling resistances can be defined by numerical analysis, which is naturally a more demanding task.

The method for predicting shear buckling resistances at non-uniform elevated temperatures (utilized in method A) gives accurate results compared to FEM analysis as shown in [Salminen, 2010]. It is more complicated to use than, for example, method B and requires iteration when considered analytically as a formula. However, the method is easy to apply, for example, in spreadsheet computation as shown in [Salminen, 2010].

The basic assumption of method A is that plate behaviour is ideal resulting in distinguishable shear buckling and post-buckling phases at ambient as well as elevated temperatures, which presumes a very small magnitude of initial imperfection (approximately $h/100\,000$ in the considered cases). According to EN 1090-2 [EN 1090-2, 2005], the value $h/100$ should be applied in the calculations. However, it was shown in this study (e.g. Tables 4.15–4.17) that the use of an imperfection of $h/100\,000$ instead of $h/100$ yields only slightly higher resistances in most cases.

The comparison of the results from method A and FEM was not as extensive as with method B because most of the reduction factors from FEM were calculated using an imperfection of $h/100$ meaning that the buckling and post-buckling phases were not distinguishable. Thus, more research is needed, for example, on the slenderness limits of method A.

Method of reference temperature (method B)

The main idea of this method is to convert the non-uniform temperature distribution into a uniform temperature distribution using the so-called reference temperature, so as to make the behaviour of the plates more similar. Method B gave reliable results for carbon and stainless steel plates. Especially in the case of carbon steel, plates with different properties were considered. In the case of aluminium plates, the scattering of the results was clearly higher perhaps due to the applied material model and reduction curve.

Method B is applicable to the cases considered in this study. It is assumed that the effects of the yield strength, slenderness and aspect ratio of the plate are similar in the case of aluminium and stainless steel plates as they are for carbon steel plates (Figs. 4.42–4.44 and 4.46). The method is not dependent on the boundary conditions of the plate. Table 5.21 presents all the cases where the proposed method can be applied. The temperature distribution across the height of the plate must also closely follow the form:

$$\theta(y) = \theta_{cold} + \left(1 - \frac{y}{h}\right)^{n} \left(\theta_{hot} - \theta_{cold}\right) \tag{5.38}$$

where n can vary from 1 to 3

It is believed that method of reference temperature (method B) can be applied to many kinds of temperature distributions. All the considered temperature distributions of this study were as presented in Equation (5.38) (see also Equations (4.1) and (4.2)).

Table 5.21. Applicability of the proposed method of reference temperature.

Material	Grades	λ_w	a/h	Temperatures [°C]
Carbon steel	S235–S460	1.5-3.5	0.5-3	20–900
Aluminium	5083–H111/O	1.5-3.5	0.5-3	20–550
Stainless steel	1.4301	1.5-3.5	0.5-3	20–1000

Method of reference temperature is based on the Eurocode equations and is easy to use in hand calculations. The difference between EN 1993-1-2 [EN 1993-1-2, 2005] and EN 1999-1-2 [EN 1999-1-2, 2007] equations and method B is that the reduction of 0.2 % proof strength is based on a reference temperature instead of average temperature. Moreover, an upper limit is given for resistance.

The factors k_y, k_a and k_d applied in method of reference temperature can be easily modified (e.g. for other stainless steel grades), or other factors can be added based on results from tests or numerical analysis, if available.

Conclusions

Based on the above discussion, it can be concluded that the advantage of method of separation of shear and post-buckling (method A) over method of reference temperature (method B) is that both phases (buckling and post-buckling) are calculated separately. Method of reference temperature, again, is easier to apply and gives more reliable results for ultimate shear resistance compared to numerical analysis in the considered cases. Figure 5.38 compares these methods where possible (cases presented in Chapter 5.1.3). Ratios k_{FEM}/k_i (i = A and B) for ultimate shear resistance are based on the FEM resistances calculated using the magnitude $h/100$ for initial imperfection.

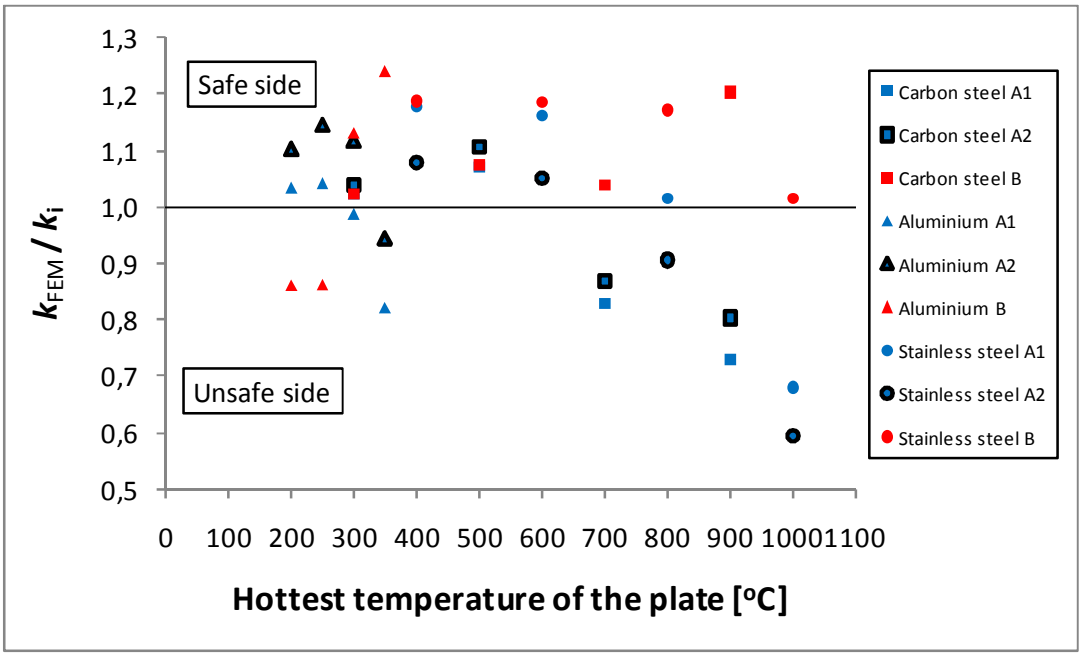

Figure 5.38. Comparison of proposed methods.

Based on Figure 5.38, it can be concluded that in the considered cases method of reference temperature (method B) gives better predictions for ultimate shear strength reduction factors than method of separation of shear and post-buckling (method A) compared to FEM results. In the considered cases, the ratios k_{FEM} / k_i of methods A1, A2 and B were, on average, 0.96, 0.98 and 1.08, respectively. The corresponding standard deviations were 0.162, 0.164 and 0.128. Especially in the cases of carbon and stainless steel plates, the reduction factors from method A were on the unsafe side when the maximum temperature of the plate was relatively hot. On the other hand, the reduction factors from method A were also quite close to those from FEM when the hottest temperature of the plate did not exceed 600 °C.

Figures 5.39–5.41 compare all the reduction factors obtained by using FEM (k_{FEM}), method of reference temperature (k_B) and based on the average (k_{EN}) and maximum temperature (k_{EN*}) for all considered cases of this study.

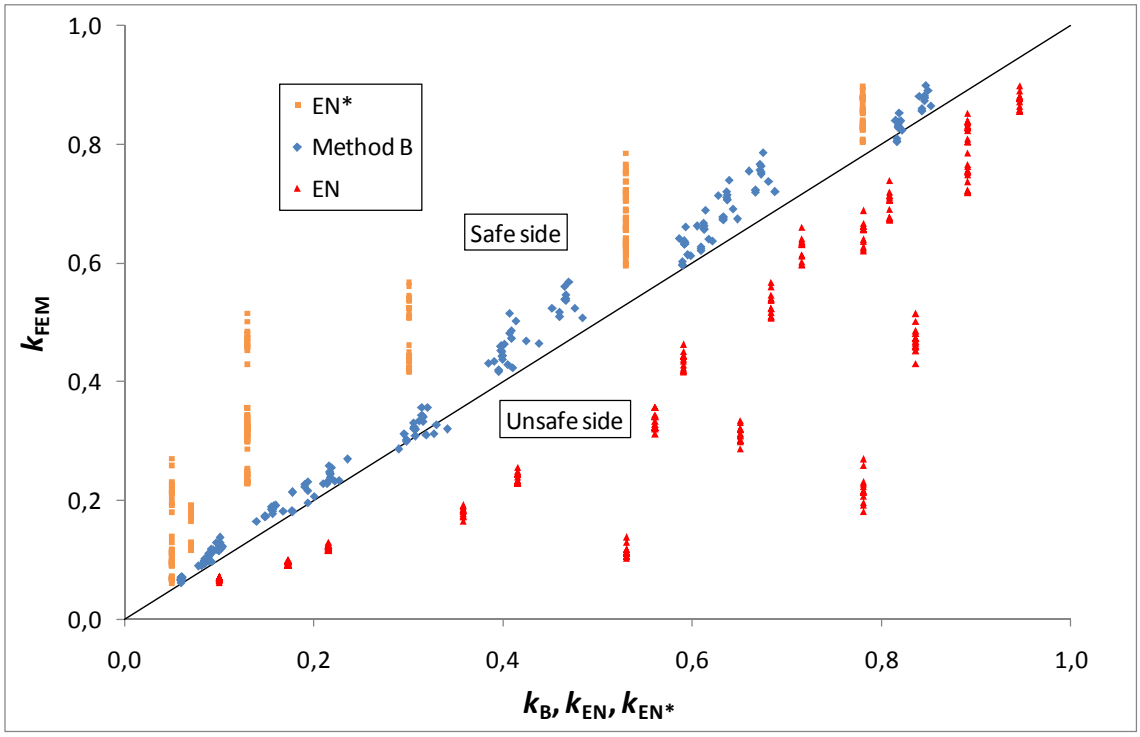

Figure 5.39. Comparison of reduction factors from FEM, method B and based on the average (EN) and hottest (EN*) temperature of the plate for carbon steel plates PL1–PL12.

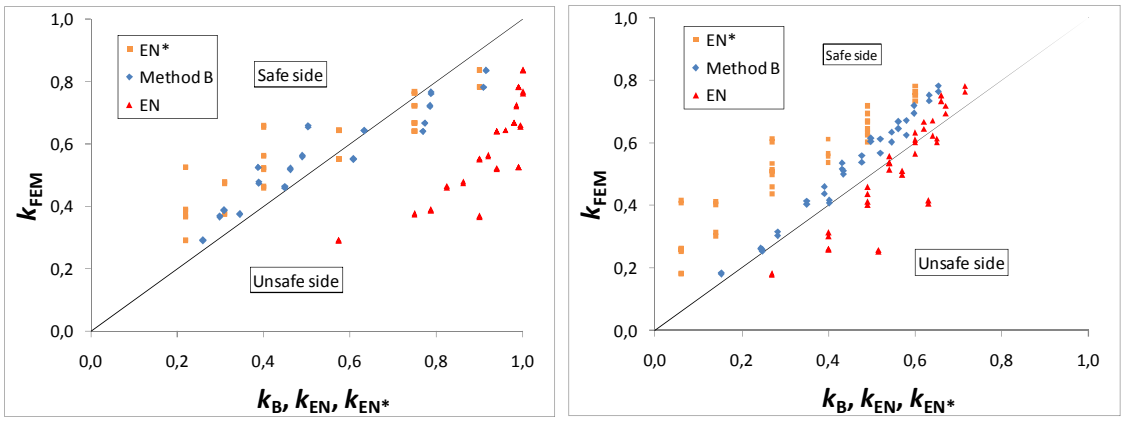

Figure 5.40. Comparison of reduction factors from FEM, method B and based on the average (EN) and hottest (EN*) temperature of the plate for aluminium and stainless steel plates PLa1, PLa2, PLs1 and PLs2.

Figure 5.41 compares the average values of the ratio k_{FEM} / k_i of method of reference temperature (method B) and reduction based on the average (EN) and maximum temperature (EN*) for all considered cases of this study. Moreover, minimum and maximum values are shown. When the ratio k_{FEM} / k_i exceeds one, the reduction factor is on the safe side compared to FEM analysis. It should be noted that in some cases involving carbon and stainless steel, the reduction factors from FEM were almost seven times higher than those based on the hottest temperature of the plate. In Figure 5.41, the maximum value of ratio k_{FEM} / k_i is limited to 2.5.

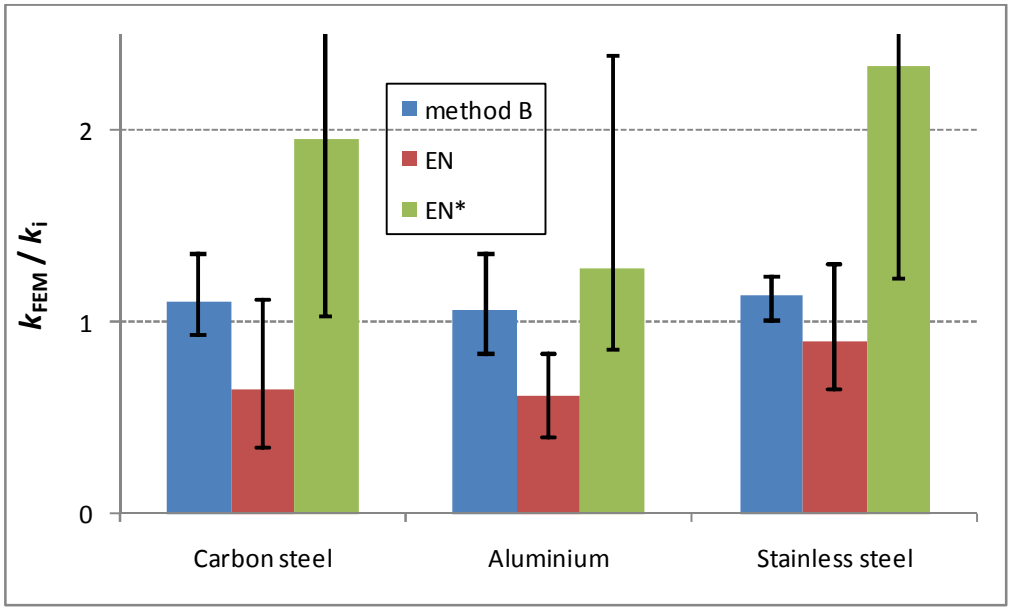

Figure 5.41. All reduction factors from FEM divided by reduction factors from method B and from Eurocodes (using average and maximum temperature).

Based on Figures 5.39–5.41 and the comparison done in Chapter 5.2.6, it can be concluded that method of reference temperature (method B) provides a reliable way to define the shear resistance of thin carbon steel and stainless steel (grade 1.4301) plates at non-uniform elevated temperatures when post-buckling strength is utilized (e.g. in Eurocodes). In the case of aluminium, the scattering of the results was higher probably due to the applied material model. More research is needed. If post-buckling strength is not utilized for some reason (appearance, limitations of standards, deflections), method A provides a reliable way to predict shear buckling strength at non-uniform elevated temperatures. Moreover, since the contribution of shear buckling can be estimated rather accurately, it might be possible to develop method of separation of shear and post-buckling (method A) so that post-buckling resistance could be calculated more reliably, especially in cases where the hottest temperature of the plate is relatively high.

The comparisons made in this chapter show that use of reduction based on average temperature of the plate at non-uniform elevated temperatures yields unconservative results in most cases. However, in some cases (e.g. stainless steel when the hottest temperature of the plate does not exceed 600 ^{o}C) the use of reduction based on average temperature is justified. The use of reduction based on the hottest temperature of the plate leads to highly conservative results in most cases.

6 DISCUSSION AND CONCLUSIONS

6.1 General

This study was conducted in order to gain knowledge about the behaviour of thin metal (carbon steel, aluminium and stainless steel) plates under shear loading at non-uniform elevated temperatures. Plates with different properties were analysed at ambient, uniform and non-uniform elevated temperatures using FEM.

Another goal of the study was to develop an analytical design method to predict reliably the shear resistance of thin metal plate at non-uniform elevated temperatures. Since no results from related tests were available, the validation of the proposed method was done by comparing its results to those of FEM calculations.

6.2 Numerical modelling

The shear resistances of metal plates with different properties were calculated at numerous non-uniform elevated temperatures using commercial ABAQUS FEM software [ABAQUS, 2010]. All the modelled plates were isolated which is why the effects of stiffeners and flanges were not considered in this study. All cases involved only the shear in the plane of the plate.

Many tension field theories, such as the rotated stress field theory [Höglund, 1972], are based on the fundamental assumption that compressive stress cannot increase after critical shear stress is reached and equilibrium is violated by stresses on the vertical and horizontal planes. If that fundamental assumption were correct, no tension field (post-buckling behaviour) could have occurred in the cases of this study. However, according to the FEM analyses conducted in this study and other recent researches, such as [Yoo, Lee, 2006], no anchoring system, such as flanges, is needed for the development of post-buckling strength. The shear resistance of an isolated plate was the basic case considered in this study, which should be solved before considering more practical cases including e.g. axial stresses.

Imperfection sensitivity analysis revealed that the magnitude of the initial imperfection (if between $h/100\ 000$–$h/100$) did not have a significant effect on ultimate shear resistance at ambient and elevated temperatures in most cases. Moreover, it was concluded that ultimate shear resistance did not depend much on the shape of the initial

imperfection in most cases, especially when using the lowest positive eigenmodes as an imperfection.

The comparisons between tested [Vimonsatit, Tan, Qian, 2007] and calculated resistances showed that the FEM model was reliable in analysing the behaviour of an isolated plate at elevated temperatures. It was also shown that supporting structures (flanges) may increase the shear resistance of a plate significantly.

Analysis at uniform elevated temperatures revealed that the ultimate shear resistance of thin metal plates at elevated temperatures can be reduced accurately using a reduction based on 0.2 % proof strength.

Reduction based on average temperature and 0.2 % proof strength at non-uniform elevated temperatures (Eurocode [EN 1993-1-2, 2005], [EN 1999-1-2, 2007] method) gave unconservative results compared to FEM results in the considered cases. Moreover, the use of maximum temperature instead of average temperature yielded highly conservative results especially in the case of carbon steel plates. Thus, it was concluded that in most of the cases, the correct reduction factor should be based on a temperature between the average and the hottest temperature of the plate.

6.3 Proposed calculation methods

Two methods for predicting the shear resistance of a thin metal plate at non-uniform elevated temperatures were proposed: method of separation of shear and post-buckling and method of reference temperature. The advantage of method of separation of shear and post-buckling compared to method of reference temperature is that both phases (buckling and post-buckling) can be calculated separately. Method of reference temperature is easier to apply and gives more reliable results for ultimate shear resistance compared to numerical analysis in the considered cases.

Based on the results of this study, it can be concluded that method of reference temperature provides a reliable way to define the shear resistance of thin carbon steel and stainless steel (grade 1.4301) plates at non-uniform elevated temperatures when post-buckling strength is utilised (e.g. in Eurocodes). For aluminium, the scattering of the results was higher probably due to the applied material model [Maljaars, 2008]. If post-buckling strength is not utilised for some reason, method of separation of shear and post-buckling provides a reliable way to predict shear buckling resistance at non-uniform elevated temperatures.

6.4 Further studies

The effects of surrounding members and interactions with other stress components were not considered in this study even though significant axial forces have been observed in heated beams due to column restraints, such as in references [Liu et al, 2002] and [Ma, Mäkeläinen, 2006]. It has been shown that many kinds of behaviour occur due to the interaction of the members, and often the behaviour of real structures is better than that predicted from standards for isolated member [Wald et al, 2006]. Thus, future studies should examine the behaviour of plates which are part of a larger structure.

The behaviour of aluminium and stainless steel plates depends significantly on the alloy and grade. In this study aluminium alloy 5083-H111 and stainless steel grade 1.4301 were considered. In the case of other other alloys and grades the behaviour of plates may be significantly different. The stress-strain relationships and reduction factors for carbon and stainless steel were taken from EN 1993-1-2 [EN 1993-1-2, 2005]. Reduction factors for aluminium were taken from EN 1999-1-2 [EN 1999-1-2, 2007] and stress-strain relationships at a few elevated temperatures from the dissertation of Maljaars [Maljaars, 2008]. In the case of aluminium, more research is needed also with regard to isolated plates of different alloys and on wider temperature distributions.

The FEM calculations were conducted using a steady-state method where the plate was first heated to the specified temperature and then a mechanical load was applied. The steady-state method was used in order to be able to observe both phases (buckling and post-buckling) separately. However, the transient-state method, which gives more realistic results [Outinen, 2001], should also be considered in future studies.

Test results at non-uniform elevated temperatures are badly needed to verify the proposed methods. Both methods can be developed and, for example, the factors applied in method of reference temperature can be easily adjusted (e.g. for other stainless steel grades) or other factors added based on results from experimental or numerical analysis, if available. Moreover, since the contribution of shear buckling can be estimated rather accurately, it might be possible to develop method of separation of shear and post-buckling so that post-buckling resistance could be calculated more reliably especially in cases where the hottest temperature of the plate is relatively high.

REFERENCES

AASHTO, *AASHTO.LRFD bridge design specifications*, 1st ed, American Association of State Highway and Transportations, Washington D.C., 1994

ABAQUS 6.10/CAE User's Manual, Dassault Systemes, 2010

AISC, *Specification for the design, fabrication and erection of structural steel for building*, American Institute of Steel Construction, New York, 1963

AISC, (a), *Seismic provisions for structural steel buildings*, American Institute of Steel Construction, Chicago, 2005

AISC, (b), *Specification for Structural Steel Buildings*, American Institute of Steel Construction, Chicago, 2005

Ala-Outinen T., Schaumann P., Kaitila O., Kettner F., Light weight structures exposed to fire: a stainless steel sandwich panel, *Proceedings of the Fourth International Workshop: Structures in Fire*, Aveiro 2006, pp. 139-150

Allam A.M., Burgess I.W., Plank R.J., Performance-based simplified model for a steel beam at large deflection in fire, *Fourth international conference on performance-based codes and fire safety*, 2002, p. 100

Alinia M.M., Gheitasi A., Erfani S., (a), Plastic shear buckling of unstiffened stocky plates, *Journal of Constructional Steel Research* 65, 2009, pp. 1631-1643

Alinia M.M., Gheitasi A., Shakiba M., Postbuckling and ultimate state of stresses in steel plate girders, *Thin-Walled Structures* 49, 2011, pp. 455-464

Alinia M.M., Habasbi H.R., Khorram A., (b) Nonlinearity in the postbuckling behaviour of thin steel shear panels, *Thin-Walled Structures* 47, 2009, pp. 412-420

Alinia M.M., Hosseinzadeh S.A.A., Habashi H.R., Buckling and post-buckling strength of shear panels degraded by near border cracks, *Journal of Constructional Steel Research* 64, 2008, pp. 1483-1494

Alinia M.M., Shakiba M., Habasbi H.R., (c) Shear failure characteristics of steel plate girders, *Thin-Walled Structures* 47, 2009, pp. 1498-1506

Basler K., (a) Strength of plate girder in shear, *Journal of the Structural Division ASCE* 87, 1961, pp. 151-180

Basler K., (b) Strength of plate girder under combined bending and shear, *Journal of the Structural Division ASCE* 87, 1961, pp. 181-197

Basler K., Thurlimann B., Plate girder research, *Proceedings of AISC national engineering conference*, 1959

BS 5950, Part 1, *Structural use of steelwork in building, Code of practice for design in simple and continous construction: Hot rolled sections*, British Standards Institution, London 1990

BS 5950, Part 8, *Structural use of steelwork in building, Code of practice for fire resistant design*, British Standards Institution, London 1990

Chern C., Ostapenko A., Ultimate strength of plate girder under shear, *Friz Engineering Laboratory Rep. No. 328.7*, Lehigh Univ., Bethlehem, Pa, 1969

COMSOL Multiphysics User's Guide, Version 3.5a, COMSOL AB, 2008

COMSOL Heat Transfer Module User's Guide, Version 3.5a, COMSOL AB, 2008

Dai X.H., Wang Y.C., Bailey C.G., Numerical modeling of structural fire behavior of restrained steel beam-column assemblies using typical joint types, *Engineering Structures* 32 (2010), pp. 2337-2351

Dubas P., Gehri E., (Eds.) *Behaviour and Design of Steel Plated Structures*, ECCS Technical Committee 8, Structural Stability, no 44, 1986

Duthinh D., McGrattan K., Khaskia A., Recent advances in fire-structure analysis, *Fire Safety Journal* 43 (2008), pp. 161-167

EN 1090-2, *Execution of steel structures and aluminium structures* – Part 2: Technical requirements for the execution of steel structures, CEN, Bryssels, 2008

EN 1991-1-2, Eurocode 1: *Actions on structures, Part 1-2: General actions – Actions on structures exposed to fire*, CEN, Bryssels, 2002

EN 1993-1-1, Eurocode 3: *Design of steel structures, Part 1-1: General rules and rules for buildings*, CEN, Bryssels, 2005

EN 1993-1-2, Eurocode 3: *Design of steel structures, Part 1-2: Structural fire design*, CEN, Bryssels, 2005

EN 1993-1-4, Eurocode 3: *Design of steel structures, Part 1-4: General rules, Supplementary rules for stainless steel*, CEN, Bryssels, 2006

EN 1993-1-5, Eurocode 3: *Design of steel structures, Part 1-5: Plated structural elements*, CEN, Bryssels, 2005

EN 1999-1-1, Eurocode 9: *Design of aluminium structures, Part 1-1: General structural rules*, CEN, Bryssels, 2007

EN 1999-1-2, Eurocode 9: *Design of aluminium structures, Part 1-2: Structural fire design*, CEN, Bryssels, 2007

Estrada I., *Shear design of stainless steel plate girders*, Doctoral thesis, Universitat Politecnica de Catalunya, Barcelona, 2005

Estrada I., Real E., Mirambell E., General behavior and effect of rigid and non-rigid end post in stainless steel plate girders loaded in shear. Part I: Experimental study, *Journal of Constructional Steel Research* 63, 2007, pp. 970-984

Estrada I., Real E., Mirambell E., A new developed expression to determine more realistically the shear buckling stress in steel plate structures, *Journal of Constructional Steel Research* 64, 2008, pp. 737-747

Feng M., Wang Y.C., Davies J.M., Axial strength of cold-formed thin-walled steel channels under non-uniform temperatures in fire, *Fire Safety Journal* 38, 2003, pp.679-707

Fujii T., *On an improved theory for Dr. Basler's theory*, Final Rep., IABSE 8th Congress, New York, 1968

Fujii T., A comparison between the theoretical values and the experimental results for the ultimate shear strength of plate girders, IABSE Rep. of the Working Commissions, Volume-Band 11, Colloquium, *Design of Plate and Box Girders for Ultimate Strength*, London, 1971, pp. 161-171

Gheitasi A., Alinia M.M., Slenderness classification of unstiffened metal plates under shear loading, *Thin-Walled Structures* 48, 2010, pp. 508-518

Habashi H.R., Alinia M.M., Characteristics of the wall-frame interaction in steel plate shear walls, *Journal of Constructional Steel Research* 66, 2010, pp.150-158

Heinisuo M., Ylihärsilä H., *All Metal Structures at Elevated Temperatures*, Tampere University of Technology, Institute of Structural Engineering, Research Report 135, Tampere, 2006

Höglund T., *Design of thin plate I-girders in shear and bending with special reference to web buckling*, Division of Building Statics and Structural Engineering, Royal Institute of Technology, Stockholm, 1972

Höglund T., Shear Buckling Resistance of Steel and Aluminium Plate Girders, *Thin-Walled Structures* 29, 1997, pp. 13-30

Johansson B., Maquoi R., Sedlacek G., New design rules for plated structures in Eurocode 3, *Journal of Constructional Steel Research* 57, 2001, pp. 279-311

Kaitila O., *Web Crippling of Cold-Formed Thin-Walled Steel Cassettes*, Doctoral Thesis, Helsinki University of Technology, Laboratory of Steel Structures, Publications 30, TKK-TER-20, Espoo, 2004

Kaitila O., Finite Element Modelling of Cold-Formed Steel Members at High Temperatures, Thesis for the Degree of Licentiate of Science in Technology, Helsinki University of Technology, Laboratory of Steel Structures, Publications 24, TKK-TER-24, Espoo, 2002

Kansallinen liite standardiin SFS-EN 1993-1-5 *Eurokoodi 3: Teräsrakenteiden suunnittelu, Osa 1-5: Tasomaiset levyrakenteet* (In Finnish), Ympäristöministeriö, 2008

Komatsu S., Ultimate strength of stiffened plate girders subjected to shear, IABSE Rep. of the Working Commissions, Volume-Band 11, Colloquium, *Design of Plate and Box Girders for Ultimate Strength*, London, 1971, pp. 49-65

Kristanic N., Korelc J., Optimization method for the determination of the most unfavourable imperfection of structures, *Computational Mechanics* 42, 2008, pp. 859-872

Lee S.C., Lee D.S., Yoo C.H., Ultimate shear strength of long web panels, *Journal of Constructional Steel Research* 64, 2008, pp. 1357-1365

Liu T.C.H., Fahad M.K., Davies J.M., Experimental investigation of behaviour of axially restrained steel beams in fire, *Journal of Constructional Steel Research* 58, 2002, pp. 1211-1230

Ma Z., Mäkeläinen P., Structural Behaviour of composite slim floor frames in fire conditions, *Journal of Constructional Steel Research* 62, 2006, pp.1282-1289

Maljaars J., *Local buckling of slender aluminium sections exposed to fire*, Doctoral thesis, Netherlands Institute for Metals Research, 2008

Maquoi R., Skaloud M., Stability of plates and plated structures, General Report, *Journal of Constructional Steel Research* 55, 2000, pp. 45-68.

Olsson A., *Stainless steel plasticity, Material modeling and structural applications*, Doctoral thesis, Luleå University of Technology, Luleå, 2001

Outinen H., Salmi T., *Lujuusopin perusteet*(In Finnish), Pressus Oy, Tampere, 2004

Outinen J., *Mechanical properties of structural steels at high temperatures and after cooling down*, Doctoral Dissertation, Helsinki University of Technology, Laboratory of Steel Structures, Publications 32, Espoo, 2007

Outinen J., Kaitila O., Mäkeläinen P., *High-temperature testing of structural steel and modelling of structures at fire temperatures*, Helsinki University of Technology, Laboratory of Steel Structures, Publications 23, Espoo, 2001

Pavlovcic L., Detzel A., Kuhlmann U., Beg D., Shear resistance of longitudinally stiffened panels – Part 1: Tests and numerical analysis of imperfections, *Journal of Constructional Steel Research* 63, 2007, pp. 337-350

Qian Z.H., Tan K.H., Deflection behaviour of plate girders loaded in shear at elevated temperatures, *Journal of Constructional Steel Research* 65, 2009, pp. 991-1000

Real E., *Aportaciones al studio del comportamiento a flexion de estructuras de acero inoxidable*, Doctoral thesis, Universitat Politecnica de Catalunya, Barcelona, 2001

Real E., Mirambell E., Estrada I., Shear response of stainless steel plate girders, *Engineering Structures* 29, 2007, pp. 1626-1640

Reddy J.N., *An introduction to nonlinear finite element analysis*, USA, Oxford University Press, 2004

Rockey K.C., Evans H.R., Porter D.M., Design method for predicting the collapse behavior of plate girders, *Proceedings of the institution of civil engineers, part 2*, 1978, pp. 85-112

Rode H.H., Beitrag zur Theorie der Knickerscheidungen, *Der Eisenbau*, 1916, pp. 210-218

Salminen M., *Shear Buckling Resistance of Thin Metal Plate at Non-Uniform Elevated Temperatures*, Licentiate Thesis, Tampere University of Technology, Tampere, 2010

Salminen M., Heinisuo M., *Shear resistance of thin plate at non-uniform elevated temperatures*, ECCS TC8, 25.6.2010, Oslo

Salminen M., Heinisuo M., (a), *Shear buckling and resistance of thin-walled metal plate in non-uniform elevated temperature*, 10th International Conference on Steel, Space and Composite Structures (SS11), North Cyprus, Turkey, May 2011

Salminen M., Heinisuo M., (b), *Shear Resistance of Metal Plates at Non-Uniform Elevated Temperatures*, XII International Conference on Metal Structures, Wroclaw, Poland, June 2011

Tan K.H., Qian Z.H., Experimental behavior of a thermally restrained plate girder loaded in shear at elevated temperature, *Journal of Constructional Steel Research* 64, 2008, pp. 596-606

Tan K.H., Yuan W.F., Buckling of elastically restrained steel columns under longitudinal non-uniform temperature distribution, *Journal of Constructional Steel Research* 64, 2008, pp. 51-61

Tan K.H., Yuan W.F., Inelastic buckling of pin-ended steel columns under longitudinal non-uniform temperature distribution, *Journal of Constructional Steel Research* 65, 2009, pp. 132-141

Teräsnormikortti N:o 21/2009, *WQ-palkin poikkileikkauksen mitoitus normaali- ja palotilanteessa* (In Finnish), TRY, 2009

Quintiere J.G., di Marzo M., Becker R., A suggested cause of the fire-induced collapse of the World Trade Towers, *Fire Safety Journal* 37 (2002), pp. 707-716

Vimonsatit V., Tan K.H., Qian Z.H., Testing of plate girder web panel loaded in shear, *Journal of Structural Engineering*, ASCE, 2007

Vimonsatit V., Tan K.H., Ting S.K., Shear strength of plate girder web panel at elevated temperature, *Journal of Constructional Steel Research* 63, 2007, pp. 1442-1451

Wagner H., *Flat sheet metal girder with very thin metal web*, National Advisory Committee for Aeronautics, 1931

Wald F., Simoes da Silva L., Moore D.B., Lennon T., Chladna M., Santiago A., Benes M., Borges L., Experimental behaviour of a steel structure under natural fire, *Fire Safety Journal* 41, 2006, pp. 509-522

Wald F., Sokol Z., Moore D., Horizontal forces in steel structures tested in fire, *Journal of Constructional Steel Research* 65, 2009, pp. 1896-1903

Wilson J.M., *On specifications for strength of iron bridges*, Trans Am Soc Civ Eng, 1886

Yin Y.Z., Wang Y.C., Numerical simulations of the effects of non-uniform temperature distributions on lateral torsional buckling resistance of steel I-beams, *Journal of Constructional Steel Research* 59, 2003, pp. 1009-1033

Yin Y.Z., Wang Y.C., (a) Analysis of catenary action in steel beams using a simplified hand calculation method, Part 1: theory and validation for uniform temperature distribution, *Journal of Constructional Steel Research* 61, 2005, pp. 183-211

Yin Y.Z., Wang Y.C., (b) Analysis of catenary action in steel beams using a simplified hand calculation method, Part 2: validation for non-uniform temperature distribution, *Journal of Constructional Steel Research* 61, 2005, pp. 213-234

Yoo C.H., Lee S.C., Mechanics of Web Panel Postbuckling Behavior in Shear, *Journal of Structural Engineering*, ASCE, 2006

APPENDIX A. TYPICAL KEYWORDS FOR ABAQUS / CAE CALCULATIONS

Model: buckling

```
*Part, name=PL_1_POST_B
*End Part
**
**
** ASSEMBLY
**
*Assembly, name=Assembly
**
*Instance, name=PL_1_POST_B-3, part=PL_1_POST_B
*Element, type=S4R
** Section: PL_1_POST_B
*Shell Section, elset=_PickedSet2, material=BM
0.0015, 5
*End Instance
**
*Nset, nset=Setti_2, instance=PL_1_POST_B-3, generate
*Elset, elset=Setti_2, instance=PL_1_POST_B-3, generate
*Surface, type=ELEMENT, name=_PickedSurf32, internal
*Surface, type=ELEMENT, name=_PickedSurf41, internal
*Surface, type=ELEMENT, name=_PickedSurf84, internal
*Surface, type=ELEMENT, name=_PickedSurf85, internal
*End Assembly
**
** MATERIALS
**
*Material, name=BM
*Elastic
   2e+11,  0.3,   0.
   2e+11,  0.3, 100.
 1.8e+11,  0.3, 200.
 1.6e+11,  0.3, 300.
 1.4e+11,  0.3, 400.
 1.2e+11,  0.3, 500.
 6.2e+10,  0.3, 600.
 2.6e+10,  0.3, 700.
 1.8e+10,  0.3, 800.
1.35e+10,  0.3, 900.
```

```
   9e+09,  0.3,1000.
 4.5e+09,  0.3,1100.
     0.1,  0.3,1200.
**
**
** BOUNDARY CONDITIONS
**
** Name: A_Y Type: Displacement/Rotation
*Boundary
_PickedSet58, 3, 3
_PickedSet58, 5, 5
_PickedSet58, 6, 6
** Name: O_V Type: Displacement/Rotation
*Boundary
_PickedSet59, 3, 3
_PickedSet59, 4, 4
_PickedSet59, 6, 6
** Name: POST_muut_pisteet Type: Displacement/Rotation
*Boundary
_PickedSet36, 3, 3
_PickedSet36, 4, 4
_PickedSet36, 5, 5
_PickedSet36, 6, 6
** Name: POST_piste_A Type: Displacement/Rotation
*Boundary
_PickedSet35, 1, 1
_PickedSet35, 2, 2
_PickedSet35, 3, 3
_PickedSet35, 4, 4
_PickedSet35, 5, 5
_PickedSet35, 6, 6
** ----------------------------------------------------------------
**
** STEP: BUCKLING
**
*Step, name=BUCKLING, perturbation
*Buckle
40, 60., 48, 30
**
** BOUNDARY CONDITIONS
**
** Name: A_Y Type: Displacement/Rotation
```

*Boundary, op=NEW, load case=1
_PickedSet58, 3, 3
_PickedSet58, 5, 5
_PickedSet58, 6, 6
*Boundary, op=NEW, load case=2
_PickedSet58, 3, 3
_PickedSet58, 5, 5
_PickedSet58, 6, 6
** Name: O_V Type: Displacement/Rotation
*Boundary, op=NEW, load case=1
_PickedSet59, 3, 3
_PickedSet59, 4, 4
_PickedSet59, 6, 6
*Boundary, op=NEW, load case=2
_PickedSet59, 3, 3
_PickedSet59, 4, 4
_PickedSet59, 6, 6
** Name: POST_muut_pisteet Type: Displacement/Rotation
*Boundary, op=NEW, load case=1
_PickedSet36, 3, 3
_PickedSet36, 4, 4
_PickedSet36, 5, 5
_PickedSet36, 6, 6
*Boundary, op=NEW, load case=2
_PickedSet36, 3, 3
_PickedSet36, 4, 4
_PickedSet36, 5, 5
_PickedSet36, 6, 6
** Name: POST_piste_A Type: Displacement/Rotation
*Boundary, op=NEW, load case=1
_PickedSet35, 1, 1
_PickedSet35, 2, 2
_PickedSet35, 3, 3
_PickedSet35, 4, 4
_PickedSet35, 5, 5
_PickedSet35, 6, 6
*Boundary, op=NEW, load case=2
_PickedSet35, 1, 1
_PickedSet35, 2, 2
_PickedSet35, 3, 3
_PickedSet35, 4, 4
_PickedSet35, 5, 5

```
_PickedSet35, 6, 6
**
** LOADS
**
** Name: BUCKLE_oikea_vasen   Type: Shell edge load
*Dsload
_PickedSurf84, EDSHR, -3278.69
** Name: BUCKLE_yla_ala   Type: Shell edge load
*Dsload
_PickedSurf85, EDSHR, 3278.69
**
** OUTPUT REQUESTS
**
*Restart, write, frequency=0
**
** FIELD OUTPUT: F-Output-2
**
*Output, field, variable=PRESELECT
*node file, nset=assembly.Setti_2,mode=1,last mode=16
u
*End Step
```

Model: post-buckling

```
*Part, name=PL_1_POST_B
*End Part
**
**
** ASSEMBLY
**
*Assembly, name=Assembly
**
*Instance, name=PL_1_POST_B-3, part=PL_1_POST_B
*Element, type=S4R
** Section: PL_1_POST_B
*Shell Section, elset=_PickedSet2, material=POST_Steel_tarkka_S332
0.0015, 5
*End Instance
**
*Nset, nset=Setti_2, instance=PL_1_POST_B-3, generate
*Elset, elset=Setti_2, instance=PL_1_POST_B-3, generate
*Surface, type=ELEMENT, name=_PickedSurf31, internal
*Surface, type=ELEMENT, name=_PickedSurf32, internal
```

```
*Surface, type=ELEMENT, name=_PickedSurf84, internal
*End Assembly
**
** MATERIALS
**
*Material, name=POST_Steel_tarkka_S332
*Elastic
   2e+11,  0.3,   0.
   2e+11,  0.3, 100.
 1.8e+11,  0.3, 200.
 1.6e+11,  0.3, 300.
 1.4e+11,  0.3, 400.
 1.2e+11,  0.3, 500.
 6.2e+10,  0.3, 600.
 2.6e+10,  0.3, 700.
 1.8e+10,  0.3, 800.
1.35e+10,  0.3, 900.
   9e+09,  0.3,1000.
 4.5e+09,  0.3,1100.
   0.001,  0.3,1200.
*Expansion
1.19e-05,  20.
1.19e-05, 100.
1.29e-05, 200.
1.33e-05, 300.
1.37e-05, 400.
1.41e-05, 500.
1.45e-05, 600.
1.49e-05, 700.
1.51e-05, 750.
1.41e-05, 800.
1.33e-05, 850.
1.34e-05, 900.
1.41e-05,1000.
1.46e-05,1100.
1.51e-05,1200.
*Plastic
3.32551e+08,      0.,     20.
 3.3316e+08, 0.00182,     20.
3.33769e+08, 0.00365,     20.
3.34378e+08, 0.00546,     20.
3.34987e+08, 0.00728,     20.
```

```
 3.35596e+08, 0.00909,     20.
 3.36204e+08,  0.0109,     20.
 3.36813e+08, 0.01271,     20.
 3.37422e+08, 0.01451,     20.
 3.38031e+08, 0.01631,     20.
  3.3864e+08, 0.01811,     20.
   3.818e+08, 0.13785,     20.
         1., 0.18232,     20.
 3.00436e+08,      0.,    150.
 3.14834e+08, 0.00176,    150.
 3.20746e+08, 0.00356,    150.
  3.2505e+08, 0.00537,    150.
 3.28446e+08, 0.00718,    150.
 3.31203e+08, 0.00899,    150.
  3.3346e+08,  0.0108,    150.
 3.35294e+08, 0.01261,    150.
 3.36753e+08, 0.01441,    150.
.
.
.
1.65375e+07, 0.01271,    950.
  1.6737e+07, 0.01457,    950.
 1.68676e+07, 0.01643,    950.
  1.6932e+07,  0.0183,    950.
   1.909e+07, 0.13807,    950.
         1., 0.18232,    950.
 8.30765e+06,      0.,   1000.
 1.04179e+07, 0.00167,   1000.
 1.12823e+07, 0.00347,   1000.
 1.18927e+07,  0.0053,   1000.
 1.23592e+07, 0.00714,   1000.
 1.27247e+07, 0.00899,   1000.
 1.30108e+07, 0.01085,   1000.
   1.323e+07, 0.01271,   1000.
 1.33896e+07, 0.01457,   1000.
 1.34941e+07, 0.01643,   1000.
 1.35456e+07,  0.0183,   1000.
  1.5272e+07, 0.13807,   1000.
         1., 0.18232,   1000.
**
** BOUNDARY CONDITIONS
**
```

```
** Name: A_Y Type: Displacement/Rotation
*Boundary
_PickedSet58, 3, 3
_PickedSet58, 5, 5
_PickedSet58, 6, 6
** Name: O_V Type: Displacement/Rotation
*Boundary
_PickedSet59, 3, 3
_PickedSet59, 4, 4
_PickedSet59, 6, 6
** Name: POST_muut_pisteet Type: Displacement/Rotation
*Boundary
_PickedSet36, 3, 3
_PickedSet36, 4, 4
_PickedSet36, 5, 5
_PickedSet36, 6, 6
** Name: POST_piste_A Type: Displacement/Rotation
*Boundary
_PickedSet35, 1, 1
_PickedSet35, 2, 2
_PickedSet35, 3, 3
_PickedSet35, 4, 4
_PickedSet35, 5, 5
_PickedSet35, 6, 6
**
** PREDEFINED FIELDS
**
** Name: Lin100-500   Type: Temperature Using Field: Lin100-500
*Initial Conditions, type=TEMPERATURE
PL_1_POST_B-3.1, 500.
PL_1_POST_B-3.2, 500.
PL_1_POST_B-3.3, 500.
PL_1_POST_B-3.4, 500.
PL_1_POST_B-3.5, 500.
PL_1_POST_B-3.6, 500.
.
.
.
PL_1_POST_B-3.2590, 100.
PL_1_POST_B-3.2591, 100.
PL_1_POST_B-3.2592, 100.
PL_1_POST_B-3.2593, 100.
```

```
PL_1_POST_B-3.2594, 100.
PL_1_POST_B-3.2595, 100.
PL_1_POST_B-3.2596, 100.
PL_1_POST_B-3.2597, 100.
PL_1_POST_B-3.2598, 100.
PL_1_POST_B-3.2599, 100.
PL_1_POST_B-3.2600, 100.
PL_1_POST_B-3.2601, 100.
*imperfection,file=buckling,step=1,nset=assembly.Setti_2
2,0.0024132
4,0.0010675
6,0.0016892
** ----------------------------------------------------------------
**
** STEP: POST_Riks
**
*Step, name=POST_Riks, nlgeom=YES, inc=80
*Static, riks
100., 100., 100., 2000., 10000.,
**
** BOUNDARY CONDITIONS
**
** Name: A_Y Type: Displacement/Rotation
*Boundary, op=NEW
_PickedSet58, 3, 3
_PickedSet58, 5, 5
_PickedSet58, 6, 6
** Name: O_V Type: Displacement/Rotation
*Boundary, op=NEW
_PickedSet59, 3, 3
_PickedSet59, 4, 4
_PickedSet59, 6, 6
** Name: POST_muut_pisteet Type: Displacement/Rotation
*Boundary, op=NEW
_PickedSet36, 3, 3
_PickedSet36, 4, 4
_PickedSet36, 5, 5
_PickedSet36, 6, 6
** Name: POST_piste_A Type: Displacement/Rotation
*Boundary, op=NEW
_PickedSet35, 1, 1
_PickedSet35, 2, 2
```

```
_PickedSet35, 3, 3
_PickedSet35, 4, 4
_PickedSet35, 5, 5
_PickedSet35, 6, 6
**
** LOADS
**
** Name: POST_oikea_vasen   Type: Shell edge load
*Dsload
_PickedSurf32, EDSHR, -3278.69
** Name: POST_yla_ala   Type: Shell edge load
*Dsload
_PickedSurf31, EDSHR, 3278.69
**
** OUTPUT REQUESTS
**
*Restart, write, frequency=0
**
** FIELD OUTPUT: F-Output-1
**
*Output, field, variable=PRESELECT
*Output, history, frequency=0
*End Step
```

Tampereen teknillinen yliopisto
PL 527
33101 Tampere

Tampere University of Technology
P.O.B. 527
FI-33101 Tampere, Finland

ISBN 978-952-15-2697-8
ISSN 1459-2045